6-18-2013 12:00 AM

Degradation Kinetics and Functional Design of Linear Self-Immolative Polymers

Ryan A. McBride
The University of Western Ontario

Supervisor
Dr. Elizabeth Gillies
The University of Western Ontario

Graduate Program in Chemical and Biochemical Engineering
A thesis submitted in partial fulfillment of the requirements for the degree in Master of Engineering Science

DEGRADATION KINETICS AND FUNCTIONAL DESIGN OF LINEAR SELF-IMMOLATIVE POLYMERS

(Thesis format: Integrated Article)

by

Ryan A. McBride

Graduate Program in Chemical and Biochemical Engineering

A thesis submitted in partial fulfillment
of the requirements for the degree of
Master of Engineering Science (M.E.Sc.)

The School of Graduate and Postdoctoral Studies
The University of Western Ontario
London, Ontario, Canada

Abstract

Linear self-immolative polymers display a potential to address many of the limitations in the control over the degradation process in traditional biodegradable polymers. These materials are unique relative to most degradable polymers, in that they undergo end-to-end depolymerization in response to the cleavage of a stabilizing end-capping agent. Although one of their cited attributes is a dependence of their degradation time on chain length, no conclusive study has been conducted to demonstrate and study this effect. Using a previously reported linear self-immolative backbone derived from alternating 4-hydroxybenzyl alcohol and *N,N'*-dimethylethylenediamine spacers, this work offers the first conclusive study demonstrating the proportional relationship between chain length and degradation time. This is accomplished using a set of monodisperse oligomers synthesized through a new convergent iterative route and a series of polymers optimized to display varying molecular weights. This work also describes the development and validation of a new linear self-immolative degradation model relating monomer kinetics to polymer degradation and shows its application in explaining oligomeric and polymeric degradation profiles. Collectively, this work provides the first quantitative evidence supporting the mixed pseudo zero- and first-order degradation kinetics of linear self-immolative polymers and proves the utility of chain length as an alternate means to tune the degradation time in linear self-immolative polymers. In the second focus of this thesis, a series of modified linear self-immolative amphiphilic block copolymer designs are proposed and evaluated in an effort to develop functional self-immolative nanoparticles for controlled release applications. Overall, the work presented in this thesis serves to expand the utility of linear self-immolative polymers for biomedical applications by demonstrating the flexibility of such systems through controlled design.

Keywords

Self-immolative polymers, self-immolative degradation, polymer degradation kinetics, cyclization kinetics, kinetic modelling, amphiphilic block copolymer, drug delivery vehicle.

Acknowledgments

I would first like to acknowledge my supervisor, Dr. Elizabeth Gillies, for giving me the opportunity to join her research group and for her support and guidance over the last two years. She has been very patient in allowing me to explore avenues of research outside of the realm of organic chemistry, and for that I am truly thankful.

My thanks also go out to the members of the Gillies group that I have crossed paths with during my time in the lab. I will always remember the experiences we have had together, both good and bad. Thanks for always keeping things new and exciting. I would especially like to thank Ali Nazemi, Darryl Knight, Mike Maris, Dr. Eric Chen, and Dr. Matt DeWit for training and continually helping me throughout my graduate studies. Last but not least, I would like to thank our laboratory technician, Aneta Borecki, for running all of my GPC samples and for keeping us a bit more balanced in the lab and office.

I would also like to thank my thesis examiners Dr. Herera, Dr. Rehmann, and Dr. Workentin for taking the time to review my thesis. Thanks to all the staff in the Department of Chemical and Biochemical Engineering, namely April Finkenhoefer and Kristen Hunt for keeping me on track over the course of my degree and for the quick responses to all my email inquiries. In the Department of Chemistry, I would like to acknowledge Doug Hairsine for running all of my samples for mass spectroscopy and Dr. Willans for helping me with all of my NMR needs.

Lastly, I would like to thank my parents for their continual support throughout my academic career. None of this would have been possible without the help I have received from the two of you.

To the rest of you who have helped me along the way, thank you.

Table of Contents

Abstract ii

Acknowledgments iii

List of Tables vii

List of Figures viii

List of Schemes xiv

List of Appendices xv

List of Abbreviations xvi

Chapter 1 1

1 Biodegradable Polymers for Biomedical Applications: From Polyesters to Self-Immolative Materials 1

1.1 General Introduction 1

1.2 Biodegradable Polyesters 2

1.2.1 Functional Designs 3

1.2.2 Limitations in the Degradation of Polyesters 5

1.3 Stimuli-Responsive Degradable Polymers 5

1.3.1 Acid Degradable Polymers 5

1.3.2 Reduction Sensitive Polymers 6

1.3.3 Photodegradable Polymers 7

1.3.4 Limitations in the Degradation of Conventional Stimuli-Responsive Degradable Polymers 7

1.4 Self-Immolative Polymers 8

1.4.1 Self-Immolative Spacers 9

1.4.2 Self-Immolative Oligomers 13

1.4.3 Self-Immolative Dendrimers 15

1.4.4 Linear Self-Immolative Polymers 21

1.5 Scope of the Thesis 30

1.6 References 31

Chapter 2 41

2 Kinetics of Self-Immolative Degradation in a Linear Polymeric System: Demonstrating the Effect of Chain Length[†] 41

2.1 Introduction 41

2.2 Experimental 44

2.2.1 General Procedures and Materials 44

2.2.2 Synthesis 45

2.2.3 Simulation Studies 50

2.2.4 Degradation Studies 50

2.2.5 Statistics 51

2.3 Results and Discussion 51

2.3.1 Choice of Model System 51

2.3.2 Oligomer Synthesis 52

2.3.3 Polymer Synthesis 56

2.3.4 Linear Self-Immolative Degradation Model 57

2.3.5 Mixed-Mode Degradation Kinetics 59

2.3.6 Simulation Studies 60

2.3.7 Oligomer Degradation Kinetics 62

2.3.8 Polymer Degradation Kinetics 65

2.4 Conclusions 67

2.5 References 68

Chapter 3 72

3 Progress Towards a Redox-Sensitive Self-Immolative Block Copolymer 72

3.1 Introduction 72

3.2 Experimental 75
3.2.1 General Procedures and Materials 75
3.2.2 Synthesis 76
3.2.3 Degradation Studies 85
3.2.4 General Procedure for Nanoparticle Assembly 87
3.2.5 Transmission Electron Microscopy 87
3.3 Results and Discussion 87
3.3.1 Motivation and Design 87
3.3.2 Synthesis 89
3.3.3 Probing the Solution Degradation Kinetics 94
3.3.4 Self-Assembly of Self-Immolative Block Copolymers 98
3.4 Self-Immolative Nanoparticle Degradation 101
3.5 Conclusion 102
3.6 References 103
Chapter 4 106
4 Conclusions and Future Perspectives 106
Appendices 109
Curriculum Vitae for Ryan A. McBride 156

List of Tables

Table 2.1: Summary of simulation studies investigating the effect of r_n and PDI on the kinetics linear self-immolative degradation 61

Table 2.2: Kinetic parameters for the degradation of oligomers 2.1d-2.4d 64

List of Figures

Figure 1.1. Conventional synthetic biodegradable polymers with hydrolyzable bonds 1

Figure 1.2: Popular synthetic biodegradable polyesters for biomedical applications 2

Figure 1.3: Ring opening polymerization of polyesters from (a) lactone or (b) cyclic dimer species. 2

Figure 1.4: Example of a 4th generation dendritic polyester scaffold derived from 2,2-bis(hydroxymethyl)propionic acid (bisMPA) 3

Figure 1.5: Self-assembly of block copolymers into functional polymer assemblies: (a) spherical micelles and (b) polymer vesicles. 4

Figure 1.6: Acid-sensitive linkers used in acid-degradable polymer backbones 6

Figure 1.7: (a) General structure of a poly(disulfide) and its reduction to thiols. (b) An example of a poly(disulfide) synthesized from a linear disulfide monomer. 6

Figure 1.8: Example of a photodegradable block copolymer incorporating a photolabile *ortho*-nitrobenzyl carbonyl group 7

Figure 1.9: Self-immolative degradation in (a) dendritic and (b) linear polymeric systems 8

Figure 1.10: (a) Classic and (b) self-immolative prodrug strategies 9

Figure 1.11: General schematics for (a) electronic cascade spacers, (b) cyclization, and (c) hemiacetal spacers. 10

Figure 1.12: Self-immolative cyclization spacers derived from 4-hydroxybutanoyl esters. (a) Trimethyl lock lactonization and (b) Coumarin based prodrug design. 11

Figure 1.13: Activation of carbamate prodrugs by intramolecular cyclization of the ethylenediamine pro-moiety[117] 12

Figure 1.14: Other hemiacetal based self-immolative linkers based on acyloxyalkyl and phosphoryloxyalkyl systems 13

Figure 1.15: Oligomeric prodrugs based on (a) multiple 1,6-elimination spacers and (b) multiple 1,6-elimination spacers followed by a cyclization spacer in series (PG – protecting group, D – drug, n=1,2). 14

Figure 1.16: Linear self-eliminating prodrug design incorporating double-release linkers to achieve amplification in the amount of drug released 15

Figure 1.17: 2nd generation linear disassembling dendrimer that degrades through a 1,6-elimination pathway upon cleavage of a terminal allyl-ether to release a single 4-nitrophenol reporter molecule 16

Figure 1.18: 2nd generation geometric disassembling dendrimer that degrades through a 1,4 and 1,6-elimination pathway upon cleavage of a terminal allyl-ether to release a four molecules of 4-nitrophenol 17

Figure 1.19: 2nd generation self-immolative polycarbamate dendrimer that degrades through a cascade of cyclization, 1,4-elimination, and decarboxylation reactions to release aminomethylpyrene upon exposure to UV light 18

Figure 1.20: 2nd generation polycarbamate dendrimer derived from branched 2-(4-aminobenzylidene)propane-1,3-diol spacers and designed to degrade through a cascade of 1,8-elimination reactions 19

Figure 1.21: Schematic representation of all currently available dendrimer designs. (a) Basic amplifier in which one triggering event leads to release of multiple reporter molecules. (b) Molecular OR logic trigger in which cleavage of one of two different triggers leads to the release of multiple reporter molecules. (c) Receiver-amplifier design with high sensitivity and gain whereby a low-level signal can be detected and amplified through the release of multiple reporter molecules. Adapted with permission from Wong et *al.*[80] Copyright 2012 Elsevier. 20

Figure 1.22: Dendrimer system capable of exponential signal amplification through the dendritic chain reaction. Cleavage of the phenylboronic acid triggering group by H_2O_2 leads to the liberation of a 4-nitroaniline reporter and two molecules of choline, which in turn generate four additional molecules of H_2O_2 upon reaction with choline oxidase. 21

Figure 1.23: Linear self-immolative polymer that degrades through a cascade of 1,6-elimination/decarboxylation reactions in the presence of BSA to release fluorescent monomer units and a terminal 4-nitroaniline reporter molecule (n=16). 22

Figure 1.24: Linear self-immolative polymer that degrades through 1,6-elimination/decarboxylation reactions in the presence of PGA in aqueous solution. Liberation of 4-nitroaniline molecules occurs following main chain degradation via a 1,6-elimination/decarboxylation reaction at a vinylogous 2-benzyl position on a released monomer unit. 23

Figure 1.25: Design of self-immolative microcapsules for self-healing autonomous repair systems. Selective removal of Boc and Fmoc end-caps triggers the degradation of the polycarbamate backbone through a cascade of 1,6-elimination/decarboxylation reactions to promote the release of the microcapsule contents through ruptures in the shell wall. Adapted with permission from Esser-Kahn *et al.*[171] Copyright 2010 American Chemical Society. 24

Figure 1.26: (a) First reported self-immolative poly(phthaldehyde)s that depolymerize through a cascade of 1,2-hemiacetal eliminations following end-cap removal. (b) Fabrication of a patterned plastic using a self-immolative poly(phthaldehyde). 25

Figure 1.27: Recent improvements to the design and synthesis of self-immolative poly(phthaldehyde)s. (a) Copolymerization of ortho-phthalaldehyde with substituted benzaldehydes to allow for the formation of functionalized PPAs. (b) Generalized procedure for the synthesis of PPAs with two stimuli-responsive end-caps appended to both ends of the polymer. 26

Figure 1.28: Linear self-immolative polymer backbones derived from alternating 1,6 elimination and cyclization spacers and their degradation kinetics in 3:2 pH 7.4 phosphate buffer:acetone at 37˚C. Reprinted with permission from Chen et al. Copyright 2012 American Chemical Society. 27

Figure 1.29: Reduction sensitive linear self-immolative polymer derived from alternating 2-mercaptoethanol and *N,N'*-dimethylethylenediamine cyclization spacers. 28

Figure 1.30: (a) 4-aminobutyric acid spacers that display rapid cyclization kinetics and their subsequent incorporation into linear self-immolative polymer frameworks based on (b) alternating cyclization/elimination reactions and (c) alternating cyclization reactions. 29

Figure 1.31: Design of a self-immolative block copolymer micellular drug delivery vehicle. (a) General structure of the self-immolative polymer backbone based on alternating 1,6-elimination and cyclization spacers and the hydrolytically sensitive PEG end-cap. (b) Structure and the degradation of micellular drug delivery vehicle. 30

Figure 2.1: Illustration of linear self-immolative degradation. (a) Generic overview depicting the end-to-end depolymerization of the polymer backbone following the removal of the stabilizing end-cap. (b) Previously reported linear self-immolative polymer derived from alternating cyclization and 1,6-elimination spacers and its mechanism of degradation. 42

Figure 2.2: Size exclusion chromatograms of compounds 2.2a (- · -), 2.3a (- - -), and 2.4a (—) prior to the removal of the Boc-protecting group (black) and after complete degradation (grey). (b) Size exclusion chromatograms of polymers 2.6 (- - -) and 2.7 (—) before (black) and after degradation (grey). All chromatograms acquired at a sample concentration of 5 mg/mL and calibrated using PMMA standards. 54

Figure 2.3: ^{1}H NMR spectra of monodisperse oligomers 2.1a-2.4a showing the evolution of oligomeric peaks relative to the Boc-terminus and the absence of *N,N'*-dimethylimidazolidinone during the iterative convergent synthesis (600 MHz, $CDCl_3$) 55

Figure 2.4: Mixed-mode degradation profile for the degradation of linear self-immolative polymers involving an initial pesudo zero-order domain followed by a gradual transition towards first-order behaviour 60

Figure 2.5: Calculated influence of chain length (a and b) and polydispersity index (c-d) on the rate of self-immolative degradation. Initial weight fraction (wi) distributions are shown in (a and c) and the resultant degradation plots are shown in (b and d). (a and b): PDI=1.6, r_n =10 (—), 20 (- - -), 30(···), 40(– · –). (c and d): r_n=10, PDI=1(—), 1.25(- - -), 1.5(···), 1.75 (– · –), 2(—). All distribution and kinetic plots were derived from numerical solutions to Eqs. (2.2), (2.3) and (2.5) with k=1.61 × 10^{-1} min^{-1}. 62

Figure 2.6: Degradation kinetics of compounds 2.1d-2.4d, as measured by ^{1}H NMR spectroscopy in 0.1 M phosphate buffer (D_2O):acetone-d_6 (3:2) at 37˚C. Representative samples from triplicate runs of 2.1d (●), 2.2d (■), 2.3d (▲), 2.4d (◆). Solid lines correspond to the regressed fits of Eq. (2.8) to each generation of oligomer (n=1,2,4,8). (b) Degradation kinetics of polymers 2.6 (▲) and 2.7 (■), as measured by ^{1}H NMR spectroscopy in 0.1 M phosphate buffer (D_2O):acetone-d_6 (3:2) at 37˚C. Overlayed lines correspond to the self-immolative model fits for both polymers..... 65

Figure 3.1: Linear self-immolative block copolymers synthesized using a poly(ethylene glycol) (PEG) end cap. (a) Generic diagram depicting the basic structure and mechanism of degradation. (b) Previously reported linear self-immolative block copolymer synthesized using a PEG acid end cap. (c) Diagram showing the self-assembly of amphiphilic linear self-immolative block copolymers in aqueous solution to form micelles for the encapsulation of hydrophobic drug molecules..... 73

Figure 3.2: Chemical structures, proposed depolymerization mechanisms, and expected depolymerization products of (a) target PEG succinic acid based self-immolative block copolymer and (b) target PEG disulfide based self-immolative block copolymer..... 88

Figure 3.3. Size exclusion chromatograms of block copolymers 3.7a (M_n = 3600 g/mol, PDI=1.47) (grey) and 3.7b (M_n = 7170 g/mol, PDI=1.21) (black). All chromatograms obtained a concentration of 5 mg/mL and calibrated against PEG in THF..... 91

Figure 3.4: Size exclusion chromatograms of polymers 3.14 (M_n = 3150 g/mol, PDI=1.73) (grey), 3.15 (M_n = 4300 g/mol, PDI=1.01) (- - -), and 3.16 (M_n = 5200 g/mol, PDI=1.41) (dark grey). All chromatograms obtained a concentration of 5 mg/mL and calibrated against PEG-PEO in THF. 94

Figure 3.5: Kinetics of cyclization in 0.1 M phosphate buffered D_2O:acetone-d_6 as measured by ^{1}H NMR spectroscopy for (a) compound 3.19 and (b) compound 3.21 and (c) polymer 3.14 after reduction of the thiopyridyl disulfide moeity in a highly reducing environment (0. 1 M DTT). Dashed lines correspond to the first-order fits for compounds 3.19 and 3.21 and the modified Avrami fit for polymer 3.14. 96

Figure 3.6: ^{1}H NMR spectra of compound 3.19: (a) immediately following dissolution in 0.1 M pH 7.4 phosphate buffered D_2O:acetone-d_6 (3:2) at 37˚C; (b) 5 min and (c) 5 h following DTT addition; and (d) following 40 h in a reducing environment. 97

Figure 3.7: ^{1}H NMR spectra of polymer 3.14: (a) immediately following dissolution in 0.1 M pH 7.4 phosphate buffered D_2O:acetone-d_6 (3:2) at 37˚C; (b) after complete disulfide reduction 5 min after DTT addition; and (c) following complete degradation after 40 h in a highly reducing environment (0.1 M DTT). 98

Figure 3.8: Dynamic light scattering traces of nanoparticles derived from (a) PEG succinic acid based block copolymers 3.7a (d=78.5 ± 1.4 nm, PDI=1.51 ± 0.17 × 10^{-1}) (grey) and 3.7b (d=332 ± 8.1 nm, PDI=1.84 ± 0.14 × 10^{-1}) (black) or (b) PEG thiol based block copolymer 3.16 (d=499 ± 22 nm, PDI=2.81 ± 0.27 × 10^{-1}) (dark grey). All traces obtained at a concentration of 0.1 mg/mL..... 99

Figure 3.9: Transmission electron microscopy images of the nanoparticles formed from copolymers 3.7a (a), 3.7b (b), and 3.16 (c)..... 100

Figure 3.10: Kinetics of self-immolative nanoparticle degradation in 0.1 M pH 7.4 phosphate buffer (D_2O) for copolymer 3.7a (●) and 3.7b (▲) as measured by ^{1}H NMR spectroscopy.102

List of Schemes

Scheme 2.1: Iterative convergent synthesis of monodisperse oligomers 53

Scheme 2.2: Synthesis of Polymers 2.6 and 2.7 56

Scheme 2.3: Degradation of compounds 2.1-2.4d to form dimethylimidazolidinone and 4-hydroxybenzyl alcohol 63

Scheme 3.1: Synthesis of a PEG succinic acid based end cap 89

Scheme 3.2: Polymerization of linear self-immolative block copolymers 3.7a and 3.7b using a PEG end capping agent 90

Scheme 3.3: Synthesis of a redox sensitive end cap incorporating a *N*-methylaminoethanethiol cyclization spacer 92

Scheme 3.4: Synthesis of a redox sensitive block copolymer using a thiol/disulfide exchange reaction 93

Scheme 3.5: Synthesis of model *N*-methylaminoethane thiol compound 3.19 and its cyclization to form 3-methylthiazolidinone 95

Scheme 3.6: Synthesis of model *N,N'*-dimethylethylenediamine compound 3.22 and its cyclization to form *N,N'*-dimethylimidazolidinone 95

List of Appendices

Appendix A: NMR Characterization Data 109

Appendix B: HPLC Chromatograms 128

Appendix C: Supplemental Degradation Study Spectra 132

Appendix D: Factorial DOE Experiments 144

Appendix E: Regression Fits 146

Appendix F: Permission to Reuse Copyrighted Material 154

List of Abbreviations

AIC	Akaike information criterion
Alloc	allyloxycarbonyl
ANOVA	analysis of variance
BIC	Bayesian information criterion
Boc	*tert*-butoxycarbonyl
br	broad
d	doublet
DBTL	dibutyltin dilaurate
DIPEA	*N,N*-diisopropylethylamine
DMAP	4-(dimethylamino)pyridine
DMF	*N,N*-dimethylformamide
DP	degree of polymerization
EI	electron impact
ESI	electrospray ionization
HPLC	high pressure liquid chromatography
HPLC	High pressure liquid chromatography
HRMS	high resolution mass spectrometry
Hz	hertz
IR	infrared
M	molar
m	multiplet
MALDI-TOF	matrix-assisted laser desorption ionization – time of flight
M_n	number average molecular weight
M_w	weight average molecular weight
MWCO	molecular weight cut-off
NIR	near infrared
NMR	nuclear magnetic resonance
PABC	*p*-aminobenzyl oxycarbonyl
PDI	polydispersity index
PEG	poly(ethylene glycol)
PPA	polyphthaldehyde
r_n	number average chain length
RT	room temperature
s	singlet
SEC	size exclusion chromatography
t	triplet
TBS	*tert*-butyldimethylsilyl
TEGMME	triethylene glycol monomethyl ether
TFA	trifluoracetic acid
THF	tetrahydrofuran
TLC	thin layer chromatography
UV	ultraviolet

Chapter 1

1 Biodegradable Polymers for Biomedical Applications: From Polyesters to Self-Immolative Materials

1.1 General Introduction

Advances in the field of polymer science over the last 50 years have led to the development of biodegradable polymers for a wide variety of applications. Once limited to the domain of academic research, biodegradable polymers have now emerged as environmentally-friendly alternatives to commodity plastics and are finding widespread use in biomedical applications ranging from tissue engineering to drug delivery.[1-6] In general, a biodegradable polymer can be defined as a polymeric system that is prone to a deleterious change in its chemical structure or physical properties under specific, practical environmental conditions.[7] In addition, these polymers should be biologically inert and not generate any substances that are harmful to the environment during the degradation process.[8]

Biodegradable polymers are typically comprised of systems with hydrolyzable bonds in the polymer backbone. Such polymers can be produced from natural materials such as polysaccharides, proteins, and bacterial polyesters or generated synthetically through the polymerization of polyamides, polyureas, polyurethanes, polyesters, polyethers, polyanhydrides, polypeptides and other corresponding copolymer systems (Figure 1.1).[1,2] Similar to the physical properties of polymeric materials, the degradation behaviour of biodegradable polymers is influenced by the chemical composition of the polymer backbone, molecular weight, polydispersity, and crystallinity.[1] To this end, the proper design and application of biodegradable polymers relies on a thorough understanding of polymer properties and their effect on the degradation process.

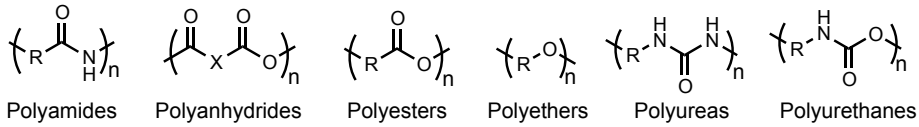

Figure 1.1. Conventional synthetic biodegradable polymers with hydrolyzable bonds

1.2 Biodegradable Polyesters

Aliphatic polyesters have received the most attention for biomedical applications out of all the available biodegradable backbones due to their ease of synthesis, desirable mechanical properties, and high biocompatibility.[9] Additionally, the degradation of these polymers is well tolerated *in vivo*, as the hydrolytic and/or enzymatic cleavage of backbone esters yields hydroxy-carboxylic acid species that can ultimately be metabolized.[1] Popular synthetic polyesters such as poly(lactic acid) (PLA), poly(glycolic acid) (PGA), poly(lactic-*co*-glycolic acid) (PLGA), and poly(ε-caprolactone) (PCL) are widely used in the field of biomedicine as biodegradable stents and sutures[10,11], tissue engineering scaffolds[12,13], and drug delivery vehicles[14-18] (Figure 1.2).

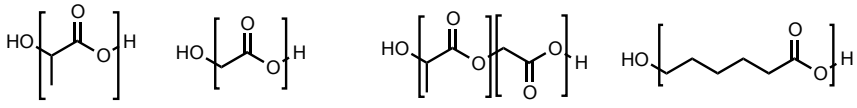

Figure 1.2: Popular synthetic biodegradable polyesters for biomedical applications

The synthesis of polyesters has evolved significantly since the initial method proposed and developed by Wallace Carothers in the 1930s.[19] High molecular weight polyesters are now typically synthesized by means of a ring opening polymerization reaction involving coordinative catalysts or anionic, cationic, or nucleophilic initiators (Figure 1.3).[2,5] This strategy allows for a high degree of control over the polymerization process as well as the functionalization of polyesters through the homopolymerization or copolymerization of cyclic monomers bearing specific functional groups. Control over the polymer composition, molecular weight distribution, and stereochemistry has permitted a modulation of the time required for polyester degradation in the span of weeks to years under physiological conditions.[9]

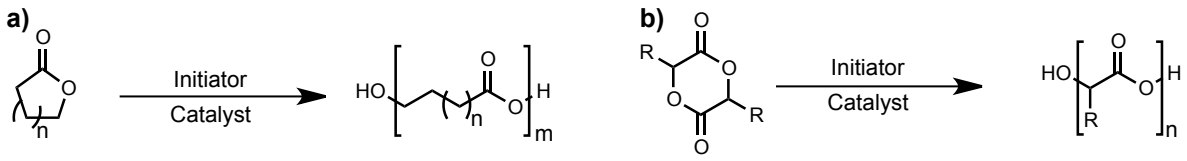

Figure 1.3: Ring opening polymerization of polyesters from (a) lactone or (b) cyclic dimer species.

1.2.1 Functional Designs

In addition to the versatility offered through controlled polymerization, biodegradable polyesters can also be incorporated into a number of different functional designs for biomedical applications. One particularly important example of a functional polyester design is the 2,2-bis(hydroxymethyl)propionic acid (bisMPA)-based dendrimer scaffold (Figure 1.4).[20-22] Dendrimers are highly branched, tree-like macromolecules comprised of a number of repeated branches emanating outward from a central core.[23,24] Each concentric layer, referred to as a generation, gives rise to an exponential growth of peripheral groups, which can be used to conjugate other molecules. Dendrimers are ideal candidates for biomedical applications due to their well-defined structures and monodispersity that come as a result of their stepwise synthesis. Prior to the development of the bisMPA scaffold, however, the biomedical utility of dendrimers was limited by their toxicity and poor aqueous solubility.[25] Since the initial reports on the design and synthesis of bisMPA scaffolds,[20-22] an extensive amount of promising work has been conducted on the use of bisMPA dendrimers in biomedical applications.[25-30]

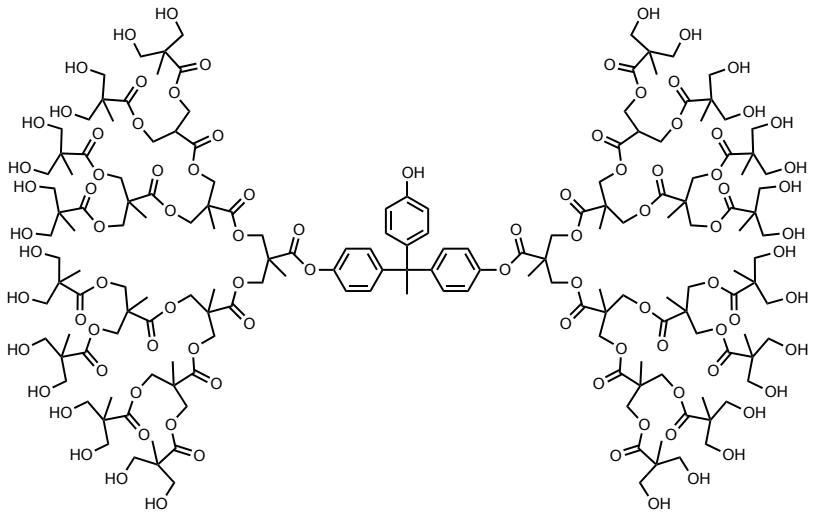

Figure 1.4: Example of a 4th generation dendritic polyester scaffold derived from 2,2-bis(hydroxymethyl)propionic acid (bisMPA)

Biodegradable polyesters have also been explored in the design of amphiphilic block copolymers capable of self-assembly into supramolecular structures. When incorporated

into a block copolymer architecture with a hydrophilic polymer such as poly(ethylene glycol) (PEG), polyesters can self-assemble in aqueous solution to form polymeric micelles[31,32], vesicles[33,34], and other nanoparticles.[18] This phenomenon is attributed to two competing thermodynamic factors: (i) the enthalpic contribution from the interfacial energy between the two blocks and (ii) the entropic contribution due to chain stretching. In an attempt to minimize the interfacial energy between the two blocks and adopt the highest configurational entropy, block copolymers will self-assembly into the lowest energy conformation as dictated by the volume fractions of the blocks, the total degree of polymerization, and the Flory–Huggins parameter.[35] In general, block copolymers will form vesicles if the volume fraction of the hydrophobic block is between 25 and 40%, or micelles if the volume fraction exceeds 50%.[33]

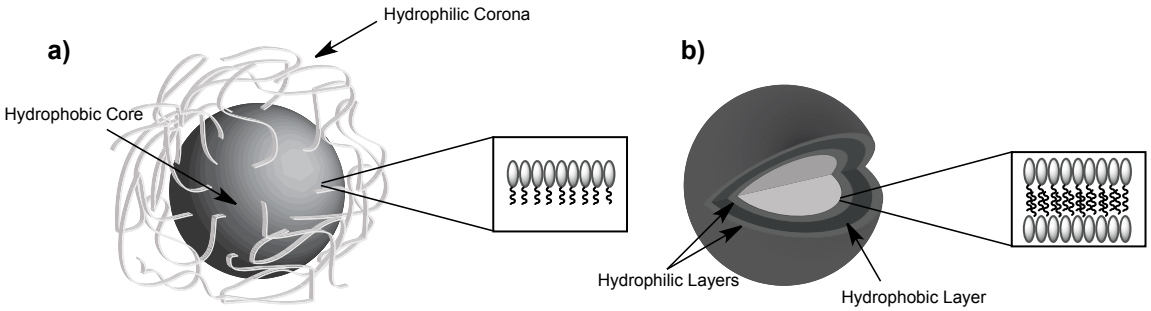

Figure 1.5: Self-assembly of block copolymers into functional polymer assemblies: (a) spherical micelles and (b) polymer vesicles.

PEG-polyester based micelles and vesicles are particularly important as drug delivery vehicles due to their ability to encapsulate and release hydrophobic and hydrophilic molecules, respectively.[36] Spherical micelles are composed of a hydrophobic core surrounded by hydrophilic coronal chains (Figure 1.5a). The hydrophilic portion of these assemblies allows for aqueous solubility of the micelles, while the core can be used to encapsulate hydrophobic molecules. Polymer vesicles, on the other hand, are hollow spheres with a bilayer wall composed of a hydrophobic layer sandwiched between an internal and external hydrophilic corona (Figure 1.5b).[35] When used as drug delivery vehicles, both of these assemblies have been demonstrated to increase the bioavailability of the encapsulated drug and enhance the efficacy of therapeutic treatment.[36-41]

1.2.2 Limitations in the Degradation of Polyesters

Despite the proven utility of biodegradable polyesters, the degradation of these systems suffers from a lack of fine-control. The reliance of these materials on random hydrolytic cleavage of the ester linkages throughout the polymer backbone raises two concerns in the context of biomedicine: (i) the degradation process is not initiated by a specific stimulus and (ii) the cleavage of the polymer backbone is dictated by an uncontrolled process that can reduce the polymer molecular weight by up to 50% upon every cleavage event.[42] In part, the overall rate of degradation can be influenced by pH and chain length[43,44]; however, there is no means to direct the degradation process along a specific pathway throughout the polymer backbone. Hence, many of the physical properties of polyesters are prone to unpredictable changes from the onset of degradation that can lead to the poor performance or failure of polyester-based biomedical devices *in vivo*. [43,45]

1.3 Stimuli-Responsive Degradable Polymers

The issue of non-specific degradation in biodegradable polymer systems has been mediated through the development of stimuli-responsive degradable polymer backbones. Not to be confused with the general class of stimuli-responsive materials, these polymers undergo complete backbone degradation in response to specific environmental conditions or an applied stimulus.[46-48] In general, there are 3 major classes of stimuli-responsive degradable polymers: (i) acid degradable polymers, (ii) reduction sensitive polymers, and (iii) photodegradable polymers. A small handful of other polymer systems have also been developed to degrade in response to biologically mediated events such as enzymatic cleavage[49] or changes in chemical concentration.[50,51] However, the biomedical applications of these materials will not be discussed in the following sections.

1.3.1 Acid Degradable Polymers

A large number of pH-sensitive linkers are available for the development of acid-degradable polymers (Figure 1.6). Despite the structural diversity of these linkers, they all contain chemical linkages that are stable at neutral pH and prone to hydrolysis in acidic solution.[52] This unique property has been exploited in the field of biomedicine to promote degradation of polymers derived from these units following an abrupt change in

environmental pH.[48] To this end, acid-degradable polymers are commonly used to form drug delivery vehicles for the triggered release of therapeutics following intracellular uptake into mildly acidic endosomes or lysosomes or for the targeted delivery of drugs to cancerous tissues possessing a slightly acidic tumour environment.[53-58]

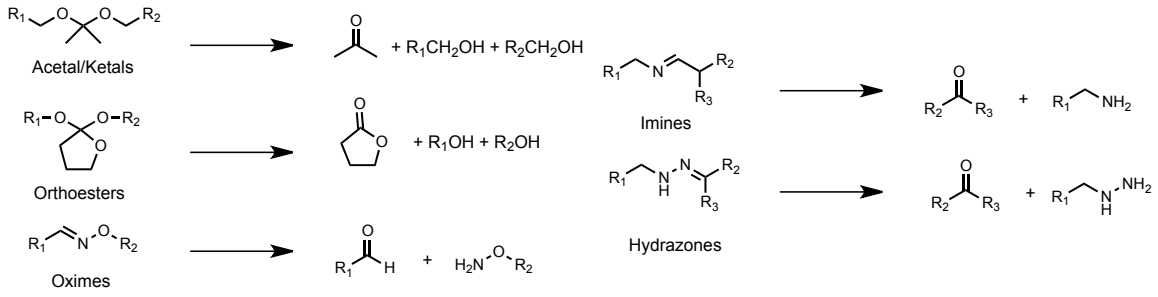

Figure 1.6: Acid-sensitive linkers used in acid-degradable polymer backbones

1.3.2 Reduction Sensitive Polymers

Reduction sensitive polymers are a broad class of materials that incorporate disulfide linkages throughout the polymer backbone (Figure 1.7). The disulfide bond is a highly versatile linkage that can be cleaved and reformed under the appropriate conditions, but is stronger than most non-covalent interactions.[59] This gives poly(disulfide) systems the ability to adapt, self-repair, and degrade in response to physical and/or chemical stimuli.[59] However, the use of poly(disulfide)s in applications requiring complete degradation relies on a total reduction of these bonds into their thiol constituents (Figure 1.7a). Typically used in drug and gene delivery systems, disulfide-based carriers operate on a difference between the intracellular and extracellular redox potential. These systems are stable in the extracellular environment in which the glutathione concentration is on the order of 1 μM, but degrade upon cellular uptake where the glutathione concentration is on the order of several millimolar.[60-64]

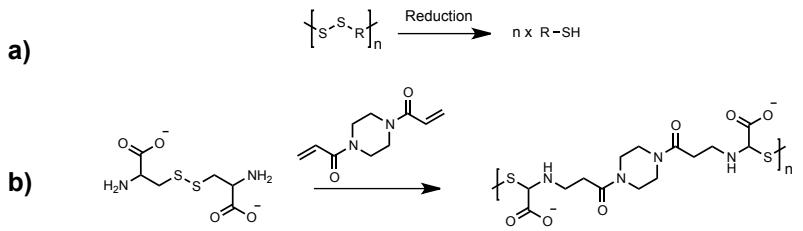

Figure 1.7: (a) General structure of a poly(disulfide) and its reduction to thiols. (b) An example of a poly(disulfide) synthesized from a linear disulfide monomer.

1.3.3 Photodegradable Polymers

The third major class of stimuli-responsive degradable polymers involve polymer backbones that are susceptible to cleavage following exposure to ultraviolet (UV)/near infrared (NIR) light. These systems typically employ *ortho*-nitrobenzyl alcohol derivatives[65] to promote cleavage by a single-photon process upon exposure to UV light (Figure 1.8).[66-72] Due to the potential for photodamage caused by UV light, more recent investigations have focused on the use of 4-bromo 7-hydroxycoumarin derivatives[73] to promote photolysis by the less efficient two-photon process using biologically benign NIR light.[74-78] Although in the early stages of development, these materials display immense promise for the fabrication of drug delivery vehicles that release their payload in response to UV/NIR irradiation.

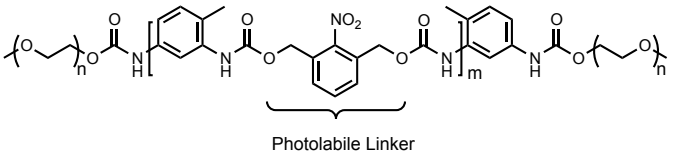

Figure 1.8: Example of a photodegradable block copolymer incorporating a photolabile *ortho*-nitrobenzyl carbonyl group

1.3.4 Limitations in the Degradation of Conventional Stimuli-Responsive Degradable Polymers

Stimuli-responsive degradable polymers circumvent the issues associated with the non-specific degradation of polyesters. However, the degradation of these materials still relies on random chain scissions throughout the polymer backbone. This reliance limits the overall control of the degradation process and prevents the reliable prediction of the degradation behavior *in vivo*. Additionally, the complete degradation of these materials requires many environmentally-mediated cleavage events, thereby restricting their usage to applications in which triggering events are abundant

1.4 Self-Immolative Polymers

Self-immolative polymers have been developed over the past 10 years as alternatives to conventional biodegradable polymers and address the limitations associated with the lack of fine-control over the degradation process. Self-immolative polymers are a general class of compounds that can undergo end-to-end depolymerization through a cascade of intramolecular reactions upon the selective removal of a stimuli-responsive, stabilizing end-cap (Figure 1.9).[79-81] Inspired by and derived from their prodrug counterparts, self-immolative polymers are typically comprised of a number self-immolative monomeric spacers covalently linked in an iterative fashion and terminated with a protective end-capping agent. At the current stage in development, self-immolative polymers are limited to either a dendritic (Figure 1.9a) or linear architecture (Figure 1.9b).

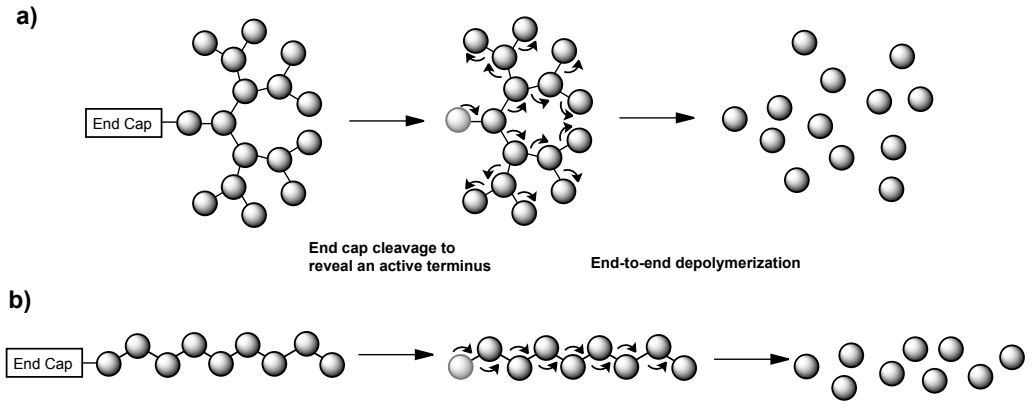

Figure 1.9: Self-immolative degradation in (a) dendritic and (b) linear polymeric systems

Under the appropriate environmental conditions, self-immolative polymers are not susceptible to random backbone cleavage, thereby restricting their degradation to a well-defined pathway that can only be triggered by end-cap removal. This controlled mechanism of self-immolative degradation allows for three main advantages over conventional biodegradable polymers. Firstly, the stimuli-responsiveness of self-immolative polymers can be readily tuned and adjusted through the incorporation of different end-capping agents. Secondly, self-immolative degradation permits the amplification of a given stimulus in that only one triggering event is required to achieve

complete degradation. Lastly, the degradation rate of self-immolative polymers is dictated by, and dependent on, the chemistry and architecture of the polymer backbone. As a result, self-immolative polymers can be engineered to degrade under a specific set of conditions with a degradation rate that is regulated by the composition and structure of the polymer backbone.

1.4.1 Self-Immolative Spacers

Self-immolative spacers were developed for prodrug systems as a means to overcome steric limitations by increasing the physical distance between the conjugated drug and active cleavage site.[82] In the most basic prodrug design, the trigger group (also described as a protecting group) is attached directly to the drug molecule via a scissile bond (Figure 1.10a). While this strategy has proven useful for a large number of small molecule[83,84] and macromolecular prodrug systems[85], it relies on an easily accessible linkage between the conjugated molecules. When the trigger and/or drug are sterically bulky, their spatial proximity can restrict enzymatic access to the linkage site, thereby preventing cleavage and release of the active drug molecule.[86-88] Modification of this design to incorporate a self-immolative spacer between the trigger and drug moieties bypasses any steric restrictions and allows for the release of the drug molecule through an alternate pathway.[89,90] In the self-immolative prodrug design, removal of the triggering group reveals an active terminus on the self-immolative spacer that initiates a spontaneous and irreversible intramolecular reaction to liberate the active drug molecule (Figure 1.10b).[91,92]

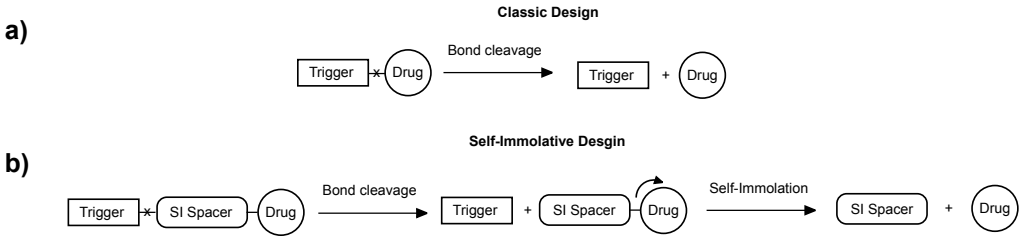

Figure 1.10: (a) Classic and (b) self-immolative prodrug strategies

The basic process of self-immolation can be described as the spontaneous and irreversible disassembly of multi-component compounds into their constituent components through

an intramolecular reaction. This process is driven by an increase in entropy and by the irreversible formation of thermodynamically stable products (eg. CO_2, cyclic species).[79] In general, self-immolative spacers can be grouped into three classes based on their mechanism of disassembly: (i) electronic cascade spacers; (ii) cyclization spacers; and (iii) hemiacetal spacers (Figure 1.11).

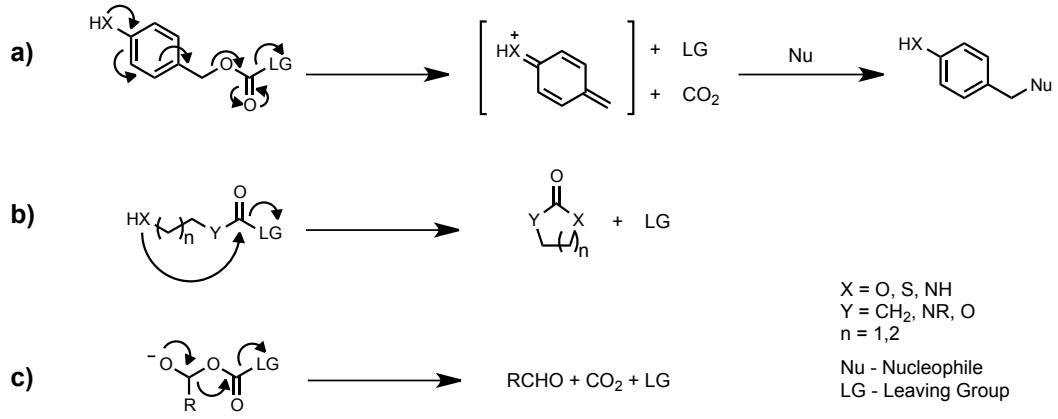

Figure 1.11: General schematics for (a) electronic cascade spacers, (b) cyclization, and (c) hemiacetal spacers.

1.4.1.1 Electronic Cascade Spacers

The first class of self-immolative linkers, known as electronic cascade spacers, involve compounds capable of undergoing an elimination reaction caused by the shifting of electron pairs in a conjugated aromatic system (Figure 1.11a). The predominant majority of electronic cascade spacers are based on the initial 1,6-elimination spacer developed by Katzenellenbogen and coworkers in 1981.[82] Often considered to be the first application of a self-immolative spacer in prodrug chemistry, this system involved a lysine functionalized 4-aminobenzyl alcohol spacer conjugated to a 4-nitroaniline reporter molecule through a carbamate linkage at the benzylic position. Following enzymatic cleavage of the lysine residue, the strongly electron-donating 4-aminobenzyl group initiates a 1,6-elimination reaction, followed by a spontaneous decarboxylation to release the 4-nitroaniline reporter.[82]

This initial design has since been adapted to other polysubstituted electron-rich aromatic systems that feature a masked electron-donating group (hydroxyl[93] or thiol[94] moeities)

conjugated to a benzylic leaving group at either the *ortho* (1,4-elimination) or *para* (1,6-elimination) positions.[95] Highly electron-donating substituents are required to lower the energy-barrier associated with dearomatisation to form the quinone, azaquinone or thioquinone methide intermediates, while benzylic carbonate and carbamate linkages are often employed to provide a thermodynamically favourable decarboxylation following elimination. Electronic cascade eliminations are typically quite rapid under the appropriate conditions and require proper modulation or masking of the electron-donating substituent using an appropriate triggering group to avoid premature elimination.[79] Despite the complexities associated with electronic cascade spacers, a number of homoaromatic[49,86,87,90,96-108] and heteroaromatic[109] systems have been developed for use in a variety of prodrug systems.

1.4.1.2 Cyclization Spacers

The second major class of self-immolative linkers, known as cyclization spacers, involves compounds capable of undergoing intramolecular cyclization reactions (Figure 1.11b). These compounds most commonly involve activation of a latent nucleophile and subsequent nucleophilic attack on a carbonyl center to liberate an active drug molecule.[79] Although a large variety of cyclization spacers exist, the predominant majority of these compounds are based on either 4-amino or 4-hydroxybutanoyl esters or ethylenediamine species.[110] The first reported self-immolative cyclization prodrugs were developed simultaneously by the Lane and Borchardt research groups and involved the use of hydroxyl amide lactonization reactions[110] to release an active reporter molecule (Figure 1.12a).[111-114] This strategy was later applied to coumarin based prodrug systems by Wang and coworkers to take advantage of the relative non-toxicity of the released coumarin species and to increase the rate of lactonization (Figure 1.12b).[115,116]

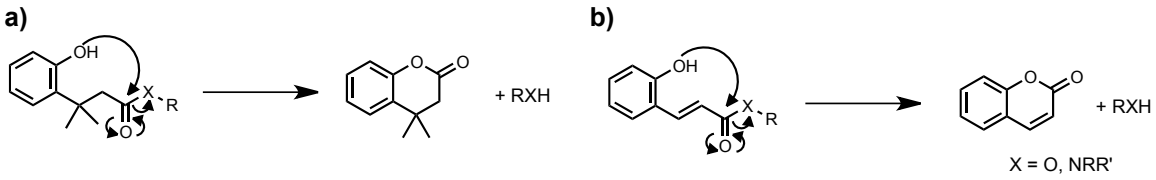

Figure 1.12: Self-immolative cyclization spacers derived from 4-hydroxybutanoyl esters. (a) Trimethyl lock lactonization and (b) Coumarin based prodrug design.

The other common class of cyclizaton spacers based on ethylenediamine compounds were first reported by Saari and coworkers in 1990 for a series of carbamate and ester prodrugs.[117,118] In these systems, selective cleavage of a *tert*-butoxycarbonyl (Boc)-protecting group reveals an active amine terminus, which then undergoes an intramolecular cyclization reaction to form the corresponding cyclic urea or amide species and liberate a reporter molecule (Figure 1.13). Varying the substituents on both the nucleophilic and electrophilic nitrogen atoms in the carbamate design allowed for tuning of the cyclization rate between 24 and 942 min in aqueous buffer maintained at pH 7.4 and 37˚C, thereby demonstrating the inherent flexibility of such systems.[117] Similar strategies have also been adopted using mercaptoethanol[119], aminoethanol[120-122], and cysteamine[123] based spacers to further tune the rates of cyclization and expand the variety of chemical linkages permitted in self-immoaltive cyclization systems. In general, cyclization reactions are much slower than 1,4- and 1,6-eliminations and are often used to control the release kinetics in self-immolative prodrug systems.[92,124-127]

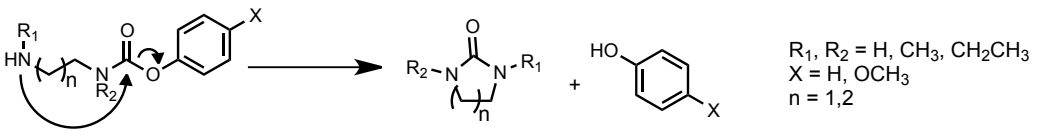

Figure 1.13: Activation of carbamate prodrugs by intramolecular cyclization of the ethylenediamine pro-moiety[117]

1.4.1.3 Hemiacetal Spacers

A third minor class of self-immolative spacers based on hemiacetal systems does exist, but these spacers are not as widely employed in prodrug designs as electronic cascade or cyclization based spacers (Figure 1.11c). First introduced as potential spacers for amine prodrugs to address the relative instability of *N*-acyl groups, these spacers often involve *N*-acyloxyalkoxycarbonyl derivatized drug molecules. This strategy was first reported by Alexander and coworkers in 1987 and involved *N*-acyloxyalkoxycarbonyl derivatized model compounds terminated with an esterase sensitive trigger group.[128-130] Following hydrolytic cleavage, the exposed hydroxyl group initiates a spontaneous 1,2-elimination followed by a decarboxylation reaction to decompose the (hydroxyalkoxy)carbonyl

derivative and liberate the active drug molecule. Similar prodrug strategies also exist for acyloxyalkyl and phosphoryloxyalkyl systems (Figure 1.14)[131-135]; however, the applicability of such systems is often limited by the generation of toxic aldehydes during degradation.[136]

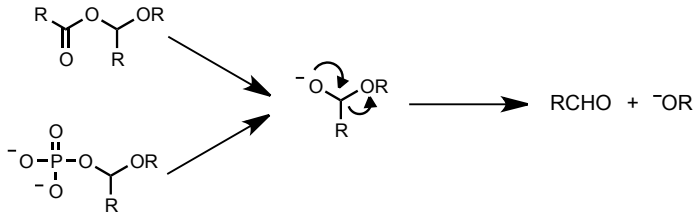

Figure 1.14: Other hemiacetal based self-immolative linkers based on acyloxyalkyl and phosphoryloxyalkyl systems

1.4.2 Self-Immolative Oligomers

The first extension of self-immolative spacers towards incorporation into oligomeric designs was introduced by Schereen and coworkers in 2001.[137] It was hypothesized that the use of elongated and extended self-immolative spacers would enhance cleavage rates by further increasing the distance between the active trigger site and sterically bulky drug molecule. To this end, several biaromatic spacers based on napthyl (1,8-elimination) and biphenyl (1,10-elimination) moieties were prepared; however, these systems failed to undergo any electronic cascade reactions, which was attributed to the high cost of dearomatization required for the 1,8 and 1,10-elimination reactions, respectively. Conversely, the combination of multiple 1,6-elimination *p*-aminobenzyl oxycarbonyl (PABC) spacers into an elongated oligomeric design (Figure 1.15a) involving a plasmin sensitive trigger significantly enhanced the release rate of paclitaxel when compared to the analogous monomeric system. These PABC oligomers were subsequently modified with an additional *N,N'*-dimethylethylenediamine cyclization spacer to allow for the attachment of hydroxyl containing drugs using a carbamate linkage instead of the less-stable carbonate linkage, available using the PABC spacers alone (Figure 1.15b). These combination 1,6-elimination and cyclization based oligomers displayed slower release kinetics compared to the purely 1,6-elimination systems, but demonstrated the potential

for fine control over the degradation process using cyclization linkers in conjunction with electronic cascade spacers.

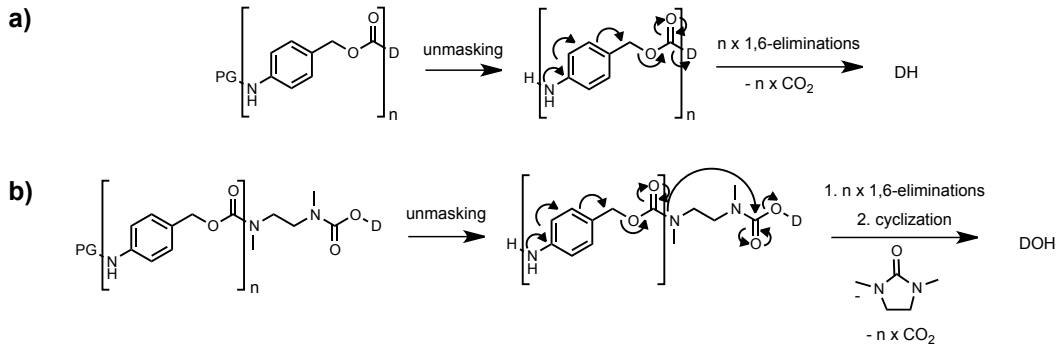

Figure 1.15: Oligomeric prodrugs based on (a) multiple 1,6-elimination spacers and (b) multiple 1,6-elimination spacers followed by a cyclization spacer in series (PG – protecting group, D – drug, n=1,2).

While the first self-immolative oligomer system is important in the evolution of self-immolative linkers from prodrugs to polymers, it failed to exploit the opportunity for chemical amplification in the design. The first self-immolative oligomer possessing chemical amplification was not developed until several years later in 2008 by Warnecke and Kratz.[138] This system used a modified PABC linker design involving 2,4-bis(hydroxymethyl)aniline molecules capable of undergoing both 1,4 and 1,6-eliminations (Figure 1.16). By using a "double release linker", this system was able to concomitantly liberate reporter molecules through 1,4-eliminations during the linear degradation of the main chain through the faster 1,6-elimination pathway. Such a strategy allowed for an enhanced release rate compared to oligomeric prodrug systems in which drug molecules are simply conjugated at a single terminus. It was suggested that this oligomeric design would be highly versatile for the development of combination therapeutic strategies, particularly in cases in which steric hindrances could limit drug conjugation in dendrimer based systems. However, the complicated stepwise iterative synthesis required for such a system has limited any further development in the literature.

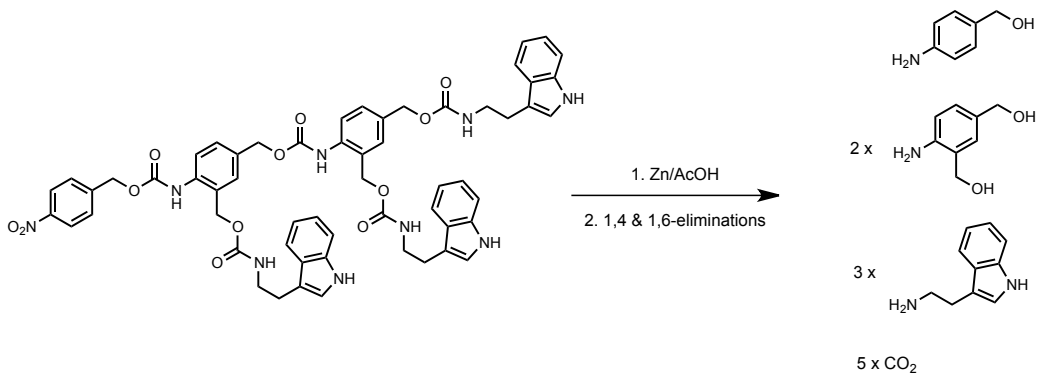

Figure 1.16: Linear self-eliminating prodrug design incorporating double-release linkers to achieve amplification in the amount of drug released

Despite the potential of self-immolative oligomers, only a handful of systems have been developed over the past decade for drug delivery and sensing applications.[121,139-141] The main limitation in the design of such systems is the lengthy stepwise iterative syntheses that typically only result in arithmetic growth. As a result, an increased focus has been placed on the development of dendrimer systems that can be synthesized through iterative convergent methods and grown geometrically.[80] More recently, however, self-immolative oligomers have emerged as useful models to investigate the mechanism and degradation kinetics of self-immolative polymers.[101,102,142-144]

1.4.3 Self-Immolative Dendrimers

The first incorporation of self-immolative spacers into a polymeric framework was reported almost simultaneously by three different groups in 2003.[145-147] All three groups utilized dendritic architectures in their designs with variations on the triggering groups, self-immolative spacers, conjugated molecules, and potential applications. McGrath and coworkers described the synthesis of up to the 2nd generation “linear disassembling" benzyl(aryl ether) dendrimers derived from *O*-functionalized 3,4-dihydroxybenzyl alcohol and 4-hydroxybenzyl alcohol spacers (Figure 1.17).[145] In this design, selective removal of a terminal allyl-ether group initiated a sequence of 1,6-eliminations to degrade the dendrimer backbone and ultimately release a single 4-nitrophenol reporter molecule. Interestingly, the time required to achieve complete degradation displayed no generational dependence in DMF, indicating that the cleavage of the allyl trigger group

under these conditions was strongly rate limiting. The degradation of these dendrimers was significantly slower in THF and allowed for the tracking of intermediate phenoxide species that supported the degradation through a 1,6-elimination pathway, rather than simple cleavage of the ether linkages.

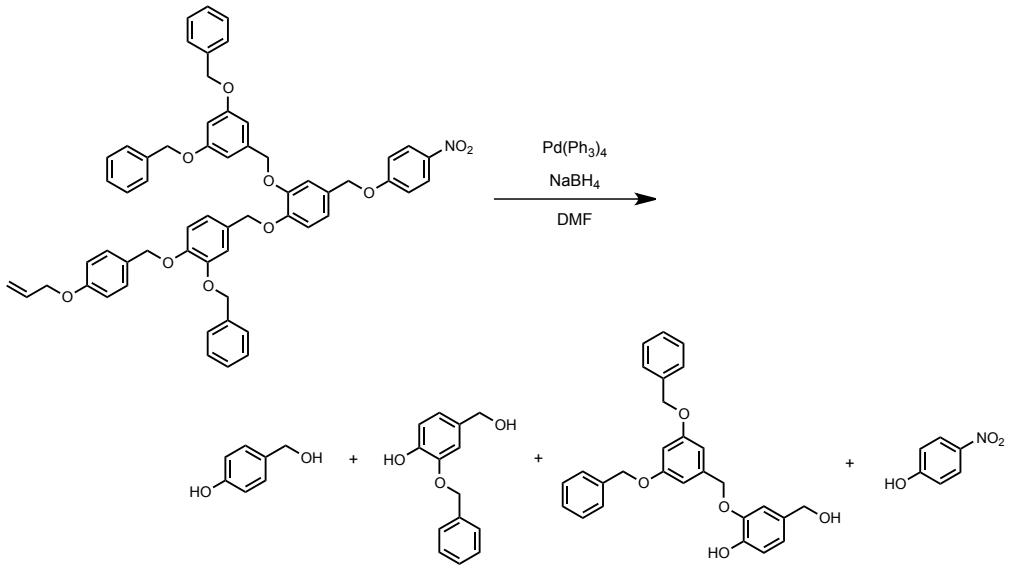

Figure 1.17: 2nd generation linear disassembling dendrimer that degrades through a 1,6-elimination pathway upon cleavage of a terminal allyl-ether to release a single 4-nitrophenol reporter molecule

This work was succeeded in the same year by the same group with an alternate dendritic design derived from 2,4-bis(hydroxymethyl)phenol spacers that permitted an amplified release of reporter molecules.[148] Upon cleavage of the terminal allyl-ether group at the dendrimer focal point, this system degraded through a combination of 1,4- and 1,6-eliminations to fragment the polymer backbone and release 4-nitrophenol molecules from the dendrimer periphery (Figure 1.18). Unlike the previous example in which only a single reporter molecule was liberated, this system released 4-nitrophenol molecules geometrically according to the following relation:

$$\text{Number of molecules released} = 2^n \qquad (1.1)$$

where n is the dendrimer generation. This system was also subsequently modified with a photolabile 2-nitrobenzyl alcohol based triggering group to allow for phototriggered dendrimer degradation.[149]

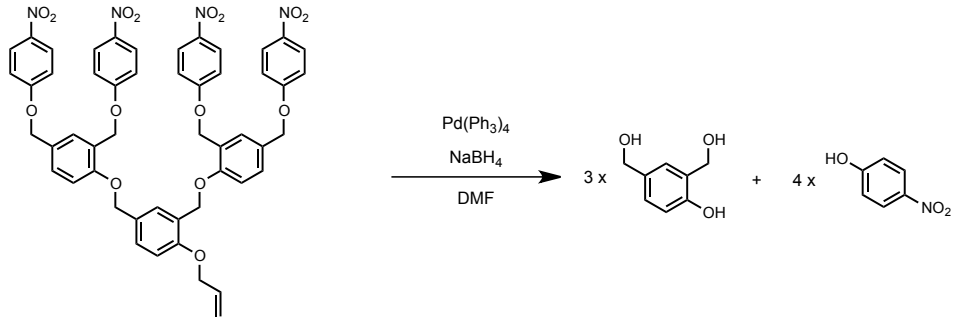

Figure 1.18: 2nd generation geometric disassembling dendrimer that degrades through a 1,4 and 1,6-elimination pathway upon cleavage of a terminal allyl-ether to release a four molecules of 4-nitrophenol

The first self-immolative dendrimer reported by Shabat and coworkers in 2003 utilized a stable polycarbamate backbone derived from alternating 2,6-bis(hydroxymethyl)-4-cresol elimination and *N,N'*-dimethylethylenediamine cyclization spacers (Figure 1.19).[146] Using this system, 1st and 2nd generation dendrimers were synthesized with a photolabile 2-nitrobenzyl alcohol trigger and were shown to degrade through a cascade of cyclization, 1,4-elimination, and decarboxylation reactions to ultimately release aminomethylpyrene reporter molecules from the dendrimer periphery following exposure to UV light. Exploiting the dendritic potential for chemical amplification, this system released a geometrically amplified amount of reporter molecules in response to a single triggering event according to the relation described in Eq. (1.1). Additionally, the incorporation of cyclization spacers into the polymeric design allowed for higher degree of control over the degradation process, as the overall kinetics of degradation were dictated by the rate limiting cyclization reactions. Tracking the evolution of degradation products over time by HPLC verified the proposed mechanism of degradation, but also revealed two important aspects pertaining to the degradation of self-immolative dendrimers: (i) the overall time for degradation is dependent on the generation of the dendrimer; and (ii) terminal self-immolative cyclization reactions are independent of the

polymer size. This system was extended to a third generation dendrimer, however, a smaller 4-nitroaniline reporter molecule had to be used, as steric crowding prevented the attachment of 8 aminomethylpyrene molecules.

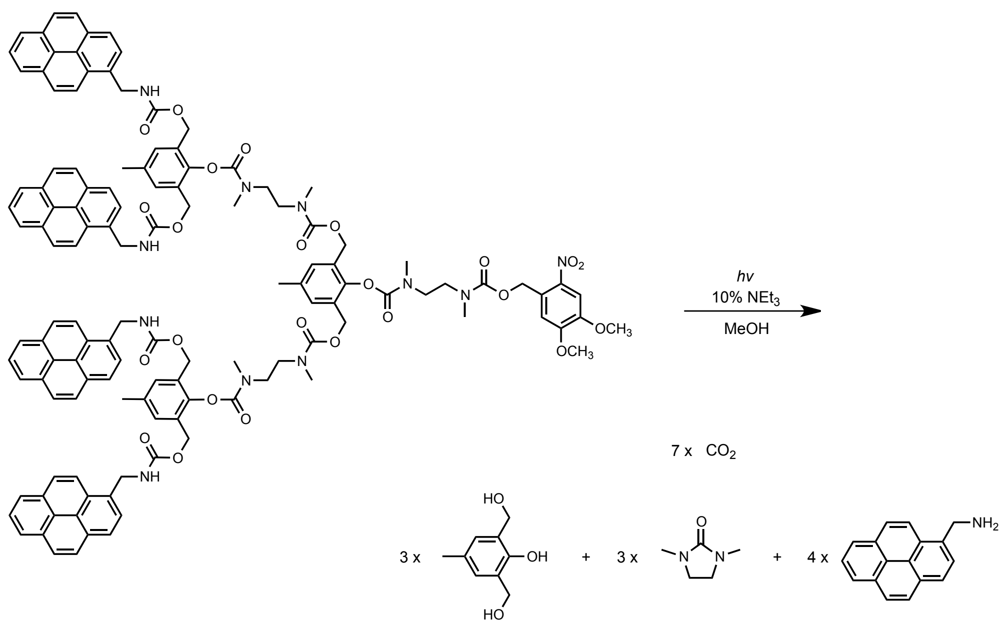

Figure 1.19: 2[nd] generation self-immolative polycarbamate dendrimer that degrades through a cascade of cyclization, 1,4-elimination, and decarboxylation reactions to release aminomethylpyrene upon exposure to UV light

The 2003 report on self-immolative dendrimers by de Groot and coworkers was the first system to explicitly demonstrate the amplified release of actual drug molecules from a self-immolative dendritic device.[147] Using a polycarbamate system derived from branched 2-(4-aminobenzylidene)propane-1,3-diol spacers, de Groot and coworkers were able to construct dendrimers up to the 2[nd] generation with an oxidized aniline trigger and releasable units of the anticancer drug paclitaxel on the dendrimer periphery (Figure 1.20). Since each branched monomer unit was designed to undergo two 1,8-eliminations, the entire dendrimer backbone was degraded through a cascade of 1,8-elimination and decarboxylation reactions to release 4 molecules of paclitaxel following reduction of the terminal nitro-group. Kinetic evaluation of these devices was rather limited, but indicated a complete release of paclitaxel after 30 minutes in organic solution. Subsequent cytotoxicity testing of the 2-(4-aminobenzylidene)propane-1,3-diol degradation product

using human cell lines also revealed that the dendrimer backbone displayed negligible adverse effects following degradation. Hence, this dendritic prodrug system was shown to be an effective and viable means of amplified paclitaxel release.

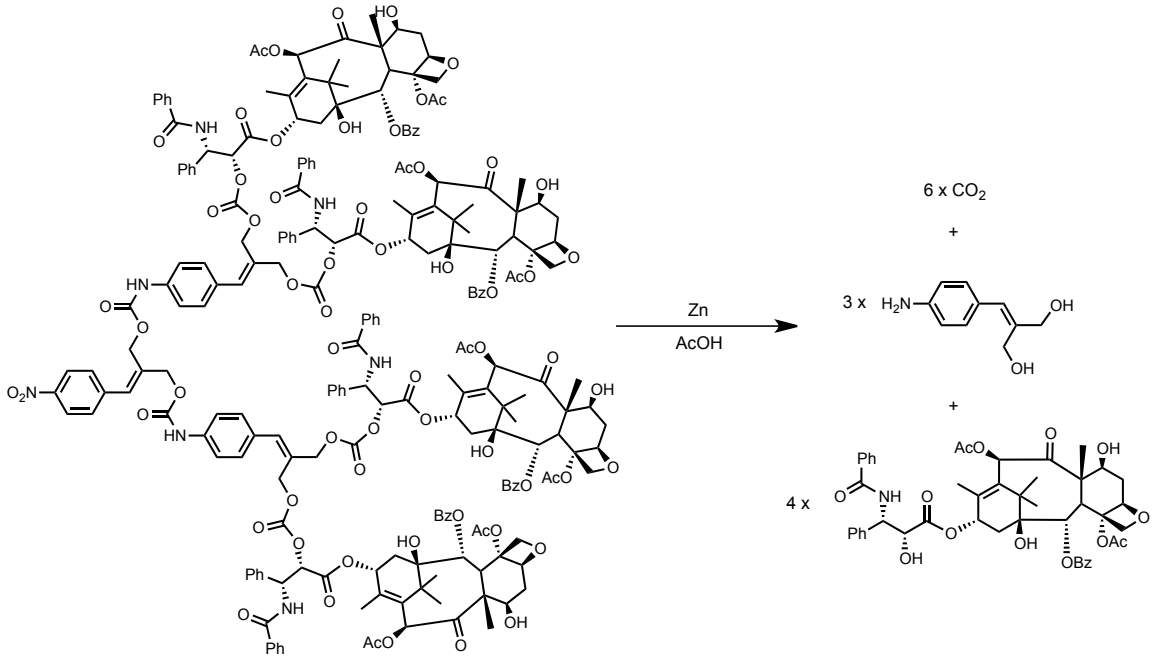

Figure 1.20: 2nd generation polycarbamate dendrimer derived from branched 2-(4-aminobenzylidene)propane-1,3-diol spacers and designed to degrade through a cascade of 1,8-elimination reactions

Most of the work in the field of self-immolative dendrimers following the seminal reports has focused on expanding the utility of these systems by improving the initial designs. McGrath and coworkers have since reported an improved synthesis for their initial linear diassembling dendrimer design that enables the synthesis of 1st, 2nd, and 3rd generation dendrimers on a multigram scale.[150] They have also reported a convergent synthesis of their geometrically disassembling dendrimer through a copper-mediated coupling reaction that avoids exposure of an active phenol and prevents issues associated with premature degradation during the synthetic procedure.[151]

Shabat and coworkers have been monumental in the development and expansion of self-immolative dendrimers for a wide variety of different drug delivery[126,141,152-158] and sensing[159-166] applications. In the field of drug delivery, the Shabat group has developed

self-immolative dendrimer systems incorporating PGA and catalytic antibody (Ab) 38C2 sensitive triggers for both mono[126,152,155,156,158] and combination[153] therapeutic strategies. In the field of signal amplification, the Shabat group has developed probes for the detection of enzymes[167], hydrogen peroxide[161-163], triacetyl triperoxide[160], fluoride anions[165], and sulfhydryl compounds.[164] The predominant majority of these systems are based on simple variants of the initial dendrimer backbones discussed above but arranged into one of three design categories: the simple amplifier, the molecular OR logic trigger, or the receiver amplifier design (Figure 1.21).

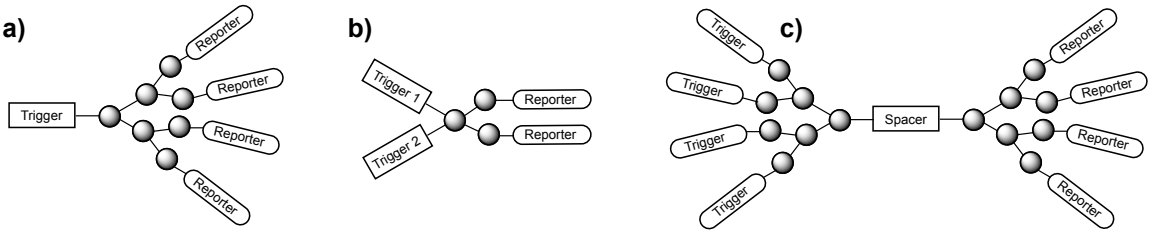

Figure 1.21: Schematic representation of all currently available dendrimer designs. (a) Basic amplifier in which one triggering event leads to release of multiple reporter molecules. (b) Molecular OR logic trigger in which cleavage of one of two different triggers leads to the release of multiple reporter molecules. (c) Receiver-amplifier design with high sensitivity and gain whereby a low-level signal can be detected and amplified through the release of multiple reporter molecules. Adapted with permission from Wong et *al.*[80] Copyright 2012 Elsevier.

The most promising strategy developed by the Shabat group involves a series of dendrimer-based probes capable of exponential signal amplification through a semi-autocatalytic effect referred to as the "dendritic chain reaction (DCR)".[161-164,166] The first reported system to exploit this effect was derived from a 1st generation dendrimer with two bound molecules of choline, a single 4-nitroaniline reporter molecule and a H_2O_2 sensitive phenylboronic acid triggering group (Figure 1.22). Exposure of this system to low levels of H_2O_2 triggered the degradation of a portion of these dendrimers, resulting in the release of 4-nitroaniline and two molecules of choline. In turn, the released choline molecules reacted with choline oxidase *in situ* to generate 4 molecules of H_2O_2 capable of activating an additional 4 dendrimer molecules. In theory, a single molecule of H_2O_2

could initiate the dendritic chain reaction and ultimately catalyze the release of all the bound reporter groups in solution. However, this system only resulted in a 53–fold increase in signal amplification through the dendritic chain reaction. This potentially exponential amplification has been further improved through a slight modification to use releasable molecules of methanol in conjunction with alcohol oxidase to improve the stability of carbonate linkages in the dendritic design and reduce background signal amplification.[166] Upon further improvements to reduce background signal generation, it is presumable that this dendritic chain reaction will offer a practical means for diagnostic signal amplification comparable to that of the immuno-polymerase chain reaction.

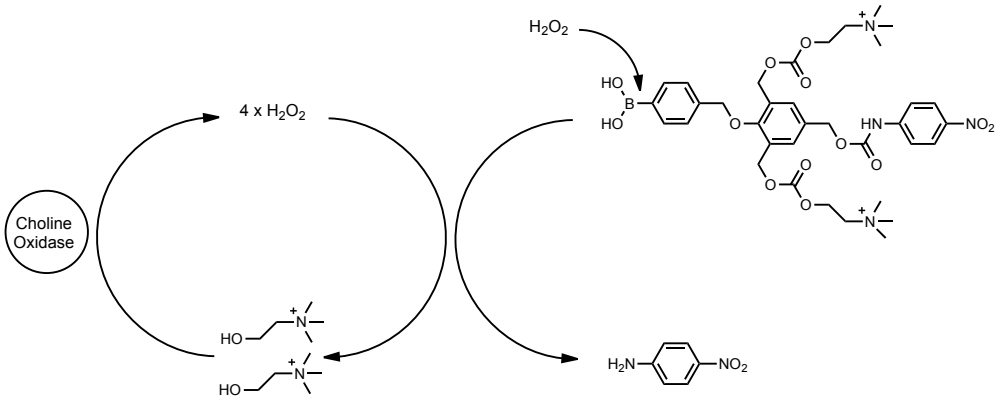

Figure 1.22: Dendrimer system capable of exponential signal amplification through the dendritic chain reaction. Cleavage of the phenylboronic acid triggering group by H_2O_2 leads to the liberation of a 4-nitroaniline reporter and two molecules of choline, which in turn generate four additional molecules of H_2O_2 upon reaction with choline oxidase.

1.4.4 Linear Self-Immolative Polymers

Self-immolative oligomeric and dendritic frameworks lend themselves well towards simple adaptations of existing prodrug chemistries. The main issue associated with these designs, however, is the lengthy stepwise iterative procedures required to generate high molecular weight species. Consequently, the next logical step in the evolution of self-immolative materials was to adapt self-immolative chemistry to allow for polymerization of simple monomeric units. Although linear self-immolative polymers are no longer

monodisperse, they can be synthesized in a single step and allow for a practical and scalable means of generating self-immolative polymers. Additionally, these polymers possess an inherent capability for a higher degree of signal amplification compared to oligomeric or dendritic designs since they can incorporate more spacers while bypassing any steric constraints. Such linear systems also display a potential to generate self-immolative drug delivery vehicles through the generation of micelles, vesicles, and nanoparticles.

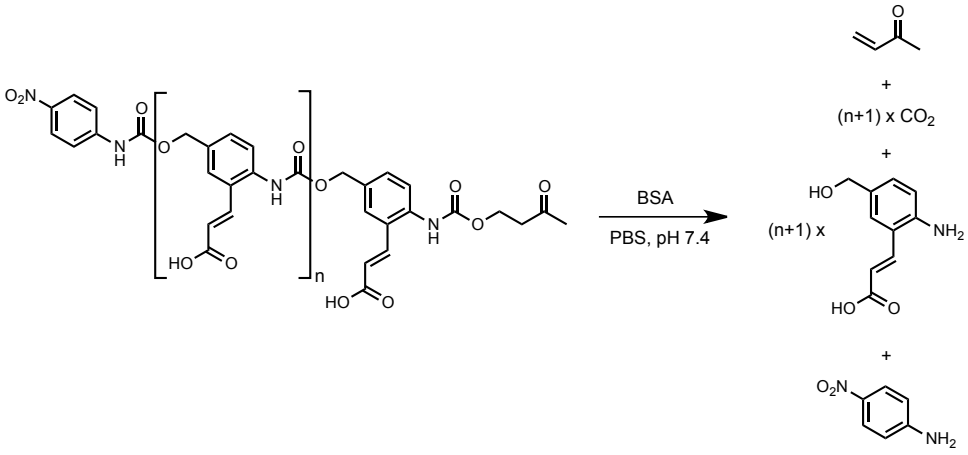

Figure 1.23: Linear self-immolative polymer that degrades through a cascade of 1,6-elimination/decarboxylation reactions in the presence of BSA to release fluorescent monomer units and a terminal 4-nitroaniline reporter molecule (n=16).

The first linear self-immolative polymer system was reported by Shabat and coworkers in 2008.[168] This system was derived from monomeric units of 4-aminobenzylalcohol derivatives terminated with a blocked isocyanate, phenyl carbamate moiety. Polymerization of this monomer was carried out at elevated temperatures in the presence of catalytic dibutyltin dilaurate (DBTL) to promote nucleophilic attack of the benzylic alcohol on the terminal blocked isocyanate. Addition of 4-nitrophenyl isocyanate during polymerization and a BSA sensitive trigger-alcohol complex following polymerization allowed for the incorporation of a terminal reporter and end-cap into the polymer framework (Figure 1.23). Following cleavage of the end-cap in the presence of BSA, this polymer was shown to degrade through a cascade of 1,6-elimination/decarboxylation reactions to release fluorescent monomer units and liberate a 4-nitroaniline reporter

molecule. With an average chain length of 16 units, this polymer displayed the promising potential of linear self-immolative polymers for heightened signal amplification. This same polymer backbone was later used by the same group for activity-linked labeling of enzymes[169], while subsequent modifications allowed for the development of a water soluble variant capable of releasing pendent 4-nitroaniline reporters through an additional 1,6-elimination-decarboxylation reaction at vinylogous 2-benzyl positions (Figure 1.24).[170]

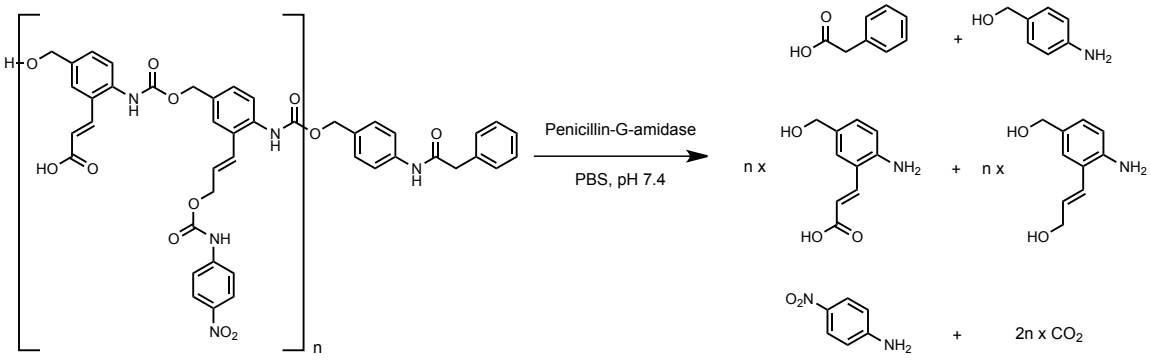

Figure 1.24: Linear self-immolative polymer that degrades through 1,6-elimination/decarboxylation reactions in the presence of PGA in aqueous solution. Liberation of 4-nitroaniline molecules occurs following main chain degradation via a 1,6-elimination/decarboxylation reaction at a vinylogous 2-benzyl position on a released monomer unit.

This basic polycarbamate backbone was further developed in 2010 by Moore and coworkers to allow for the generation of self-immolative microcapsules.[171] Fabrication of these microcapsules was accomplished using a 4-aminobenzyl alcohol derivative that permitted crosslinking of the linear polymers through an interfacial polymerization method. Selective removal of Boc or fluorenylmethyloxycarbonyl (Fmoc) end-capping agents triggered the degradation of the polymer backbone and promoted the release of the microcapsule contents through ruptures in the capsule shell wall (Figure 1.25). Due to aqueous insolubility of the polymer backbone, it was suggested that these microcapsules may be useful for self-healing autonomous repair systems, rather than for drug delivery applications.

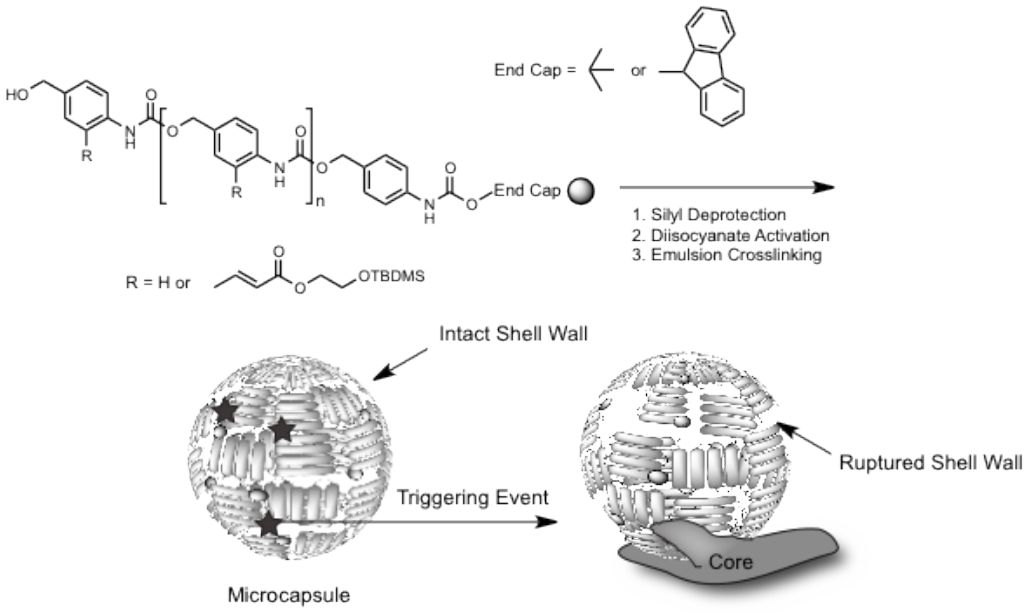

Figure 1.25: Design of self-immolative microcapsules for self-healing autonomous repair systems. Selective removal of Boc and Fmoc end-caps triggers the degradation of the polycarbamate backbone through a cascade of 1,6-elimination/decarboxylation reactions to promote the release of the microcapsule contents through ruptures in the shell wall. Adapted with permission from Esser-Kahn *et al.*[171] Copyright 2010 American Chemical Society.

In recent years, poly(phthaldehyde) (PPA) based systems have also been developed for a variety of self-immolative applications. These linear self-immolative systems are fundamentally different than those based on 4-aminobenzyl alcohol derivatives as they rely on the low ceiling temperature (temperature at which polymerization and depolymerization are in equilibrium) of polyaldehydes to achieve depolymerization through hemiacetal decompositions.[172] Through careful design, however, these systems can be end-capped with a stimuli-responsive agent that stabilizes the polymer above its ceiling temperature and permits triggered degradation through a self-immolative pathway involving a cascade of 1,2-hemiacetal eliminations. The first reported self-immolative PPA system was designed by Phillips and coworkers in 2010.[173] Using allyloxycarbonyl (Alloc) and *tert*-butyldimethylsilyl (TBS) end-capped PPAs, they were able to create stimuli-responsive plastics that were sensitive to Pd(0) and F^-, respectively (Figure

1.26a). Similar to the 4-aminobenzyl alcohol polymers, these PPAs displayed rapid solution phase degradation kinetics. Exposure of the Alloc end-capped polymer to 0.40 equivalents of Pd(0) resulted in complete depolymerization within 5 minutes, while exposure of the TBS end-capped polymer to 0.5 equivalents of F^- caused complete depolymerization within 1 minute. With a clever application of these polymers, Phillips and coworkers were able to fabricate patterned plastics that changed their physical structure in response to an applied stimulus by depositing a non-degradable PPA around a stimuli-responsive one in a plastic sheet (Figure 1.26b). In a subsequent report, Phillips and coworkers were also able generate self-powered microscale pumps by depositing a thin-film of the TBS end-capped PPA on a microscale slide.[173]

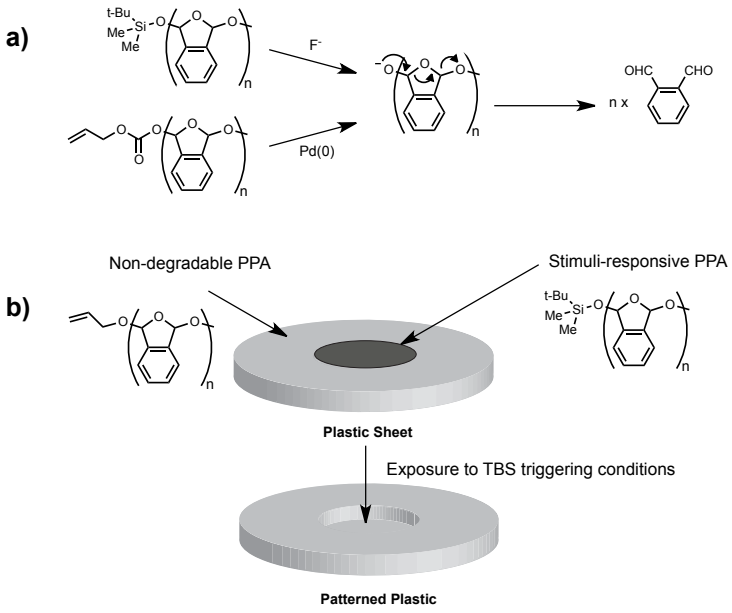

Figure 1.26: (a) First reported self-immolative poly(phthaldehyde)s that depolymerize through a cascade of 1,2-hemiacetal eliminations following end-cap removal. (b) Fabrication of a patterned plastic using a self-immolative poly(phthaldehyde).

Since the initial reports, the focus in the development of self-immolative PPAs has shifted towards improving the design and synthesis of these polymers. Kaitz and Moore addressed the lack of functional monomer diversity through a copolymerization of *ortho*-phthalaldehyde with substituted benzaldehydes (Figure 1.27a).[174] In addition to

overcoming the thermodynamic barriers required for copolymerization, this revised synthesis reduced the polymerization time from 72 h to 4-6 h and allowed for the formation of functionalized PPAs through post-polymerization modifications. Phillips and coworkers have also further improved their initial design by developing a generalized procedure for the synthesis of PPAs that is: (i) reproducible and scalable; (ii) requires 4 h to complete; (iii) allows for end-caps to be appended to either side of the polymer; and (iv) provides a high-degree of control over the molecular weight (Figure 1.27b).[175] Phillips and coworkers subsequently expanded the utility of these polymers by fabricating stimuli-responsive core-shell PPA microcapsules using a flow-focusing microfluidics technique.[176]

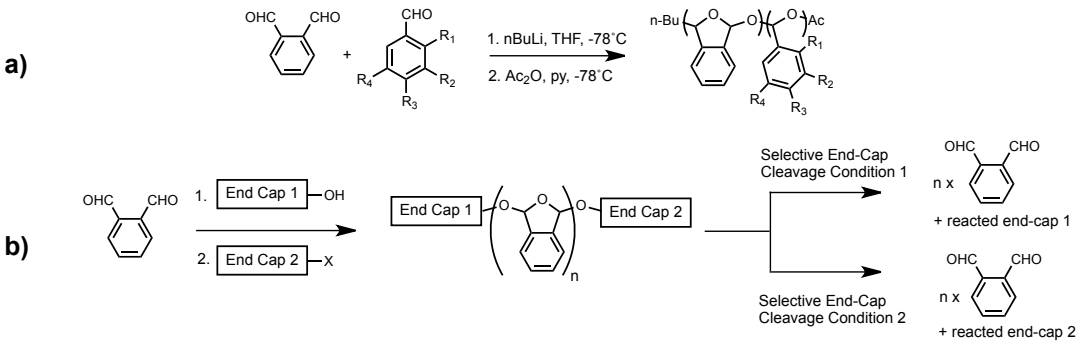

Figure 1.27: Recent improvements to the design and synthesis of self-immolative poly(phthaldehyde)s. (a) Copolymerization of ortho-phthalaldehyde with substituted benzaldehydes to allow for the formation of functionalized PPAs. (b) Generalized procedure for the synthesis of PPAs with two stimuli-responsive end-caps appended to both ends of the polymer.

Despite the proven utility of linear self-immolative polymers derived from PABC and PPA systems, the rapid degradation kinetics associated with 1,2 and 1,6-eliminations restricts the use of such polymers for applications involving controlled degradation at a slower rate. In general, PABC and PPA based systems display rapid solution phase degradation kinetics and depolymerize over the span of several minutes. Gillies and coworkers have addressed this limitation in degradation kinetics over the past 5 years through the design and synthesis of new linear self-immolative polymer backbones involving cyclization spacers. In 2009, DeWit and Gillies reported the first of such

designs with a linear self-immolative polymer backbone derived from alternating 1,6-elimination and cyclization spacers.[177] This system was based on a monomer comprised of 4-hydroxybenzyl alcohol and *N,N'*-dimethylethylenediamine units and was synthesized through a step-growth polycondensation reaction. Selective removal of a Boc end-cap initiated a cascade of cyclization, 1,6-elimination, and decarboxylation reactions that ultimately led to complete depolymerization of the polymer over 7 days in a 3:2 pH 7.4 buffer:acetone mixture at 37˚C (Figure 1.28a). Subsequent modifications to the nucleophilic and electrophilic sites in the cyclization spacer enabled tuning of the degradation rate in this system to reduce the time required to achieve complete depolymerization.[120] Enhancing the electrophilic character of the active carbonyl using a *N*-methylaminoethanol spacer reduced the degradation time to 4 hours (Figure 1.28b), while further enhancing the strength of the nucleophile using a 2-mercaptoethanol spacer reduced the degradation time to 2 hours (Figure 1.28c).

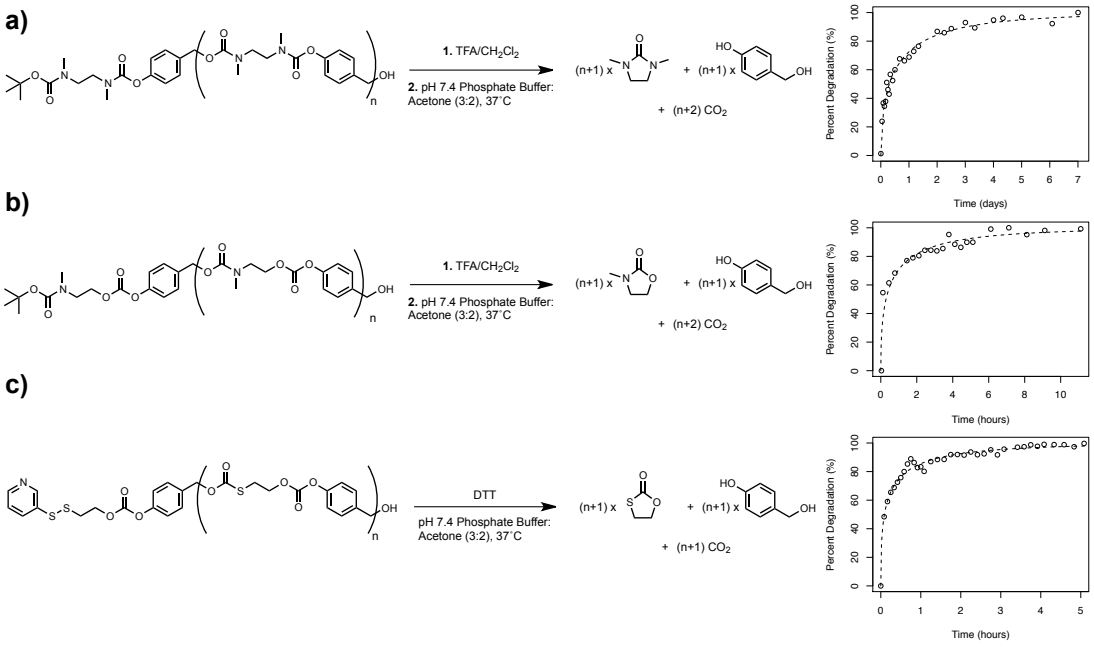

Figure 1.28: Linear self-immolative polymer backbones derived from alternating 1,6 elimination and cyclization spacers and their degradation kinetics in 3:2 pH 7.4 phosphate buffer:acetone at 37˚C. Reprinted with permission from Chen et al. Copyright 2012 American Chemical Society.

Using different cyclization polymer frameworks, the degradation rate of linear self-immolative polymers can also be further tuned in either direction. In 2010, Gillies and coworkers reported the design of a reduction sensitive, purely cyclization based polymer derived from alternating 2-mercaptoethanol and *N,N'*-dimethylethylenediamine spacers (Figure 1.29). Selective cleavage of the terminal thiopyridyl end-cap under reducing conditions initiated a cascade of cyclization reactions that ultimately led to depolymerization of the polymer over 2 weeks in a 3:2 pH 7.4 buffer:acetone mixture at 37˚C. [178] The design of a purely cyclization based polymer was motivated by the potential toxicity of the quinone methide species released during the degradation of 1,6-elimination based systems. However, the major limitation of this design was the tendency of the system to form cyclic oligomers during polymerization that were not prone to degradation under reducing conditions.

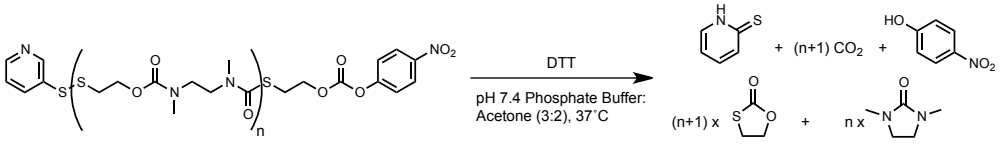

Figure 1.29: Reduction sensitive linear self-immolative polymer derived from alternating 2-mercaptoethanol and *N,N'*-dimethylethylenediamine cyclization spacers.

In an attempt to further bridge the gap between elimination and cyclization based polymers, DeWit and Gillies have also designed a series of 4-aminobutyric acid spacers that display rapid cyclization kinetics.[179] It was demonstrated that the kinetics of these 4-aminobutyric acid compounds display a remarkable substituent dependency, with cyclization half-lives varying between 2 and 39 s at physiological temperature and pH (Figure 1.30a). The incorporation of these spacers into polymer frameworks based on alternating cyclization/elimination or pure cyclization systems has been investigated, but the polymerization conditions required have yet to be optimized (Figure 1.30b-c).[180] Upon successful optimization of these systems, it is expected that a linear self-immolative system involving cyclization spacers can be used in applications requiring depolymerization times on the order of several minutes to several weeks.

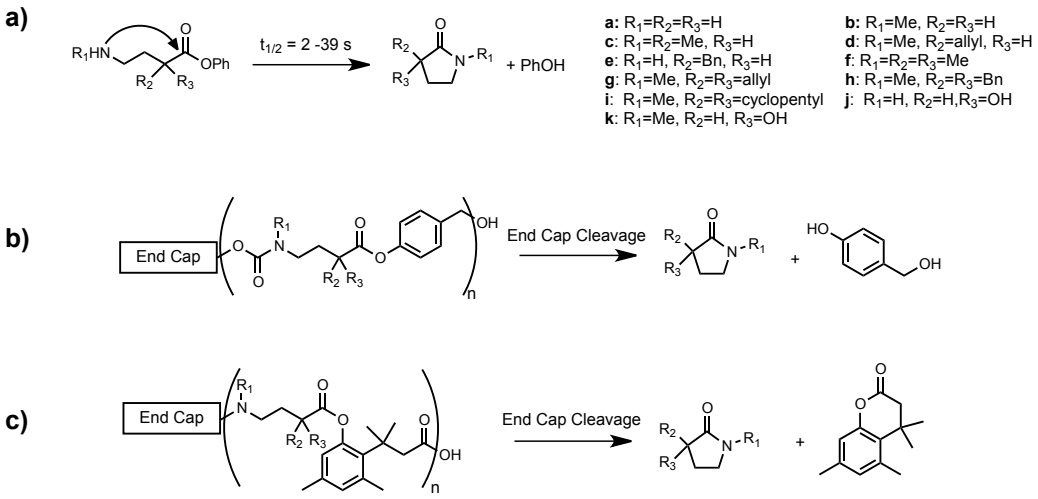

Figure 1.30: (a) 4-aminobutyric acid spacers that display rapid cyclization kinetics and their subsequent incorporation into linear self-immolative polymer frameworks based on (b) alternating cyclization/elimination reactions and (c) alternating cyclization reactions.

Due to their longer timescales of degradation, linear self-immolative polymers involving cyclization spacers are ideal candidates for controlled release applications. DeWit and Gillies have explored this potential using their initial system derived from 4-hydroxybenzyl alcohol and *N,N'*-dimethylethylenediamine to design a self-immolative amphiphilic block copolymer (Figure 1.31).[177] This polymeric system was synthesized with a modified PEG end-cap possessing a hydrolytically sensitive ester linkage between the hydrophilic PEG block and hydrophobic polycarbamate backbone. When subjected to aqueous conditions, this system self-assembled into micelles capable of encapsulating hydrophobic molecules. As a proof of concept, this system was able to provide a controlled release of a model hydrophobic drug, nile red, over a period of approximately 15 days in aqueous solution. Almutairi and coworkers have recently adopted an alternate approach to generate nanoparticles using the same self-immolative polycarbamate backbone with UV and NIR sensitive end-caps.[181] Using an emulsion method, they were able to generate hydrophobic nanoparticles capable of encapsulating nile red. However, when exposed to UV/NIR light, these nanoparticles displayed a burst release profile that is unsuited for prolonged release applications. Subsequent cytotoxicity testing of this system and its degradation products revealed that is equally as well tolerated as

poly(lactic-*co*-glycolic acid), which is currently approved by the FDA for biomedical applications.[181] As such, this polymer system displays immense promise for the fabrication of functional drug delivery vehicles, despite the limited work conducted in the field.

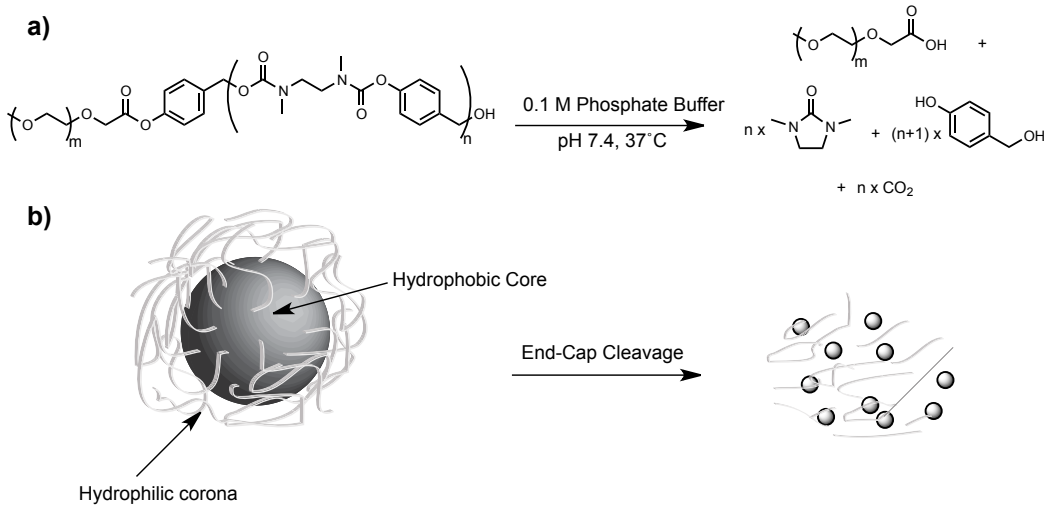

Figure 1.31: Design of a self-immolative block copolymer micellular drug delivery vehicle. (a) General structure of the self-immolative polymer backbone based on alternating 1,6-elimination and cyclization spacers and the hydrolytically sensitive PEG end-cap. (b) Structure and the degradation of micellular drug delivery vehicle.

1.5 Scope of the Thesis

The work described in this thesis focuses on two currently underexplored areas in the field of linear self-immolative polymers: degradation kinetics and functional designs. Chapter 2 of this thesis offers a theoretical and experimental evaluation of the kinetics of self-immolative degradation in a linear polymeric system. This section is geared towards developing and validating a theoretical model to explain the observed degradation behaviour in systems involving cyclization spacers. Overall, the goal of this section is to prove the proportional relationship between chain length and the degradation time while demonstrating chain length as a functional means to control the depolymerization time in linear self-immolative systems.

Chapter 3 focuses on the controlled design of linear self-immolative block copolymer nanoparticles for drug delivery applications. Expanding on the initial work conducted by DeWit and Gillies in 2009, this section first explores the potential to form alternate self-assemblies by varying the fraction of the hydrophilic PEG chain in the previously reported PEG-self-immolative copolymer system.[177] This chapter also describes the design and synthesis of a redox sensitive PEG-self-immolative block copolymer using a new modular approach to conjugate the PEG and self-immolative blocks. Preliminary evaluation of the degradation kinetics and self-assembly characteristics associated with this copolymer are also presented throughout this chapter.

The work described in this thesis involves the use of the previously reported linear self-immolative polymer system derived from alternating 4-hydroxybenzyl alcohol and *N,N'*-dimethylethylenediamine spacers. Practical considerations associated with the reproducibility, scale-up, and purification of this system are presented throughout with a focus on improving the utility of this system for further development and future applications.

1.6 References

(1) Tschan, M. J. L.; Brulé, E.; Haquette, P.; Thomas, C. M. *Polym. Chem.* **2012**, *3*, 836.

(2) Tian, H.; Tang, Z.; Zhuang, X.; Chen, X.; Jing, X. *Prog. Polym. Sci.* **2012**, *37*, 237.

(3) Amass, W.; Amass, A.; Tighe, B. *Polym. Int.* **1998**, *47*, 89.

(4) Gross, R. A.; Kalra, B. *Science* **2002**, *297*, 803.

(5) Gupta, A. P.; Kumar, V. *Eur. Polym. J.* **2007**, *43*, 4053.

(6) Nair, L. S.; Laurencin, C. T. *Prog. Polym. Sci.* **2007**, *32*, 762.

(7) Shi, B.; Topolkaraev, V.; Wang, J. In *Renewable and Sustainable Polymers*; Payne, G. F., Smith, P. B., Eds.; Amer Chemical Soc: Washington, 2011; Vol. 1063, p 117.

(8) Mecking, S. *Angew. Chem. Int. Ed.* **2004**, *43*, 1078.

(9) Sisson, A. L.; Schroeter, M.; Lendlein, A. In *Handbook of Biodegradable Polymers*; Wiley-VCH Verlag GmbH & Co. KGaA: 2011, p 1.

(10) Gilding, D. K.; Reed, A. M. *Polymer* **1979**, *20*.

(11) Reed, A. M.; Gilding, D. K. *Polymer* **1981**, *22*, 494.

(12) Li, Y.; Thouas, G. A.; Chen, Q.-Z. *RSC Advances* **2012**, *2*, 8229.

(13) Langer, R.; Vacanti, J. *Science* **1993**, *260*, 920.

(14) Jeong, B.; Bae, Y. H.; Lee, D. S.; Kim, S. W. *Nature* **1997**, *388*.

(15) Uhrich, K. E.; Cannizzaro, S. M.; Langer, R. S.; Shakesheff, K. M. *Chemical Reviews* **1999**, *99*, 3181.

(16) Kataoka, K.; Harada, A.; Nagasaki, Y. *Adv. Drug Delivery Rev.* **2001**, *47*, 113.

(17) Yih, T. C.; Al-Fandi, M. *J. Cell. Biochem.* **2006**, *97*, 1184.

(18) Kumari, A.; Yadav, S. K.; Yadav, S. C. *Colloids and Surfaces B: Biointerfaces* **2010**, *75*, 1.

(19) Carothers, W. H.; Dorough, G. L.; Van Natta, F. J. *J. Am. Chem. Soc.* **1932**, *54*, 761.

(20) Ihre, H.; Hult, A.; Soderlind, E. *J. Am. Chem. Soc.* **1996**, *118*, 6388.

(21) Ihre, H.; Hult, A.; Fréchet, J. M. J.; Gitsov, I. *Macromolecules* **1998**, *31*, 4061.

(22) Ihre, H.; Padilla De Jesús, O. L.; Fréchet, J. M. J. *J. Am. Chem. Soc.* **2001**, *123*, 5908.

(23) Vögtle, F.; Richardt, G.; Werner, N. In *Dendrimer Chemistry*; Wiley-VCH Verlag GmbH & Co. KGaA: 2009, p 1.

(24) Tomalia, D. A.; Fréchet, J. M. J. In *Dendrimers and Other Dendritic Polymers*; John Wiley & Sons, Ltd: 2002, p 1.

(25) Gillies, E. R.; Fréchet, J. M. J. *J. Am. Chem. Soc.* **2002**, *124*, 14137.

(26) Ihre, H. R.; Padilla De Jesús, O. L.; Szoka, F. C.; Fréchet, J. M. J. *Bioconjugate Chem.* **2002**, *13*, 443.

(27) Padilla De Jesús, O. L.; Ihre, H. R.; Gagne, L.; Fréchet, J. M. J.; Szoka, F. C. *Bioconjugate Chem.* **2002**, *13*, 453.

(28) Gillies, E. R.; Jonsson, T. B.; Fréchet, J. M. J. *J. Am. Chem. Soc.* **2004**, *126*, 11936.

(29) Gillies, E. R.; Fréchet, J. M. J. *Drug Discovery Today* **2005**, *10*, 35.

(30) Carlmark, A.; Malmström, E.; Malkoch, M. *Chem. Soc. Rev.* **2013**.

(31) Mikhail, A. S.; Allen, C. *J. Controlled Release* **2009**, *138*, 214.

(32) Kataoka, K.; Harada, A.; Nagasaki, Y. *Adv. Drug Delivery Rev.* **2012**, *64*, 37.

(33) Christian, D. A.; Cai, S.; Bowen, D. M.; Kim, Y.; Pajerowski, J. D.; Discher, D. E. *European Journal of Pharmaceutics and Biopharmaceutics* **2009**, *71*, 463.

(34) Tanner, P.; Baumann, P.; Enea, R.; Onaca, O.; Palivan, C.; Meier, W. *Acc. Chem. Res.* **2011**, *44*, 1039.

(35) Mai, Y.; Eisenberg, A. *Chem. Soc. Rev.* **2012**, *41*, 5969.

(36) Saltzman, W. M. *Drug Delivery : Engineering Principles for Drug Therapy: Engineering Principles for Drug Therapy*; Oxford University Press, 2001.

(37) Jain, R.; Shah, N. H.; Malick, A. W.; Rhodes, C. T. *Drug Dev. Ind. Pharm.* **1998**, *48*, 703.

(38) Aliabadi, H. M.; Lavasanifar, A. *Expert Opinion on Drug Delivery* **2006**, *3*, 139.

(39) Zhang, J.; Li, S.; Li, X. *Recent Pat. Nanotechnol.* **2009**, *3*, 225.

(40) Li, G.; Liu, J.; Pang, Y.; Wang, R.; Mao, L.; Yan, D.; Zhu, X.; Sun, J. *Biomacromolecules* **2011**, *12*, 2016.

(41) Miyata, K.; Christie, R. J.; Kataoka, K. *Reactive and Functional Polymers* **2011**, *71*, 227.

(42) Vert, M. *Biomacromolecules* **2005**, *6*, 538.

(43) Hofmann, D.; Entrialgo-Castaño, M.; Kratz, K.; Lendlein, A. *Advanced Materials* **2009**, *21*, 3237.

(44) Rahman, M. In *Degradation of Polyesters in Medical Applications*; Saleh, H. E.-D., Ed. 2012.

(45) Van Damme, H.; Deprez, M.; Creemers, E.; Limet, R. *Acta chirurgica Belgica* **2005**, *105*, 249.

(46) Esser-Kahn, A. P.; Odom, S. A.; Sottos, N. R.; White, S. R.; Moore, J. S. *Macromolecules* **2011**, *44*, 5539.

(47) Morachis, J. M.; Mahmoud, E. A.; Almutairi, A. *Pharmacological Reviews* **2012**, *64*, 505.

(48) Wei, H.; Zhuo, R.-X.; Zhang, X.-Z. *Prog. Polym. Sci.* **2012**, *38*, 503.

(49) Karton-Lifshin, N.; Vogel, U.; Sella, E.; Seeberger, P. H.; Shabat, D.; Lepenies, B. *Org. Biomol. Chem.* **2013**, *11*, 2903.

(50) Wu, Q.; Wang, L.; Yu, H.; Wang, J.; Chen, Z. *Chemical Reviews* **2011**, *111*, 7855.

(51) de Gracia Lux, C.; Joshi-Barr, S.; Nguyen, T.; Mahmoud, E.; Schopf, E.; Fomina, N.; Almutairi, A. *J. Am. Chem. Soc.* **2012**, *134*, 15758.

(52) Binauld, S.; Stenzel, M. H. *Chem. Commun.* **2013**, *49*, 2082.

(53) Zhao, C.; Nie, S.; Tang, M.; Sun, S. *Prog. Polym. Sci.* **2011**, *36*, 1499.

(54) Park, I.-K.; Singha, K.; Arote, R. B.; Choi, Y.-J.; Kim, W. J.; Cho, C.-S. *Macromol. Rapid Commun.* **2010**, *31*, 1122.

(55) Gao, W.; Chan, J. M.; Farokhzad, O. C. *Mol. Pharm.* **2010**, *7*, 1913.

(56) Dai, S.; Ravi, P.; Tam, K. C. *Soft Matter* **2008**, *4*, 435.

(57) Jain, R.; Standley, S. M.; Fréchet, J. M. J. *Macromolecules* **2007**, *40*, 452.

(58) Heffernan, M. J.; Murthy, N. *Bioconjugate Chem.* **2005**, *16*, 1340.

(59) Bang, E.-K.; Lista, M.; Sforazzini, G.; Sakai, N.; Matile, S. *Chem. Sci.* **2012**, *3*, 1752.

(60) Ko, N. R.; Yao, K.; Tang, C.; Oh, J. K. *J. Polym. Sci. A Polym. Chem.* **2012**, n/a.

(61) Bauhuber, S.; Hozsa, C.; Breunig, M.; Göpferich, A. *Advanced Materials* **2009**, *21*, 3286.

(62) Emilitri, E.; Ranucci, E.; Ferruti, P. *J. Polym. Sci. A Polym. Chem.* **2005**, *43*, 1404.

(63) Meng, F.; Hennink, W. E.; Zhong, Z. *Biomaterials* **2009**, *30*, 2180.

(64) Wang, Y.-J. P. Y.-Y. C. D.-R. W. C. W. J. G. D.-R. L. C.-C. C. C.-C.; Chen, Y.-Y.; Wang, D.-R.; Wei, C.; Guo, J.; Lu, D.-R.; Chu, C.-C.; Wang, C.-C. *Biomaterials* **2012**, *33*, 6570.

(65) Zhao, H.; Sterner, E. S.; Coughlin, E. B.; Theato, P. *Macromolecules* **2012**, *45*, 1723.

(66) Fomina, N.; Sankaranarayanan, J.; Almutairi, A. *Adv. Drug Delivery Rev.* **2012**, *64*, 1005.

(67) Griffin, D. R.; Schlosser, J. L.; Lam, S. F.; Nguyen, T. H.; Maynard, H. D.; Kasko, A. M. *Biomacromolecules* **2013**, *14*, 1199.

(68) Han, D.; Tong, X.; Zhao, Y. *Macromolecules* **2011**, *44*, 437.

(69) Johnson, J. A.; Finn, M. G.; Koberstein, J. T.; Turro, N. J. *Macromolecules* **2007**, *40*, 3589.

(70) Lv, C.; Wang, Z.; Wang, P.; Tang, X. *International Journal of Molecular Sciences* **2012**, *13*, 16387.

(71) Nazemi, A.; Schon, T. B.; Gillies, E. R. *Org. Lett.* **2013**, *15*, 1830.

(72) Pasparakis, G.; Manouras, T.; Argitis, P.; Vamvakaki, M. *Macromol. Rapid Commun.* **2011**, *33*, 183.

(73) Furuta, T.; Wang, S. S.; Dantzker, J. L.; Dore, T. M.; Bybee, W. J.; Callaway, E. M.; Denk, W.; Tsien, R. Y. *Proc. Natl. Acad. Sci. U. S. A.* **1999**, *96*, 1193.

(74) Fomina, N.; McFearin, C. L.; Almutairi, A. *Chem. Commun.* **2012**, *48*, 9138.

(75) Goodwin, A. P.; Mynar, J. L.; Ma, Y.; Fleming, G. R.; Fréchet, J. M. J. *J. Am. Chem. Soc.* **2005**, *127*, 9952.

(76) Hagen, V.; Kilic, F.; Schaal, J.; Dekowski, B.; Schmidt, R.; Kotzur, N. *J. Org. Chem.* **2010**, *75*, 2790.

(77) Mynar, J. L.; Goodwin, A. P.; Cohen, J. A.; Ma, Y.; Fleming, G. R.; Fr chet, J. M. J. *Chem. Commun.* **2007**, 2081.

(78) Sun, L.; Yang, Y.; Dong, C.-M.; Wei, Y. *Small* **2010**, *7*, 401.

(79) Blencowe, C. A.; Russell, A. T.; Greco, F.; Hayes, W.; Thornthwaite, D. W. *Polym. Chem.* **2011**, *2*, 773.

(80) Wong, A. D.; DeWit, M. A.; Gillies, E. R. *Adv. Drug Delivery Rev.* **2012**, *64*, 1031.

(81) Peterson, G. I.; Larsen, M. B.; Boydston, A. J. *Macromolecules* **2012**, *45*, 7317.

(82) Carl, P. L.; Chakravarty, P. K.; Katzenellenbogen, J. A. *J. Med. Chem.* **1981**, *24*, 479.

(83) Skwarczynski, M.; Hayashi, Y.; Kiso, Y. *J. Med. Chem.* **2006**, *49*, 7253.

(84) Rautio, J.; Kumpulainen, H.; Heimbach, T.; Oliyai, R.; Oh, D.; Järvinen, T.; Savolainen, J. *Nat. Rev. Drug Discovery* **2008**, *7*, 255.

(85) Duncan, R. *Nat. Rev. Cancer* **2006**, *6*, 688.

(86) Madec-Lougerstay, R.; Florent, J.-C.; Monneret, C. *J. Chem. Soc., Perkin Trans. 1* **1999**, 1369.

(87) Leenders, R. G.; Damen, E. W.; Bijsterveld, E. J.; Scheeren, H. W.; Houba, P. H.; van der Meulen-Muileman, I. H.; Boven, E.; Haisma, H. J. *Bioorg. Med. Chem.* **1999**, *7*, 1597.

(88) Dubowchik, G. M.; Firestone, R. A. *Bioorg. Med. Chem. Lett.* **1998**, *8*, 3341.

(89) Chakravarty, P. K.; Carl, P. L.; Weber, M. J.; Katzenellenbogen, J. A. *J. Med. Chem.* **1983**, *26*, 638.

(90) de Groot, F. M. H.; de Bart, A. C. W.; Verheijen, J. H.; Scheeren, H. W. *J. Med. Chem.* **1999**, *42*, 5277.

(91) Tranoy-Opalinski, I.; Fernandes, A.; Thomas, M.; Gesson, J. P.; Papot, S. *Anti-Cancer Agents Med. Chem.* **2008**, *8*, 618.

(92) Kratz, F.; Müller, I. A.; Ryppa, C.; Warnecke, A. *ChemMedChem* **2008**, *3*, 20.

(93) Corre, G. E.; Guibe-Jampel, E.; Wakselman, M. *Tetrahedron* **1978**, *34*, 3105.

(94) Senter, P. D.; Pearce, W. E.; Greenfield, R. S. *J. Org. Chem.* **1990**, *55*, 2975.

(95) Wakselman, M. *Nouv. J. Chem.* **1983**, *7*, 439.

(96) Andrianomenjanahary, S.; Dong, X.; Florent, J. C.; Gaudel, G.; Gesson, J. P.; Jacquesy, J. C.; Koch, M.; Michel, S.; Mondon, M.; Monneret, C.; Petit, P.; Renoux, B.; Tillequin, F. *Bioorg. Med. Chem. Lett.* **1992**, *2*, 1093.

(97) Ghosh, A. K.; Khan, S.; Farquhar, D. *Chem. Commun.* **1999**, 2527.

(98) Jobron, L.; Hindsgaul, O. *J. Am. Chem. Soc.* **1999**, *121*, 5835.

(99) Niculescu-Duvaz, D.; Niculescu-Duvaz, I.; Friedlos, F.; Martin, J.; Lehouritis, P.; Marais, R.; Springer, C. J. *J. Med. Chem.* **2003**, *46*, 1690.

(100) Rivault, F. *Bioorg. Med. Chem.* **2004**, *12*, 675.

(101) Erez, R.; Shabat, D. *Org. Biomol. Chem.* **2008**, *6*, 2669.

(102) Perry-Feigenbaum, R.; Baran, P. S.; Shabat, D. *Org. Biomol. Chem.* **2009**, *7*, 4825.

(103) Jourden, J. L. M.; Daniel, K. B.; Cohen, S. M. *Chem. Commun.* **2011**, *47*, 7968.

(104) Renoux, B.; Legigan, T.; Bensalma, S.; Chadéneau, C.; Muller, J.-M.; Papot, S. *Org. Biomol. Chem.* **2011**, *9*, 8459.

(105) Broaders, K. E.; Grandhe, S.; Fréchet, J. M. J. *J. Am. Chem. Soc.* **2011**, *133*, 756.

(106) Nuñez, S. A.; Yeung, K.; Fox, N. S.; Phillips, S. T. *J. Org. Chem.* **2011**, *76*, 10099.

(107) Schmid, K. M.; Jensen, L.; Phillips, S. T. *J. Org. Chem.* **2012**, *77*, 4363.

(108) Labruère, R.; Alouane, A.; Le Saux, T.; Aujard, I.; Pelupessy, P.; Gautier, A.; Dubruille, S.; Schmidt, F.; Jullien, L. *Angew. Chem. Int. Ed.* **2012**, *51*, 9344.

(109) Hay, M. P.; Anderson, R. F.; Ferry, D. M.; Wilson, W. R.; Denny, W. A. *J. Med. Chem.* **2003**, *46*, 5533.

(110) Cain, B. F. *J. Org. Chem.* **1976**, *41*, 2029.

(111) Johnson, C. D.; Lane, S. *J. Org. Chem.* **1988**, *53*, 5130.

(112) Amsberry, K. L.; Gerstenberger, A. E.; Borchardt, R. T. *Pharm. Res.* **1991**, *8*, 455.

(113) Amsberry, K. L.; Borchardt, R. T. *Pharm. Res.* **1991**, *8*, 323.

(114) Amsberry, K. L.; Borchardt, R. T. *J. Org. Chem.* **1990**, *55*, 5867.

(115) Wang, B.; Zhang, H.; Zheng, A.; Wang, W. *Bioorg. Med. Chem.* **1998**, *6*, 417.

(116) Wang, B.; Zhang, H.; Wang, W. *Bioorg. Med. Chem. Lett.* **1996**, *6*, 945.

(117) Saari, W. S.; Schwering, J. E.; Lyle, P. A.; Smith, S. J.; Engelhardt, E. L. *J. Med. Chem.* **1990**, *33*, 97.

(118) Saari, W. S.; Schwering, J. E.; Lyle, P. A.; Smith, S. J.; Engelhardt, E. L. *J. Med. Chem.* **1990**, *33*, 2590.

(119) Meyer, Y.; Richard, J.-A.; Massonneau, M.; Renard, P.-Y.; Romieu, A. *Org. Lett.* **2008**, *10*, 1517.

(120) Chen, E. K. Y.; McBride, R. A.; Gillies, E. R. *Macromolecules* **2012**, *45*, 7364.

(121) Schuster, H. J.; Krewer, B.; von Hof, J. M.; Schmuck, K.; Schuberth, I.; Alves, F.; Tietze, L. F. *Org. Biomol. Chem.* **2010**, *8*, 1833.

(122) El Alaoui, A.; Schmidt, F.; Monneret, C.; Florent, J.-C. *J. Org. Chem.* **2006**, *71*, 9628.

(123) El Alaoui, A.; Schmidt, F.; Amessou, M.; Sarr, M.; Decaudin, D.; Florent, J.-C.; Johannes, L. *Angew. Chem. Int. Ed.* **2007**, *46*, 6469.

(124) Shabat, D.; Lode, H. N.; Pertl, U.; Reisfeld, R. A.; Rader, C.; Lerner, R. A.; Barbas III, C. F. *Proc. Natl. Acad. Sci. U. S. A.* **2001**, *98*, 7528.

(125) Pessah, N.; Reznik, M.; Shamis, M.; Yantiri, F.; Xin, H.; Bowdish, K.; Shomron, N.; Ast, G.; Shabat, D. *Bioorg. Med. Chem.* **2004**, *12*, 1859.

(126) Amir, R. J.; Popkov, M.; Lerner, R. A.; Barbas, C. F.; Shabat, D. *Angew. Chem. Int. Ed.* **2005**, *44*, 4378.

(127) Thorn-Seshold, O.; Vargas-Sanchez, M.; McKeon, S.; Hasserodt, J. *Chem. Commun.* **2012**, *48*, 6253.

(128) Gogate, U. S.; Repta, A. J.; Alexander, J. *Int. J. Pharm.* **1987**, *40*, 235

(129) Gogate, U. S.; Repta, A. J. *Int. J. Pharm.* **1987**, *40*, 249.

(130) Alexander, J.; Cargill, R.; Michelson, S. R.; Schwam, H. *J. Med. Chem.* **1988**, *31*, 318.

(131) Varia, S. A.; Schuller, S.; Sloan, K. B.; Stella, V. J. *J. Pharm. Sci.* **1984**, *73*, 1068.

(132) Fechner, J.; Schwilden, H.; Schüttler, J. *Handbook of experimental pharmacology* **2008**, 253.

(133) Takahashi, K.; Tamagawa, S.; Haginaka, J.; Yasuda, H.; Katagi, T.; Mizuno, N. *J. Pharm. Sci.* **1992**, *81*, 226.

(134) Tang, X.; Xian, M.; Trikha, M.; Honn, K. V.; Wang, P. G. *Tetrahedron Lett.* **2001**, *42*, 2625.

(135) Lavis, L. D.; Chao, T.-Y.; Raines, R. T. *Chem. Sci.* **2011**, *2*, 521.

(136) Simplicio, A. L.; Clancy, J. M.; Gilmer, J. F. *Molecules* **2008**, *13*.

(137) de Groot, F. M. H.; Loos, W. J.; Koekkoek, R.; van Berkom, L. W. A.; Busscher, G. F.; Seelen, A. E.; Albrecht, C.; de Bruijn, P.; Scheeren, H. W. *J. Org. Chem.* **2001**, *66*, 8815.

(138) Warnecke, A.; Kratz, F. *J. Org. Chem.* **2008**, *73*, 1546.

(139) Devy, L. *FASEB J.* **2004**.

(140) Meyer, Y.; Richard, J.-A.; Delest, B.; Noack, P.; Renard, P.-Y.; Romieu, A. *Org. Biomol. Chem.* **2010**, *8*, 1777.

(141) Haba, K.; Popkov, M.; Shamis, M.; Lerner, R. A.; Barbas, C. F.; Shabat, D. *Angew. Chem. Int. Ed.* **2005**, *44*, 716.

(142) Lee, H. Y.; Jiang, X.; Lee, D. *Org. Lett.* **2009**, *11*, 2065.

(143) Kevwitch, R. M.; Shanahan, C. S.; McGrath, D. V. *New J. Chem.* **2012**, *36*, 492.

(144) Robbins, J. S.; Schmid, K. M.; Phillips, S. T. *J. Org. Chem.* **2013**, 130222154949002.

(145) Li, S.; Szalai, M. L.; Kevwitch, R. M.; McGrath, D. V. *J. Am. Chem. Soc.* **2003**, *125*, 10516.

(146) Amir, R. J.; Pessah, N.; Shamis, M.; Shabat, D. *Angew. Chem. Int. Ed.* **2003**, *42*, 4494.

(147) de Groot, F. M. H.; Albrecht, C.; Koekkoek, R.; Beusker, P. H.; Scheeren, H. W. *Angew. Chem. Int. Ed.* **2003**, *42*, 4490.

(148) Szalai, M. L.; Kevwitch, R. M.; McGrath, D. V. *J. Am. Chem. Soc.* **2003**, *125*, 15688.

(149) Kevwitch, R. M.; McGrath, D. V. *New J. Chem.* **2007**, *31*, 1332.

(150) Ortiz, A.; Shanahan, C. S.; Sisk, D. T.; Perera, S. C.; Rao, P.; McGrath, D. V. *J. Org. Chem.* **2010**, *75*, 6154.

(151) Polaske, N. W.; Szalai, M. L.; Shanahan, C. S.; McGrath, D. V. *Org. Lett.* **2010**, *12*, 4944.

(152) Amir, R. J.; Shabat, D. *Chem. Commun.* **2004**, 1614.

(153) Shamis, M.; Lode, H. N.; Shabat, D. *J. Am. Chem. Soc.* **2004**, *126*, 1726.

(154) Perry, R.; Amir, R. J.; Shabat, D. *New J. Chem.* **2007**, *31*, 1307.

(155) Sagi, A.; Segal, E.; Satchi-Fainaro, R.; Shabat, D. *Bioorg. Med. Chem.* **2007**, *15*, 3720.

(156) Gopin, A.; Ebner, S.; Attali, B.; Shabat, D. *Bioconjugate Chem.* **2006**, *17*, 1432.

(157) Shamis, M.; Shabat, D. *Chem. Eur. J.* **2007**, *13*, 4523.

(158) Erez, R.; Segal, E.; Miller, K.; Satchi-Fainaro, R.; Shabat, D. *Bioorg. Med. Chem.* **2009**, *17*, 4327.

(159) Amir, R. J.; Danieli, E.; Shabat, D. *Chem. Eur. J.* **2007**, *13*, 812.

(160) Sella, E.; Shabat, D. *Chem. Commun.* **2008**, 5701.

(161) Sella, E.; Shabat, D. *J. Am. Chem. Soc.* **2009**, *131*, 9934.

(162) Avital-Shmilovici, M.; Shabat, D. *Bioorg. Med. Chem.* **2010**, *18*, 3643.

(163) Sella, E.; Lubelski, A.; Klafter, J.; Shabat, D. *J. Am. Chem. Soc.* **2010**, *132*, 3945.

(164) Sella, E.; Weinstain, R.; Erez, R.; Burns, N. Z.; Baran, P. S.; Shabat, D. *Chem. Commun.* **2010**, *46*, 6575.

(165) Perry-Feigenbaum, R.; Sella, E.; Shabat, D. *Chem. Eur. J.* **2011**, *17*, 12123.

(166) Karton-Lifshin, N.; Shabat, D. *New J. Chem.* **2012**, *36*, 386.

(167) Danieli, E.; Shabat, D. *Bioorg. Med. Chem.* **2007**, *15*, 7318.

(168) Sagi, A.; Weinstain, R.; Karton, N.; Shabat, D. *J. Am. Chem. Soc.* **2008**, *130*, 5434.

(169) Weinstain, R.; Baran, P. S.; Shabat, D. *Bioconjugate Chem.* **2009**, *20*, 1783.

(170) Weinstain, R.; Sagi, A.; Karton, N.; Shabat, D. *Chem. Eur. J.* **2008**, *14*, 6857.

(171) Esser-Kahn, A. P.; Sottos, N. R.; White, S. R.; Moore, J. S. *J. Am. Chem. Soc.* **2010**, *132*, 10266.

(172) Köstler, S. *Polym. Int.* **2012**, *61*, 1221.

(173) Seo, W.; Phillips, S. T. *J. Am. Chem. Soc.* **2010**, *132*, 9234.

(174) Kaitz, J. A.; Moore, J. S. *Macromolecules* **2013**, *46*, 608.

(175) DiLauro, A. M.; Robbins, J. S.; Phillips, S. T. *Macromolecules* **2013**, *46*, 2963.

(176) DiLauro, A. M.; Abbaspourrad, A.; Weitz, D. A.; Phillips, S. T. *Macromolecules* **2013**, *46*, 3309.

(177) DeWit, M. A.; Gillies, E. R. *J. Am. Chem. Soc.* **2009**, *131*, 18327.

(178) DeWit, M. A.; Beaton, A.; Gillies, E. R. *J. Polym. Sci. A Polym. Chem.* **2010**, *48*, 3977.

(179) DeWit, M. A.; Gillies, E. R. *Org. Biomol. Chem.* **2011**, *9*, 1846.

(180) DeWit, M., The University of Western Ontario, 2012.

(181) de Gracia Lux, C.; McFearin, C. L.; Joshi-Barr, S.; Sankaranarayanan, J.; Fomina, N.; Almutairi, A. *ACS Macro Lett.* **2012**, *1*, 922.

Chapter 2

2 Kinetics of Self-Immolative Degradation in a Linear Polymeric System: Demonstrating the Effect of Chain Length†

2.1 Introduction

Recent advances in the field of polymer science have contributed to a paradigmatic shift in the use of biodegradable polymers as environmentally-friendly substitutes for traditional commodity plastics and in biomedical applications ranging from drug delivery to tissue engineering. While there exists a large variety of different biodegradable polymer backbones, the predominant majority of such systems are polyester-based. Despite the proven utility of popular synthetic polyesters such as poly(caprolactone), poly(lactic acid), and poly(glycolic acid), the degradation of polyesters suffers from a lack of fine control, as it initiated by a non-specific triggering event and relies on random hydrolytic cleavage of ester bonds throughout the polymer backbone.[1-3] In part, the limited control over the degradation of polyesters has been addressed through the development of stimuli-responsive, biodegradable polymers in which polymer degradation is triggered[4] by specific environmental conditions such as changes in pH[5-7] or redox potential,[8-10] biologically mediated events including enzymatic cleavage[11] and changes in chemical concentration,[12,13] or by an applied external stimulus such as UV/NIR light.[14-17] Such systems are an improvement over basic polyesters in that they circumvent the issue of non-specific degradation. However, these systems still require many environmentally-mediated cleavage events to ensure complete degradation, thereby restricting their usage to applications in which triggering events are abundant.

Self-immolative polymers have been developed over the past decade as an alternative to traditional biodegradable polymers and offer new levels of control and amplification to the degradation process. Self-immolative polymers undergo end-to-end depolymerization through a cascade of intramolecular reactions upon the removal of a stimuli-responsive, stabilizing end-cap (Figure 2.1a).[18-20] This particular mechanism of degradation possesses three main advantages over the degradation of traditional biodegradable polymers: (i) it

†This chapter contains work that has been published: McBride, R. A.; Gillies, E. R. G. *Macromolecules* **2013**, doi: 10.1021/ma4009753.

permits the amplification of a given stimulus, in that only one triggering event is required to achieve complete degradation of the polymer backbone; (ii) the stimuli-responsive degradation of a given polymer can be readily adjusted and tuned through the incorporation of different end-capping agents; and (iii) the degradation kinetics of these polymers are dictated and controlled by the chemical composition of the polymer backbone.

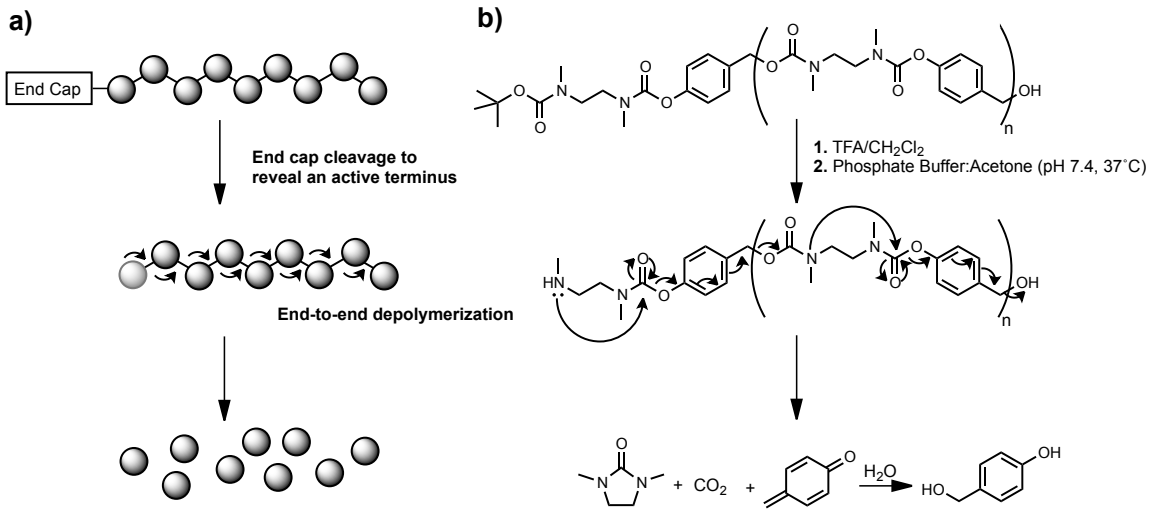

Figure 2.1: Illustration of linear self-immolative degradation. (a) Generic overview depicting the end-to-end depolymerization of the polymer backbone following the removal of the stabilizing end-cap. (b) Previously reported linear self-immolative polymer derived from alternating cyclization and 1,6-elimination spacers and its mechanism of degradation.

Following the seminal reports on the design and synthesis of self-immolative dendrimers,[21-23] a number of different self-immolative polymer backbones and architectures have been designed for signal amplification,[24-27] drug delivery,[28-31] microfluidics,[32] protein labeling,[33] self-healing,[34] and shape-memory applications.[35] Our group, along with several others, have focused predominantly on the design and synthesis of linear self-immolative polymers with a special consideration towards fine-tuning the degradation rate.[26,33-41] Despite being no longer monodisperse, linear self-immolative polymers provide a high-degree of amplification in a limited number of synthetic steps while bypassing any restrictions associated with steric constraints.

The first reported linear self-immolative polymer was derived entirely from monomers that underwent 1,6-elimination reactions to degrade the polymer into fluorescent monomer units.[36] Our group subsequently developed linear polymer backbones that were comprised of alternating cyclization and 1,6-elimination spacers or purely cyclization spacers and showed that the degradation kinetics of such polymers could be significantly slowed through the incorporation of cyclization spacers.[37,38] More recently, we have shown that the degradation rate of such polymers can be effectively tuned by exploiting the structure-property relationships of the monomer cyclization spacers.[39,41] A similar approach has also been utilized by Phillips and coworkers for linear self- immolative oligomers derived from 1,6-elimination spacers.[42,43] While this approach is a proven means to induce large changes to the depolymerization rate, it should be possible to effectively tune the depolymerization rate by simply changing the length of the polymer. In particular, since the depolymerization of linear self-immolative polymers involves a cascade of reactions across a defined architecture, the degradation rate of these polymers should be inversely proportional to chain length. In the absence of more complicated effects arising from alternative reaction pathways or electronic communication between adjacent monomer units, the relative depolymerization rates of linear self-immolative oligomers and polymers should be inversely proportional to chain length. While several studies have been performed to investigate the effect of chain length on the degradation rate of short self-immolative oligomers, with varying results,[44-47] the length dependence of self-immolative polymer degradation has not yet been demonstrated, and no comprehensive model has been developed to describe their behaviour.

Using our previously reported linear polycarbamate backbone derived from alternating 1,6-elimination and cyclization spacers (Figure 2.1b) [37] we herein report the first conclusive study demonstrating the effect of chain length on the kinetics of linear self-immolative degradation. This is accomplished using a set of monodisperse oligomers synthesized through a new convergent iterative route and a series of polymers optimized to display varying molecular weights. We also report the development and validation of a new linear self-immolative degradation model relating monomer kinetics to polymer degradation and show its application in explaining oligomeric and polymeric degradation profiles. Collectively, this work offers the first quantitative evidence supporting the

mixed pseudo zero- and first-order degradation kinetics of linear self-immolative polymers and proves the utility of chain length as an alternate means to tune the degradation time in linear self-immolative polymers.

2.2 Experimental

2.2.1 General Procedures and Materials

All reagents were purchased from commercial suppliers and used without further purification unless otherwise noted. Anhydrous toluene was obtained from a solvent purification system using aluminum oxide columns. Dichloromethane (CH_2Cl_2), pyridine, triethylamine (NEt_3), and *N,N*- diisopropylethylamine (DIPEA) were distilled from CaH_2 immediately prior to use. Unless otherwise stated, all reactions were performed under an Ar atmosphere using flame-dried glassware. Column chromatography was performed using silica gel (0.040 – 0.063 mm particle size, 230 – 430 mesh). Thin layer chromatography (TLC) was carried out using EMD silica gel 60 F254 plates (20 cm × 20 cm, 250 *μm).* Deionized water was purified using a Millipore purification system. Dialyses were performed using Spectra/Por® regenerated cellulose membranes with either a 6000-8000 g/mol or 25000 g/mol molecular weight cutoff (MWCO).

^{1}H NMR spectra were obtained at 400 MHz or 600 MHz using a Varian INOVA spectrometer, while ^{13}C NMR spectra were obtained at 100 MHz using a Varian INOVA spectrometer. Chemical shifts are reported in ppm versus tetramethylsilane and referenced to residual solvent signals of $CDCl_3$ (δ 7.26, 77.2), $(CD3)_2CO$ (δ 2.05), or D_2O (δ 4.79). Coupling constants are expressed in Hz. High resolution mass spectrometry (HRMS) was performed on either a Finnigan MAT 8400 or a PE-Sciex API 365 mass spectrometer using electron impact (EI) or electrospray (ESI) ionization, respectively. Fourier transform infrared spectra were obtained using a Bruker Tensor 27 from CH_2Cl_2 films on KBr plates. Size exclusion chromatography (SEC) was carried out at a flow rate of 1 mL/min in *N,N*- dimethylformamide (DMF) with 10 mM LiBr and 1% (v/v) NEt_3 at 85˚C using a Waters 2695 separations module equipped with a Waters 2414 differential refractometer and two PLgel 5 *μm* mixed-D (300 mm × 7.5 mm) columns from Polymer Laboratories connected in series. SEC calibrations were performed using poly(methyl

methacrylate) (PMMA) standards. Reverse phase high pressure liquid chromatography (RP-HPLC) was performed at a flow rate of 1 mL/min on a Waters 2695 separations module equipped with a Waters 2998 photodiode array detector at a wavelength of 225 nm and a Nova-Pak® C-18 analytical column (3.9 mm × 150 mm, 4 *μm).* The HPLC gradient was linear from 40/60 MeCN/H_2O to 100/0 MeCN/H_2O over 15 min. Solvent mixtures for all chromatographic analyses contained 0.1% TFA.

2.2.2 Synthesis

*Synthesis of Compound **2.1a**.* Unactivated monomer **2.1b**[37] (1.34 g, 4.0 mmol, 1.0 equiv) was dissolved in 20 mL of anhydrous CH_2Cl_2. Acetyl chloride (0.42 mL, 5.9 mmol, 1.5 equiv), pyridine (1.0 mL, 12.0 mmol, 3 equiv) and 4-(dimethylamino)pyridine (DMAP) (0.05 g, 0.4 mmol, 0.1 equiv) were successively added to the reaction flask and the solution was stirred at room temperature until completion (~ 1.25 h) as determined by TLC. The reaction mixture was then diluted with CH_2Cl_2 and washed with 1 M HCl. The organic layer was dried over $MgSO_4$, filtered, and concentrated *in vacuo*. The resulting oil was purified by silica gel flash chromatography (1:19 EtOAc:CH_2Cl_2, gradient to 3:7 EtOAc:CH_2Cl_2) to afford 1a as a pale yellow oil (1.31 g, 87%). ^{1}H NMR ($CDCl_3$, 400 MHz):δ 7.31 (m, 2H), 7.11–7.03 (m, 2H), 5.04 (s, 2H), 3.61–3.49 & 3.48–3.37 (2 m, 4H total, rotamers), 3.09 & 3.00 (2 s, 3H total, rotamers), 2.93–2.82 (m, 3H, rotamers), 2.05 (s, 3H), 1.48–1.39 (m, 9H, rotamers). ^{13}C NMR ($CDCl_3$, 150 MHz): δ 170.7, (155.9, 155.7 & 155.5, rotamers), (154.7, 154.5, & 154.4, rotamers), (151.4 & 151.2, rotamers), (133.0 & 132.9, rotamers), 129.4, (122.0 & 121.8, rotamers), (79.8, 79.7, 79.6, & 79.4, rotamers), 69.7, (47.3, 47.1, 46.9, 46.7, 46.5, 46.4, & 45.6, methylenes, rotamers), (35.4, 35.2, 35.1, 34.7, & 34.5, methyls, rotamers), 28.4, 21.0. FT-IR (ν_{max}/cm^{-1}): 2976, 2934, 1724, 1693, 1515. HRMS: calcd $[M]^+$ ($C_{19}H_{28}N_2O_6$): 380.1947. Found (EI) 380.1948. RP-HPLC: t_R=3.8 min (purity, >99%).

*Synthesis of Compound **2.2a**.* Acetylated monomer **2.1a** (1.12 g, 2.9 mmol, 1.2 equiv) was dissolved in 6 mL of 1:1 TFA:CH_2Cl_2 and stirred at room temperature for 2 h. The reaction mixture was then diluted with CH_2Cl_2 and the solvent was removed under reduced pressure. This dilution/evaporation cycle was repeated an additional three times

to remove residual TFA, yielding the deprotected-acetylated monomer **2.1d**. 4-Nitrophenyl-activated activated monomer **2.1c**[37] (1.25 g, 2.5 mmol, 1.0 equiv) was then added and the resulting mixture was dissolved in anhydrous toluene and cooled to 0˚C. DIPEA (1.3 mL, 7.4 mmol, 3.0 equiv) and DMAP (35 mg, 0.29 mmol, 0.12 equiv) were sequentially added and the solution was stirred at 0˚C for 8 h. The reaction was allowed to warm to room temperature and stirred an additional 8 h. The reaction mixture was then diluted with CH_2Cl_2 and washed with 1 M HCl followed by 1 M Na_2CO_3. The organic layer was dried over $MgSO_4$, filtered, and concentrated *in vacuo.* The resulting oil was then purified by silica gel flash chromatography (1:4 EtOAc:CH_2Cl_2, gradient to 3:2 EtOAc:CH_2Cl_2) to afford **2.2a** as a colourless oil (1.34 g, 84%). ^{1}H NMR ($CDCl_3$, 400 MHz): δ 7.38–7.27 (m, 4H), 7.11–7.00 (m, 4H), 5.13–5.01 (m, 4H), 3.64–3.36 (m, 8H), 3.12–2.82 (m, 12H), 2.06 (s, 3H), 1.52–1.37 (m, 9H, rotamers). FT-IR (ν_{max}/cm^{-1}): 2932, 1722, 1699, 1512. HRMS: calcd $[M+Na]^+$ ($C_{32}H_{44}N_4O_{10}Na$): 667.2955. Found (ESI): 667.2929. RP-HPLC: t_R=5.1 min (purity, >99%). SEC: M_n=*875* g/mol, PDI=1.03 (PMMA standards).

*Synthesis of Compound **2.2b**.* Acetylated dimer **2.2a** (0.64 g, 1.0 mmol, 1.0 equiv) and LiOH·H_2O (59 mg, 1.4 mmol, 1.4 equiv) were dissolved in 15 mL of 3:2 THF:H_2O and stirred at room temperature for 16 h. Upon completion of the reaction, the solvent mixture was poured over 1 M HCl and the product was extracted with CH_2Cl_2. The combined organic layers were dried over MgSO4, filtered, and concentrated *in vacuo* to yield compound **2.2b** (0.55 g, 92%) as a white solid. ^{1}H NMR ($CDCl_3$, 400 MHz): δ 7.38–7.17 (m, 4H), 7.10–6.89 (m, 4H), 5.13–5.03 (m, 2H, rotamers), 4.58 (d, J=5.4, 2H, rotamers), 3.67–3.37 (m, 8H), 3.16–2.78 (m, 12H), 1.48–1.37 (m, 9H, rotamers). FT-IR (ν_{max}/cm^{-1}): 3468, 2928, 2872, 2856, 1718, 1701, 1510. HRMS: calcd $[M+Na]^+$ ($C_{30}H_{42}N_4O_9Na$): 625.2850. Found (ESI) 625.2858. RP-HPLC: t_R=3.4 min (purity, >99%).

*Synthesis of Compound **2.2c**.* Unactivated dimer **2.2b** (0.50 g, 0.84 mmol, 1.0 equiv) and pyridine (20 *μL,* 2.5 mmol, 3.0 equiv) were dissolved in 6 mL of anhydrous CH_2Cl_2. 4-Nitrophenyl chloroformate (0.34 g, 1.7 mmol, 2.0 equiv) was added slowly to the reaction flask and the solution was stirred at room temperature until completion (~ 3 h) as

determined by TLC. The reaction mixture was then diluted with CH_2Cl_2 and washed with 1 M HCl followed by saturated $NaHCO_3$. The organic layer was dried over $MgSO_4$, filtered, and concentrated *in vacuo.* The resulting oil was purified by silica gel flash chromatography (1:4 EtOAc:CH_2Cl_2, then 2:3 EtOAc:CH_2Cl_2) to afford **2.2c** as a white solid (0.51 g, 79%). ^{1}H NMR ($CDCl_3$, 400 MHz): δ 8.23 (d, J=9.0, 2H), 7.46–7.27 (m, 6H), 7.14–7.01 (m, 4H), 5.24 (s, 2H), 5.13–5.03 (m, 2H), 3.66–3.35 (m, 8H), 3.15– 2.82 (m, 8H), 1.50–1.37 (m, 9H, rotamers). FT-IR (νmax/cm^{-1}): 2972, 2934, 1767, 1720, 1697, 1614, 1593, 1526. HRMS: calcd $[M+Na]^+$ ($C_{37}H_{45}N_5O_{13}Na$): 790.2912. Found (ESI) 790.2898. RP-HPLC:t_R=7.2 min (purity, 99%).

*Synthesis of Compound **2.3a**.* Acetylated tetramer **2.3a** was prepared using similar conditions to those described for compound **2.2a**. The quantities of reagents used were **2.2a** (0.55 g, 0.86 mmol, 1.4 equiv), **2.2c** (0.48 g, 0.63 mmol, 1.0 equiv), DIPEA (0.33 mL, 1.8 mmol, 3.0 equiv), and DMAP (13 mg, 0.11 mmol, 0.17 equiv). The product was purified by silica gel flash chromatography (4:1 EtOAc:CH_2Cl_2, gradient to EtOAc) to afford **2.3a** as a white solid (0.65 g, 88%). ^{1}H NMR ($CDCl_3$, 400 MHz): δ 7.40–7.28 (m, 8H), 7.12–7.00 (m, 8H), 5.15–5.03 (m, 8H), 3.64–3.39 (m, 16H), 3.16–2.84 (m, 24H), 2.07 (s, 3H), 1.50–1.38 (m, 9H, rotamers). FT-IR (νmax/cm^{-1}): 2934, 1720, 1701, 1510. HRMS: calcd $[M+Na]^+$ ($C_{58}H_{76}N_8O_{18}Na$): 1195.5176. Found (ESI) 1195.5133. RP-HPLC: t_R=6.8 min (purity, 97%). SEC: M_n=*1940* g/mol, PDI=1.02 (PMMA standards).

*Synthesis of Compound **2.3b**.* Deprotected tetramer **2.3b** was prepared using similar conditions to those described for compound **2.2b**. The quantities of reagents used were **2.3a** (0.27 g, 0.23 mmol, 1.0 equiv) and $LiOH{\cdot}H_2O$ (19 mg, 0.46 mmol, 2.0 equiv). The product alcohol was purified by silica gel flash chromatography (1:24 MeOH:CH_2Cl_2) to afford **2.3b** as a white solid (0.19 g, 73%). ^{1}H NMR ($CDCl_3$, 400 MHz): δ 7.39–7.18 (m, 8H), 7.11–6.91 (m, 8H), 5.14–4.99 (m, 6H), 4.59 (d, J=4.4, 2H), 3.66–3.36 (m, 16H), 3.14–2.84 (m, 24H), 1.51–1.39 (m, 9H, rotamers). FT-IR (ν_{max}/cm^{-1}): 3479, 2934, 1718, 1703, 1510. HRMS: calcd $[M+Na]^+$ ($C_{56}H_{74}N_8O_{17}Na$): 1153.5070. Found (ESI) 1153.5031. RP-HPLC: t_R=5.5 min (purity, >99%).

*Synthesis of Compound **2.3c**.* 4-Nitrophenyl-activated tetramer **2.3c** was prepared using similar conditions to those described for compound **2.2c**. The quantities of reagents used were **2.3b** (0.12 g, 0.11 mmol, 1 equiv), pyridine (30 *μL,* 0.3 mmol, 3 equiv), and 4-nitrophenyl chloroformate (60 mg, 0.30 mmol, 2.7 equiv). The product was purified by silica gel flash chromatography (EtOAc, then 1:24 MeOH:EtOAc) to afford **2.3c** as a white solid (0.1 g, 70%). ^{1}H NMR ($CDCl_3$, 400 MHz): δ 8.22 (m, 2H), 7.44–7.26 (m, 10H), 7.13–6.97 (m, 8H), 5.23 (s, 2H), 5.13–5.01 (m, 2H), 3.63–3.34 (m, 16H), 3.15–2.80 (m, 24H), 1.48–1.38 (m, 9H, rotamers). FT-IR (ν_{max}/cm^{-1}): 2930, 2856, 1767, 1720, 1701, 1614, 1593, 1525, 1512. HRMS: calcd $[M+Na]^+$ ($C_{63}H_{77}N_9O_{21}Na$): 1318.5132. Found (ESI) 1318.5132. RP-HPLC: t_R=8.4 min (purity, 96%).

*Synthesis of Compound **2.4a**.* Acetylated octamer **2.4a** was prepared using similar conditions to those described for compound **2.2a**. The quantities of reagents used were **2.3a** (0.14 g, 0.12 mmol, 1.6 equiv), **2.3c** (0.09 g, 0.07 mmol, 1 equiv), DIPEA (60 *μL,* 0.4 mmol, 5 equiv) and DMAP (1 mg, 0.007 mmol, 0.1 equiv). The product was purified by silica gel flash chromatography (1:49 MeOH:CH_2Cl_2, then 3:47 MeOH:CH_2Cl_2) to afford **2.4a** as a white solid (0.14 g, 74%). ^{1}H NMR ($CDCl_3$, 400 MHz): δ 7.40 –7.28 (m, 16H), 17.12–6.99 (m, 16H), 5.14–5.05 (m, 16H), 3.65–3.39 (m, 32H), 3.19–2.86 (m, 48H), 2.08 (s, 3H), 1.50–1.41 (m, 9H, rotamers). FT-IR (ν_{max}/cm^{-1}): 2936, 1718, 1701, 1512. HRMS: calcd $[M+Na]^+$ ($C_{110}H_{140}N_{16}O_{34}Na$): 2251.9610. Found (ESI) 2251.9593. RP-HPLC: t_R =8.9 min (purity, 96%). SEC: M_n =3660 g/mol, PDI=1.03 (PMMA standards).

*Synthesis of Polymer **2.6**.* Activated monomer **2.1c**[37] (0.28 g,0.55 mmol, 1 equiv) was dissolved in 3 mL of 1:1 TFA:CH_2Cl_2 and stirred at room temperature for 2 h. The solvent was then removed under a stream of nitrogen in the fume hood prior to subjecting the reaction mixture three times to a repeat cycle of dilution with CH_2Cl_2 followed by concentration under reduced pressure to remove residual TFA and provide the deprotected monomer **2.5**.[37] End-cap **2.1c**[37] (0.014 g, 0.027 mmol, 0.05 equiv) was added and the resulting mixture was dissolved in 3 mL of anhydrous toluene. DIPEA (0.48 mL, 2.75 mmol, 5.0 equiv) and DMAP (0.016 g, 0.13 mmol, 0.24 equiv) were sequentially added and the solution was stirred at room temperature for 6 h. The solvent was then

evaporated under reduced pressure and the crude polymer was dissolved in 2 mL of DMF and dialyzed against DMF for 24 h (200, mL, 1 solvent change) using a regenerated cellulose membrane (6000-8000 g/mol MWCO). The contents of the dialysis membrane were then concentrated *in vacuo* and lyophilized to afford polymer **2.6** (0.063 g, 42%). ^{1}H NMR indicated a degree of polymerization of ~ 25 by integrating the benzylic peak against the Boc end-cap. ^{1}H NMR ($CDCl_3$, 600 MHz): δ 7.46–7.26 (m, 51H), 7.18–6.95 (m, 44H), 5.18–4.97 (m, 50H), 3.70–3.37 (m, 103H), 3.25–2.80 (m, 158H), 1.50–1.41 (m, 9H, rotamers). SEC: M_n=5250 g/mol, M_w=7730 g/mol, PDI=1.47 (PMMA standards).

*Synthesis of Polymer **2.7**.* Activated monomer **2.1c**[37] (1.25 g, 2.49 mmol, 1 equiv) was dissolved in 6 mL of 1:1 TFA:CH_2Cl_2 and stirred at room temperature for 2 h. The solvent was then removed under a stream of nitrogen in the fume hood prior to subjecting the reaction mixture three times to a repeat cycle of dilution with CH_2Cl_2 followed by concentration under reduced pressure to remove residual TFA and provide the deprotected monomer. End-cap **2.1c**[37] (0.013 g, 0.025 mmol, 0.01 equiv) was added and the resulting mixture was dissolved in 12 mL of anhydrous toluene and cooled to 0˚C. NEt_3 (1.73 mL, 12.43 mmol, 5 equiv) and DMAP (0.066 g, 0.54 mmol, 0.22 equiv) were sequentially added and the solution was stirred at 0˚C for 24 h. The reaction mixture was then diluted with CH_2Cl_2 and washed with 1M HCl followed by 1 M Na_2CO_3. The organic layer was dried over $MgSO_4$, filtered, and concentrated *in vacuo* to provide the crude polymer (0.60 g, 92%). The crude polymer was then dissolved in 5 mL of DMF and dialyzed against DMF for 24 h (500, mL, 1 solvent change) using a regenerated cellulose membrane (25000 g/mol MWCO). The contents of the dialysis membrane were then concentrated *in vacuo* and lyophilized to afford polymer **2.7** (0.25 g, 37%). ^{1}H NMR indicated a degree of polymerization of ~ 101 by integrating the benzylic peak against the Boc end-cap. ^{1}H NMR ($CDCl_3$, 600 MHz): δ 7.39–7.29 (m, 181H), 7.12–6.99 (m, 178H), 5.17–5.02 (m, 203H), 3.70–3.36 (m, 409H), 3.21–2.79 (m, DMF, 700H), 1.49–1.42 (m, 9H, rotamers). SEC: M_n=13600 g/mol, M_w=21500 g/mol kDa, PDI=1.58 (PMMA standards).

2.2.3 Simulation Studies

Lognormal polymer distributions were simulated using the Statistics Toolbox in MATLAB® (R2012 A). Solutions to the set of differential equations (Eqs. (2.2), (2.3) and (2.5)) were solved numerically in MATLAB using a non-stiff ordinary differential equation solver (ode45) using simulated lognormal weight-fraction distributions for the initial concentrations of each polymeric species.

2.2.4 Degradation Studies

*Degradation of oligomers **2.1d–2.4d**.* Acetylated oligomers **2.1a-2.4a** were Boc-deprotected using the same procedures described above to yield compounds **2.1d-2.4d**. Deprotected oligomer (10 mg) was dissolved in CH_2Cl_2 and washed with a 1:1 mixture of brine:1 M citric acid. The product was then re-extracted from the aqueous layer 5 times with CH_2Cl_2. The combined organic layers were dried over $MgSO_4$, filtered, and concentrated *in vacuo.* The product was then taken up in 1 mL of 0.1 M phosphate buffer (D_2O):acetone-d_6 (3:2) preheated to 37˚C and filtered through a Promax® PTFE membrane (0.22 *μm).* The filtered solution was then incubated at 37˚C using an INOVA variable temperature controller calibrated using ethylene glycol. ^{1}H NMR spectra were recorded at 3 min intervals over a period of 4 hours. Following depolymerization, the pH of the solution was tested to ensure that the sample did not fall outside of the buffer region during the degradation process. The extent of depolymerization was quantified by integrating the methyl peak of the *N,N'*-dimethylimidazolidinone degradation product relative to the $(CHD_2)(CD_3)CO$ in the sample. The plateau region corresponding to 100% degradation was defined as the region in which the mean fluctuation between successive integral values was less than or equal to 2%. Oligomer degradation data was treated by non-linear regression and fit to the appropriate form of Eq. (8) to assess the degradation kinetics.

*Degradation of polymers **2.6** and **2.7**.* Polymer (10 mg) was dissolved in 1 mL of 1:1 TFA:CH_2Cl_2 and stirred at room temperature for 2 h. The solvent was blown off and the product was taken up in CH_2Cl_2 and washed with a 1:1 mixture of brine:1 M citric acid. The deprotected polymer was then re-extracted from the aqueous layer 5 times with

CH_2Cl_2. The combined organic layers were dried over $MgSO_4$, filtered, and concentrated *in vacuo.* The product was then taken up in 1 mL of 0.1 M phosphate buffer (D_2O):acetone-d_6 (3:2) preheated to 37˚C and filtered through a Promax® PTFE membrane (0.22 *μm).* The filtered solution was then incubated at 37˚C using an INOVA variable temperature controller calibrated using ethylene glycol. ^{1}H NMR spectra were recorded at 5 min intervals over a period of 8 hours. Following depolymerization, the pH of the solution was tested to ensure that the sample did not fall outside of the buffer region during the degradation process. The extent of depolymerization was quantified by integrating the methyl peak of the *N,N'*- dimethylimidazolidinone degradation product relative to the $(CHD_2)(CD_3)CO$ in the sample. The plateau region corresponding to 100% degradation was defined as the region in which the mean fluctuation between successive integral values was less than or equal to 5%. Polymer degradation data was treated by non-linear regression and fit to the self-immolative degradation model (Eqs. (2), (3) and (5)) to assess the degradation kinetics.

2.2.5 Statistics

Nonlinear least-squares regression was performed using a Gauss-Newton algorithm contained within the R stats package. Unless otherwise noted, the presented data represent the average plus or minus the standard deviation determined through triplicate measurement.

2.3 Results and Discussion

2.3.1 Choice of Model System

The chemical structure of our previously reported linear self-immolative polycarbamate derived from alternating *N,N'*-dimethylethylenediamine and 4-hydroxybenzyl alcohol-based spacers is shown in Figure 2.1a.[37] Selective removal of the *N-tert*-butoxycarbonyl (Boc) end-cap reveals a terminal amine that cyclizes to form *N,N'*-dimethylimidazolidinone, exposing a phenol, which then spontaneously undergoes 1,6-elimination followed by a decarboxylation to regenerate an amine on the polymer terminus. This cascade of alternating cyclization, 1,6-elimination, and decarboxylation reactions is repeated along the length of the polymer backbone until complete

depolymerization of the polymer into *N,N'*-dimethylimidazolidinone, 4-hydroxybenzyl alcohol, and CO_2 occurs. This linear polymeric framework was selected as the model system for the kinetic study as the cyclization of *N,N'*-dimethylethylenediamine spacers is well studied and occurs over a moderate time frame under physiological conditions.[48] Additionally, the polymer is sufficiently stable as a trifluoroacetic acid (TFA)-salt following end-cap removal. As a result, end-cap removal can be effectively decoupled from the degradation of the polymer backbone, allowing the kinetics of self-immolation to be studied independent from the end-cap removal.

2.3.2 Oligomer Synthesis

In order to test the effect of chain length on the kinetics of linear self-immolative degradation, a series of monodisperse oligomers were synthesized using a convergent iterative scheme (Scheme 2.1). The use of monodisperse oligomers was driven by the fact that chain length and polydispersity are inherently difficult to control in the previously reported polycondensation of the model polymer. The use of a monodisperse sample set also eliminates any competing effects of polydispersity on the overall degradation kinetics, thereby allowing for a more accurate assessment of the influence of chain length on self-immolative degradation. A monomer and three oligomers, dimer, tetramer, and octamer, were prepared using a modified route used to synthesize the model polymer.[37] As in the previously reported monomer synthesis,[37] a Boc group was selected as a protecting group and end-cap for the amine termini of the oligomers. An acetyl protecting group was chosen for the hydroxyl termini of the oligomers because it can be selectively removed in the presence of carbamates and can tolerate TFA deprotections of the Boc group.[41] As shown in Scheme 2.1, the previously reported unactivated monomer (**2.1b**)[37] was reacted with acetyl chloride to provide the acetyl-protected monomer (**2.1a**). The Boc group of **2.1a** was then removed by treatment with 1:1 TFA:CH_2Cl_2 to provide monomer **2.1d**. The monomer **2.1d** was then reacted with the 4-nitrophenyl carbonate-activated monomer (**2.1c**)[37] to afford the acetyl-protected dimer (**2.2a**). From here a convergent, iterative strategy was employed in which the acetyl-protected oligomers (**2.2a,2.3a**) were treated with $LiOH \cdot H_2O$ in 3:2 THF:H_2O to hydrolyze the acetate and provide the unactivated alcohol species (**2.2b,2.3b**). These compounds were then

activated with 4-nitrophenyl chloroformate to afford the activated carbonate species (**2.2c,2.3c**), which were subsequently reacted with the Boc-deprotected acetyl compounds (**2.2d,2.3d**) in the presence of DIPEA and DMAP to produce the acetyl-protected oligomers (**2.3a,2.4a**). For example, the tetramer **2.3a** was obtained from the reaction of dimer **2.2c** with dimer **2.2d**, while the octamer **2.4a** was obtained from tetramer **2.3c** and **2.3d**.

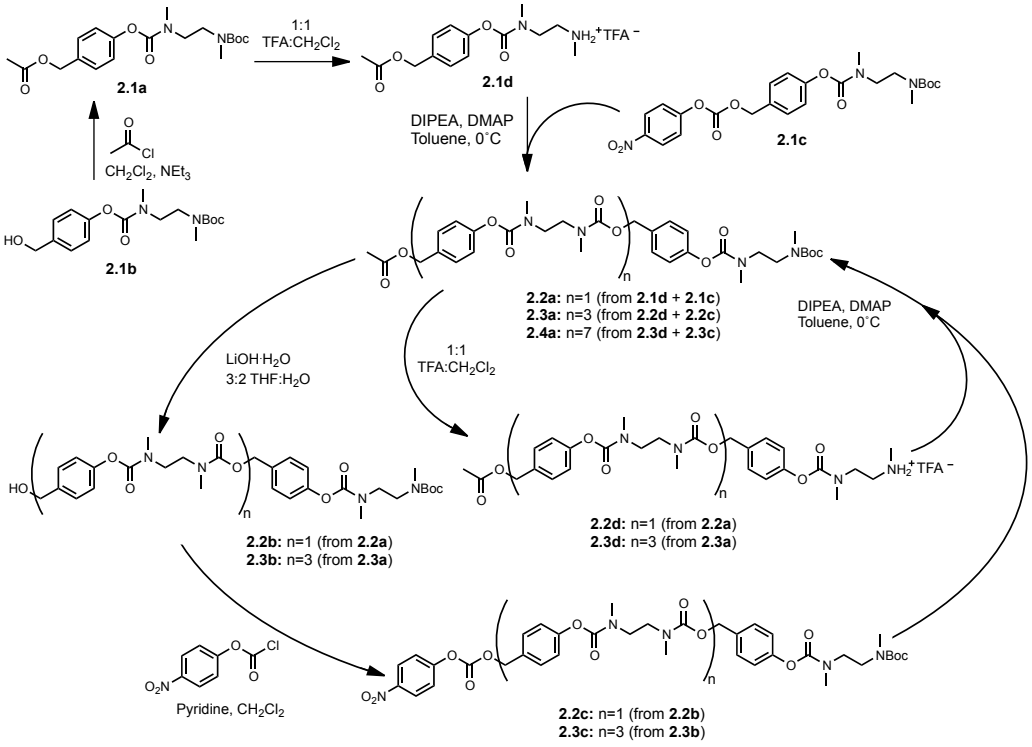

Scheme 2.1: Iterative convergent synthesis of monodisperse oligomers

The oligomers were characterized by NMR spectroscopy, IR spectroscopy, SEC, and HPLC. Notably, the absence of *N,N'*-dimethylimidazolidinone that would be formed from the competing intramolecular cyclization reaction during each coupling step was assessed using ^{1}H NMR spectroscopy. NMR spectra for the acetylated compounds **2.1a**-**2.4a** showing the evolution of oligomeric peaks relative to the Boc-terminus as well as the absence of *N,N'*-dimethylimidazolidinone are shown in Figure 2.3. Due to the presence of many carbamate rotameric centres, standard ^{13}C NMR analysis could not be used to assess purity in each of the oligomer samples above the monomer generation. Therefore, the absence of different oligomeric species from each sample was assessed

using reverse phase HPLC analysis and it was demonstrated that the purity of each oligomer was > 95% (Appendix B). Ensuring the absence of both cyclic urea and unwanted oligomer contaminants was crucial to allow proper experimental model validation, as the presence of cyclic urea would result in an overestimation of the degradation rate and the presence different oligomer species would invalidate the assumption of monodispersity in the subsequent model development and validation. As shown in Figure 2.2a, SEC traces for **2.2a**, **2.3a**, and **2.4a** exhibited monomodal distributions and very narrow polydispersities ranging from 1.02-1.03. The number average molecular weights for **2.2a**, **2.3a**, and **2.4a** were 875, 1940, and 3660 g/mol relative to PMMA standards, in comparison with the theoretical molecular weights of 644, 1173, and 2230 g/mol, respectively.

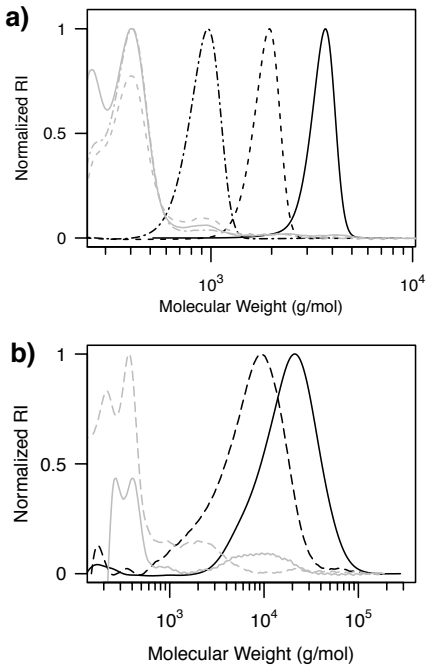

Figure 2.2: Size exclusion chromatograms of compounds 2.2a (- ˙ -), 2.3a (- - -), and 2.4a (—) prior to the removal of the Boc-protecting group (black) and after complete degradation (grey). (b) Size exclusion chromatograms of polymers 2.6 (- - -) and 2.7 (—) before (black) and after degradation (grey). All chromatograms acquired at a sample concentration of 5 mg/mL and calibrated using PMMA standards.

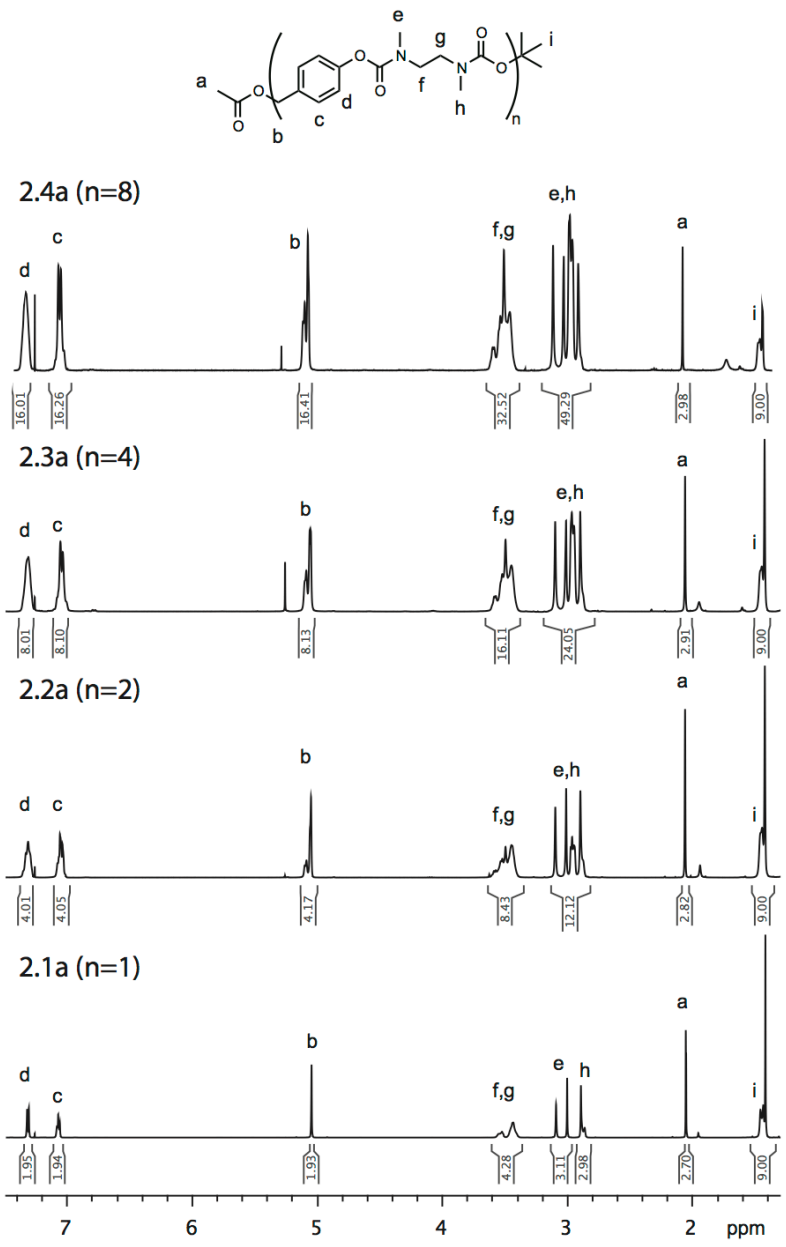

Figure 2.3: ^{1}H NMR spectra of monodisperse oligomers 2.1a-2.4a showing the evolution of oligomeric peaks relative to the Boc-terminus and the absence of *N,N'*-dimethylimidazolidinone during the iterative convergent synthesis (600 MHz, $CDCl_3$)

2.3.3 Polymer Synthesis

In addition to the oligomers that possessed exact molecular weights, it was also a goal of this work to demonstrate the dependence of the depolymerization time on chain length in longer polymeric systems. As shown in Scheme 2.2, the polycarbamate can be synthesized from the activated carbonate **2.5**,[37] along with **2.1c** as an end-cap in the presence of a tertiary amine base. In order to obtain a reference set of polymers displaying varying chain lengths, a two-level, four factor designed experiment was conducted to investigate the effects of end-cap ratio, temperature, reaction duration, and the nucleophilicity of the amine base on the degree of polymerization in the previously reported polycondensation of the model polymer (Scheme 2.2).[37] The results of this study (Appendix D) were used to select adequate polymerization conditions to synthesize both a low and high molecular weight polymer. Polymer **2.6** was synthesized using the previously reported polymerization conditions[37] and purified by dialyses in DMF against a 6000-8000 g/mol molecular weight cutoff (MWCO) membrane to yield a polymer with a M_n of 5250 g/mol and a PDI of 1.47 (Figure 2.2b). Analysis by ^{1}H NMR spectroscopy revealed a monomer to end-cap ratio of 25:1, which was similar to the monomer feed ratio of 20:1. Polymer **2.7** was synthesized using similar conditions to those previously reported except that a lower end-cap ratio was used (0.01 equiv), NEt_3 was used instead of DIPEA, and the polymerization was carried out at 0˚C for a longer period of time. Polymer **2.7** was purified by dialyses in DMF against a 25000 g/mol MWCO membrane to yield a polymer with a M_n of 13600 g/mol and a PDI of 1.58 (Figure 2.2b). Analysis by ^{1}H NMR spectroscopy revealed a monomer to end-cap ratio of 101:1, which was similar to the monomer feed ratio of 100:1.

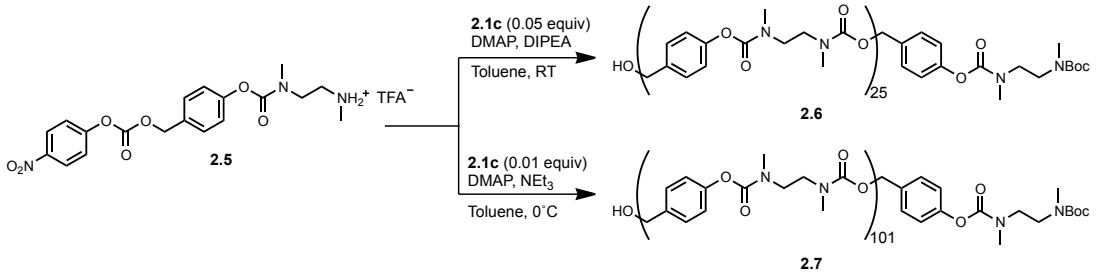

Scheme 2.2: Synthesis of Polymers 2.6 and 2.7

2.3.4 Linear Self-Immolative Degradation Model

As part of this work, we aimed to probe the kinetics of linear self-immolative degradation using computational simulations. Despite the growing popularity of self-immolative polymers, there has been very little work conducted into developing models that describe the self-immolative degradation process. It has long been inferred that the degradation kinetics of self-immolative polymers are dictated by the kinetics of the monomer repeat units, yet no conclusive study has been conducted to relate the two on a theoretical and quantitative basis. The kinetics of linear self-immolative degradation have been previously explored on a number of oligomers based on 1,4 and 1,6-elimnation spacers and on elongated cyclization spacers, however, analysis of the degradation kinetics has either been qualitative or limited to the fitting of higher order models.[44,46,47] The Shabat group have shown that the kinetics between successive dendrimer generations in systems derived from cyclization and elimination spacers approximately follows first-order cyclization kinetics and used this observation to derive theoretical release models for second generation dendrons.[21,30] In this work we also sought to build off the promising results observed for dendrimer systems and derive a theoretical model for the degradation of linear self-immolative polymers that relates monomer kinetics to the overall kinetics of polymer degradation and use this model to predict and explain experimental degradation trends.

The linear self-immolative degradation of the model polymer may be described as a sequence of elementary reactions proceeding from the chain terminus. Such a model is mechanistically similar to the end-wise depolymerization models that have been developed for linear protein systems to describe microtubulin disassembly.[49,50] Assuming that the rate of cyclization is significantly slower than the rate of 1,6-elimination, the degradation of the model polymer can be treated as a series of first-order intramolecular cyclization reactions between successive chain lengths as follows:

$$P_n \underset{k_n}{\overset{-M}{\rightarrow}} P_{n-1} \underset{k_{n-1}}{\overset{-M}{\rightarrow}} \cdots \underset{k_2}{\overset{-M}{\rightarrow}} P_1 \underset{k_1}{\overset{-M}{\rightarrow}} M \tag{2.1}$$

where P_i is the polymer chain of length *i*, M is the released monomer unit, and k_i is the rate of intramolecular cyclization for a terminal cyclization spacer on a polymer chain of length *i*. This assumption is valid, as the rate of 1,6-elimination is generally much faster than the rate of intramolecular cyclization, especially when followed by a thermodynamically favourable carbamate decarboxylation reaction.[46,51] 1,6-eliminations in hydroxybenzyl alcohol-based system are typically quite rapid with complete conversion to the quinone methide occurring in several seconds,[46] while the cyclization of *N,N'*-dimethylethylenediamine in aqueous systems is much slower with a previously reported half-life of 36.3 min at pH 7.4.[48] In the simplest case, the intramolecular cyclization rate constant is independent of chain length and Eq. (2.1) can be reduced to the following set of linear ordinary differential equations:

$$\frac{d[P_n]}{dt} = -k[P_n] \tag{2.2}$$

$$\frac{d[P_i]}{dt} = k([P_{i+1}]-[P_i]) \quad \forall\, i \leq n-1 \tag{2.3}$$

where [Pi] is the concentration of polymer chains of length *i* and *t* is the time elapsed in the degradation process. This assumption has been previously shown to hold true for dendritic systems[21] and is later validated through our experimental systems. Using an integrating factor, Eqs. (2.2) and (2.3) can be solved for all chain lengths and generalized into the following form:

$$[P_{n-i}] = e^{-kt} \sum_{j=0}^{i} \frac{(kt)^{i-j}}{(i-j)!} [P_{n-j}]_0 \tag{2.4}$$

Since *N,N'*-dimethylimidazolidone and 4-hydroxybenzyl alcohol are ultimately released upon every cyclization, the concentration of either released monomer unit can be used as a measure of polymer degradation as follows:

$$\frac{d[M]}{dt} = k \sum_{i=1}^{n} P_i \tag{2.5}$$

$$D(t)=\frac{M(t)}{M_\infty}=\frac{M(t)}{\sum_{i=1}^{n} i[P_i]_0} \tag{2.6}$$

where D(t) is the relative degradation of the self-immolative polymers at time t. Although not a true measure of molecular weight, the trend in the appearance of degradation byproducts is inversely related to the number average molecular weight. Tracking the degradation in this manner also allows for a more robust method of practical measurement in that small changes in the concentration of degradation products can be measured with a higher degree of accuracy compared to small changes in M_n or M_w.

In the case of initial monodispersity, Eqs. (2.2), (2.3) and (2.5) can be solved algebraically to yield the following expression for the evolution of degradation products during the linear self-immolative process:

$$M(t)=[P_n]_0\left(n-e^{-kt}\sum_{i=1}^{n}\sum_{j=1}^{i}\frac{(kt)^{j-1}}{(j-1)!}\right) \tag{2.7}$$

Where n is the chain length of the initial monodisperse polymer species. Substituting into Eq. (2.6):

$$D(t)=\frac{M(t)}{n[P_n]_0}=[P_n]_0\left(1-e^{-kt}n^{-1}\sum_{i=1}^{n}\sum_{j=1}^{i}\frac{(kt)^{j-1}}{(j-1)!}\right) \tag{2.8}$$

2.3.5 Mixed-Mode Degradation Kinetics

Analysis of the system of differentials describing the linear self-immolative degradation process reveals a mixed-mode kinetic phenomenon unique to linear self-immolative polymers. Unlike traditional biodegradable polyesters that display pseudo first-order degradation kinetics, linear self-immolative polymers exhibit mixed-mode kinetics in which the degradation displays an initial pseudo zero-order phase followed by a gradual transition towards first-order behavior over the course of degradation. This theoretical behavior is consistent with our previous experimental findings for the degradation of linear self-immolative polymer systems that required fitting of a modified first-order

model to account for the sharp rise in the initial pseudo zero-order domain.[39] Such behavior can be explained by considering that the concentration of polymer chains is not affected until complete degradation of a given chain into monomer units occurs (Figure 2.4). This causes the concentration of polymer chains to remain relatively constant during the initial stages of degradation, thereby imparting pseudo zero-order characteristics to Eq. (2.5). The length and duration of the apparent zero-order phase is dependent on PDI, but also on the length of polymer chains, as the resistance to first-order behavior (polynomial term in Eq. (2.4)) is enhanced by the presence of high molecular weight species.

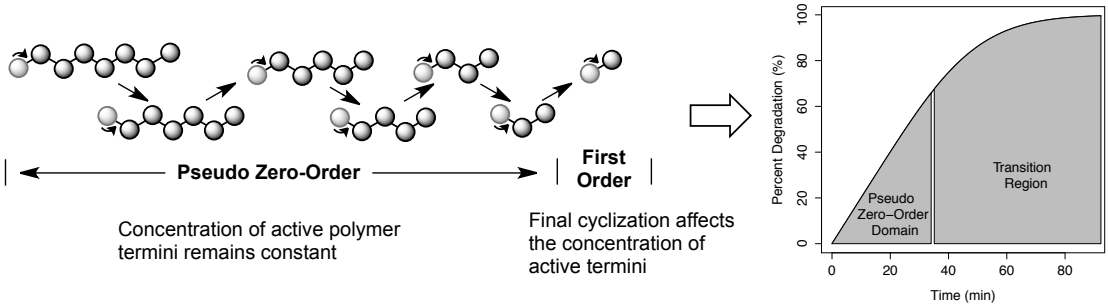

Figure 2.4: Mixed-mode degradation profile for the degradation of linear self-immolative polymers involving an initial pesudo zero-order domain followed by a gradual transition towards first-order behaviour

2.3.6 Simulation Studies

Prior to the experimental investigation of the degradation kinetics for the oligomer and polymer samples, computational studies were conducted to investigate the effects of degree of polymerization (r_n) and PDI on the kinetics of self-immolative degradation. A series of artificial polymer distributions with varying number average chain lengths (Figure 2.5a) and polydispersities (Figure 2.5c) were simulated on a lognormal basis according to the following probability density function:

$$n(r)=\left(\frac{1}{2\pi}\right)^{\frac{1}{2}}\frac{1}{\sigma_n}\exp\left(\frac{-(r-r_n)^2}{2\sigma_n^2}\right) \tag{2.9}$$

$$\sigma_n = r_n(\text{PDI}-1)^{\frac{1}{2}} \tag{2.10}$$

where r is chain length, n(r) is the number fraction of chains of length r, r_n is the number average chain length, σ_n is the standard deviation, and PDI is the polydispersity index.

The set of linear differentials describing the self-immolation process (Eqs. (2.2), (2.3) and (2.5)) were solved numerically on the artificial polymer distributions using the experimentally determined rate constant for intramolecular cyclization of 1.61×10^{-1} min^{-1} (Figure 2.5). Using the times required to reach 50% (t_{50}) and 95% (t_{95}) degradation, the computational simulations suggest that the overall degradation time is proportional to r_n at a fixed PDI. Analysis of the effect of PDI, however, is slightly more complicated. The mixed-mode degradation kinetics are most pronounced for monodisperse samples and become skewed as PDI is increased (Figure 2.5d). This can be explained by considering that the fraction of both low and high molecular weight species increases as PDI is raised at a fixed r_n. Consequently, the degradation kinetics become more heavily weighted towards both small and large chain lengths, which results in a minor increase to the relative rate of degradation early in the process and a substantial reduction to the rate during the latter stages. This trend is evidenced in Figure 2.5 and Table 2.1, as increases to the PDI resulted in a minor increase to the time required to reach 50% degradation and a substantial increase to the time required to reach complete degradation.

Table 2.1: Summary of simulation studies investigating the effect of r_n and PDI on the kinetics linear self-immolative degradation

r_n	PDI	t_{50} (min)[a]	t_{95} (min)[b]
10	-	37.1	161.5
20	-	71.6	309.5
30	-	106.1	458.3
40	-	140.8	608.5
20	1.00	62.3	137.2
-	1.25	65.4	211.7
-	1.50	69.8	281.7
-	1.75	74.2	351.4
-	2.00	78.7	422.5

[a] – time required to reach 50% degradation
[b] – time required to reach 95% degradation

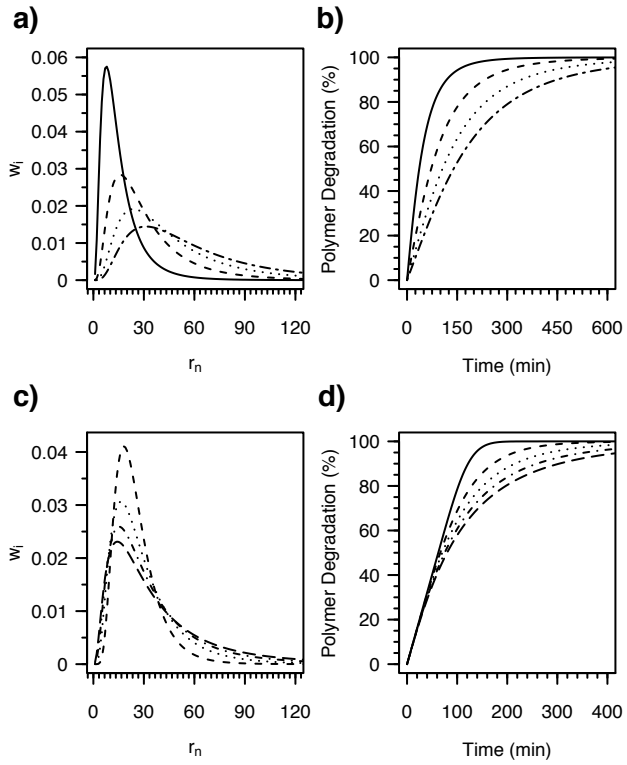

Figure 2.5: Calculated influence of chain length (a and b) and polydispersity index (c-d) on the rate of self-immolative degradation. Initial weight fraction (wi) distributions are shown in (a and c) and the resultant degradation plots are shown in (b and d). (a and b): PDI=1.6, r_n =10 (—), 20 (- - -), 30(···), 40(– · –). (c and d): r_n=10, PDI=1(—), 1.25(- - -), 1.5(···), 1.75 (– · –), 2(—). All distribution and kinetic plots were derived from numerical solutions to Eqs. (2.2), (2.3) and (2.5) with k=1.61 × 10^{-1} min^{-1}.

2.3.7 Oligomer Degradation Kinetics

Based on the promising results of the simulation studies, the degradation kinetics for the oligomer samples were investigated and compared to the expected theoretical behaviour. The solution degradation kinetics for compounds **2.1d-2.4d** were studied by ^{1}H NMR spectroscopy in 3:2 0.1 M pH 7.4 phosphate buffer (D_2O):acetone-d_6 at 37˚C (Scheme 2.3). The Boc protecting groups of compounds **2.1a-2.4a** were cleaved by treatment with

TFA/CH_2Cl_2 and the solvent was removed to afford compounds **2.1d-2.4d**. The oligomer-TFA salts were then washed with 1 M citric acid/brine and concentrated under reduced pressure to remove any residual TFA immediately prior to dissolving the resulting oligomers in 1 mL of buffer:acetone. Incorporation of the wash step was necessary to ensure the pH was maintained at 7.4 during the degradation process. Citric acid was selected as its pKa (3.15) was sufficiently high to remove the residual TFA, but also acidic enough to ensure no premature degradation occurred during the wash step (Figures C1-C2). The relative degradation of the oligomeric species was quantified and assessed by integrating the methyl peak of *N,N'*-dimethylimidazolidinone relative to residual solvent peaks in the samples. The complete degradation of all oligomer species except the monomer was assessed by SEC before and after the degradation studies. Model validation and kinetic analysis were carried out by fitting the degradation model to the oligomeric degradation profiles. As stated beforehand, application of the linear self-immolative degradation model to a monodisperse sample set allows for an algebraic solution to the system of differentials (Eq. (2.8)) and requires no approximations in determining the initial polymer distribution relative to chain length. This is particularly important in comparing the fitted monomer cyclization rate constant between oligomer samples of different lengths, as any approximations in the calculation of chain length would alter the form of the nonlinear degradation model and introduce an artificial dampening or inflation to the rate constant.

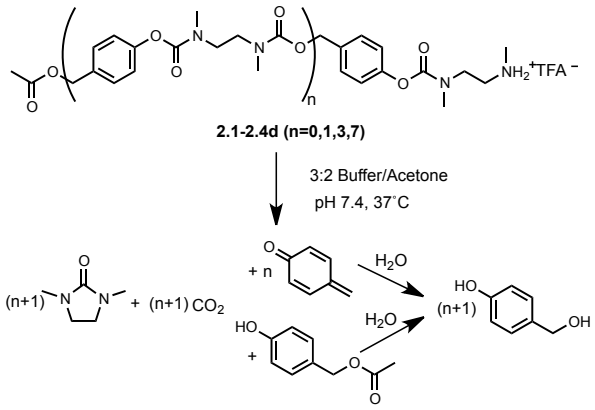

Scheme 2.3: Degradation of compounds 2.1-2.4d to form dimethylimidazolidinone and 4-hydroxybenzyl alcohol

As shown in Table 2.2 and Figure 2.6, the relative rate of degradation was inversely proportional to the length of the oligomer species, with longer oligomers requiring more time to degrade than shorter ones. This trend was quantified using the time to reach 50% degradation (t_{50}), which was found to be proportional to the size of the oligomer species within experimental error (Tabe 2.2). Fitting the degradation data for each oligomer species to the respective solutions to Eq. (2.8) using non-linear regression provided reasonable fits to all of the experimental data with significant parameter estimations (P<0.001) and low residual standard errors (<5%) (Appendix E). Additionally, the fitting of all oligomeric species past the monomer stage to Eq. (2.8) offered better fits to the experimental data than the standard first-order degradation model (Eq. (2.8), n=1), evaluated based on the Akaike information criterion (AIC) and Bayesian information criterion (BIC) (Appendix E). More importantly, however, the monomer cyclization rate constants determined through non-linear regression (Table 2.2) displayed no significant difference based on a one-way ANOVA test (P=0.82), thereby validating the linear self-immolative degradation model relating monomer kinetics to polymer degradation.

Table 2.2: Kinetic parameters for the degradation of oligomers 2.1d-2.4d

Compound	k $\times 10^1$ (min^{-1})	t_{50} (min)[a]
2.1d	1.61 ± 0.37	4.5 ± 0.9
2.2d	1.48 ± 0.10	8.1 ± 0.9
2.3d	1.60 ± 0.38	13.2 ± 1.7
2.4d	1.73 ± 0.34	23.9 ± 4.3

[a] – time to reach 50% degradation

Complete degradation of the starting oligomers to the intended degradation byproducts was observed by ^{1}H NMR spectroscopy (Figures C3-C6) and verified by SEC analysis (Figure 2.2a). The half-life for monomer cyclization of 4.5 min determined in this study was significantly shorter than the previously reported half-life of 35 min.[37] The large discrepancy in the cyclization kinetics can likely be attributed to insufficient buffering of residual TFA from the Boc deprotection step in the previously reported case, as we found that the half-life was significantly longer and pH values of the solution measured using a microelectrode were lower when the citric acid wash was not performed. Use of the citric acid wash led to reproducible data for all oligomers, as demonstrated in triplicate experiments (Appendix E).

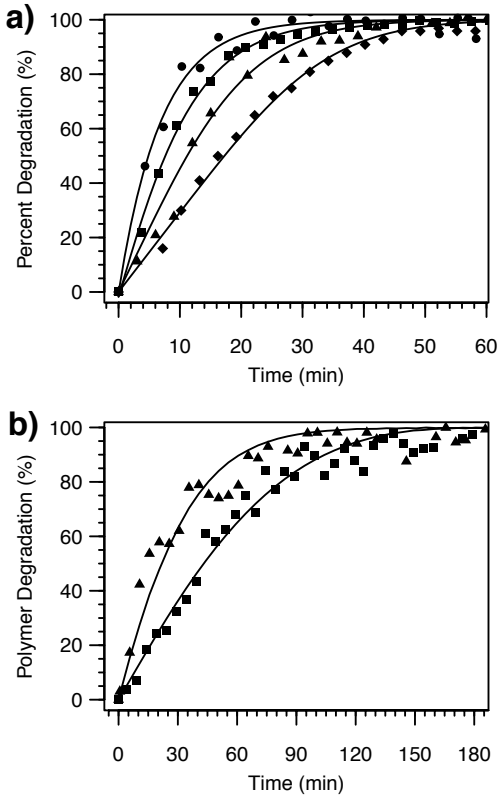

Figure 2.6: Degradation kinetics of compounds 2.1d-2.4d, as measured by ^{1}H NMR spectroscopy in 0.1 M phosphate buffer (D_2O):acetone-d_6 (3:2) at 37˚C. Representative samples from triplicate runs of 2.1d (●), 2.2d (■), 2.3d (▲), 2.4d (◆). Solid lines correspond to the regressed fits of Eq. (2.8) to each generation of oligomer (n=1,2,4,8). (b) Degradation kinetics of polymers 2.6 (▲) and 2.7 (■), as measured by ^{1}H NMR spectroscopy in 0.1 M phosphate buffer (D_2O):acetone-d_6 (3:2) at 37˚C. Overlayed lines correspond to the self-immolative model fits for both polymers.

2.3.8 Polymer Degradation Kinetics

The solution degradation kinetics of polymers **2.6** and **2.7** were investigated under the same conditions used for compounds **2.1d-2.4d** (Figure 2.1b). ^{1}H NMR spectroscopy supported complete degradation of the polymers into the expected degradation products (Figures C7-C8), however, SEC analysis revealed the presence of a small fraction of

polymers **2.6** (M_n=2020 g/mol, PDI=1.26) and **2.7** (M_n=8000 g/mol, PDI=1.07) remaining after degradation (Figure 2.2b). Similar to other studies involving linear self-immolative polymers, this non-degraded fraction is likely related to the presence of non-end-capped cyclic oligomers that are formed during polymerization.[38-40] These peaks were neglected in the treatment of the degradation data as fractional analysis revealed that they were present at less than 3 wt% in the initial distributions.

As shown in Figure 2.6b, the polymer degradation times were proportional to M_n, with polymer **2.6** reaching 50% degradation by 17.4 min and complete degradation by 150 min, while polymer **2.7** reached 50% degradation by 41.5 min and complete degradation by 200 min. These trends are in agreement with the differences in M_n and follow the trends depicted in Figure 2.5b, as polymer 2 displayed a 2.6-fold difference in M_n and required 2.4 times longer to reach 50% degradation. Based on the simulation results shown in Figure 2.5, the slight discrepancy between the relative differences in M_n and t_{50} can be attributed to the low molecular weight tailing observed for polymer **2.6**, which leads to an increased rate of degradation in the early stages of the self-immolation process. Although this slight tailing would have a minor influence on the degradation time, the determining factor in these studies was the large difference in M_n. Consequently, the results of this study indicate that altering the chain length is an effective means to tune the rate of degradation in linear self-immolative polymers involving cyclization spacers.

The degradation profile for polymers **2.6** and **2.7** were also fit to the self-immolative model using a modified non-linear regression algorithm in which the numerical solution to Eqs. (2.2), (2.3) and (2.5) was applied to the SEC chromatograms for both polymers. As shown in Figure 2.6b, the linear self-immolative model offered reasonable fits to the degradation data with standard errors of 6.6% and 4.7% and coefficients of determination (R^2) of 0.94 and 0.98 for polymers **2.6** and **2.7**, respectively (Figures E7-E8). The regressed monomer cyclization rate constants of 5.26×10^{-1} min^{-1} and 4.79×10^{-1} min^{-1} for polymers **2.6** and **2.7** were higher than expected based on the oligomer data but were within experimental error based on the spread of rate constants determined for the oligomer samples (Table 2.2). Hence, the self-immolative degradation model was an

adequate predictor of polymer degradation and offered quantitative evidence supporting the influence of chain length on the degradation time. Despite the promising results observed in this study, further investigation into the application of the linear self-immolative degradation model to polymeric profiles is necessary, as the degradation studies for polymer **2.6** and **2.7** were not performed in triplicate. In the absence of error measurements, no conclusive comments can be made on the potential influence of diffusive effects during self-immolative polymer degradation, which may limit the quality of the model fit available for higher molecular weight samples.

The one major limitation of the linear self-immolative degradation model developed in this work is the requirement for an a priori knowledge of the chain fraction distribution for a given polymer sample. Absolute molecular weight data could not be obtained for these polymers, thereby necessitating the use of relative molecular weight data in the fitting of the self-immolative degradation model. Although molecular weight data relative to PMMA offered a more reasonable approximation compared to polystyrene in DMF, the molecular weights reported in this study were still overestimated by a factor of at least 1.6 based on the limited SEC data obtained for the monodisperse oligomers. Therefore, the rapid monomer cyclization rate constants determined through non-linear regression on the polymeric data were subject to an artificial inflation due to the use of relative molecular weight data. Work in our group is currently underway to extend the results and improve the fitting of the polymer degradation model to different systems to further broaden the applicability of the self-immolative degradation model as a means of predicting and explaining experimental degradation profiles.

2.4 Conclusions

In conclusion, chain length was shown as an alternate means to tune the rate of degradation in linear self-immolative polymers. In this work we presented a new convergent iterative synthesis of a set of monodisperse oligomers based on the previously reported linear self-immolative polymer backbone derived from alternating 4-hydroxybenzyl alcohol and *N,N'*-dimethylethylenediamine spacers. The degradation time of these oligomers in 0.1 M pH 7.4 phosphate buffered (D_2O):acetone-d_6 (3:2) was shown to be proportional to chain length within experimental error. This finding was then

extended to the polydisperse case using a set of polymers synthesized to display varying molecular weights. A theoretical model describing linear self-immolative degradation was also proposed and fit to the experimental degradation profiles to provide quantitative evidence supporting the influence of chain length on the rate of degradation. This model offers new insight to the kinetics of linear self-immolative degradation in systems involving cyclization spacers and provides a means of relating monomer kinetics to the relative rate of polymer degradation. In conjunction with rational monomer design, the controlled use of chain length should allow for two-dimensional tuning of the depolymerization times in linear self-immolative polymers and thus significantly expand the usefulness of these materials for diverse applications such as sensing and programmable release.

2.5 References

(1) Kulkarni, R. K.; Moore, E. G.; Hegyeli, A. F.; Leonard, F. J. *Biomed. Mater. Res.* **1971**, *5*, 169.

(2) Vert, M. *Biomacromolecules* **2005**, *6*, 538.

(3) Antheunis, H.; van der Meer, J.-C.; de Geus, M.; Heise, A.; Koning, C. E. *Biomacromolecules* **2010**, *11*, 1118.

(4) Esser-Kahn, A. P.; Odom, S. A.; Sottos, N. R.; White, S. R.; Moore, J. S. *Macromolecules* **2011**, *44*, 5539.

(5) Gao, W.; Chan, J. M.; Farokhzad, O. C. *Mol. Pharm.* **2010**, *7*, 1913.

(6) Zhao, C.; Nie, S.; Tang, M.; Sun, S. *Prog. Polym. Sci.* **2011**, *36*, 1499.

(7) Xin, Y.; Yuan, J. *Polym. Chem.* **2012**, *3*, 3045.

(8) Bauhuber, S.; Hozsa, C.; Breunig, M.; Göpferich, A. *Advanced Materials* **2009**, *21*, 3286.

(9) Meng, F.; Hennink, W. E.; Zhong, Z. *Biomaterials* **2009**, *30*, 2180.

(10) Wei, H.; Zhuo, R.-X.; Zhang, X.-Z. *Prog. Polym. Sci.* **2012**, *38*, 503.

(11) Zelzer, M.; Todd, S. J.; Hirst, A. R.; McDonald, T. O.; Ulijn, R. V. *Biomaterials Science* **2012**, *1*, 11.

(12) Wu, Q.; Wang, L.; Yu, H.; Wang, J.; Chen, Z. *Chemical Reviews* **2011**, *111*, 7855.

(13) de Gracia Lux, C.; Joshi-Barr, S.; Nguyen, T.; Mahmoud, E.; Schopf, E.; Fomina, N.; Almutairi, A. *J. Am. Chem. Soc.* **2012**, *134*, 15758.

(14) Pasparakis, G.; Manouras, T.; Argitis, P.; Vamvakaki, M. *Macromol. Rapid Commun.* **2011**, *33*, 183.

(15) Fomina, N.; Sankaranarayanan, J.; Almutairi, A. *Adv. Drug Delivery Rev.* **2012**, *64*, 1005.

(16) Liu, G.; Liu, W.; Dong, C.-M. *Polym. Chem.* **2013**.

(17) Mejia, J. S.; Gillies, E. R. *Polym. Chem.* **2013**.

(18) Wong, A. D.; DeWit, M. A.; Gillies, E. R. *Adv. Drug Delivery Rev.* **2012**, *64*, 1031.

(19) Blencowe, C. A.; Russell, A. T.; Greco, F.; Hayes, W.; Thornthwaite, D. W. *Polym. Chem.* **2011**, *2*, 773.

(20) Peterson, G. I.; Larsen, M. B.; Boydston, A. J. *Macromolecules* **2012**, *45*, 7317.

(21) Amir, R. J.; Pessah, N.; Shamis, M.; Shabat, D. *Angew. Chem. Int. Ed.* **2003**, *42*, 4494.

(22) de Groot, F. M. H.; Albrecht, C.; Koekkoek, R.; Beusker, P. H.; Scheeren, H. W. *Angew. Chem. Int. Ed.* **2003**, *42*, 4490.

(23) Szalai, M. L.; Kevwitch, R. M.; McGrath, D. V. *J. Am. Chem. Soc.* **2003**, *125*, 15688.

(24) Amir, R. J.; Danieli, E.; Shabat, D. *Chem. Eur. J.* **2007**, *13*, 812.

(25) Sella, E.; Shabat, D. *Chem. Commun.* **2008**, 5701.

(26) Weinstain, R.; Sagi, A.; Karton, N.; Shabat, D. *Chem. Eur. J.* **2008**, *14*, 6857.

(27) Sella, E.; Shabat, D. *J. Am. Chem. Soc.* **2009**, *131*, 9934.

(28) Amir, R. J.; Shabat, D. *Chem. Commun.* **2004**, 1614.

(29) Shamis, M.; Lode, H. N.; Shabat, D. *J. Am. Chem. Soc.* **2004**, *126*, 1726.

(30) Perry, R.; Amir, R. J.; Shabat, D. *New J. Chem.* **2007**, *31*, 1307.

(31) Sagi, A.; Segal, E.; Satchi-Fainaro, R.; Shabat, D. *Bioorg. Med. Chem.* **2007**, *15*, 3720.

(32) Zhang, H.; Yeung, K.; Robbins, J. S.; Pavlick, R. A.; Wu, M.; Liu, R.; Sen, A.; Phillips, S. T. *Angew. Chem. Int. Ed.* **2012**, *51*, 2400.

(33) Weinstain, R.; Baran, P. S.; Shabat, D. *Bioconjugate Chem.* **2009**, *20*, 1783.

(34) Esser-Kahn, A. P.; Sottos, N. R.; White, S. R.; Moore, J. S. *J. Am. Chem. Soc.* **2010**, *132*, 10266.

(35) Seo, W.; Phillips, S. T. *J. Am. Chem. Soc.* **2010**, *132*, 9234.

(36) Sagi, A.; Weinstain, R.; Karton, N.; Shabat, D. *J. Am. Chem. Soc.* **2008**, *130*, 5434.

(37) DeWit, M. A.; Gillies, E. R. *J. Am. Chem. Soc.* **2009**, *131*, 18327.

(38) DeWit, M. A.; Beaton, A.; Gillies, E. R. *J. Polym. Sci. A Polym. Chem.* **2010**, *48*, 3977.

(39) Chen, E. K. Y.; McBride, R. A.; Gillies, E. R. *Macromolecules* **2012**, *45*, 7364.

(40) de Gracia Lux, C.; McFearin, C. L.; Joshi-Barr, S.; Sankaranarayanan, J.; Fomina, N.; Almutairi, A. *ACS Macro Lett.* **2012**, *1*, 922.

(41) DeWit, M. A.; Gillies, E. R. *Org. Biomol. Chem.* **2011**, *9*, 1846.

(42) Schmid, K. M.; Jensen, L.; Phillips, S. T. *J. Org. Chem.* **2012**, *77*, 4363.

(43) Robbins, J. S.; Schmid, K. M.; Phillips, S. T. *J. Org. Chem.* **2013**, 130222154949002.

(44) de Groot, F. M. H.; Loos, W. J.; Koekkoek, R.; van Berkom, L. W. A.; Busscher, G. F.; Seelen, A. E.; Albrecht, C.; de Bruijn, P.; Scheeren, H. W. *J. Org. Chem.* **2001**, *66*, 8815.

(45) Warnecke, A.; Kratz, F. *J. Org. Chem.* **2008**, *73*, 1546.

(46) Lee, H. Y.; Jiang, X.; Lee, D. *Org. Lett.* **2009**, *11*, 2065.

(47) Kevwitch, R. M.; Shanahan, C. S.; McGrath, D. V. *New J. Chem.* **2012**, *36*, 492.

(48) Saari, W. S.; Schwering, J. E.; Lyle, P. A.; Smith, S. J.; Engelhardt, E. L. *J. Med. Chem.* **1990**, *33*, 97.

(49) Kristofferson, D.; Karr, T. L.; Purich, D. L. *The Journal of biological chemistry* **1980**, *255*, 8567.

(50) Purich, D. L.; Karr, T. L.; Kristofferson, D. *Methods Enzymol.* **1982**, *85 Pt B*, 439.

(51) Meyer, Y.; Richard, J.-A.; Delest, B.; Noack, P.; Renard, P.-Y.; Romieu, A. *Org. Biomol. Chem.* **2010**, *8*, 1777.

Chapter 3

3 Progress Towards a Redox-Sensitive Self-Immolative Block Copolymer

3.1 Introduction

Self-immolative polymers have emerged as promising alternatives to traditional biodegradable polymers and offer new levels of control to the degradation process.[1-5] In contrast to traditional biodegradable materials, self-immolative polymers undergo end-to-end depolymerization through a cascade of intramolecular reactions upon response to a specific trigger (Figure 3.1a). This mechanism of degradation possesses several key advantages over the random hydrolytic cleavage of conventional biodegradable polymers as it permits stimuli-responsive degradation, allows for an amplified response to a triggering agent, and is regulated by the composition and architecture of the polymer backbone. To exploit these effects, a wide variety of self-immolative polymer backbones and architectures have been designed for signal amplification,[6-12] shape-memory,[13] protein labeling,[14] self-healing,[15] microfluidics,[16] and drug delivery applications[17-20] following their initial development in dendritic systems.[21-23]

Our group,[19,24-26] along with several others,[13-16,27-31] have focused on the design and synthesis of linear self-immolative polymers for biomedical applications. Although no longer monodisperse, linear self-immolative polymers can be synthesized in a single step and allow for a practical and scalable means of preparing self-immolative materials. At the current stage of development, these polymers can be grouped into four general classes based on the their mechanism of degradation and include those that degrade through: (i) 1,6-eliminations,[14,15,27,28] (ii) cyclization reactions,[24] (iii) alternating 1,6-eliminations and cyclizations,[19,20,26] or (iv) hemiacetal decompositions.[13,16,29-31] The predominant focus of our group over the last several years has been to develop linear self-immolative polymer backbones incorporating different cyclization spacers to control and tune the rate of self-immolative degradation. Compared to the systems that depolymerize through 1,6-eliminations and hemiacetal decompositions, cyclization based systems display slower degradation kinetics, making them ideal candidates for controlled release applications.

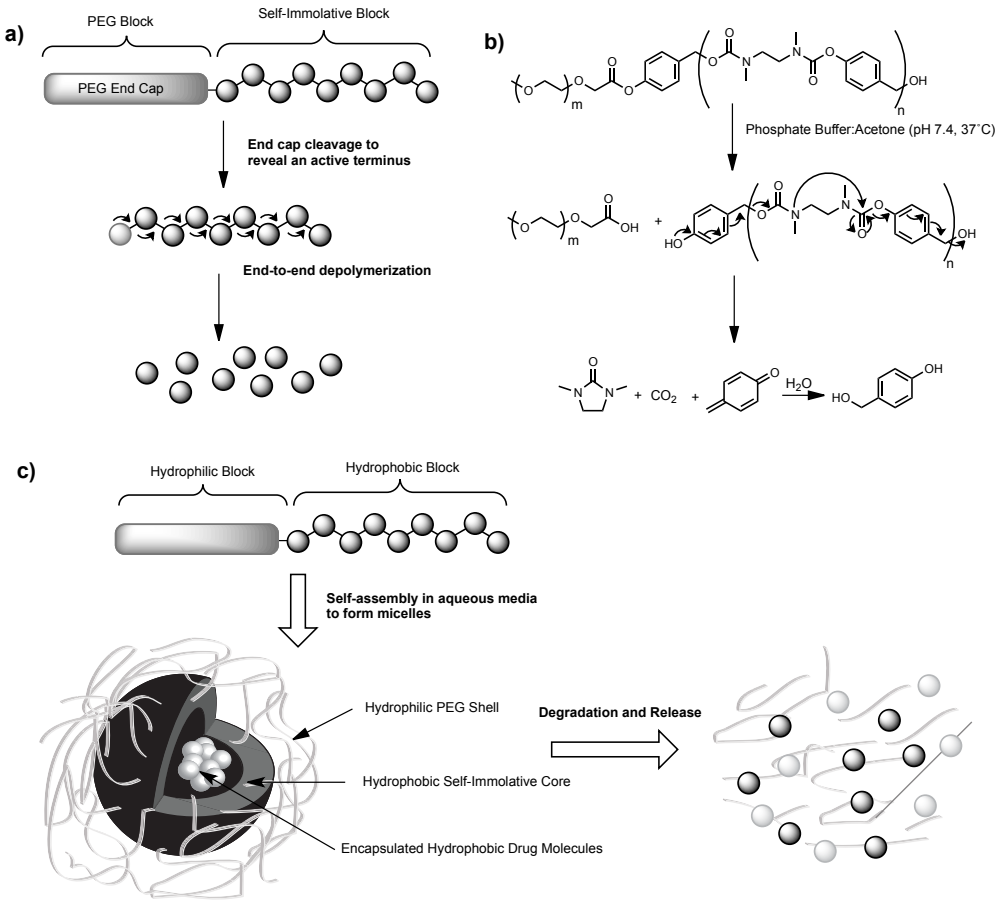

Figure 3.1: Linear self-immolative block copolymers synthesized using a poly(ethylene glycol) (PEG) end cap. (a) Generic diagram depicting the basic structure and mechanism of degradation. (b) Previously reported linear self-immolative block copolymer synthesized using a PEG acid end cap. (c) Diagram showing the self-assembly of amphiphilic linear self-immolative block copolymers in aqueous solution to form micelles for the encapsulation of hydrophobic drug molecules.

The investigation of self-immolative polymers incorporating cyclization spacers for controlled release applications is limited to two different and fundamentally distinct studies. Our group was the first to explore this potential using our initial polycarbamate backbone derived from alternating 4-hydroxybenzyl alcohol and *N,N'*-dimethylethylenediamine spacers.[19] Utilizing a poly(ethylene glycol) end-cap we were able to generate an amphiphilic self-immolative block copolymer that self-assembled in

aqueous solution to form micelles. Hydrolytic cleavage of the PEG end-cap following incubation in a pH 7.4 phosphate buffer at 37˚C initiated a cascade of alternating 1,6-elimination, decarboxylation, and cyclization reactions to degrade the polymer backbone over a period of approximately 30 days (Figure 3.1b). These block copolymer micelles were also demonstrated to encapsulate a model hydrophobic drug, nile red, and provide a controlled release throughout a 15 day period (Figure 3.1c). The major design flaw of this block copolymer system, however, was the incorporation of the PEG end-cap through a hydrolytically sensitive ester linkage. As a result, this design relied on a non-specific triggering factor to initiate degradation, and thus, failed to exploit the potential for stimuli-responsive degradation in self-immolative systems.

Using the same polycarbamate backbone, Almutairi and coworkers have recently generated hydrophobic nanoparticles incorporating UV and NIR sensitive end-caps through an emulsification method.[20] These nanoparticles were capable of encapsulating nile red, but demonstrated a significant burst release profile following exposure to UV/NIR light due to the poor aqueous solubility of the polymer backbone. Nevertheless, this system and its degradation products were well tolerated *in vitro* and displayed comparable non-toxicity to the FDA approved poly(lactic acid-*co*-glycolic acid) (PLGA). The results of these two studies have laid a promising groundwork for the use self-immolative polymers incorporating cyclization spacers for controlled release applications. However, additional development of functional self-immolative nanoparticles is necessary before this system can be effectively applied for the controlled release of hydrophobic molecules.

We herein report a follow-up study to our self-immolative block copolymer system to address the limitations of our initial design[19] (Figure 3.1). We first develop an alternative pathway to synthesize a low-cost alternative to our initial design using a PEG-succinic acid end cap and use this system to investigate the potential for self-assembly into different block copolymer morphologies. Furthermore, we propose and develop a reduction sensitive PEG-self-immolative block copolymer using a new modular approach in which backbone polymerization and PEG incorporation are decoupled from one another. This is accomplished using a *N*-methylaminoethanethiol end-cap during

polymerization and subsequently modifying this polymer with a PEG thiol derivative to produce a PEG-self-immolative block copolymer incorporating a disulfide linkage between both blocks. This strategy should offer more control over the synthesis of such block copolymer systems as it minimizes the steps required to incorporate the PEG end cap and permits a higher degree of control over the length of either block. Lastly, the degradation kinetics and self-assembly characteristics of this reduction sensitive block copolymer system are investigated under physiological conditions. This reduction sensitive PEG-self-immolative block copolymer system displays promise for the controlled release of hydrophobic drugs in mildly reducing environments. Such conditions are typically encountered in hypoxic tumour tissues, in which the concentration of the reducing agent glutathione is 4-fold higher than in healthy tissues,[32] or intracellularly where the concentration of glutathione is 0.5-1.0 mM compared to 2-20 μM in the extracellular environment.[33,34]

3.2 Experimental

3.2.1 General Procedures and Materials

All reagents were purchased from commercial suppliers and used without further purification unless otherwise noted. Anhydrous toluene was obtained from a solvent purification system using aluminum oxide columns. Dichloromethane (CH_2Cl_2), pyridine, triethylamine (NEt_3), and *N,N*-diisopropylethylamine (DIPEA) were distilled from CaH_2 immediately prior to use. Unless otherwise stated, all reactions were performed under an Ar atmosphere using flame-dried glassware. Column chromatography was performed using silica gel (0.040 – 0.063 mm particle size, 230 – 430 mesh). Thin layer chromatography (TLC) was carried out using EMD silica gel 60 F254 plates (20 cm × 20 cm, 250 *μm).* Deionized water was purified using a Millipore purification system. Dialyses were performed using Spectra/Por® regenerated cellulose membranes with either a 6000-8000 g/mol or 25000 g/mol molecular weight cutoff (MWCO).

^{1}H NMR spectra were obtained at 400 MHz or 600 MHz using a Varian INOVA spectrometer, while ^{13}C NMR spectra were obtained at 100 MHz using a Varian INOVA spectrometer. Chemical shifts are reported in ppm versus tetramethylsilane and

referenced to residual solvent signals of $CDCl_3$ (δ 7.26, 77.2), $(CD_3)_2CO$ (δ 2.05), or D_2O (δ 4.79). Coupling constants are expressed in Hz. High resolution mass spectrometry (HRMS) was performed on either a Finnigan MAT 8400 or a PE-Sciex API 365 mass spectrometer using electron impact (EI) or electrospray (ESI) ionization, respectively. Fourier transform infrared spectra were obtained using a Bruker Tensor 27 from CH_2Cl_2 films on KBr plates. Size exclusion chromatography (SEC) was carried out at a flow rate of 1 mL/min in *N,N*- dimethylformamide (DMF) with 10 mM LiBr and 1% (v/v) NEt_3 at 85˚C using a Waters 2695 separations module equipped with a Waters 2414 differential refractometer and two PLgel 5 *μm* mixed-D (300 mm × 7.5 mm) columns from Polymer Laboratories connected in series. SEC calibrations were performed using either poly(methyl methacrylate) (PMMA) or poly(ethylene glycol) (PEG) standards. Dynamic light scattering (DLS) data was obtained using a Zetasizer Nano ZS instrument from Malvern Instruments.

3.2.2 Synthesis

*Synthesis of Compound **3.1a**.* Poly(ethylene glycol) monomethylether (PEGMME) (2000 g/mol) (5.00 g, 2.5 mmol, 1.0 equiv) and succinic anhydride (2.50 g, 25 mmol, 10 equiv) were dissolved in 50 mL of dry CH_2Cl_2 and stirred at room temperature for 5 min. NEt_3 (7.0 mL, 50 mml, 20 equiv) and DMAP (0.32 g, 2.5 mmol, 1 equiv) were added and the solution was refluxed at 45˚C for 24 h. The reaction mixture was diluted with CH_2Cl_2 and poured over 1:1 1M HCl:brine. The product was re-extracted from the aqueous layer 5 times using CH_2Cl_2. The combined organic layers were dried over $MgSO_4$, filtered, and concentrated *in vacuo*. The crude product was then dissolved in 10 mL of DMF and dialyzed against DMF for 24 h (1 L, 1 solvent change) using a regenerated cellulose membrane (3500 g/mol MWCO). The contents of the dialysis membrane were then concentrated *in vacuo* and lyophilized to afford compound **3.1a** (4.12 g, 78%). ^{1}H NMR ($CDCl_3$, 600 MHz): δ 4.28-4.23 (m, 2H), 3.89-3.43 (m, 170H), 3.37 (s, 3H), 2.68-2.58 (m, 6H).

*Synthesis of Compound **3.1b**.* Compound **3.1b** was synthesized using an identical procedure to **3.1a** except that 5000 g/mol molecular weight PEGMME was used in place of 2000 g/mol molecular weight PEGMME. The quantities of reagents used were

PEGMME (5000 g/mol) (4.99 g, 1.0 mmol, 1.0 equiv), succinic anhydride (1.00 g, 10 mmol, 10 equiv), NEt_3 (2.0 mL, 20 mmol, 20 equiv), and DMAP (0.13 g, 1 mmol, equiv). The crude product was purified through dialysis against DMF using a regenerated cellulose membrane (3500 g/mol MWCO) and lyophilized to afford compound **3.1a** (4.34 g, 85%). ^{1}H NMR ($CDCl_3$, 600 MHz): δ 4.25-4.22 (m, 2H), 3.81-3.44 (m, 574H), 3.36 (s, 3H), 2.66-2.58 (m, 6H).

*Synthesis of Compound **3.2a**.* Compound **3.1a** (2.96 g, 1.41 mmol, 1.0 equiv) was dissolved in 30 mL of dry CH_2Cl_2. Pyridine (3.10 mL, 28.2 mmol, 20 equiv) and 4-nitrophenyl chloroformate (2.85 g, 14.2 mmol, 10 equiv) were successively added and the solution was stirred at room temperature for 24 h. The reaction mixture was diluted with CH_2Cl_2 and poured over 1:1 1M HCl:brine. The product was re-extracted from the aqueous layer 5 times using CH_2Cl_2. The combined organic layers were dried over $MgSO_4$, filtered, and concentrated *in vacuo* to a volume of approximately 5 mL. The crude product was then precipitated out of 300 mL of cold Et_2O to afford **3.2a** (2.80 g, 89%). ^{1}H NMR ($CDCl_3$, 600 MHz): δ 8.24 (m, 2H), 7.28 (m, 2H), 4.29-4.23 (m, 2H), 3.83-3.40 (m, 180H), 3.65 (s, 3H), 2.92-2.85 (m, 2H), 2.81-2.74 (m, 2H). MS (MALDI-TOF) $[M+Na]^+$: 1904.9.

*Synthesis of Compound **3.2b**.* Compound **3.2b** was synthesized using an identical procedure to **3.2a**. The quantities of reagents used were **3.1b** (4.08 g, 0.80 mmol, 1 equiv), 4-nitrophenyl chloroformate (1.61 g, 8.0 mmol, 10 equiv), and pyridine (1.74 mL, 16.0 mmol, 20 equiv). The crude product was precipitated out of 500 mL of cold Et_2O to afford **3.2b** (3.85 g, 92%). ^{1}H NMR ($CDCl_3$, 600 MHz): δ 8.25 (m, 2H), 7.29 (m, 2H), 4.28-4.26 (m, 2H), 3.77-3.48 (m, 591H), 3.36 (s, 3H), 2.92-2.88 (m, 2H), 2.81-2.76 (m, 2H).

*Synthesis of Compound **3.4a**.* Compound **3.2a** (2.72 g, 1.22 mmol, 1.0 equiv) was dissolved in 30 mL of dry CH_2Cl_2. NEt_3 (3.40 mL, 24.4 mmol, 20 equiv) and **3.3** (2.95 g, 12.4 mmol, 10 equiv) were successively added and the solution was stirred at room temperature for 24 h. The reaction mixture was diluted with CH_2Cl_2 and poured over 1:1 1M HCl:brine. The product was re-extracted from the aqueous layer 5 times using CH_2-

Cl_2. The combined organic layers were dried over $MgSO_4$, filtered, and concentrated *in vacuo* to a volume of approximately 5 mL. The crude product was then precipitated out of 300 mL of cold Et_2O to afford **3.4a** (2.17 g, 77%). ^{1}H NMR ($CDCl_3$, 600 MHz): δ 7.28 (m, 2H), 7.01 (m, 2H), 4.69 (s, 2H), 4.27-4.21 (m, 2H), 3.86-3.41 (m, 190H), 3.35 (s, 3H), 2.88-2.82 (m, 2H), 2.78-2.70 (m, 2H). MS (MALDI-TOF) $[M+Na]^+$: 2092.2.

*Synthesis of Compound **3.4b**.* Compound **3.4b** was synthesized using an identical procedure to **3.4a**. The quantities of reagents used were **3.2b** (4.08 g, 0.80 mmol, 1 equiv), **3.3** (1.88 g, 7.8 mmol, 10 equiv) and NEt_3 (2.20 mL, 15.7 mmol, 20 equiv). The crude product was precipitated out of 400 mL of cold Et_2O to afford **3.4b** (3.47 g, 86%). ^{1}H NMR ($CDCl_3$, 600 MHz): δ 7.30 (m, 2H), 7.03 (m, 2H), 4.70 (s, 2H), 4.28-4.24 (m, 2H), 3.82-3.47 (m, 590H), 3.37 (s, 3H), 2.89-2.84 (m, 2H), 2.78-2.74 (m, 2H).

*Synthesis of Compound **3.5a**.* Compound **3.4a** (2.12 g, 0.91 mmol, 1.0 equiv) was dissolved in 25 mL of 1% HCl in 3:1 EtOH:CH_2Cl_2 and stirred at room temperature for 1 h. The reaction mixture was diluted with CH_2Cl_2 and poured over saturated $NaHCO_3$. The product was re-extracted from the aqueous layer 5 times using CH_2Cl_2. The combined organic layers were dried over $MgSO_4$, filtered, and concentrated *in vacuo* to a volume of approximately 5 mL. The crude product was then precipitated out of 300 mL of cold Et_2O to afford **3.5a** (1.50 g, 75%). ^{1}H NMR ($CDCl_3$, 600 MHz): δ 7.36 (m, 2H), 7.06 (m, 2H), 4.65 (s, 2H), 4.29-4.23 (m, 2H), 3.83-3.40 (m, 181H), 3.36 (s, 3H), 2.90-2.83 (m, 2H), 2.79-2.73 (m, 2H). MS (MALDI-TOF) $[M+Na]^+$: 2066.1.

*Synthesis of Compound **3.5b**.* Compound **3.5b** was synthesized using an identical procedure to **3.5a**. The quantities of reagents used were **3.4b** (3.54 g, 0.67 mmol, 1 equiv). The crude product was precipitated out of 400 mL of cold Et_2O to afford **3.5b** (2.84 g, 81%). ^{1}H NMR ($CDCl_3$, 600 MHz): δ 7.29 (m, 2H), 7.02 (m, 2H), 4.70 (s, 2H), 4.28-4.23 (m, 2H), 3.81-3.45 (m, 558H), 3.36 (s, 3H), 2.89-2.83 (m, 2H), 2.79-2.72 (m, 2H).

*Synthesis of Compound **3.6a**.* Compound **3.5a** (0.50 g, 0.23 mmol, 1.0 equiv) was dissolved in 8 mL of dry CH_2Cl_2. Pyridine (0.40 mL, 4.6 mmol, 20 equiv) and 4-nitrophenyl chloroformate (0.47 g, 2.3 mmol, 10 equiv) were successively added and the

reaction mixture was stirred at room temperature for 24 h. The reaction mixture was diluted with CH_2Cl_2 and poured over 1:1 1M HCl:brine. The product was re-extracted from the aqueous layer 5 times using CH_2Cl_2. The combined organic layers were dried over $MgSO_4$, filtered, and concentrated *in vacuo* to a volume of approximately 3 mL. The crude product was then precipitated out of 80 mL of cold Et_2O to afford **3.6a** (0.44 g, 86%). ^{1}H NMR ($CDCl_3$, 600 MHz): δ 8.26 (m, 2H), 7.45 (m, 2H), 7.37 (m, 2H), 7.14 (m, 2H), 5.27 (s, 2H), 4.29-4.24 (m, 2H), 3.84-3.41 (m, 191H), 3.37 (s, 3H), 2.92-2.84 (m, 2H), 2.80-2.73 (m, 2H). MS (MALDI-TOF) $[M+Na]^+$: 2231.2.

*Synthesis of Compound **3.6b**.* Compound **3.6b** was synthesized using an identical procedure to **3.6a**. The quantities of reagents used were **3.5b** (0.99 g, 0.19 mmol, 1 equiv), pyridine (0.31 mL, 3.8 mmol, 20 equiv), and 4-nitrophenyl chloroformate (0.38 g, 1.9 mmol, 10 equiv). The crude product was precipitated out of 100 mL of cold Et_2O to afford **3.6b** (0.85 g, 83%).^{1}H NMR ($CDCl_3$, 600 MHz): δ 8.25 (m, 2H), 7.44 (m, 2H), 7.36 (m, 2H), 7.13 (m, 2H), 5.26 (s, 2H), 4.28-4.23 (m, 2H), 3.84-3.41 (m, 566H), 3.35 (s, 3H), 2.90-2.84 (m, 2H), 2.79-2.73 (m, 2H).

*Synthesis of Polymer **3.7a**.* Activated monomer **2.1c**[19] (1.02 g, 2.0 mmol, 1.0 equiv) was dissolved in 3 mL of 1:1 TFA:CH_2Cl_2 and stirred at room temperature for 2 h. The solvent was then removed under a stream of nitrogen in the fume hood prior to subjecting the reaction mixture three times to a repeat cycle of dilution with CH_2Cl_2 followed by concentration under reduced pressure to remove residual TFA and provide the deprotected monomer **2.5**.[19] End-cap **3.6a** (0.22 g, 0.10 mmol, 0.05 equiv) was added and the resulting mixture was dissolved in 8 mL of anhydrous toluene and stirred at room temperature for 5 min. NEt_3 (1.4 mL, 10 mmol, 5.0 equiv) and DMAP (62 mg, 0.50 mmol, 0.25 equiv) were sequentially added and the solution was then cooled to -15˚C and stirred for 24 h. The solution was then warmed to room temperature and stirred for an additional 36 h. The reaction mixture was diluted with CH_2Cl_2 and poured over 1:1 1 M citric acid:brine and extracted from the aqueous layer 5 times with CH_2Cl_2. The combined organic layers were then washed with saturated $NaHCO_3$ and extracted from the aqueous layer an additional 5 times with CH_2Cl_2. The combined organic layers were dried over $MgSO_4$, filtered, and concentrated *in vacuo*. The crude polymer was dissolved

in 2 mL of DMF and dialyzed against DMF for 24 h (200 mL, 1 solvent change) using a regenerated cellulose membrane (25000 g/mol MWCO). The contents of the dialysis membrane were then concentrated *in vacuo* and lyophilized to afford polymer **3.7a** (0.29 g, 40%). ^{1}H NMR indicated a degree of polymerization of ~ 18 by integrating the benzylic peak against the PEG end-cap. ^{1}H NMR ($CDCl_3$, 600 MHz): δ 7.44-7.28 (br, 36H), 7.14-7.00 (br, 35H), 5.16-5.04 (m, 35 H), 4.29-4.25 (m, 2H), 3.81-3.40 (m, 369H), 3.38 (s, 4H), 3.21-2.84 (m, 102H), 2.80-2.74 (m, 2H). SEC: M_n=3600 g/mol, M_w=5290 g/mol, PDI=1.47 (PEG standards).

*Synthesis of Polymer **3.7b**.* Activated monomer **2.1c**[19] (1.02 g, 2.0 mmol, 1.0 equiv) was dissolved in 3 mL of 1:1 TFA:CH_2Cl_2 and stirred at room temperature for 2 h. The solvent was then removed under a stream of nitrogen in the fume hood prior to subjecting the reaction mixture three times to a repeat cycle of dilution with CH_2Cl_2 followed by concentration under reduced pressure to remove residual TFA and provide the deprotected monomer **2.5**.[19] End-cap **3.6b** (0.51 g, 0.10 mmol, 0.05 equiv) was added and the resulting mixture was dissolved in 8 mL of anhydrous toluene and stirred at room temperature for 5 min. NEt_3 (1.4 mL, 10 mmol, 5.0 equiv) and DMAP (62 mg, 0.50 mmol, 0.25 equiv) were sequentially added and the solution was stirred at -15˚C for 24 h. The reaction was then warmed to room temperature and stirred for an additional 36 h. The reaction mixture was diluted with CH_2Cl_2 and poured over 1:1 1M citric acid:brine and extracted from the aqueous layer 5 times with CH_2Cl_2. The combined organic layers were then washed with saturated $NaHCO_3$ and extracted from the aqueous layer an additional 5 times with CH_2Cl_2. The combined organic layers were dried over $MgSO_4$, filtered, and concentrated *in vacuo*. The crude polymer was dissolved in 2 mL of DMF and dialyzed against DMF for 24 h (200 mL, 1 solvent change) using a regenerated cellulose membrane (25000 g/mol MWCO). The contents of the dialysis membrane were then concentrated *in vacuo* and lyophilized to afford polymer **3.7b** (0.55 g, 51%). ^{1}H NMR indicated a degree of polymerization of ~ 10 by integrating the benzylic peak against the PEG end-cap. ^{1}H NMR ($CDCl_3$, 600 MHz): δ 7.41-7.27 (br, 20H), 7.12-7.00 (br, 18H), 5.15-5.04 (m, 19H), 4.29-4.25 (m, 2H), 3.80-3.41 (m, 712H), 3.37 (s, 4H),

3.16-2.83 (m, 56H), 2.79-2.74 (m, 2H). SEC: M_n=7170 g/mol, M_w=8650 g/mol, PDI=1.21 (PEG standards).

*Synthesis of Compound **3.11***. Compound **3.8**[35] (0.88 g, 2.9 mmol, 1.4 equiv) was dissolved in 3 mL of 1:1 TFA:CH_2Cl_2 and stirred at room temperature for 2 h. The solvent was then removed under a stream of nitrogen in the fume hood prior to subjecting the reaction mixture three times to a repeat cycle of dilution with CH_2Cl_2 followed by concentration under reduced pressure to remove residual TFA and provide the Boc-deprotected compound **3.9**. Compound **3.10** (2.0 mmol, 1.0 equiv) was added and the resulting mixture was dissolved in 10 mL of anhydrous toluene. DIPEA (1.80 mL, 10.3 mmol, 5.3 equiv) and DMAP (40 mg, 0.4 mmol, 0.2 equiv) were successively added to the reaction flask and the solution was stirred at room temperature overnight. The reaction mixture was diluted with CH_2Cl_2 and washed once with 1 M HCl, twice with 1 M Na_2CO_3, and once with brine. The organic layer was then dried over $MgSO_4$, filtered, and concentrated *in vacuo*. The resulting oil was purified through silica gel chromatography (1:9 EtOAc:CH_2Cl_2) to afford compound **3.11** as a pale yellow oil (0.65 g, 71%). ^{1}H NMR ($CDCl_3$, 600 MHz): δ 8.49 (d, J=4.8, 1H), 7.74-7.59 (m, 2H), 7.29 (m, 2H), 7.12-7.09 (m, 1H), 7.08-7.00 (m, 2H), 4.71 (s, 2H), 3.76 & 3.66 (m, rotamers, 2H), 3.14 & 3.03 (m, rotamers, 3H), 3.10-3.03 (m, 2H), 0.93 (s, 9H), 0.09 (s, 6H). ^{13}C NMR ($CDCl_3$, 100 MHz): δ 159.8, (154.9 &154.7, rotamers), (150.2 & 149.9, rotamers), 138.5, 137.2, 127.0, 121.5, 121.4, (121.0 & 120.9, rotamers), (120.1 & 120.0, rotamers), 64.6, (49.0 & 48.4, rotamers),(36.6, 36.1, & 35.9, rotamers), 26.0, 18.5, -5.1. FT-IR (ν_{max}/cm^{-1}): 2955, 2930, 2885, 2856, 1722, 1574, 1562, 1510. HRMS: calcd $[M]^+$ ($C_{22}H_{32}N_2O_3S_2Si$): 464.1624. Found (EI): 464.1619.

*Synthesis of Compound **3.12***. Compound **3.11** (0.49 g, 1.1 mmol, 1 equiv) was dissolved in 4 mL of 1% HCl in EtOH and stirred at room temperature for 1.5 h. The reaction mixture was diluted with CH_2Cl_2 and washed with saturated $NaHCO_3$. The organic layer was then dried over $MgSO_4$, filtered, and concentrated *in vacuo*. The resulting oil was purified through silica gel chromatography (2:3 EtOAc:CH_2Cl_2) to afford compound **3.12** as a pale yellow oil (0.33 g, 88%). ^{1}H NMR ($CDCl_3$, 600 MHz): δ 8.48 (d, J=5.0, 1H), 7.74-7.60 (m, 2H), 7.37 (m, 2H), 7.13-7.08 (m, 2H), 7.06 (d, J=8.5, 1H), 4.66 (s, 2H),

3.77 & 3.67 (m, rotamers, 2H), 3.14 & 3.03 (m, rotamers, 3H), 3.09-3.03 (m, 2H). ^{13}C NMR ($CDCl_3$, 100 MHz): δ (159.7 & 159.5, rotamers), (154.9 & 154.6, rotamers), (150.6 & 150.5, rotamers), 138.3, 137.2, 127.9, (121.7 &121.6, rotamers), (121.0 & 120.9, rotamers), (120.1 & 120.0, rotamers), 64.5, (48.9 & 48.3, rotamers), (36.5 & 36.0, rotamers), (35.9 & 35.5). FT-IR (ν_{max}/cm^{-1}): 2926, 2870, 1717, 1576, 1562, 1510. HRMS: calcd $[M]^+$ ($C_{16}H_{18}N_2O_3S_2$): 350.0759. Found (EI): 350.0768.

*Synthesis of Compound **3.13***. Compound **3.12** (0.25 g, 0.64 mmol, 1.0 equiv) was dissolved in 4 mL of dry CH_2Cl_2. Pyridine (0.16 mL, 1.9 mmol, 2.0 equiv) and 4-nitrophenyl chloroformate (0.26 g, 1.3 mmol, 2.0 equiv) were successively added to the reaction flask and the solution was stirred for 1.5 h at room temperature until completion as determined by TLC. The reaction mixture was diluted with CH_2Cl_2 and washed with 1M HCl followed by saturated $NaHCO_3$. The organic layer was then dried over $MgSO_4$, filtered, and concentrated *in vacuo*. The resulting oil was purified through silica gel chromatography (CH_2Cl_2, then 1:9 EtOAc:CH_2Cl_2) to afford compound **3.13** as a pale yellow oil (0.31 g, 92%). ^{1}H NMR ($CDCl_3$, 600 MHz): δ 8.46 (d, J=4.2, 1H), 7.70-7.59 (m, 2H), 7.45-7.39 (m, 2H), 7.35 (m, 2H), 7.15 (m, 2H), 7.13-7.07 (m, 2H), 5.25 (s, 2H), 3.77 & 3.66 (m, rotamers, 2H), 3.13 & 3.02 (m, roatmers, 3H), 3.08-3.03 (m, 2H). ^{13}C NMR ($CDCl_3$, 100 MHz): (159.9 & 159.4, rotamers), 155.5, (154.5 & 154.2, rotamers), 152.4, 151.9, (149.9 & 149.8, rotamers), 145.5, 137.1, 131.2, 130.0, 125.3, (122.1 &122.0, rotamers), 121.9, (121.0 & 120.9, rotamers), (120.1 & 120.0, rotamers), 70.4, (48.9 & 48.2, rotamers), (36.4 & 36.0, rotamers), (35.9 & 35.4, rotamers). FT-IR (ν_{max}/cm^{-1}): 3117, 3080, 3047, 2957, 2930, 1767, 1720, 1616, 1593, 1574, 1562, 1524. HRMS: calcd $[M]^+$ ($C_{23}H_{21}N_3O_7S_2$): 515.0821. Found (EI): 515.0845.

*Synthesis of Polymer **3.14***. Activated monomer **2.1c**[19] (0.67 g, 1.3 mmol, 1.0 equiv) was dissolved in 3 mL of 1:1 TFA:CH_2Cl_2 and stirred at room temperature for 2 h. The solvent was then removed under a stream of nitrogen in the fume hood prior to subjecting the reaction mixture three times to a repeat cycle of dilution with CH_2Cl_2 followed by concentration under reduced pressure to remove residual TFA and provide the deprotected monomer **2.5**.[19] End-cap **3.13** (30 mg, 0.07 mmol, 0.05 equiv) was added and the resulting mixture was dissolved in 4.4 mL of anhydrous toluene and cooled to 0˚C.

NEt_3 (0.92 mL, 6.6 mmol, 5.0 equiv) and DMAP (33 mg, 0.27 mmol, 0.2 equiv) were sequentially added and the solution was stirred at 0˚C for 8h, let warm to room temperature, and stirred an additional 16 h. The solvent was then evaporated under reduced pressure and the crude polymer was dissolved in 2 mL of DMF and dialyzed against DMF for 24 h (200, mL, 1 solvent change) using a regenerated cellulose membrane (12000-14000 g/mol MWCO). The contents of the dialysis membrane were then concentrated *in vacuo* and lyophilized to afford polymer **3.14** (0.21 g, 60%). ^{1}H NMR indicated a degree of polymerization of ~ 25 by integrating the benzylic peak against the thiopyridyl end-cap. ^{1}H NMR ($CDCl_3$, 400 MHz): δ 8.46 (d, J=5.3, 1H), 7.70-7.59 (m, 2H), 7.40-7.27 (br, 48H), 7.11-6.99 (br, 50H), 5.14-5.01 (m, 48H), 3.62-3.37 (m, 94H), 3.75 & 3.65 (m, rotamers, 2H), 3.16-2.83 (m, 209H). SEC: M_n=3150 g/mol, M_w=5440 g/mol, PDI=1.73 (PEG-PEO standards). M_n=5580 g/mol, M_w=9720 g/mol, PDI=1.74 (PEG-PEO standards).

*Synthesis of Polymer **3.16.*** Poly(ethylene glycol) thioacetate derivative (5000 g/mol) **3.17**[36,37] (20 mg, 4 μmol, 0.6 equiv) was dissolved in 2 mL of 1:2 freshly distilled CH_2Cl_2:MeOH and cooled to 0˚C. Polymer **3.14** (30 mg, 7 μmol, 1.0 equiv) and NaOMe (6 mg, 0.1 mmol, 16 equiv) were added and the solution was stirred at 0˚C for 8 h and then stirred an additional 8 h at room temperature. The crude reaction mixture was concentrated *in vacuo* and then dissolved in CH_2Cl_2 and washed with a 1:1 mixture of 1 M HCl:brine. The product was re-extracted from the aqueous layer an additional 5 times with CH_2Cl_2. The combined organic layers were dried over $MgSO_4$, filtered, and concentrated *in vacuo*. The crude product was dissolved in 2 mL of DMF and dialyzed against DMF for 24 h (200 mL, 1 solvent change) using a regenerated cellulose membrane (12000-14000 g/mol MWCO). The contents of the dialysis membrane were then concentrated *in vacuo* and lyophilized to afford polymer **3.16** (37 mg, 57%). ^{1}H NMR indicated a degree of polymerization of ~ 28 by integrating the benzylic peak against the PEG end-cap. ^{1}H NMR ($CDCl_3$, 600 MHz): δ 7.39-7.27 (br, 56H), 7.11-6.95 (br, 56H), 5.16-5.02 (m, 57H), 3.78-3.41 (m, 644H), 3.37 (s, 3H), 3.16-2.84 (m, 179H). SEC: M_n=5200 g/mol, M_w=7330 g/mol, PDI=1.41 (PEG-PEO standards).

*Synthesis of Compound **3.18***. Compound **3.17**[38] (0.40 g, 2.9 mmol, 1.0 equiv) and NEt_3 (0.70 mL, 9.5 mmol , 3.3 equiv) were added to 10 mL of dry CH_2Cl_2 cooled to 0˚C. 4-Nitrophenyl chloroformate (0.65 g, 3.2 mmol, 1.1 equiv) dissolved in 5 mL of CH_2Cl_2 was added dropwise to the reaction mixture over 20 min. The solution was warmed to room temperature and stirred an additional 1.5 h until completion as determined by TLC. Freshly distilled triethylene glycol monomethyl ether (0.36 mL, 1.3 mmol, 0.45 equiv) was added and the reaction was stirred for 30 min to quench the remaining 4-nitrophenyl chloroformate. The reaction mixture was diluted with CH_2Cl_2 and washed with 1 M HCl. The organic layer was dried over $MgSO_4$, filtered, and concentrated *in vacuo*. The crude solid was purified through silica gel chromatography (1:49 EtOAc:CH_2Cl_2) to afford **3.18** as a white solid (0.71 g, 80%). ^{1}H NMR ($CDCl_3$, 600 MHz): δ 8.28 (m, 2H), 7.45 (m, 2H), 7.37 (m, 2H), 7.23 (m, 2H), 4.44 (s, 2H), 3.37 (s, 3H). ^{13}C NMR ($CDCl_3$, 100 MHz): δ 155.3,151.0,150.1,145.6,128.9, 125.4, 121.8, 120.7, 73.9, 58.3. FT-IR (ν_{max}/cm^{-1}): 2928, 2854, 1763, 1726, 1618, 1595, 1526. HRMS: calcd $[M]^+$ ($C_{15}H_{13}NO_6$): 303.0743. Found (EI): 303.0749.

*Synthesis of Compound **3.19***. Compound **3.9** was synthesized using the same procedure outlined above. Compound **3.9** (0.24 g, 0.77 mmol, 1.5 equiv) and compound **3.18** (0.16 g, 0.51 mmol, 1.0 equiv) were dissolved in 5 mL of dry toluene. DIPEA (0.42 mL, 3.9 mmol, 5.0 equiv) and DMAP (20 mg, 0.15 mmol, 0.30 equiv) were successively added to the reaction flask and the solution was stirred at room temperature overnight. The reaction mixture was then diluted with CH_2Cl_2 and washed with 1M HCl, followed by 1 M Na_2CO_3 and brine. The organic layer was dried over $MgSO_4$, filtered, and concentrated *in vacuo*. The resulting oil was purified through silica gel chromatography (3:20 EtOAc:CH_2Cl_2) to afford **3.19** as a pale yellow oil (0.13 g, 70%). ^{1}H NMR ($CDCl_3$, 600 MHz): δ 8.48 (d, J=5.3, 1H), 7.72-7.59 (m, 2H), 7.33-7.28 (m, 2H), 7.13-7.06 (m, 2H), 7.06-7.02 (d, J=8.0, 1H), 4.43 (s, 2H), 3.76 & 3.66 (m, rotamers, 2H), 3.36 (s, 3H), 3.14 & 3.02 (rotamers, 3H), 3.09-3.03 (m, 2H).^{13}C NMR ($CDCl_3$, 100 MHz): δ (159.7 & 159.4, rotamers), (154.7 & 154.5, rotamers), 150.7, (149.8, & 149.7, rotamers), 137.1, 135.3, 128.6, 121.6, (121.0 & 120.9, rotamers), (120.0 & 119.9, rotamers), 74.1, (48.9 & 48.3, rotamers), (36.5 & 36.0, rotamers), (35.8, & 35.5, rotamers). FT-IR (ν_{max}/cm^{-1}):

2926, 2854, 2822, 1722, 1574, 1562, 1510. HRMS: calcd $[M]^+$ ($C_{17}H_{20}N_2O_3S_2$): 364.0915. Found (EI): 364.0916.

*Synthesis of Compound **3.21***. Compound **3.20** (0.14 g, 0.76 mmol, 1.5 equiv) and compound **3.18** (0.15 g, 0.50 mmol, 1.0 equiv) were dissolved in 3 mL of dry toluene. DIPEA (0.26 mL, 1.5 mmol, 3.0 equiv) and DMAP (13 mg, 0.11 mmol, 0.21 equiv) were successively added to the reaction flask and the solution was stirred at room temperature overnight. The reaction mixture was then diluted with CH_2Cl_2 and washed with 1M HCl, followed by 1 M Na_2CO_3 and brine. The organic layer was dried over $MgSO_4$, filtered, and concentrated *in vacuo*. The resulting oil was purified through silica gel chromatography (3:20 EtOAc:CH_2Cl_2) to afford **3.20** as a pale yellow oil (0.16 g, 92%). ^{1}H NMR ($CDCl_3$, 600 MHz): 7.32-7.28 (m, 2H), 7.10-7.05 (m, 2H), 4.42 (s, 2H), 3.61-3.39 (m, methylenes, rotamers, 4H), 3.37-3.34 (m, 3H), 3.11 & 3.02 (rotamers, 3H), 2.94-2.86 (m, rotamers, 3H), 1.50-1.40 (m, 9H).^{13}C NMR ($CDCl_3$, 100 MHz): δ (155.9, 155.7, & 155.5, rotamers), (154.9 & 154.6, rotamers), (150.9 & 150.8, rotamers), (135.2 & 135.1, rotamers), 128.6, (121.8 & 121.6, rotamers), (79.9, 79.7, 79.6, & 79.5, rotamers), 74.1, 58.0, (47.4, 47.2, 47.0, 46.8, 46.6, 46.5, CH_2 rotamers), (35.4 & 35.2, rotamers), (34.7 & 34.6, rotamers), 28.4. FT-IR (ν_{max}/cm^{-1}): 2976, 2930, 1722, 1693, 1510. HRMS: calcd $[M]^+$ ($C_{18}H_{28}N_2O_5$): 352.1998. Found (EI): 352.1996.

3.2.3 Degradation Studies

*Degradation of Compounds **3.19***. Compound **3.19** (10 mg) was dissolved in 1 mL of 0.1 M phosphate buffer (D_2O):acetone-d_6 (3:2) and sparged under argon for 10 minutes. The solution was then heated to 37˚C using an INOVA variable temperature controller calibrated using ethylene glycol and maintained at 37˚C for 3 hours while ^{1}H NMR spectra were recorded at 15-minute intervals. Following the control period, DTT (20 mg, 5 equiv) was added to the NMR tube and the solution was incubated at 37˚C for 48 hours. Following complete degradation, the pH of the solution was tested to ensure that the sample did not fall outside of the buffer region during the degradation process. The extent of cyclization was quantified by integrating the aromatic peak of the 4-(methoxymethyl)phenol degradation product relative to the corresponding aromatic peak in the undegraded sample. The plateau region corresponding to 100% degradation was

defined as the region in which the mean fluctuation between successive integral values was less than or equal to 3%. Degradation data was treated by non-linear regression and fit to a first-order degradation model.

*Degradation of Compounds **3.22**.* Compound **3.21** (10 mg) was dissolved in 1 mL of 1:1 TFA:CH2Cl2 and stirred at room temperature for 2 h. The solvent was blown off and the product was taken up in CH_2Cl_2 and washed with a 1:1 mixture of brine:1 M citric acid. The deprotected polymer was then re-extracted from the aqueous layer 5 times with CH_2Cl_2. The combined organic layers were dried over $MgSO_4$, filtered, and concentrated *in vacuo* to afford the deprotected compound **3.22**. Compound **3.22** was then taken up in 1 mL of 0.1 M pH 7.4 phosphate buffer (D_2O):acetone-d_6 (3:2) preheated to 37˚C and filtered through a Promax® PTFE membrane (0.22 μm*)*. The filtered solution was then incubated at 37˚C using an INOVA variable temperature controller calibrated using ethylene glycol. ^{1}H NMR spectra were recorded at 5 min intervals over a period of 2 hours. Following complete degradation, the pH of the solution was tested to ensure that the sample did not fall outside of the buffer region during the degradation process. The extent of cyclization was quantified by integrating the methyl peak of the *N,N'*-dimethylimidazolidinone degradation product relative to the $(CHD_2)(CD_3)CO$ in the sample. The plateau region corresponding to 100% degradation was defined as the region in which the mean fluctuation between successive integral values was less than or equal to 3%. Degradation data was treated by non-linear regression and fit to a first-order degradation model.

*Degradation of Polymers **3.7a** and **3.7b**.* Polymer (10 mg) was dissolved in 1 mL of 0.1 M pH 7.4 phosphate buffer (D_2O) and sonicated for 10 minutes. The nanoparticle solution was then incubated at 37˚C over a 30-day period with ^{1}H NMR spectra taken at roughly 2-day intervals throughout the degradation process. Following complete degradation, the pH of the solution was tested to ensure that the sample did not fall outside of the buffer region during degradation. The extent of degradation was quantified by integrating the methyl peak of the *N,N'*-dimethylimidazolidinone degradation product relative to residual solvent in the sample. The plateau region corresponding to 100%

degradation was defined as the region in which the mean fluctuation between successive integral values was less than or equal to 3%.

*Degradation of Polymer **3.14***. Polymer **3.14** (12 mg, 3 μmol, 1 equiv) was dissolved in 1.0 mL of 0.1 M pH 7.4 phosphate buffer (D_2O):acetone-d_6 (3:2) preheated to 37˚C. DTT (7.5 mg, 50 μmol, 17 equiv) was added and the degradation mixture was incubated at 37˚C over a period of 30 d with ^{1}H NMR spectra taken throughout the degradation process. Following complete degradation, the pH of the solution was tested to ensure that the sample did not fall outside of the buffer region during degradation. The extent of degradation was quantified by integrating the methyl peak of the *N,N'*-dimethylimidazolidinone degradation product relative to residual DMF in the sample. The plateau region corresponding to 100% degradation was defined as the region in which the mean fluctuation between successive integral values was less than or equal to 3%.

3.2.4 General Procedure for Nanoparticle Assembly

Self-immolative block copolymer (5 mg) was dissolved in 0.5 mL of THF and stirred vigorously while 2 mL of deionized water was added dropwise to the stirred solution over a period of 10 minutes. Following the addition of water, the nanoparticle suspension was dialyzed against distilled water for 36 h (2 L, 2 changes) using a 12000-14000 g/mol MWCO regenerated cellulose membrane to remove THF.

3.2.5 Transmission Electron Microscopy

The suspension of nanoparticles (20 μL, 0.1 mg mL^{-1}) was placed on a carbon formvar grid and was dried in air overnight before imaging. Imaging was performed using a Phillips CM10 microscope operating at 80 kV with a 40 lm aperture.

3.3 Results and Discussion

3.3.1 Motivation and Design

Two designs were proposed to investigate different aspects of the amphiphilic PEG-self-immolative block copolymer system based on our previously reported polycarbamate

backbone derived from alternating 1,6-elimination and cyclization spacers (Figure 3.1b). The first proposed design, depicted in Figure 3.2a, involves the use of a PEG succinic acid end-cap in place of the PEG acetic-acid version utilized in our initial report. Our attempts to synthesize PEG acetic acids were plagued by incomplete conversions and PEG-dimerizations. Furthermore, commercial sources of PEG acetic acid are relatively expensive, making our initial system costly to investigate. As a result, this alteration was proposed to provide a low-cost, efficient method of incorporating PEG derivatives, while at the same time bypassing any issues associated with the synthesis of PEG acetic acid. Overall, this system was designed to probe the self-assembly characteristics of the amphiphilic block copolymer system and investigate the morphological effect of varying the size fraction of either block.

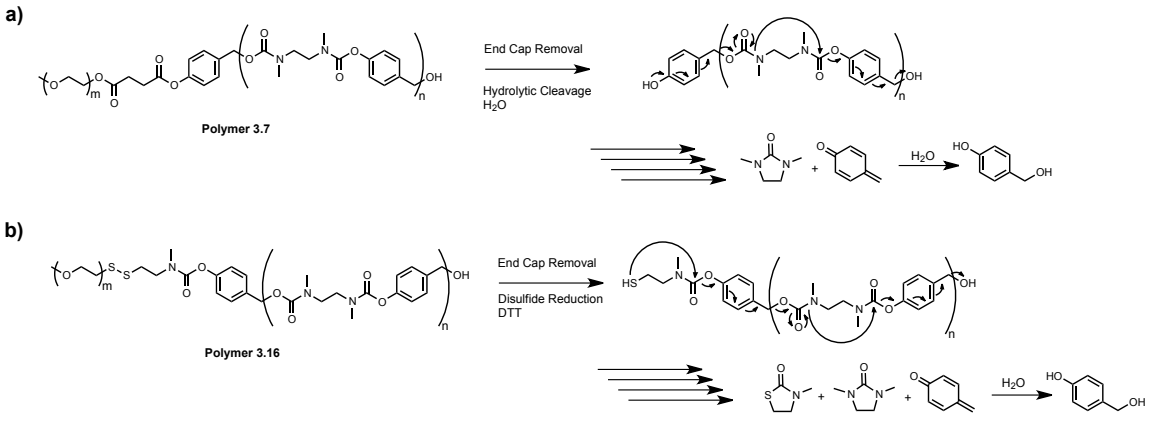

Figure 3.2: Chemical structures, proposed depolymerization mechanisms, and expected depolymerization products of (a) target PEG succinic acid based self-immolative block copolymer and (b) target PEG disulfide based self-immolative block copolymer.

The second proposed design was aimed to address the lack of stimuli-responsive degradation in the initial system by introducing a disulfide linkage between the hydrophilic PEG block and hydrophobic polycarbamate backbone. This target polymer, shown in Figure 3.2b, involves the use of a *N*-methylaminoethanethiol spacer to conjugate PEG through a disulfide linkage. This linker has been previously explored in the development of self-immolative prodrugs, but never incorporated into a polymeric

framework.[35] It was envisioned that the use of *N*-methylaminoethanethiol instead of 2-mercaptoethanol would permit an enhanced stability of the block copolymer system due to end-cap incorporation through a carbamate linkage instead of the hydrolytically labile carbonate. This enhanced stability should limit unwanted end-cap hydrolysis and restrict the degradation of these block copolymers to a single pathway involving a reduction sensitive trigger. In this design, reduction of the disulfide linkage between the two blocks reveals an active thiol terminus that then cyclizes to initiate degradation of the polycarbamate backbone through alternating 1,6-elimination and cyclization reactions. This strategy also marks the first time a heterogeneous cyclization spacer has been used in an end-cap design to influence the overall kinetics of polymer degradation.

3.3.2 Synthesis

3.3.2.1 PEG Succinic Acid Block Copolymer Model System

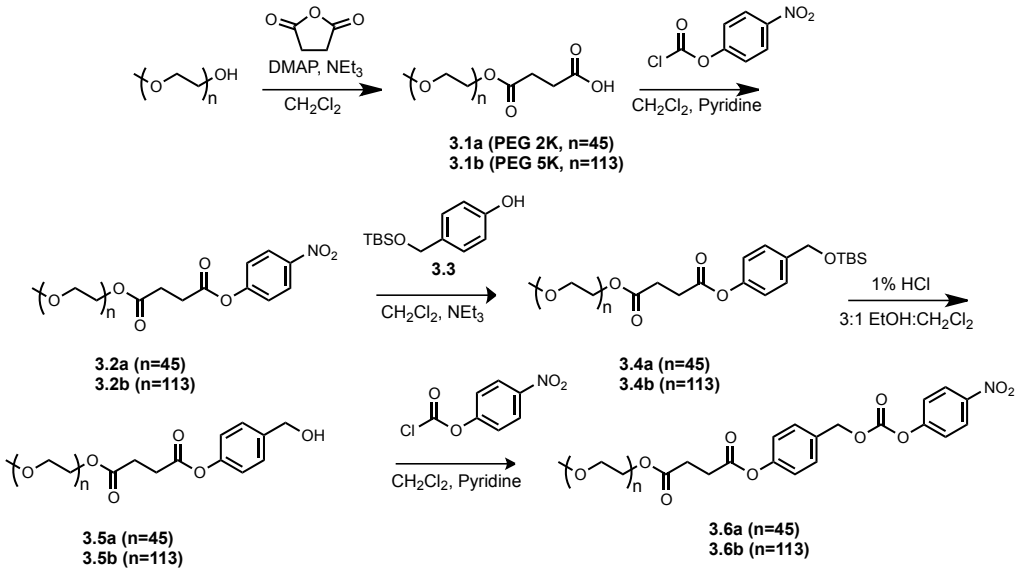

Scheme 3.1: Synthesis of a PEG succinic acid based end cap

Synthesis of the hydrolytically sensitive linear self-immolative block copolymer was carried out using a macromolecular PEG end-cap during polymerization of the polycarbamate backbone. As shown in Scheme 3.1, a modified synthetic route to that used in our previously reported system was adopted to allow for incorporation of PEG succinic acid. Monofunctional PEG succinic acids (**3.1a** & **3.1b**) were prepared through a

ring-opening of succinic anhydride using commercial PEG monomethylether alcohols having molecular weights of approximately 2000 and 5000 g/mol in the presence of DMAP and NEt_3. This ring-opening reaction provided a facile means to generate PEG acids that resulted in high conversion of the alcohol as measured by NMR spectroscopy in a moderate yield following purification. These PEG succinic acids were then reacted with 4-nitrophenyl chloroformate to generate the highly electrophilic 4-nitrophenyl ester species **3.2a** and **3.2b**, which were subsequently substituted with the TBS-protected phenol **3.3** to yield the TBS-protected esters **3.4a** and **3.4b**. The TBS groups of these esters were removed by treatment with HCl in 3:1 EtOH:CH_2Cl_2, and the resulting alcohols **3.5a** and **3.5b** were then activated with 4-nitrophenyl chloroformate to afford the PEG end-caps **3.6a** and **3.6b**.

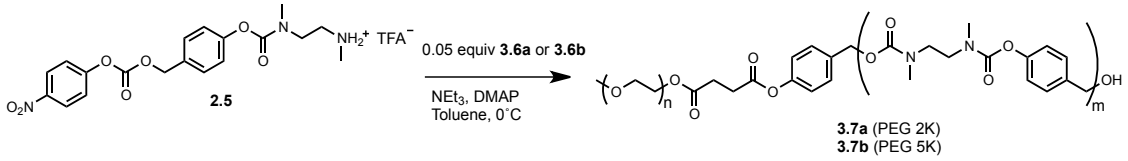

Scheme 3.2: Polymerization of linear self-immolative block copolymers 3.7a and 3.7b using a PEG end capping agent

As shown in Scheme 3.2, the amphiphilic block copolymers **3.7a** and **3.7b** were synthesized by polymerizing the activated carbonate monomer **2.5** in the presence of DMAP and NEt_3, while using PEG end-caps **3.6a** and **3.6b**, respectively. Our initial report utilized preparative size exclusion chromatography to purify the analogous block copolymer. However, in this work it was sought to improve the scalability of this design by purifying these compounds through dialysis. Self-immolative polymer systems synthesized through polycondensations are often hindered by poor end-cap incorporation. This is only a minor limitation when using small molecule end caps, as unreacted end caps and low molecular weight, non-end capped species can be removed by dialysis. On the other hand, this can be problematic when using macromolecular end caps due to the increased difficulty separating heterogeneous polymer species from one another.

Polymers **3.7a** and **3.7b** were purified by dialysis in DMF against a 25000 g/mol MWCO membrane to yield polymers with number average molecular weights of 3600 and 7170 g/mol and PDIs of 1.37 and 1.21, respectively, as measured by SEC relative to PEG-PEO standards. (Figure 3.3). Analysis by ^{1}H NMR spectroscopy revealed monomer to end cap ratios of 18:1 for polymer **3.7a** and 10:1 for polymer **3.7b (**Figures A21 and A22). This underestimation of the ratio for polymer **3.7b** is indicative of residual unreacted 5000 g/mol PEG end cap, which can be clearly seen in the bimodal SEC chromatogram (Figure 3.3). Conversely, dialysis was an effective means to remove the unreacted 2000 g/mol PEG end cap for polymer **3.7a**, leaving only a slight shoulder in the SEC chromatogram. Future attempts to purify these polymers will focus on alternate techniques such as gel filtration or precipitation in MeOH to remove any unreacted PEG species.

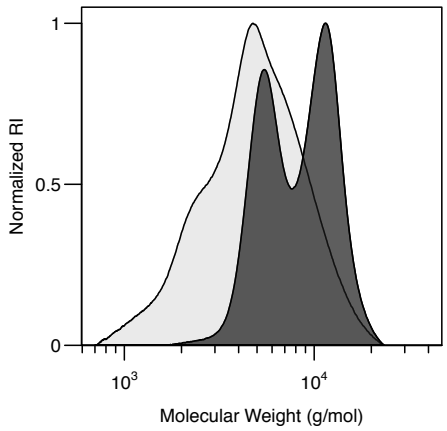

Figure 3.3. Size exclusion chromatograms of block copolymers 3.7a (M_n = 3600 g/mol, PDI=1.47) (grey) and 3.7b (M_n = 7170 g/mol, PDI=1.21) (black). All chromatograms obtained a concentration of 5 mg/mL and calibrated against PEG in THF.

3.3.2.2 Redox Sensitive Linear Self-Immolative Block Copolymer

An alternate synthetic strategy was employed for the synthesis of the redox sensitive self-immolative block copolymer due to the issues encountered in the removal of unreacted macromolecular end caps following polymerization. It was envisioned that use of a modular design in which polymerization is separated from PEG incorporation would alleviate any purification issues and reduce the overall number of synthetic steps

necessary to generate amphiphilic self-immoaltive block copolymers. Such a strategy also allows for a higher degree of control over the size fraction of both blocks in the design due to the decoupling between polymerization and block copolymer formation.

A small molecule disulfide end cap bearing a thiopyridyl group for subsequent reaction with PEG thiol was synthesized as shown in Scheme 3.3. Boc-protected *N*-methylaminoethanethiopyridine **3.8**[35] was deprotected using trifluoroacetic acid (TFA) and subsequently reacted with the 4-nitrophenyl activated carbonate **3.10** to yield the TBS-protected carbamate **3.11**. The TBS group on **3.11** was removed by treatment with HCl in EtOH, and the alcohol **3.12** was reacted with 4-nitrophenyl chloroformate to generate the thiopyridyl end cap **3.13**.

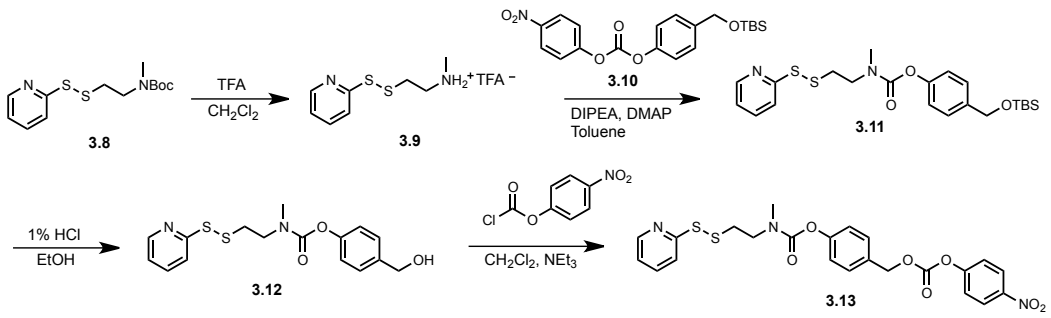

Scheme 3.3: Synthesis of a redox sensitive end cap incorporating a *N*-methylaminoethanethiol cyclization spacer

Synthesis of the thiopyridyl disulfide polymer **3.14** was carried out using a similar strategy to that described for polymer **3.7** with the use of the small molecule end cap **3.13**. Purification of this polymer through dialysis in DMF against a 12000-14000 g/mol MWCO membrane yielded a polymer with a M_n of 3150 g/mol and a PDI of 1.73 as measured by SEC relative to PEG-PEO standards (Figure 3.4). Analysis by ^{1}H NMR spectroscopy revealed a monomer to end cap ratio of 24, which was similar to the feed ratio of 20:1 (Figure A29). Our attempts to react this polymer with PEG thiol were unsuccessful due to the tendency of PEG thiol to dimerize in storage. To address this issue, this polymer was reacted with monofunctional PEG thioacetate **3.15** derived from commercial PEG monomethylether alcohol with a molecular weight of approximately 5000 g/mol, in the presence of NaOMe. This strategy for block copolymer formation

through a thiol/disulfide reaction does not suffer PEG dimerization issues as PEG thiol is generated *in situ* through the hydrolysis of PEG thioacetate under basic conditions. Purification of this polymer by dialysis in DMF against a 12000-14000 g/mol MWCO membrane yielded copolymer **3.16** with a M_n of 5200 g/mol and a PDI of 1.41 as measured by SEC relative to PEG-PEO standards (Figure 3.4). Analysis by ^{1}H NMR spectroscopy revealed a monomer to end cap ratio of 28, which was similar to the ratio observed for the homopolymer **3.14** (Figure A30).

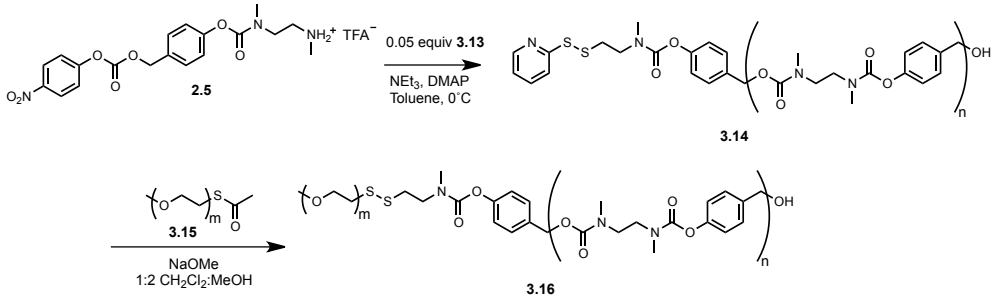

Scheme 3.4: Synthesis of a redox sensitive block copolymer using a thiol/disulfide exchange reaction

Another benefit to the generation of self-immolative block copolymers through a modular approach is the tracking of the molecular weight evolution through SEC. As shown in Figure 3.4, the peak molecular weight of **3.16** is approximately equal to the cumulative contribution of polymers **3.14** and **3.15**, therefore supporting the successful conjugation of the PEG block through the thiol/disulfide exchange reaction. A small shoulder is evident in the SEC chromatogram of copolymer **3.16** that appears to correspond to a residual amount of homopolymer **3.14** that was not detected in the ^{1}H NMR spectrum. In the absence of absolute molecular weight data, the equivalents of PEG thioacetate to be added were determined by end group analysis through ^{1}H NMR spectroscopy. It is likely that the conjugation efficiency of this design can be further improved with the use of absolute molecular weight data for the self-immolative homopolymer. Interestingly, the PDI of the block copolymer was significantly less than that observed for the self-immolative homopolymer. This narrowing of the polymer distribution is due to the degradation of non-end-capped species of polymer **3.14** under the basic/polar conditions encountered during block copolymer formation. ^{1}H NMR of the crude copolymer

revealed the presence of 4-hydroxybenzyl alcohol and *N,N'*- dimethylimidazolidinone, which are formed during the degradation of the polycarbamate backbone. This backbone degradation lowered the overall yield during block copolymer formation, but removed any non-end-capped homopolymer species that could potential interfere with the subsequent generation of nanoparticles.

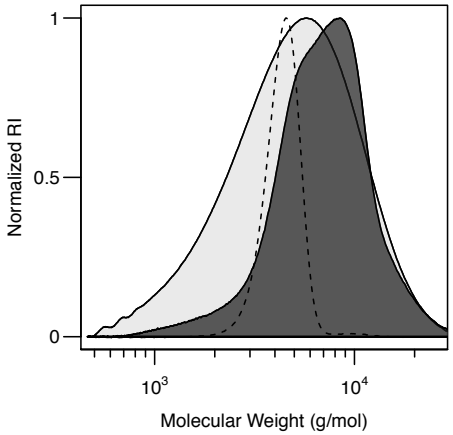

Figure 3.4: Size exclusion chromatograms of polymers 3.14 (M_n = 3150 g/mol, PDI=1.73) (grey), 3.15 (M_n = 4300 g/mol, PDI=1.01) (- - -), and 3.16 (M_n = 5200 g/mol, PDI=1.41) (dark grey). All chromatograms obtained a concentration of 5 mg/mL and calibrated against PEG-PEO in THF.

3.3.3 Probing the Solution Degradation Kinetics

The solution phase degradation kinetics of *N,N'*-dimethylethylenediamine and the corresponding polymer derived from alternating 4-hydroxybenzyl alcohol and *N,N'*-dimethylethylenediamine spacers have been previously explored in our group.[19] However, the cyclization kinetics of *N*-methylaminoethanethiol have yet to be investigated and its rate of degradation is currently unknown relative to the more conventional *N,N'*-dimethylethylenediamine cyclization spacer. To this end, a model *N*-methylaminoethanethiol compound **3.19** was prepared by reacting **3.9** with the 4-nitrophenyl-activated carbonate species **3.18** derived from 4-hydroxybenzyl methylether **3.17**[38] (Scheme 3.5). Our previous experimental findings have suggested that unwanted reactivity of benzylic alcohols can adversely influence kinetic experiments[26] so a benzylmethylether compound was selected to alleviate such effects. For an accurate

comparison, an analogous *N,N'*-dimethylethylenediamine model compound **3.22** was prepared by reacting **3.20** with the 4-nitrophenyl-activated carbonate species **3.18** followed by treatment with TFA to remove the Boc group (Scheme 3.6).

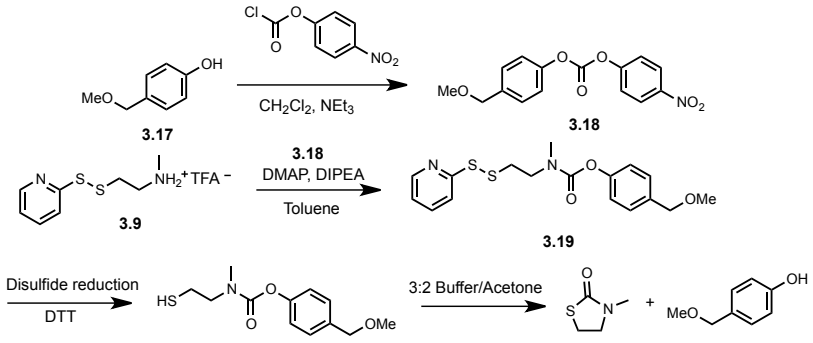

Scheme 3.5: Synthesis of model *N*-methylaminoethane thiol compound 3.19 and its cyclization to form 3-methylthiazolidinone

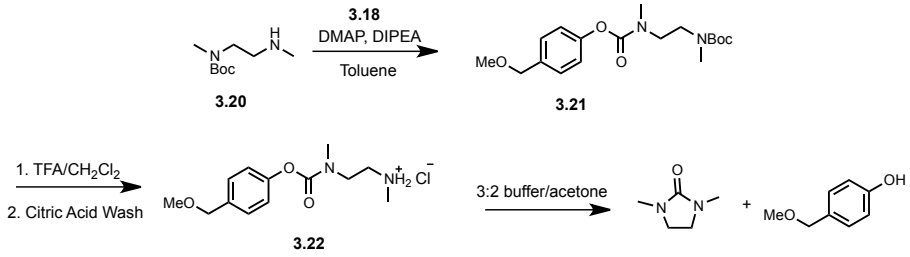

Scheme 3.6: Synthesis of model *N,N'*-dimethylethylenediamine compound 3.22 and its cyclization to form *N,N′*-dimethylimidazolidinone

The cyclization kinetics of model compounds **3.19** and **3.22** were investigated by ^{1}H NMR spectroscopy under pseudo-physiological conditions in a 3:2 mixture of 0.1 M pH 7.4 phosphate buffer (D_2O):acetone-d_6 maintained at 37˚C. Compound **3.22** displayed a first-order rate constant of $6.48 \pm 0.16 \times 10^{-2}$ min^{-1} and a half-life of 10.7 ± 0.3 min following dissolution in the buffer/acetone mixture, as determined through triplicate measurement (Figure 3.5a). Since end cap removal cannot be studied independently of cyclization for compound **3.19**, the rate of end cap removal had to be increased such that its influence on the overall kinetics could be neglected. Under normal conditions, disulfide cleavage is a second order bimolecular reaction that is dependent on the concentrations of the reducing agent and the compound bearing the disulfide bond.[39]

Hence in our design, using a large excess of reducing agent can therefore increase the rate of disulfide cleavage to point where the subsequent cyclization is largely rate limiting. As shown in Figure 3.7, a complete removal of the thiopyridyl end cap on compound **3.19** was observed by the time of the first NMR reading following the addition of DTT to a concentration of 0.1 M. Subsequent cyclization of the *N*-methylaminoethanethiol linker required an additional 24 hours to reach completion (Figure 3.5b). A first-order model was fit to the experimental data to yield a rate constant of $1.56 \pm 0.16 \times 10^{-1}$ h^{-1} and a half-life of 4.5 ± 0.4 h for compound **3.19**, thereby indicating that the *N*-methylaminoethanethiol spacer cyclizes approximately 25 times slower than *N,N'*-dimethylethylenediamine under the conditions examined.

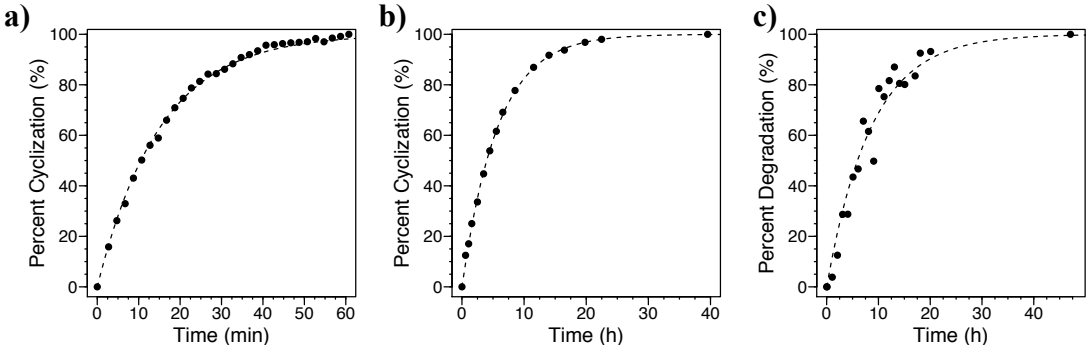

Figure 3.5: Kinetics of cyclization in 0.1 M phosphate buffered D_2O:acetone-d_6 as measured by ^1H NMR spectroscopy for (a) compound 3.19 and (b) compound 3.21 and (c) polymer 3.14 after reduction of the thiopyridyl disulfide moeity in a highly reducing environment (0. 1 M DTT). Dashed lines correspond to the first-order fits for compounds 3.19 and 3.21 and the modified Avrami fit for polymer 3.14.

The large difference in the rate of cyclization for two spacers prompted an additional degradation study to investigate the overall influence of incorporating the slower *N*-methylaminoethanethiol end cap on the kinetics of polymer degradation. Polymer **3.14** was investigated under similar conditions to that used for compound **3.19** in order to minimize the effects of disulfide cleavage on the observed rate of polymer depolymerization (Figure 3.7). Under these conditions, the degradation of polymer **3.14** required approximately 5.9 h to reach 50% degradation and 24 h to reach complete degradation. Consequently, the kinetics of end cap cyclization were rate limiting in this design, with the overall rate of depolymerization roughly mirroring that of the *N*-

methylaminoethanethiol cyclization spacer (Figure 3.5c). Such an observation is interesting in the context of tuning the rate of polymer degradation, as the use of a slower cyclization spacer in the end cap design can be used a means of gated rate control. Varying the electrophilic character of the carbamate cyclization center in the end cap through the incorporation of different electron withdrawing or donating groups should allow for an additional means of depolymerization rate control in future designs. It should be noted that the preliminary investigation of the degradation kinetics of polymer **3.14** were not performed in triplicate. Consequently, the modified Avrami equation fit was prone to significant leverage effects related to the location of the final time point measurement.

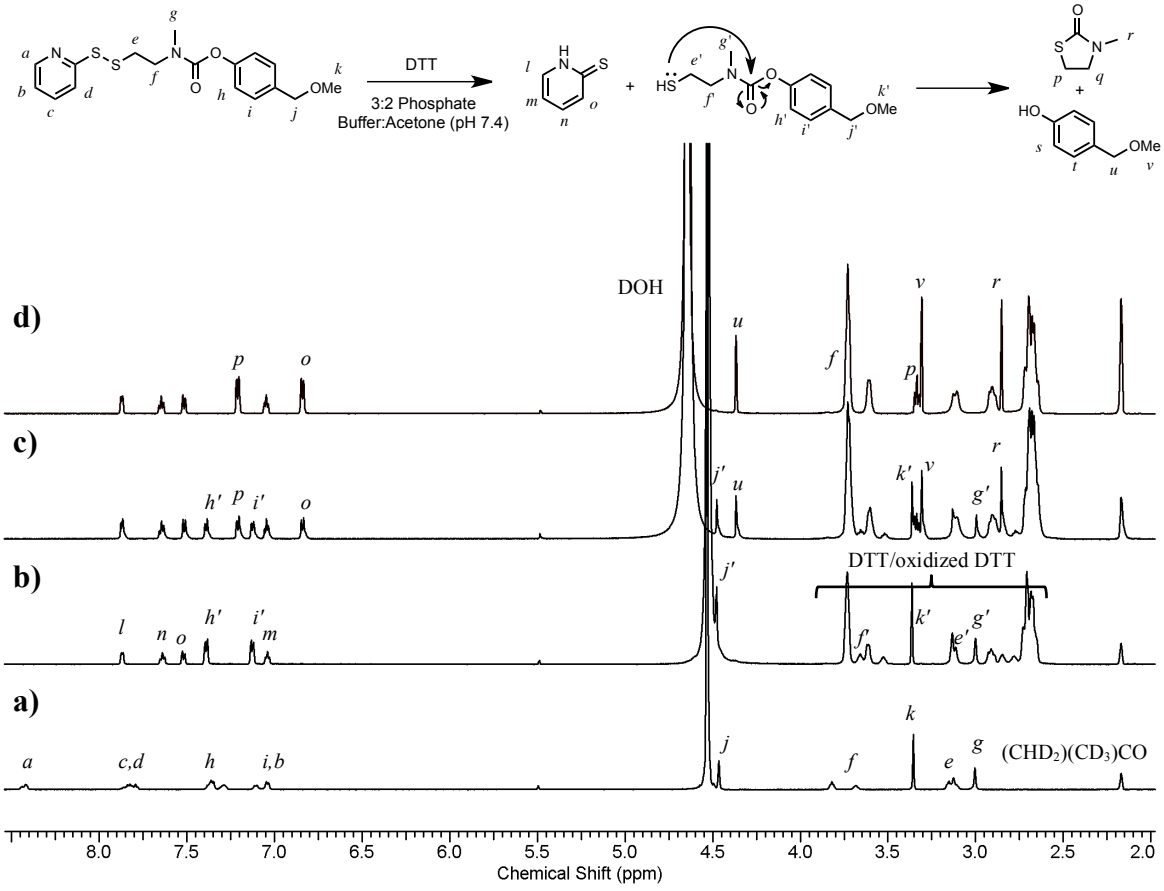

Figure 3.6: ^{1}H NMR spectra of compound 3.19: (a) immediately following dissolution in 0.1 M pH 7.4 phosphate buffered D_2O:acetone-d_6 (3:2) at 37°C; (b) 5 min and (c) 5 h following DTT addition; and (d) following 40 h in a reducing environment.

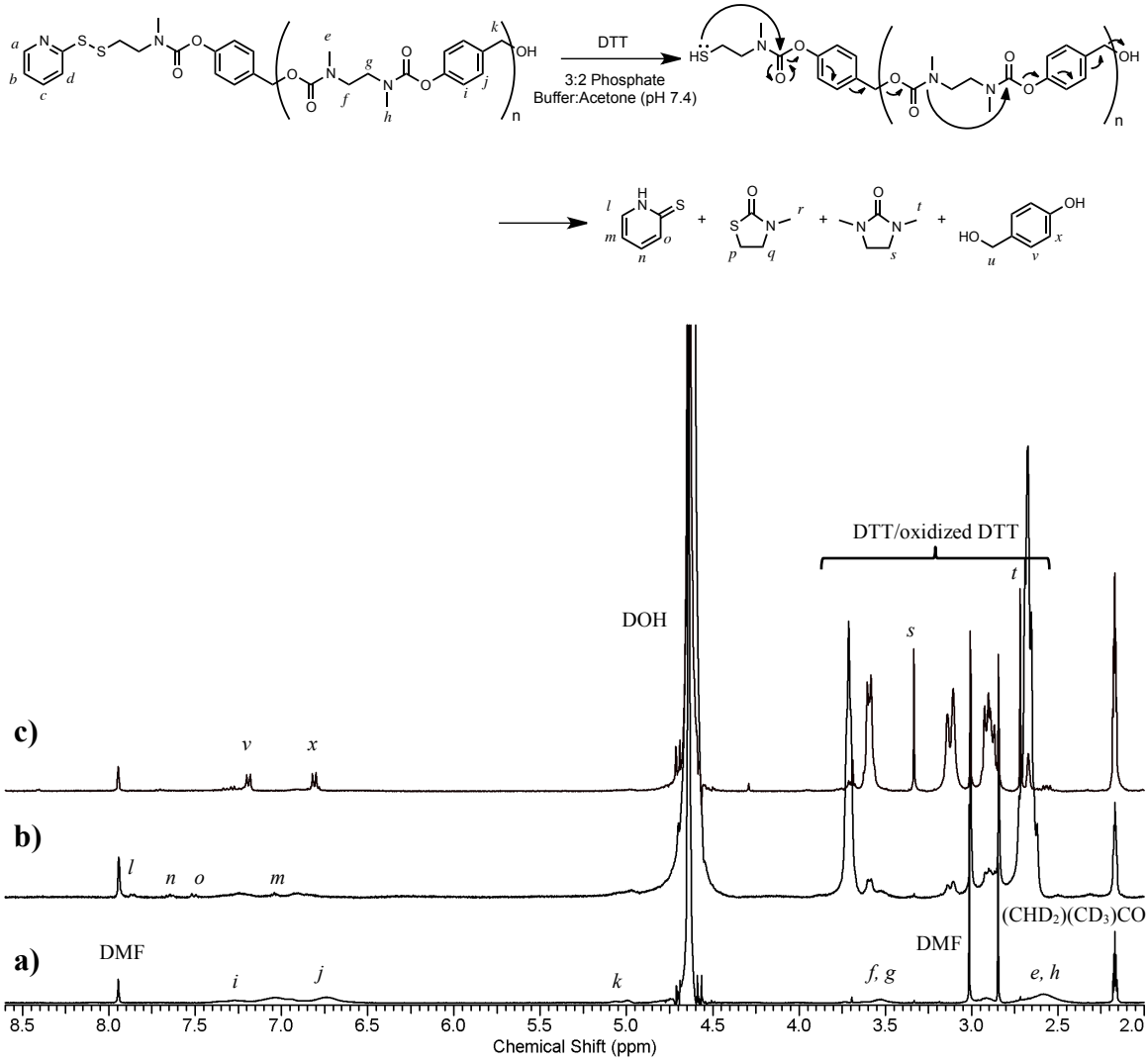

Figure 3.7: ^{1}H NMR spectra of polymer 3.14: (a) immediately following dissolution in 0.1 M pH 7.4 phosphate buffered D_2O:acetone-d_6 (3:2) at 37˚C; (b) after complete disulfide reduction 5 min after DTT addition; and (c) following complete degradation after 40 h in a highly reducing environment (0.1 M DTT).

3.3.4 Self-Assembly of Self-Immolative Block Copolymers

The formation of PEG-self-immolative nanoparticles in our group was initially accomplished through sonication of the amphiphilic block copolymers in aqueous solution over a prolonged period of time.[19] Although effective in generating micelles, this method resulted in a broad size distribution and suffered from a lack of reproducibility. Our more recent attempts have focused on the use of nanoprecipitation techniques to

generate functional nanoparticles with controllable diameters and uniform size distributions.[40,41] In this work, the use of a nanoprecipitation technique involving dissolution of copolymers **3.7a**, **3.7b**, and **3.16** in THF followed by a gradual addition of H_2O led to the reproducible formation of different nanoparticles. Copolymer **3.7a** was found to assemble into micelles with an average diameter of approximately 80 nm, while copolymer **3.7b** assembled into larger, non-spherical nanoparticles with an average diameter of approximately 330 nm as determined by dynamic light scattering (DLS) (Figure 3.8a) and transmission electron microscopy (TEM) (Figure 3.9a & b). It was originally anticipated that the incorporation of the smaller 2000 g/mol PEG end cap in copolymer **3.7a** could lead to the formation of polymer vesicles by reducing the fraction of the hydrophilic block to within 25 to 45%, as required for vesicle formation. Although vesicles were not observed in this preliminary study, further investigation of the PEG-self-immolative system may still yield such assemblies. In particular, further increases to the fraction of the polycarbamate backbone, incorporation of smaller PEG end caps, a reduction to the PDI of the copolymer, or an alternate method of preparation, such as thin film hydration, may promote the assembly of polymer vesicles.[42-44]

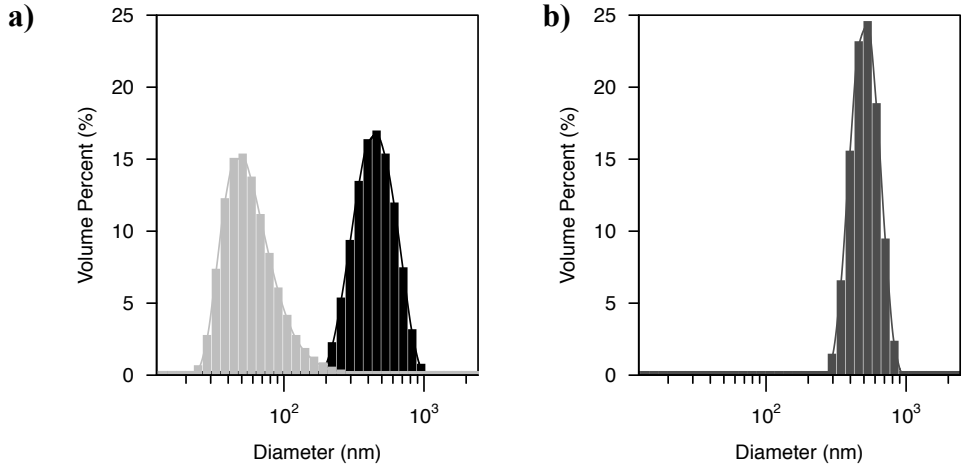

Figure 3.8: Dynamic light scattering traces of nanoparticles derived from (a) PEG succinic acid based block copolymers 3.7a (d=78.5 ± 1.4 nm, PDI=1.51 ± 0.17 × 10^{-1}) (grey) and 3.7b (d=332 ± 8.1 nm, PDI=1.84 ± 0.14 × 10^{-1}) (black) or (b) PEG thiol based block copolymer 3.16 (d=499 ± 22 nm, PDI=2.81 ± 0.27 × 10^{-1}) (dark grey). All traces obtained at a concentration of 0.1 mg/mL.

Nanoprecipitation of copolymer **3.16** led to the formation of spherical nanoparticles with an average diameter of approximately 500 nm as measured by DLS (Figure 3.8b) and TEM (Figure 3.9c). Notably, the nanoparticles derived from this amphiphilic block copolymer displayed a narrower size distribution compared to that of either **3.7a** or the more closely related **3.7b**, bearing a 5000 g/mol PEG end cap. The narrowing of the particle size distribution is attributed to the differences in the molecular weight distributions and the presence of unreacted PEG end caps in **3.7a** and **3.7b**. It has been previously shown that the presence of homopolymers and surfactants has a strong influence on nanoparticle size and polydispersity.[42,45] Therefore, the inefficient macromolecular end cap incorporation method utilized for **3.7a** and **3.7b** may have adverse effects on the polydispersity of the resultant nanoparticles.

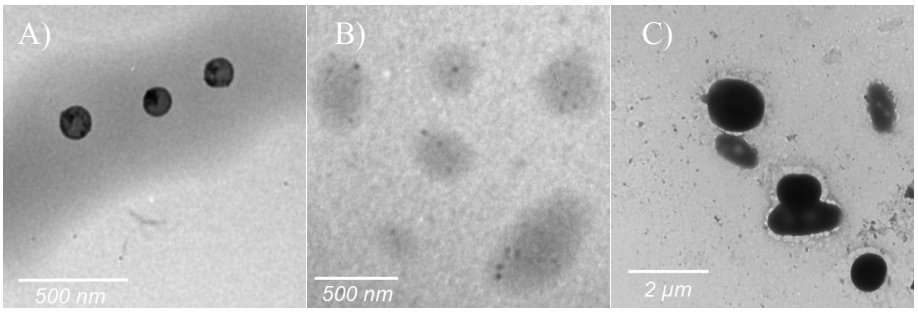

Figure 3.9: Transmission electron microscopy images of the nanoparticles formed from copolymers 3.7a (a), 3.7b (b), and 3.16 (c).

Collectively, the results observed for **3.7b** and **3.16** indicate that the incorporation of the larger 5000 g/mol PEG chain results in the formation of large nanoparticles with diameters in the range of 200 nm to 1 µm. In theory, the incorporation of larger PEG chains should increase the curvature and reduce the diameter of the resultant nanoparticles. The failure of the two systems investigated in this work to assemble into smaller nanoparticles may be indicative of a substantial amount of unconjugated homopolymer chains that promote the aggregation of the amphiphilic copolymers into larger, non-spherical assemblies. Since the optimum particle size to maximize blood circulation time is around 80-150 nm,[43] further modification of this system is necessary to improve the biomedical utility of self-immolative nanoparticles involving 5000 g/mol PEG chains. Based on the preliminary results observed in this study, incorporation of

PEG chains smaller than 5000 g/mol may be more ideal for the formation of nanoparticles for biomedical applications.

3.4 Self-Immolative Nanoparticle Degradation

The degradation of the nanoparticles derived from **3.7a** and **3.7b** were studied under pseudo-physiological conditions in 0.1 M pH 7.4 phosphate buffer (D_2O) by NMR spectroscopy. Our initial study suggested that the degradation of PEG-self-immolative copolymers is diffusion controlled in aqueous conditions due to the shielding of the ester linkage between the hydrophilic and hydrophobic blocks on the interior of the hydrophilic corona and that the depolymerization of the polycarbamate block was slowed due to the increased hydrophobicity in the interior of the nanoparticle core. As a result, the PEG-self-immolative nanoparticles display a much slower rate of degradation than that dictated by their solution phase degradation kinetics. It was originally envisioned that the incorporation of a smaller PEG chain to reduce the overall size of the hydrophilic layer would reduce the degradation time of these nanoparticles by decreasing the path over which diffusion must occur. Interestingly, our preliminary, single run data suggests that the size of the PEG chain has no effect on the degradation kinetics of the nanoparticles, as the degradation profile of **3.7a** roughly mirrored that of **3.7b**. However, further investigation of this system is necessary to verify such an observation. In particular, the nanoparticles derived for these NMR degradation studies should be formed by a nanoprecipitation method instead of the currently employed sonication method to exert a higher degree of control over the self-assembly process. More comprehensive studies are also required to investigate diffusion effects since the use of ^{1}H NMR spectroscopy to monitor byproduct formation only offers limited insight into the controlling processes behind nanoparticle degradation.

A preliminary investigation of the degradation kinetics for copolymer **3.16** was not carried out due to the amount of material and the time required for a NMR degradation study. The degradation and release kinetics of this system will be the subject of ongoing investigation in our laboratory due to its potential to form stimuli-responsive self-immolative nanoparticles for the controlled release of hydrophobic molecules under redox conditions.

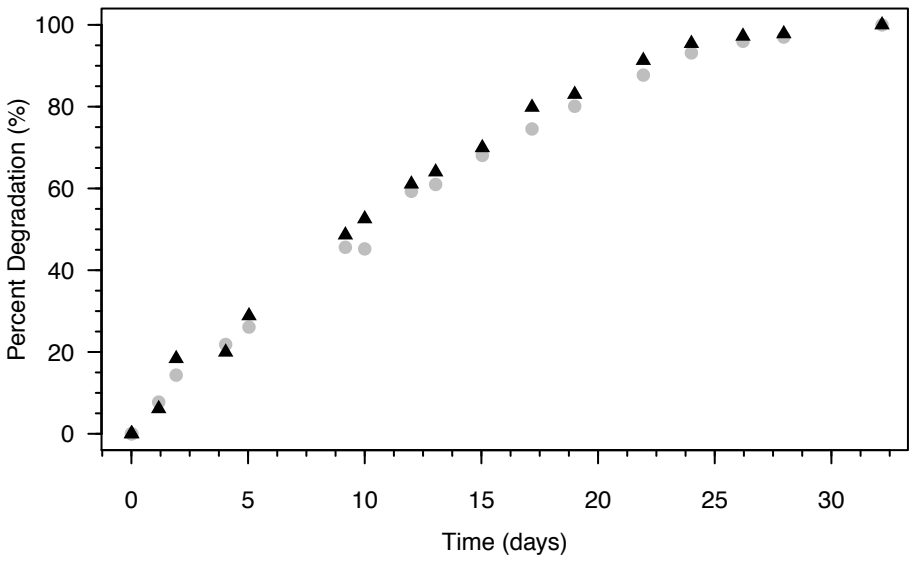

Figure 3.10: Kinetics of self-immolative nanoparticle degradation in 0.1 M pH 7.4 phosphate buffer (D_2O) for copolymer 3.7a (●) and 3.7b (▲) as measured by ^1H NMR spectroscopy.

3.5 Conclusion

In conclusion, significant advancements have been made in the development of self-immolative nanoparticles incorporating cyclization spacers for controlled release applications. In this work we presented an alternate low-cost method of generating self-immolative amphiphilic block copolymers using our previously reported linear self-immolative polymer backbone derived from alternating 4-hydroxybenzyl alcohol and *N,N'*-dimethylethylenediamine spacers. This method involved the use of PEG succinic acid-based macromolecular end capping agents during polymerization of the polycarbamate backbone. Although this system provided a versatile means of evaluating the self-assembly characteristics of the amphiphilic block copolymers, it lacks a stimuli-responsive trigger to initiate self-immolative degradation. A redox-sensitive variant of this design was developed to address this limitation by incorporating a disulfide linkage between the hydrophilic and hydrophobic blocks. This redox-sensitive amphiphilic block copolymer was synthesized through an improved modular approach in which backbone polymerization and PEG incorporation are decoupled from one another. It is expected that this modular approach will be more widely utilized than the macromolecular end cap

strategy due to an increased control over the characteristics and purity of the amphiphilic block copolymers. The self-assembly characteristics of both copolymers were investigated using a nanoprecipitation technique, however, vesicles could not be formed by reducing the size of the incorporated PEG end cap from 5000 g/mol to 2000 g/mol. Despite the immense promise, further investigation of the self-assembly characteristics as well as the degradation and release kinetics of these self-immolative nanoparticles is required before they can receive widespread biomedical application as drug delivery vehicles.

3.6 References

(1) Wang, W.; Alexander, C. *Angew. Chem. Int. Ed.* **2008**, *47*, 7804.

(2) Blencowe, C. A.; Russell, A. T.; Greco, F.; Hayes, W.; Thornthwaite, D. W. *Polym. Chem.* **2011**, *2*, 773.

(3) Esser-Kahn, A. P.; Odom, S. A.; Sottos, N. R.; White, S. R.; Moore, J. S. *Macromolecules* **2011**, *44*, 5539.

(4) Wong, A. D.; DeWit, M. A.; Gillies, E. R. *Adv. Drug Delivery Rev.* **2012**, *64*, 1031.

(5) Peterson, G. I.; Larsen, M. B.; Boydston, A. J. *Macromolecules* **2012**, *45*, 7317.

(6) Amir, R. J.; Danieli, E.; Shabat, D. *Chem. Eur. J.* **2007**, *13*, 812.

(7) Sella, E.; Shabat, D. *Chem. Commun.* **2008**, 5701.

(8) Avital-Shmilovici, M.; Shabat, D. *Bioorg. Med. Chem.* **2010**, *18*, 3643.

(9) Sella, E.; Lubelski, A.; Klafter, J.; Shabat, D. *J. Am. Chem. Soc.* **2010**, *132*, 3945.

(10) Sella, E.; Weinstain, R.; Erez, R.; Burns, N. Z.; Baran, P. S.; Shabat, D. *Chem. Commun.* **2010**, *46*, 6575.

(11) Perry-Feigenbaum, R.; Sella, E.; Shabat, D. *Chem. Eur. J.* **2011**, *17*, 12123.

(12) Karton-Lifshin, N.; Shabat, D. *New J. Chem.* **2012**, *36*, 386.

(13) Seo, W.; Phillips, S. T. *J. Am. Chem. Soc.* **2010**, *132*, 9234.

(14) Weinstain, R.; Baran, P. S.; Shabat, D. *Bioconjugate Chem.* **2009**, *20*, 1783.

(15) Esser-Kahn, A. P.; Sottos, N. R.; White, S. R.; Moore, J. S. *J. Am. Chem. Soc.* **2010**, *132*, 10266.

(16) Zhang, H.; Yeung, K.; Robbins, J. S.; Pavlick, R. A.; Wu, M.; Liu, R.; Sen, A.; Phillips, S. T. *Angew. Chem. Int. Ed.* **2012**, *51*, 2400.

(17) Shamis, M.; Lode, H. N.; Shabat, D. *J. Am. Chem. Soc.* **2004**, *126*, 1726.

(18) Erez, R.; Segal, E.; Miller, K.; Satchi-Fainaro, R.; Shabat, D. *Bioorg. Med. Chem.* **2009**, *17*, 4327.

(19) DeWit, M. A.; Gillies, E. R. *J. Am. Chem. Soc.* **2009**, *131*, 18327.

(20) de Gracia Lux, C.; McFearin, C. L.; Joshi-Barr, S.; Sankaranarayanan, J.; Fomina, N.; Almutairi, A. *ACS Macro Lett.* **2012**, *1*, 922.

(21) Li, S.; Szalai, M. L.; Kevwitch, R. M.; McGrath, D. V. *J. Am. Chem. Soc.* **2003**, *125*, 10516.

(22) Amir, R. J.; Pessah, N.; Shamis, M.; Shabat, D. *Angew. Chem. Int. Ed.* **2003**, *42*, 4494.

(23) de Groot, F. M. H.; Albrecht, C.; Koekkoek, R.; Beusker, P. H.; Scheeren, H. W. *Angew. Chem. Int. Ed.* **2003**, *42*, 4490.

(24) DeWit, M. A.; Beaton, A.; Gillies, E. R. *J. Polym. Sci. A Polym. Chem.* **2010**, *48*, 3977.

(25) DeWit, M. A.; Gillies, E. R. *Org. Biomol. Chem.* **2011**, *9*, 1846.

(26) Chen, E. K. Y.; McBride, R. A.; Gillies, E. R. *Macromolecules* **2012**, *45*, 7364.

(27) Sagi, A.; Weinstain, R.; Karton, N.; Shabat, D. *J. Am. Chem. Soc.* **2008**, *130*, 5434.

(28) Weinstain, R.; Sagi, A.; Karton, N.; Shabat, D. *Chem. Eur. J.* **2008**, *14*, 6857.

(29) Kaitz, J. A.; Moore, J. S. *Macromolecules* **2013**, *46*, 608.

(30) DiLauro, A. M.; Abbaspourrad, A.; Weitz, D. A.; Phillips, S. T. *Macromolecules* **2013**, *46*, 3309.

(31) DiLauro, A. M.; Robbins, J. S.; Phillips, S. T. *Macromolecules* **2013**, *46*, 2963.

(32) Kuppusamy, P.; Li, H.; Ilangovan, G.; Cardounel, A. J.; Zweier, J. L.; Yamada, K.; Krishna, M. C.; Mitchell, J. B. *Cancer Res.* **2002**, *62*, 307.

(33) Saito, G.; Swanson, J. A.; Lee, K.-D. *Adv. Drug Delivery Rev.* **2003**, *55*, 199.

(34) Wu, G.; Fang, Y.-Z.; Yang, S.; Lupton, J. R.; Turner, N. D. *J. Nutr.* **2004**, *134*, 489.

(35) El Alaoui, A.; Schmidt, F.; Amessou, M.; Sarr, M.; Decaudin, D.; Florent, J.-C.; Johannes, L. *Angew. Chem. Int. Ed.* **2007**, *46*, 6469.

(36) Napoli, A.; Tirelli, N.; Kilcher, G.; Hubbell, A. *Macromolecules* **2001**, *34*, 8913.

(37) Cerritelli, S.; Velluto, D.; Hubbell, J. A. *Biomacromolecules* **2007**, *8*, 1966.

(38) Kawada, A.; Yasuda, K.; Abe, H.; Harayama, T. *Chem. Pharm. Bull.* **2002**, *50*, 380.

(39) Lee, J. H.; Lim, C. S.; Tian, Y. S.; Han, J. H.; Cho, B. R. *J. Am. Chem. Soc.* **2010**, *132*, 1216.

(40) DeWit, M. A.; Nazemi, A.; Karamdoust, S.; Beaton, A.; Gillies, E. R. In *Non-Conventional Functional Block Copolymers*; Theato, P., Kilbinger, A. F. M., Coughlin, E. B., Eds.; Amer Chemical Soc: Washington, 2011; Vol. 1066, p 9.

(41) Nazemi, A.; Amos, R. C.; Bonduelle, C. V.; Gillies, E. R. *J. Polym. Sci. A Polym. Chem.* **2011**, *49*, 2546.

(42) Lim, P.; Eisenberg, A. *J. Polym. Sci., Part B: Polym. Phys.* **2004**, *42*, 923.

(43) Brinkhuis, R. P.; Rutjes, F. P. J. T.; van Hest, J. C. M. *Polym. Chem.* **2011**, *2*, 1449.

(44) Tanner, P.; Baumann, P.; Enea, R.; Onaca, O.; Palivan, C.; Meier, W. *Acc. Chem. Res.* **2011**, *44*, 1039.

(45) Huang, J.-b.; Zhu, Y.; Zhu, B.-y.; Li, R.-k.; Fu, H.-l. *J. Colloid Interface Sci.* **2001**, *236*, 201.

Chapter 4

4 Conclusions and Future Perspectives

The work described in this thesis focused on two currently underexplored areas in the field of linear self-immolative polymers: degradation kinetics and functional designs. In the first section (Chapter 2), the degradation kinetics of linear self-immolative polymers involving cyclization spacers were investigated with the overall goal of developing a generalized model to relate the kinetics of polymer degradation to monomer cyclization. In addition, it was sought to demonstrate chain length as an alternate means to tune the degradation time in linear self-immolative polymer systems. This was accomplished using the previously reported linear self-immolative polycarbamate backbone derived from alternating 4-hydroxybenzyl alcohol and *N,N'*-dimethylethylenediamine spacers. A degradation model was first derived from first principles by treating backbone degradation as a series of first-order intramolecular reactions. This model was then applied to the degradation of a set of monodisperse oligomers synthesized through a new iterative, convergent method to validate the assumptions used during model development. These results were then extended to the polydisperse case by applying the self-immolative degradation model to the degradation of a set of polymers synthesized to display varying molecular weights.

The experimental findings and computer simulations explored in the first section give proof that linear self-immolative polymer systems exhibit mixed-mode degradation kinetics with an initial pseudo zero-order domain that gradually transitions towards first order behaviour. This particular mechanism of degradation is highly controlled by the kinetics of monomer self-immolation and results in a proportional dependence of degradation time on chain length. Hence, the results presented in the first section demonstrate that varying chain length is a viable means to control and tune the degradation time in linear self-immolative polymer systems. Such a finding has significant implications on the use of linear self-immolative polymers for biomedical applications as the degradation time of these polymers can now effectively be tuned two-dimensionally through rational monomer design and molecular weight control.

The second section of this work (Chapter 3) was geared towards the development of self-immolative amphiphilic block copolymers involving cyclization spacers for controlled release applications. A modified procedure was proposed for the fabrication of self-immolative block copolymers using low-cost PEG succinic acid-based end caps. This method was demonstrated to be a versatile means of generating model compounds to investigate the self-assembly characteristics of self-immolative copolymers. However, the incorporation of the PEG block through an ester linkage failed to exploit the potential for stimuli-responsive degradation in self-immolative systems. As a result, a modified variant of the initial design was developed to incorporate a reduction sensitive disulfide linkage between the hydrophilic PEG block and hydrophobic self-immolative block. This new design was synthesized through an improved modular approach in which PEG incorporation was decoupled from polymerization of the self-immolative backbone. Such an approach allowed for an increased control over the composition and purity of the self-immolative block copolymers compared to the incorporation of the PEG block during backbone polymerization. Despite the promise of this system, additional work is required to optimize the fabrication of functional redox-sensitive nanoparticles and to study the degradation and release kinetics of this system under physiological conditions.

Collectively, the work presented in this thesis serves to expand the utility of linear self-immolative polymers for biomedical applications. The kinetic model describing linear self-immolative degradation and subsequent model validation offers the first conclusive proof of the proportional relationship between degradation time and chain length. In conjunction with rational monomer design, this property can be used to fine-tune the degradation time of these polymers with a level of precision that greatly surpasses that available in traditional biodegradable systems. It is expected that this model will serve as an initial point of reference in the design and tailoring of future linear self-immolative polymer systems with controllable degradation times. This model also offers new insight into the mixed-mode, pseudo zero- and first-order kinetic phenomenon observed in the degradation of linear self-immolative polymer systems. This property has yet to be explored in the context of controlled release and should greatly increase the usefulness of these materials relative to their dendrimer counterparts. A number of different macromolecular prodrug strategies can be envisioned to exploit this effect in order to

achieve an initial period of pseudo zero-order release, which is highly desirable in the field of drug delivery.

The functional linear self-immolative block copolymer designs presented in this thesis demonstrate the inherent flexibility of such materials. With much of the synthetic groundwork laid in the design of linear self-immolative polymer backbones, a shift in focus needs to be geared towards the application of these materials through controlled design. The two systems explored in this work are promising examples of the ease at which linear self-immolative polymers can be incorporated into amphiphilic block copolymers capable of self-assembly in aqueous solution. Future work in the development of these materials should also focus on the incorporation of different stimuli-responsive linkages to initiate block separation and self-immolative backbone degradation under a variety of conditions for programmable release. The ideal design for these systems would involve an entirely self-immolative block copolymer system in which triggering groups are contained at the terminus of the hydrophilic block, directly exposed to the external environment. To this end, additional work should be conducted into developing hydrophilic self-immolative homopolymers by modifying the currently available backbones with pendent solubilizing groups such as triethylene glycol. Upon further optimization of the self-immolative block copolymer design, it is presumable these materials will receive widespread application in the field of drug delivery due their ability to form functional nanoparticles with a highly controlled mechanism of degradation.

Appendices

Appendix A: NMR Characterization Data

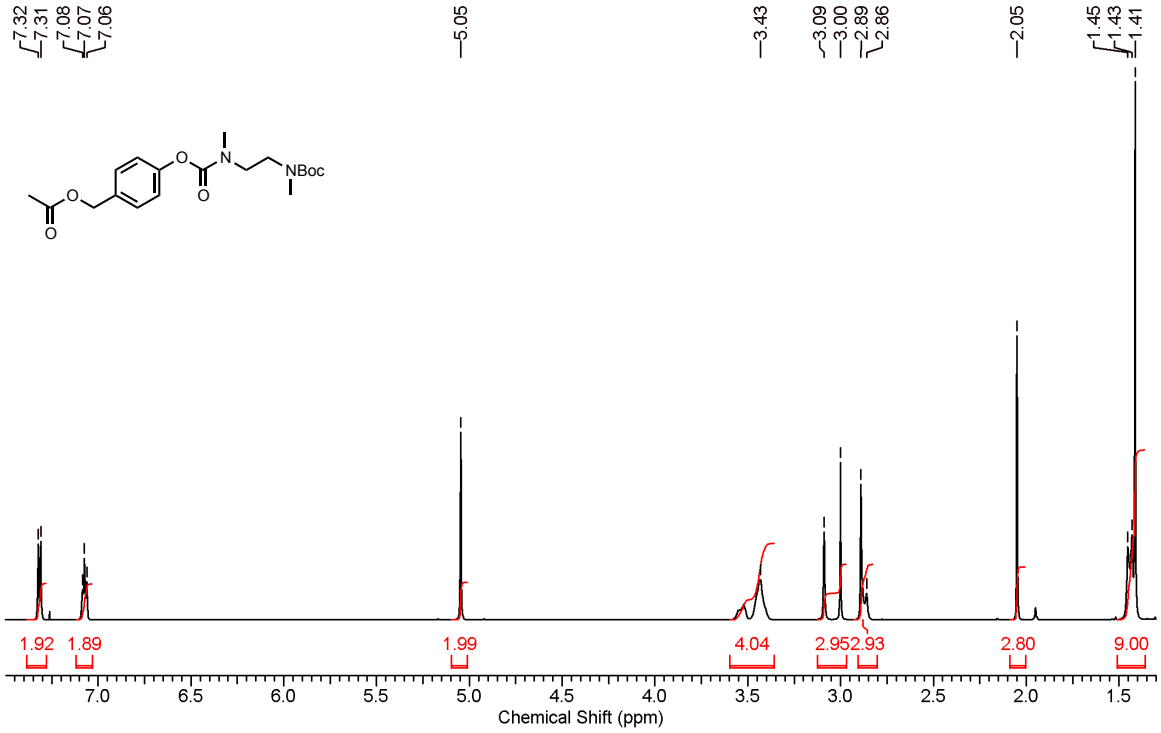

Figure A1: ^{1}H NMR spectrum of compound **2.1a** (600 MHz, $CDCl_3$)

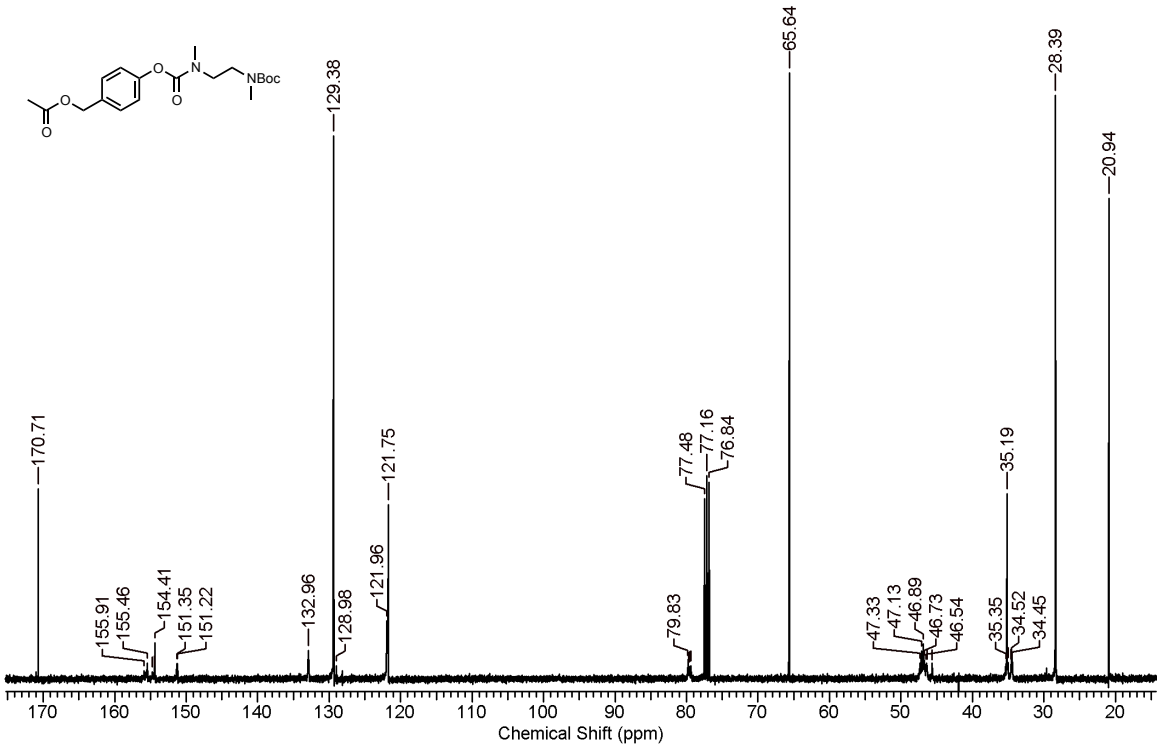

Figure A2: ^{13}C NMR spectrum of compound **2.1a** (100 MHz, $CDCl_3$)

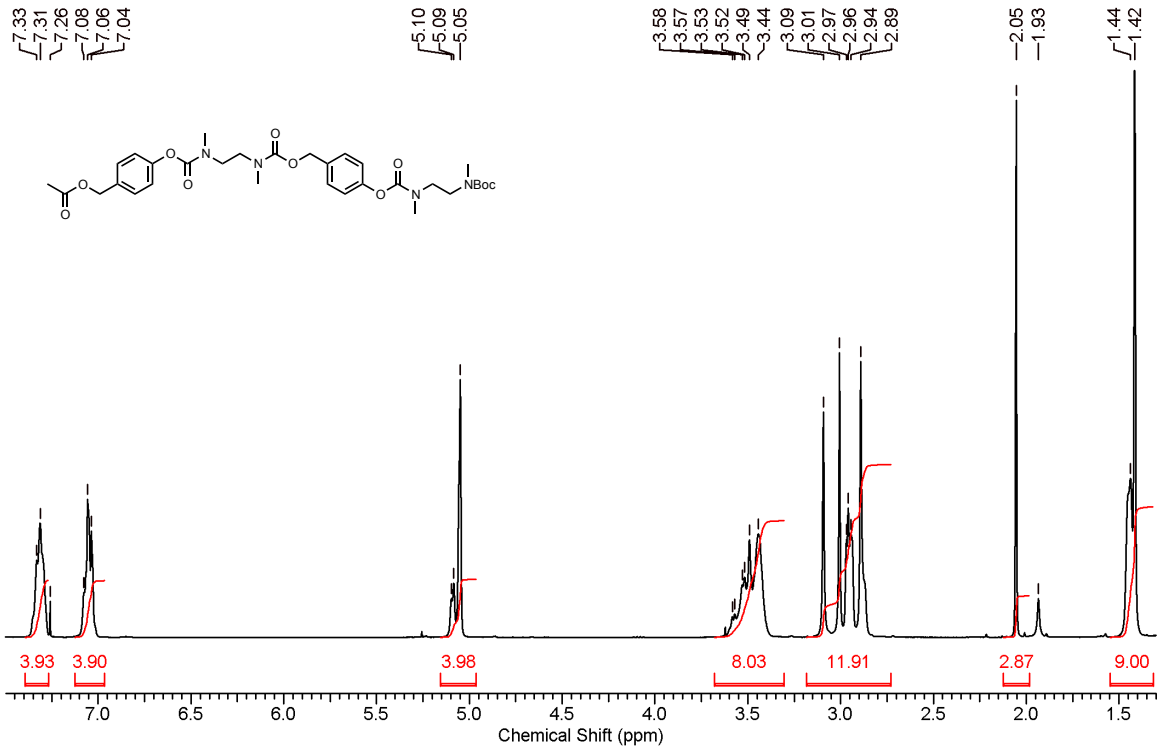

Figure A3: ^{1}H NMR spectrum of compound **2.2a** (600 MHz, $CDCl_3$)

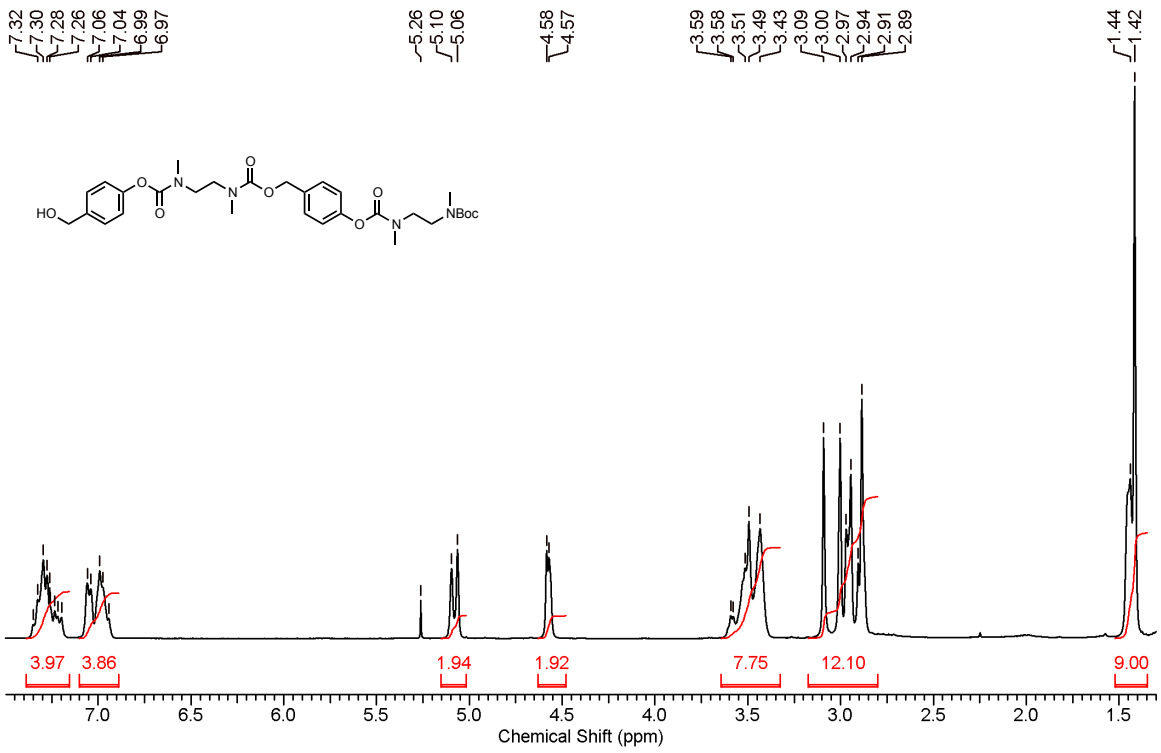

Figure A4: ^{1}H NMR spectrum of compound **2.2b** (600 MHz, $CDCl_3$)

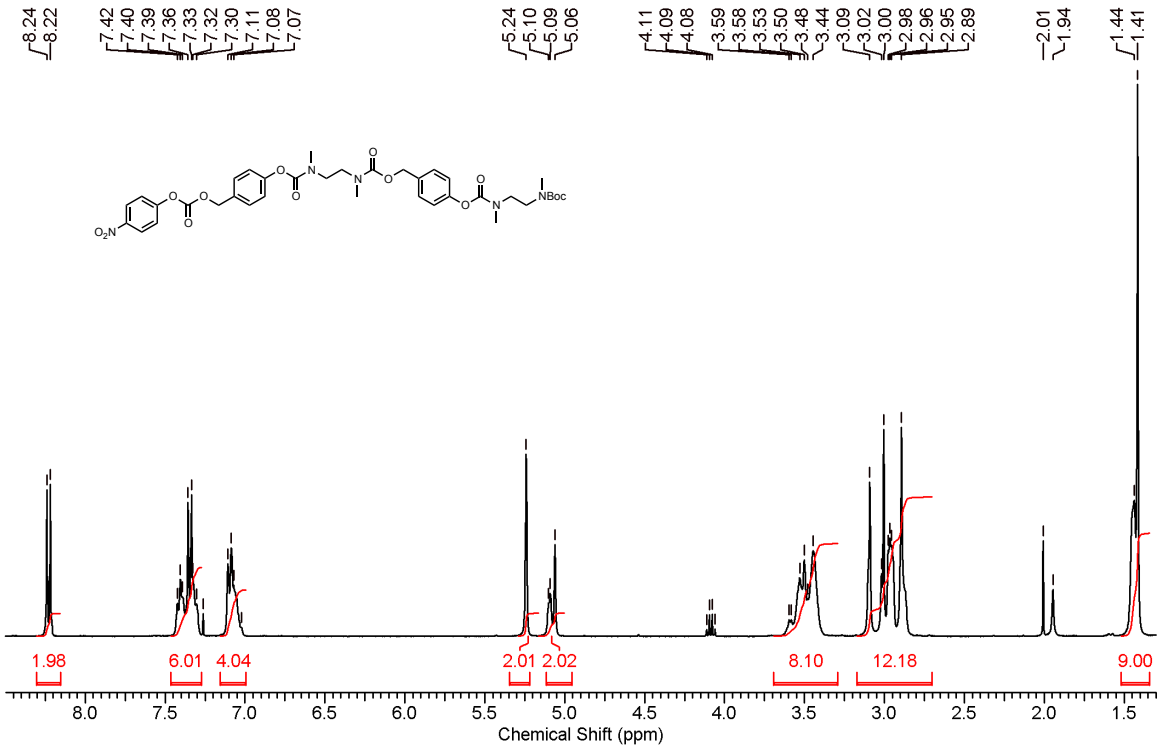

Figure A5: ^{1}H NMR spectrum of compound **2.2c** (600 MHz, $CDCl_3$)

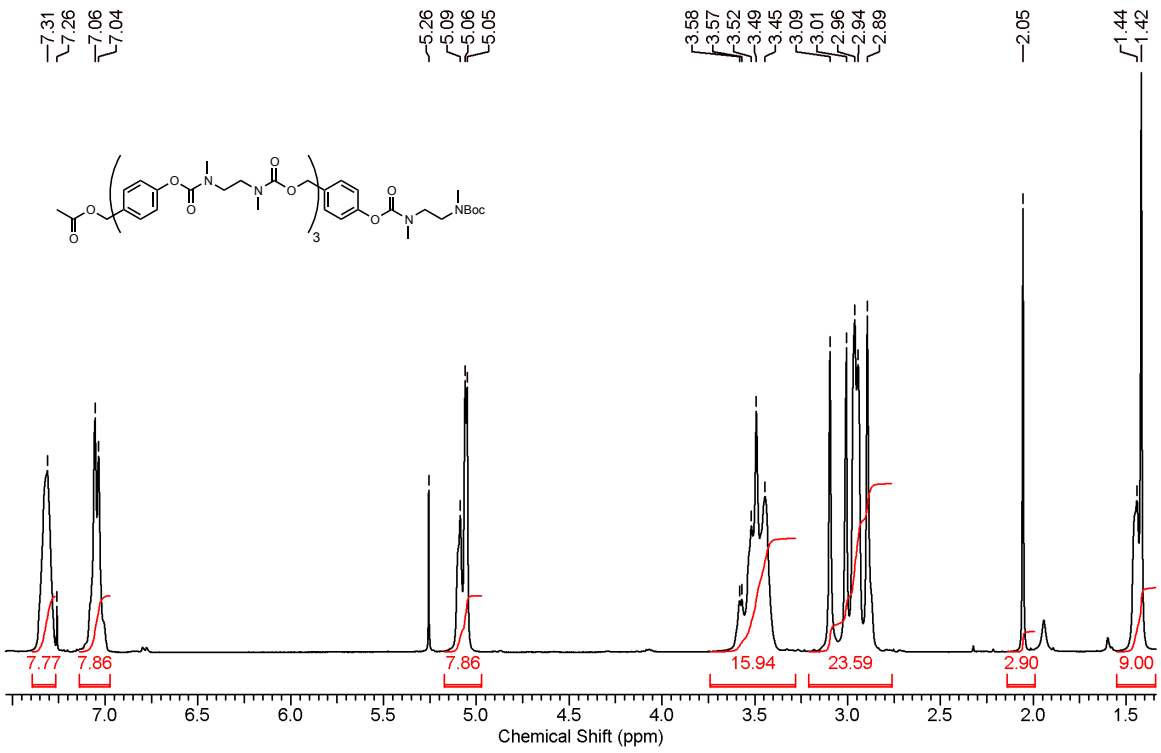

Figure A6: ^{1}H NMR spectrum of compound **2.3a** (600 MHz, $CDCl_3$)

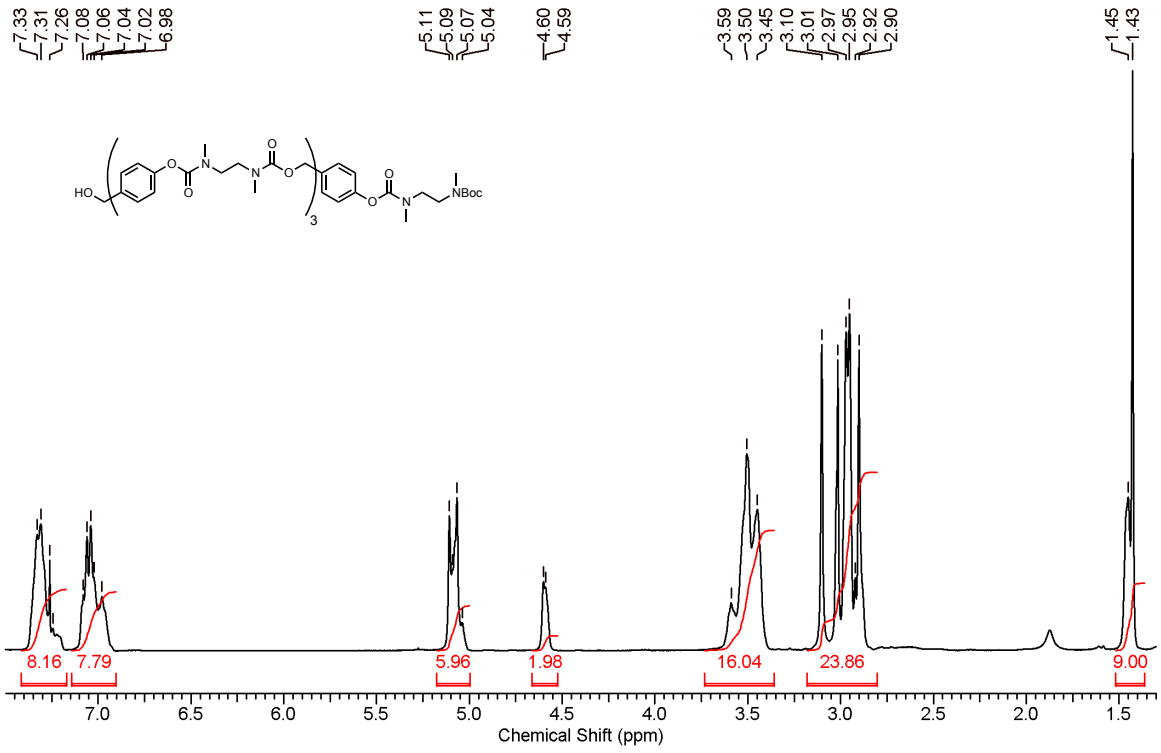

Figure A7: ^{1}H NMR spectrum of compound **2.3b** (600 MHz, $CDCl_3$)

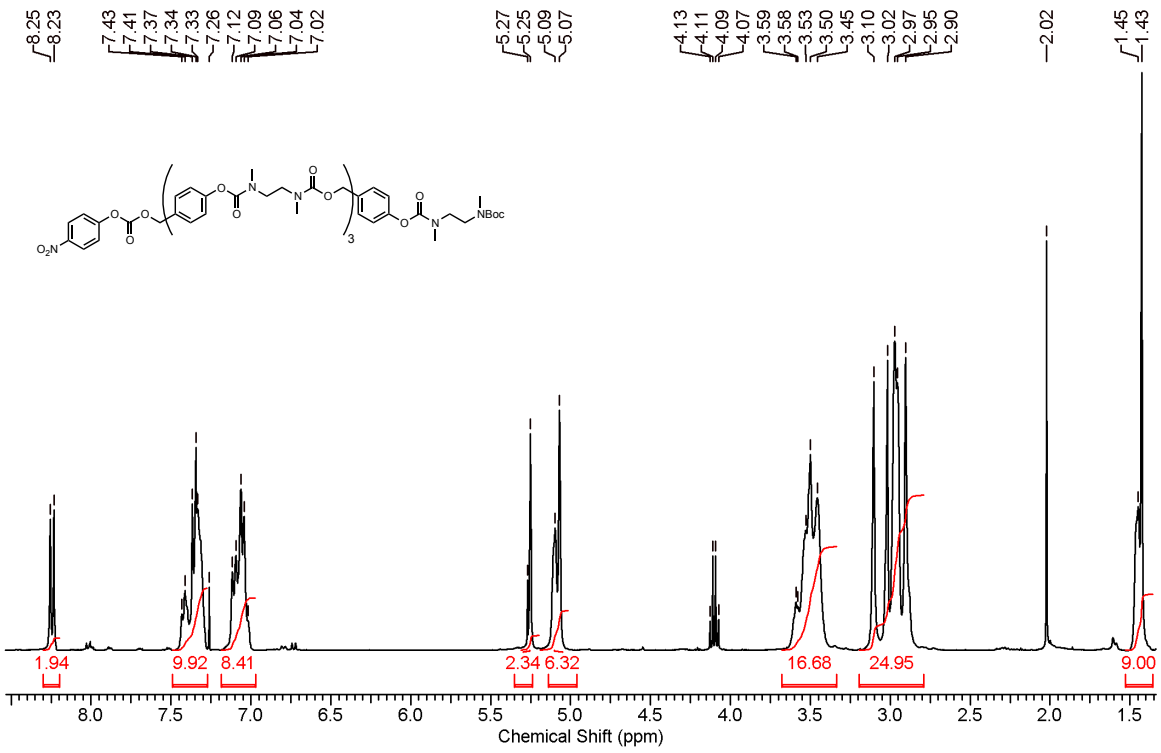

Figure A8: ^{1}H NMR spectrum of compound **2.3c** (600 MHz, $CDCl_3$)

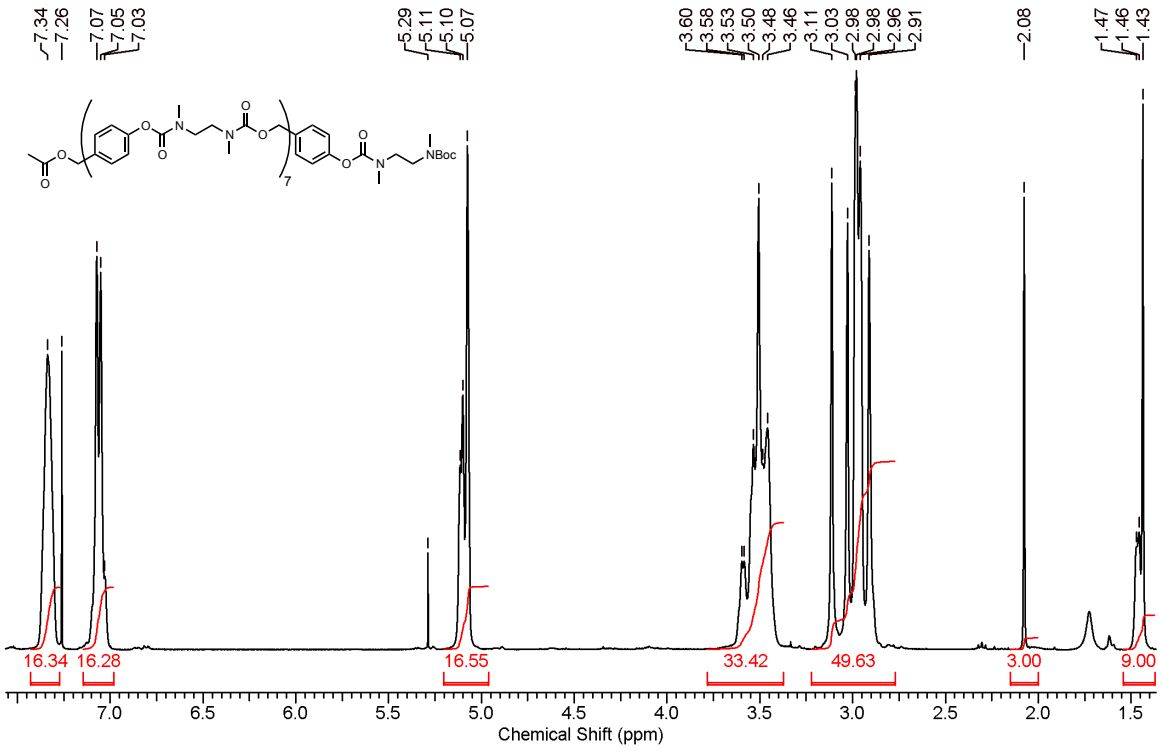

Figure A9: ^{1}H NMR spectrum of compound **2.4a** (600 MHz, $CDCl_3$)

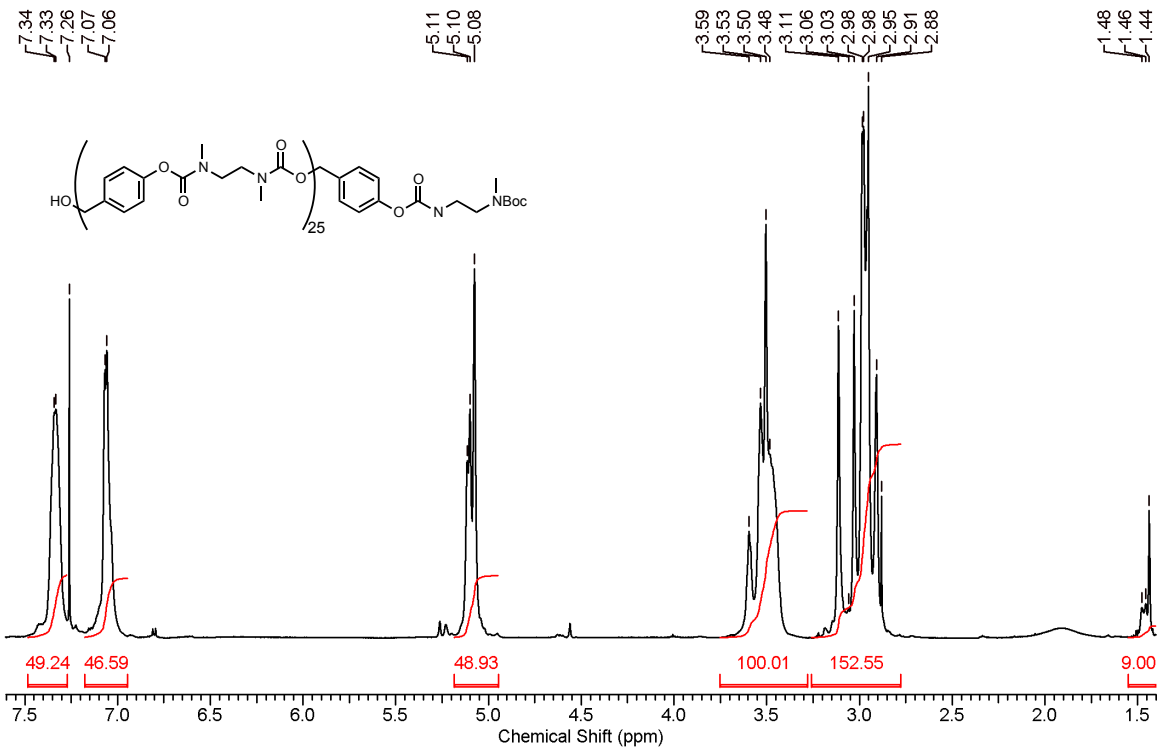

Figure A10: ^{1}H NMR spectrum of polymer **2.6** (600 MHz, $CDCl_3$)

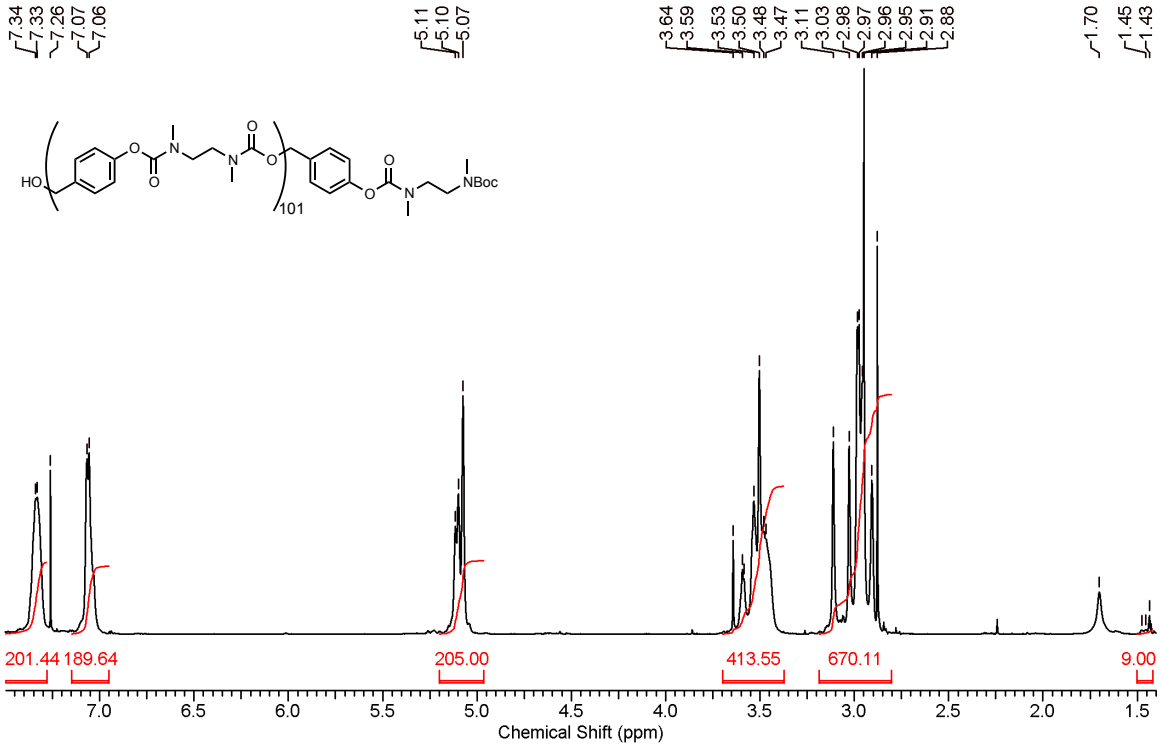

Figure A11: ^{1}H NMR spectrum of polymer **2.7** (600 MHz, $CDCl_3$)

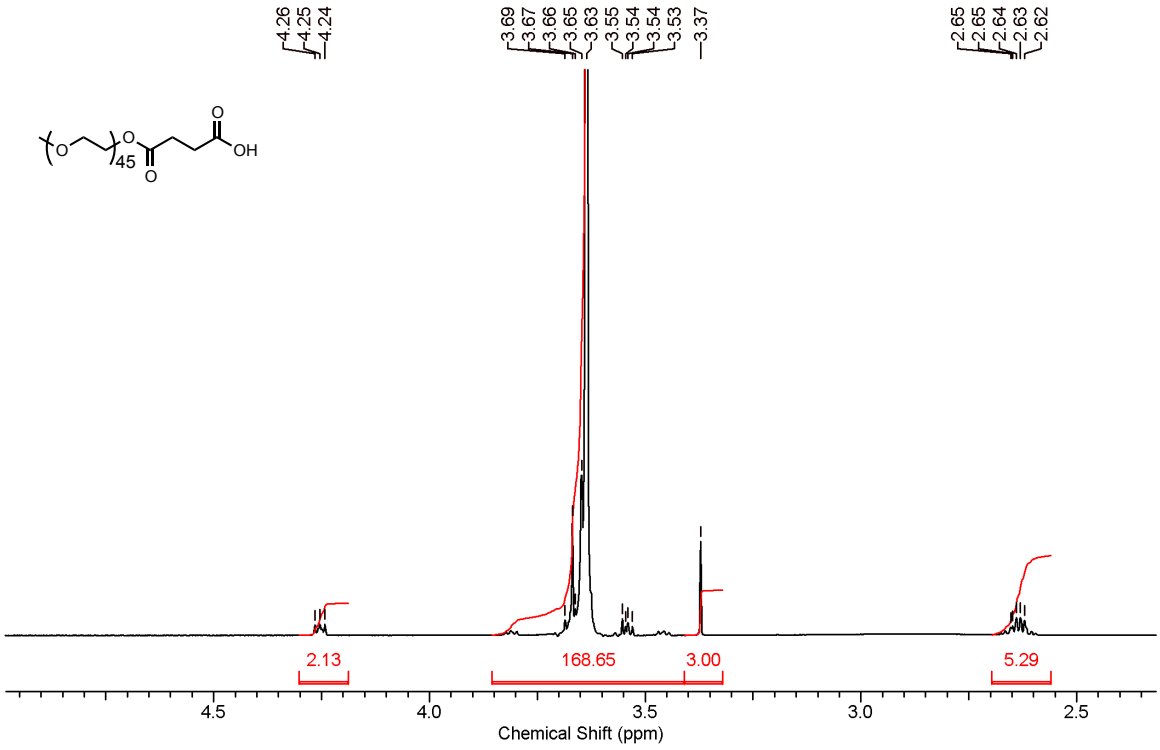

Figure A12: ^{1}H NMR spectrum of compound **3.1a** (600 MHz, $CDCl_3$)

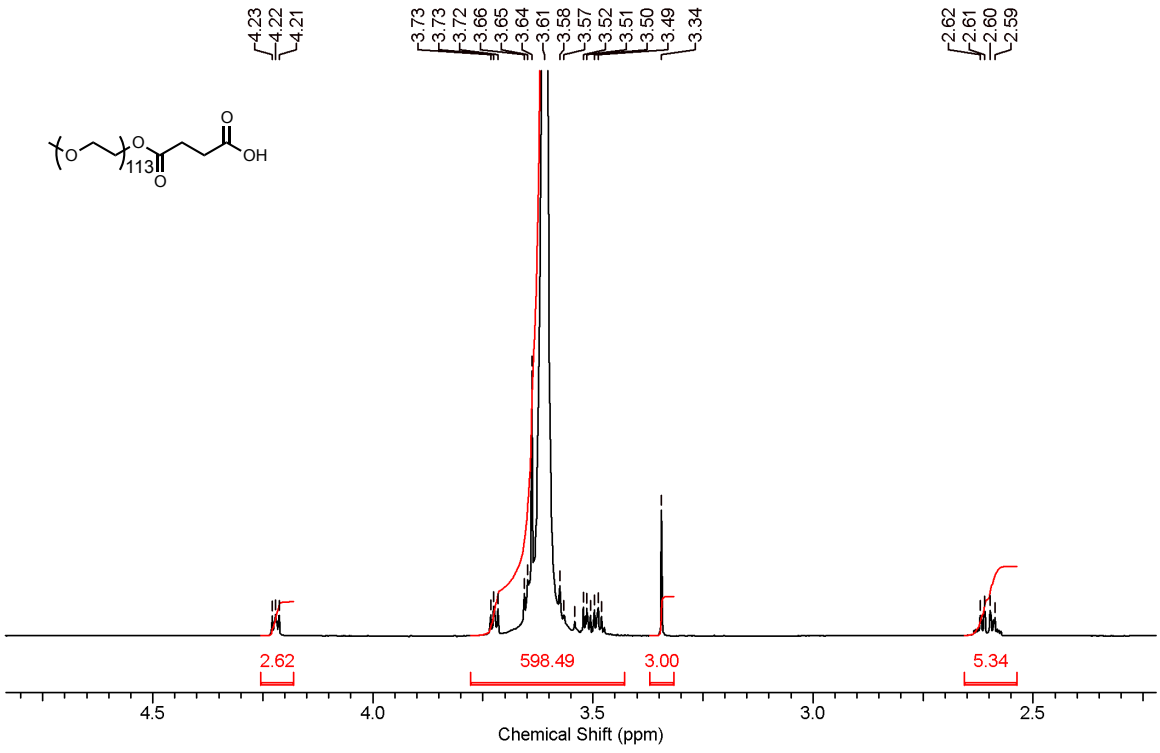

Figure A13: ^{1}H NMR spectrum of compound **3.1b** (600 MHz, $CDCl_3$)

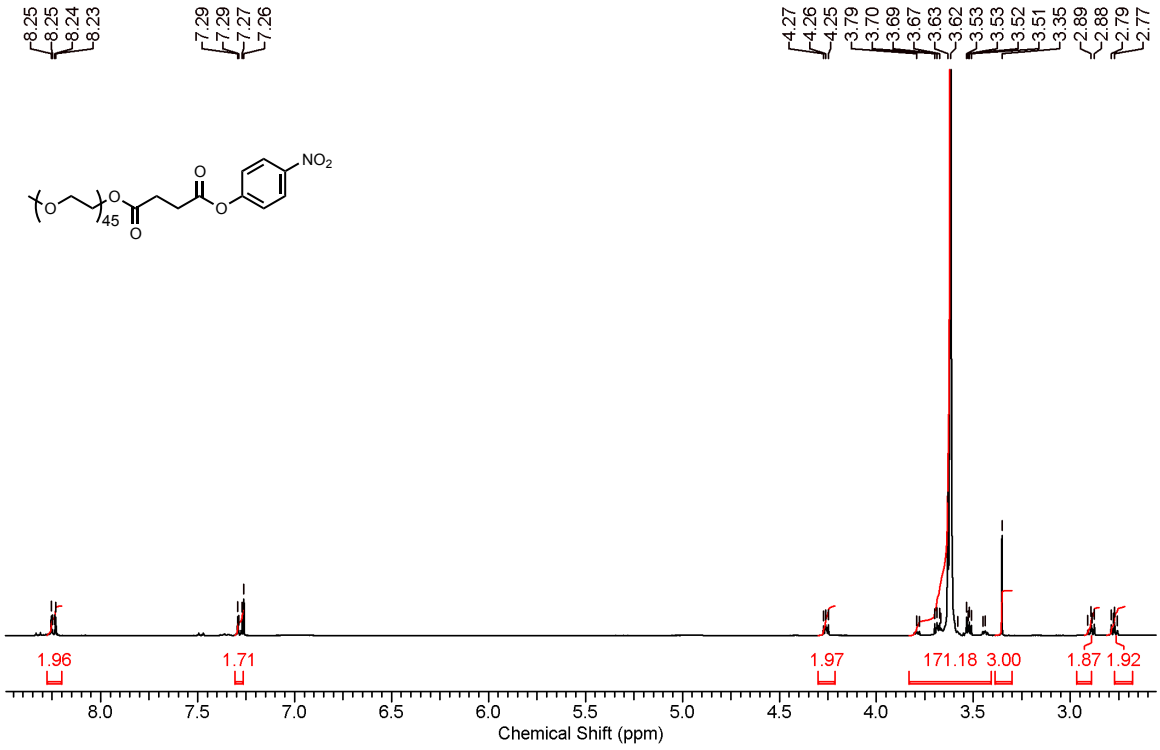

Figure A14: ^{1}H NMR spectrum of compound **3.2a** (600 MHz, $CDCl_3$)

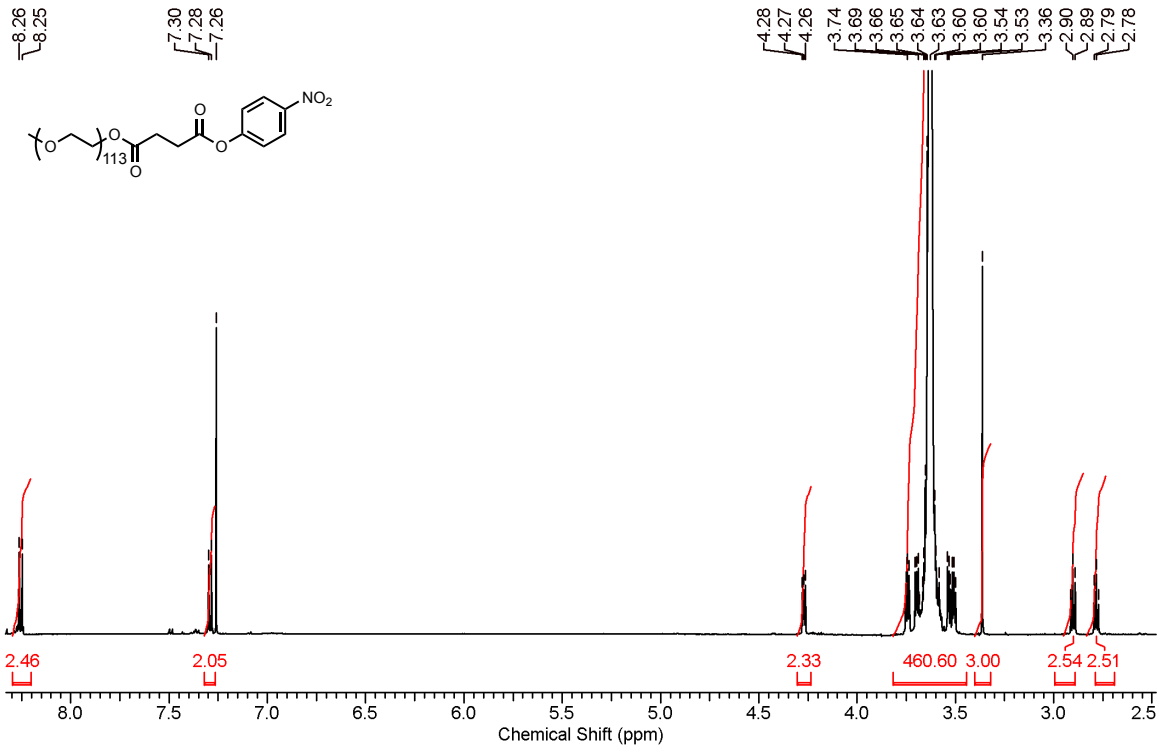

Figure A15: ^{1}H NMR spectrum of compound **3.2b** (600 MHz, $CDCl_3$)

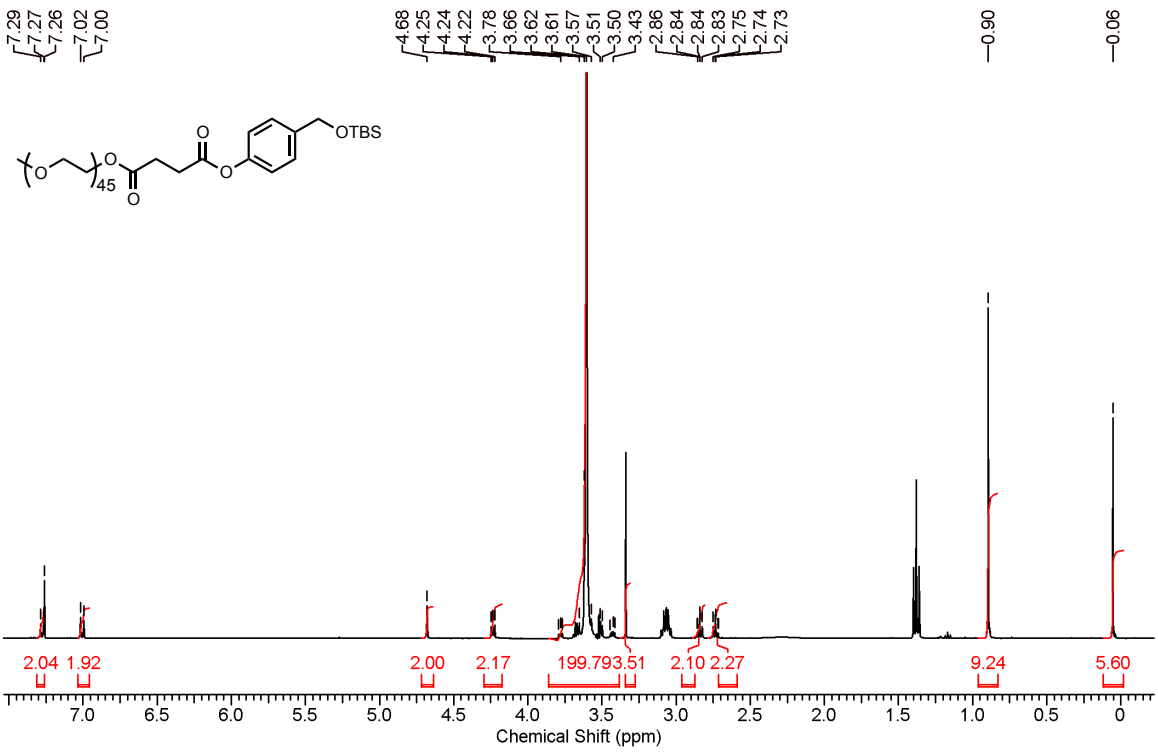

Figure A16: ^{1}H NMR spectrum of compound **3.4a** (600 MHz, $CDCl_3$)

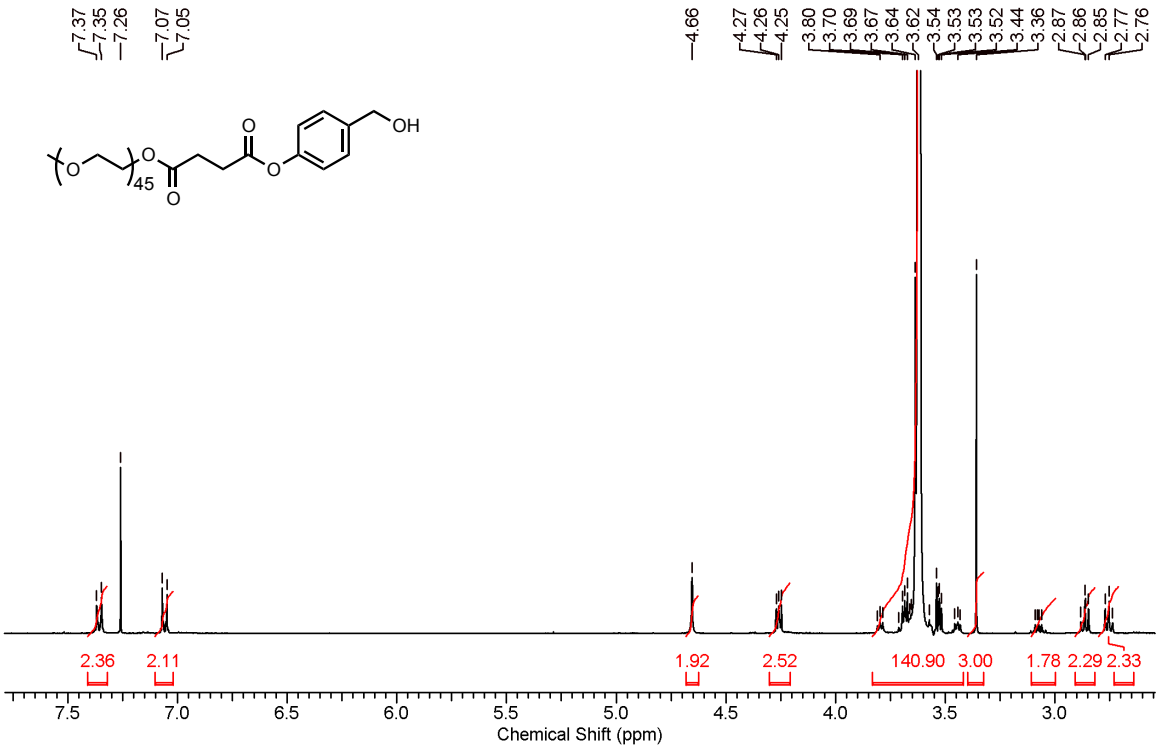

Figure A17: ^{1}H NMR spectrum of compound **3.5a** (600 MHz, $CDCl_3$)

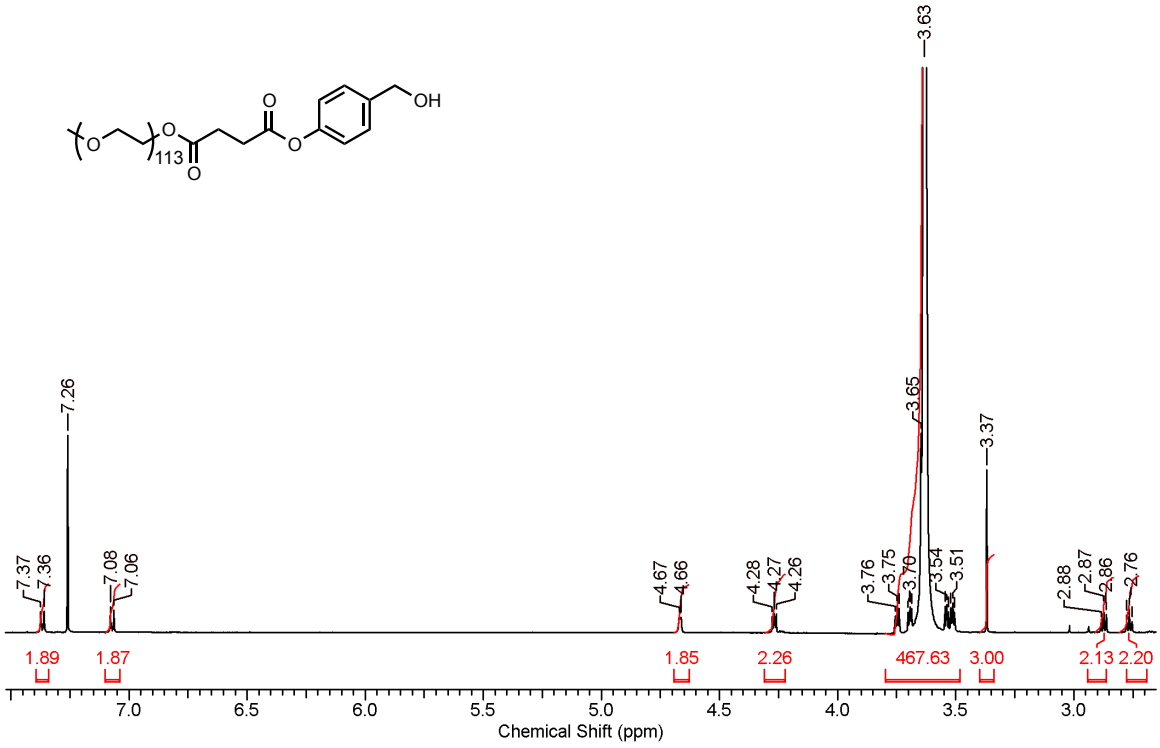

Figure A18: ^{1}H NMR spectrum of compound **3.5b** (600 MHz, $CDCl_3$)

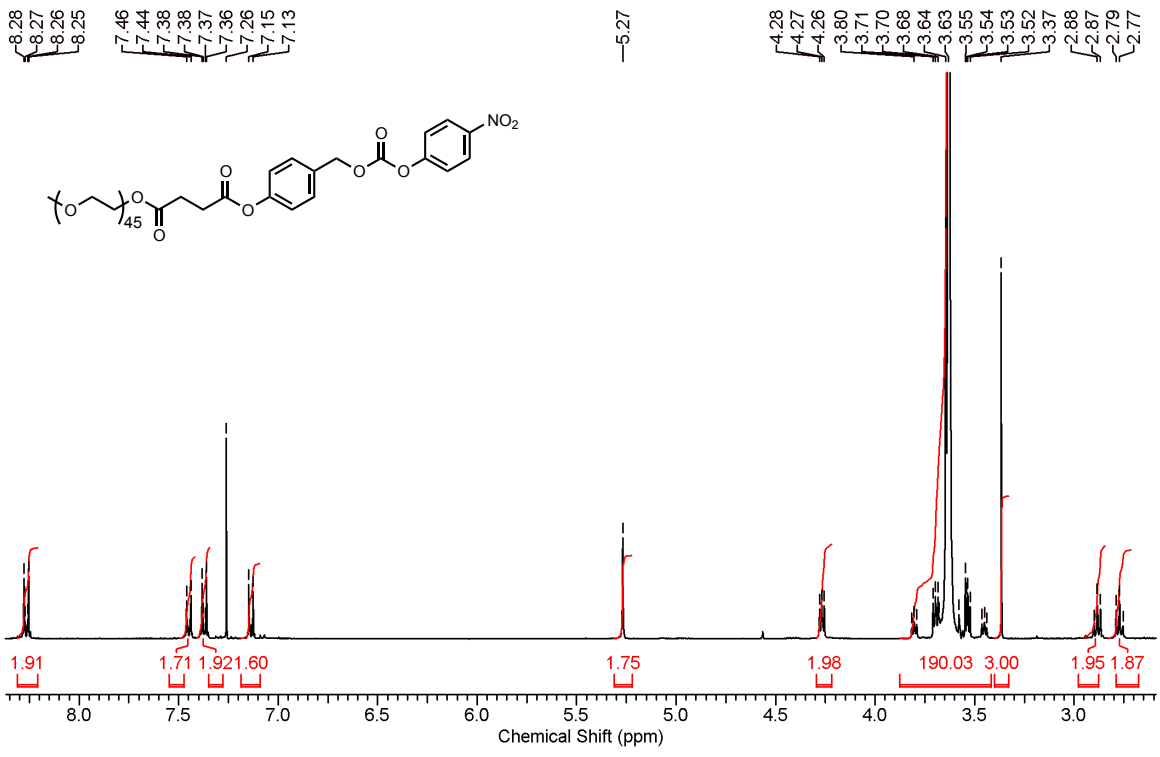

Figure A19: ^{1}H NMR spectrum of compound **3.6a** (600 MHz, $CDCl_3$)

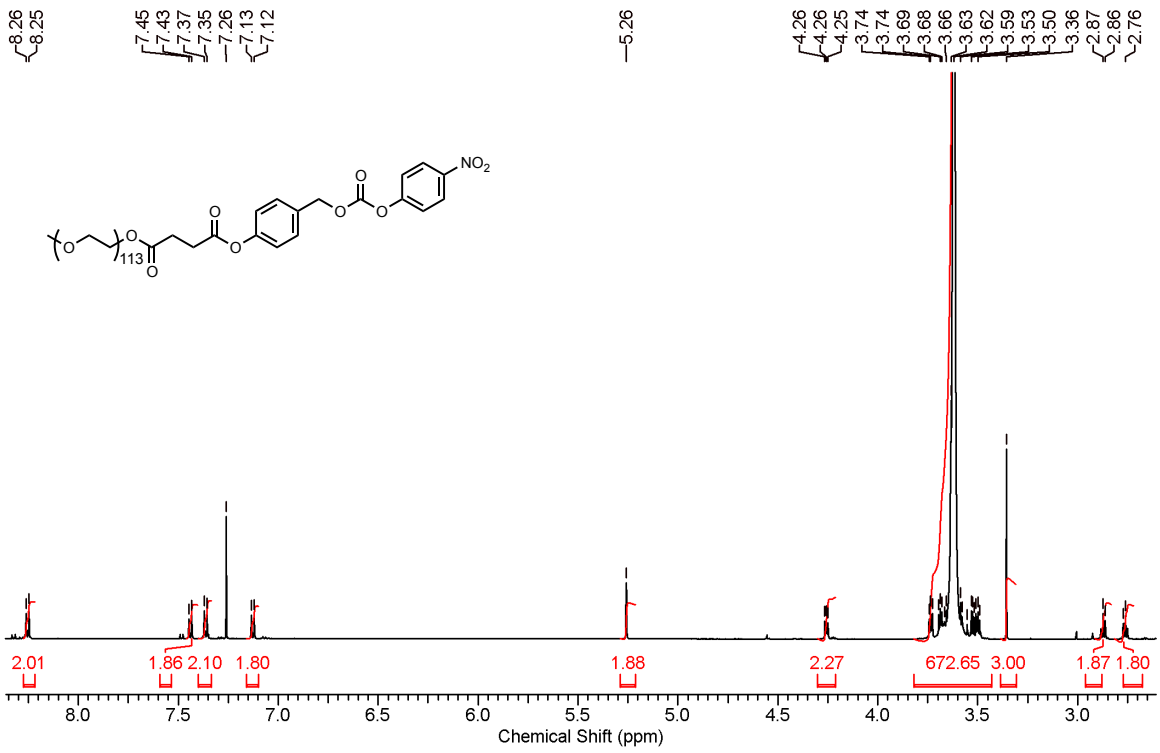

Figure A20: ^{1}H NMR spectrum of compound **3.6b** (600 MHz, $CDCl_3$)

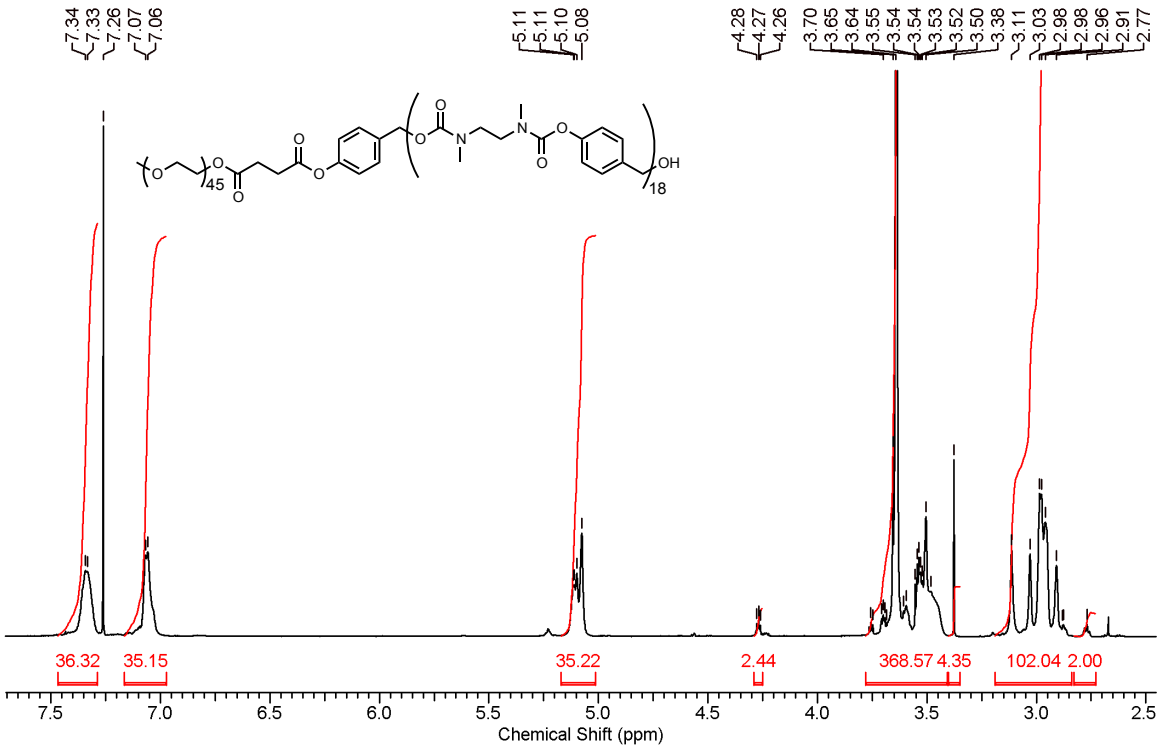

Figure A21: ^{1}H NMR spectrum of polymer **3.7a** (600 MHz, $CDCl_3$)

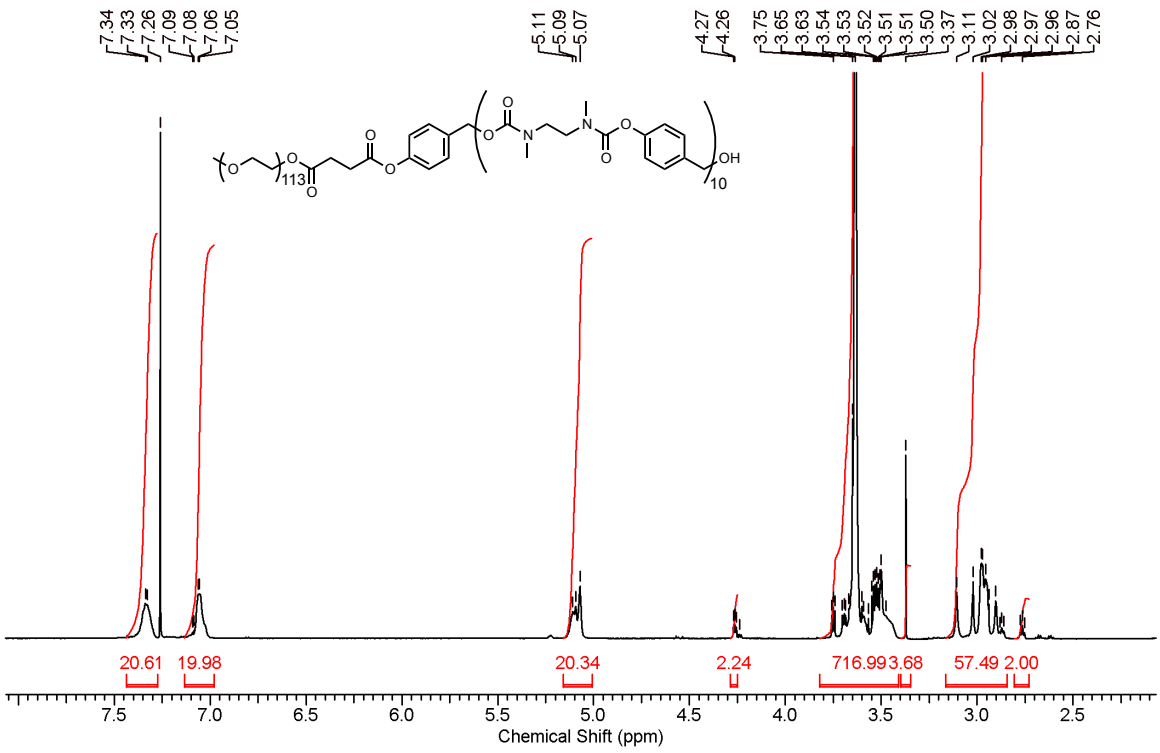

Figure A22: ^{1}H NMR spectrum of polymer **3.7b** (600 MHz, $CDCl_3$)

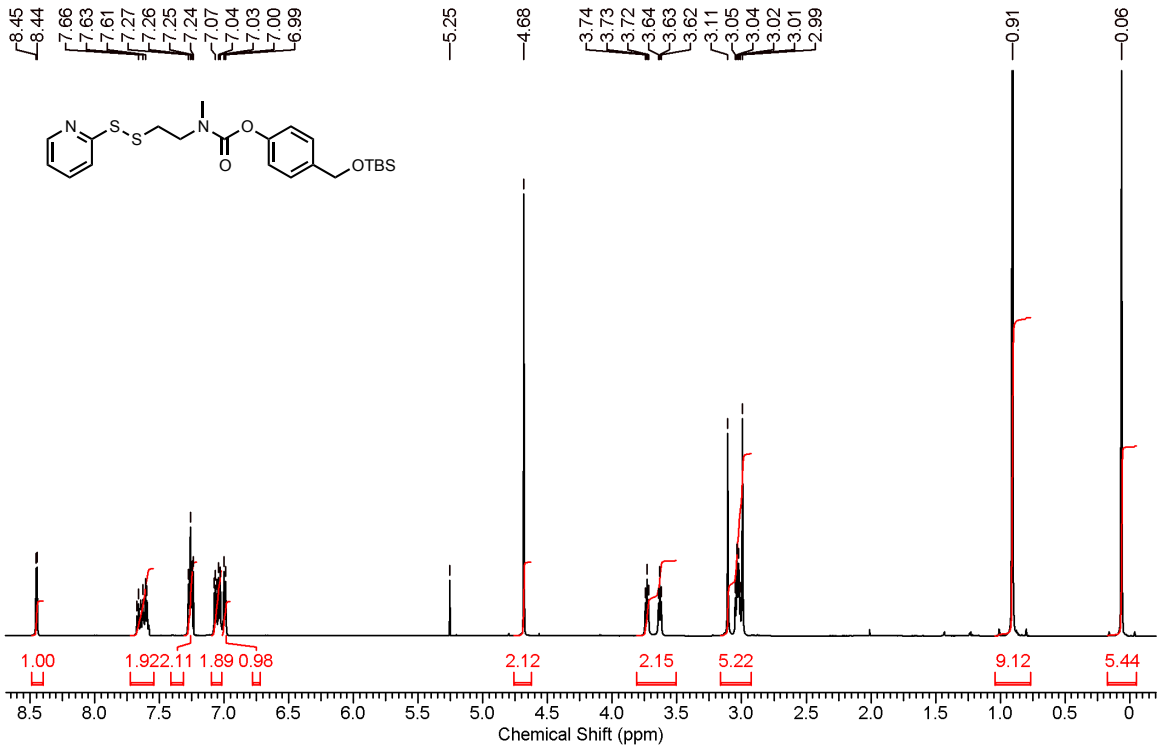

Figure A23: ^{1}H NMR spectrum of compound **3.11** (600 MHz, $CDCl_3$)

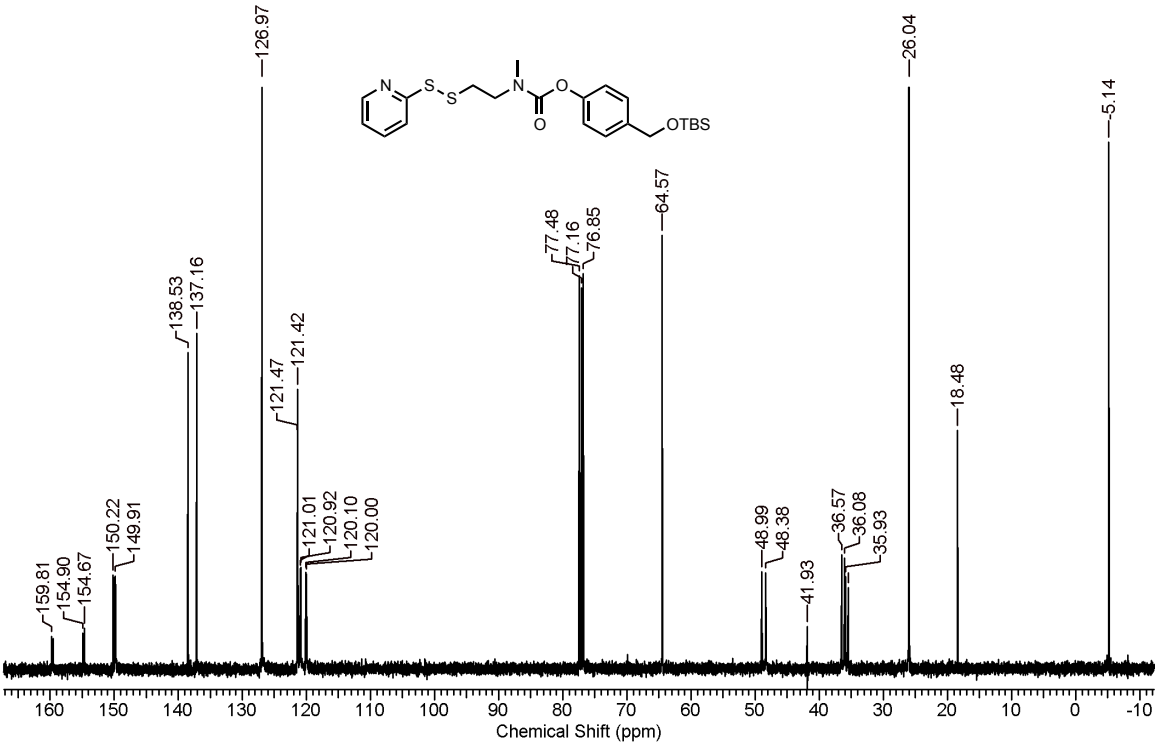

Figure A24: ^{13}C NMR spectrum of compound **3.11** (100 MHz, $CDCl_3$)

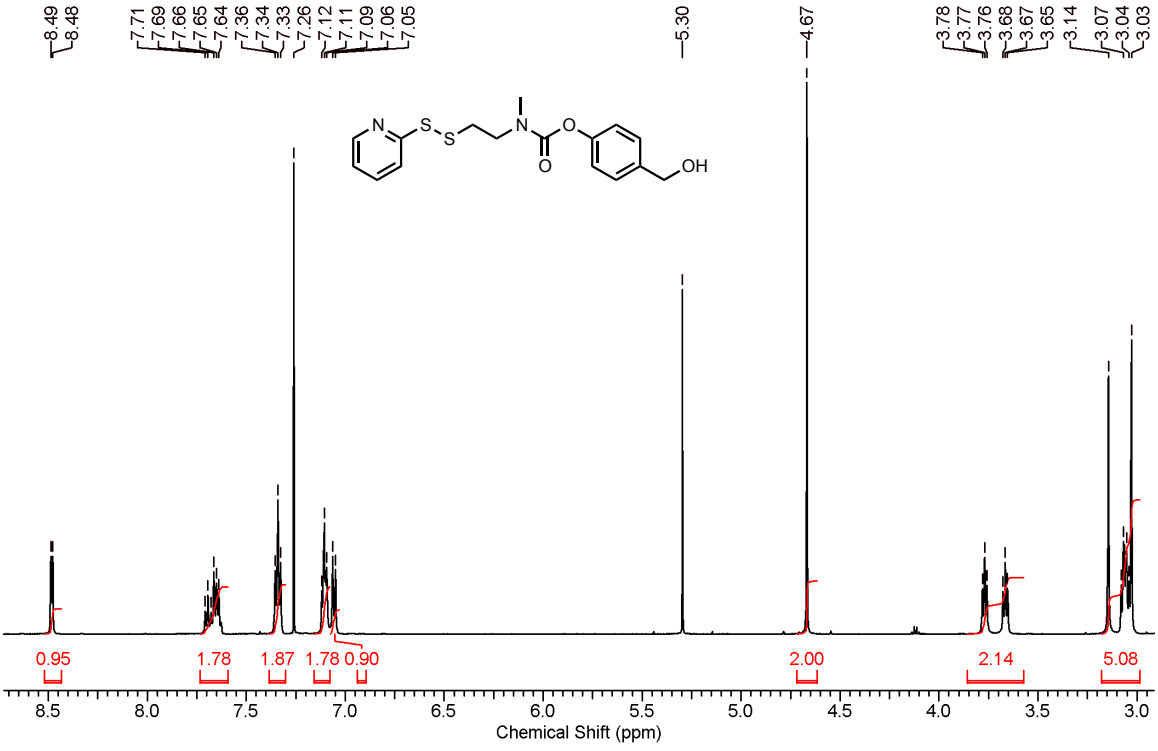

Figure A25: ^{1}H NMR spectrum of compound **3.12** (600 MHz, $CDCl_3$)

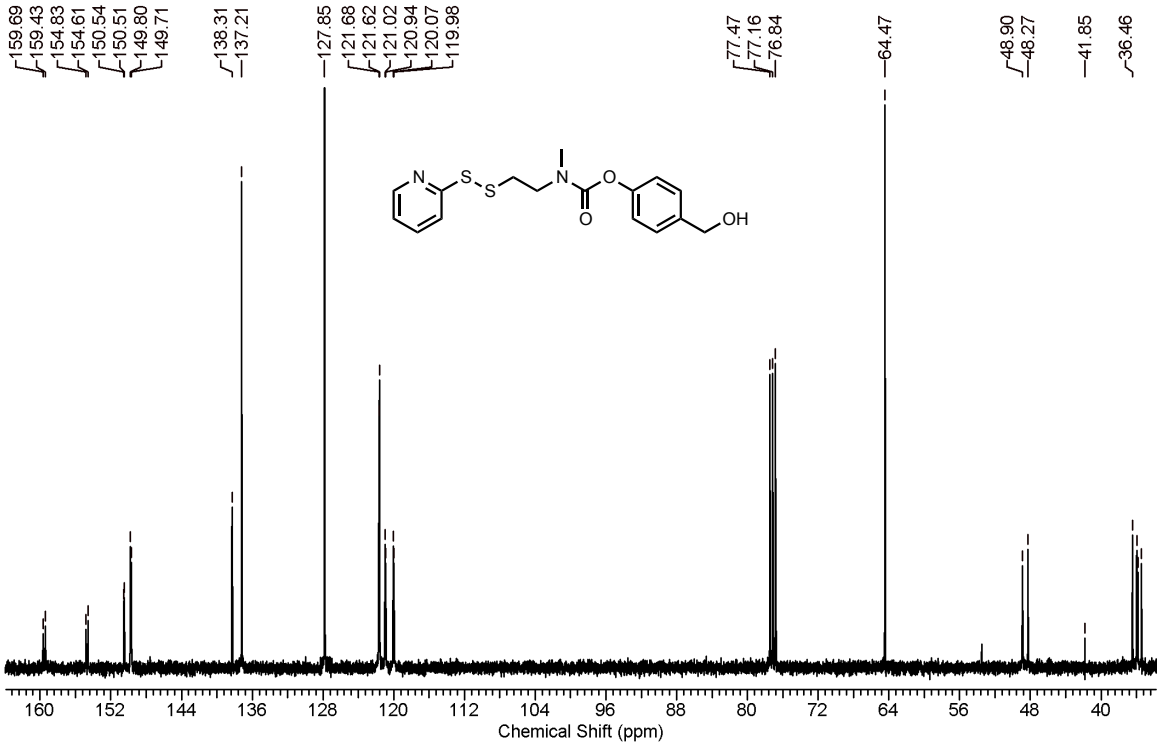

Figure A26: ^{13}C NMR spectrum of compound **3.12** (100 MHz, $CDCl_3$)

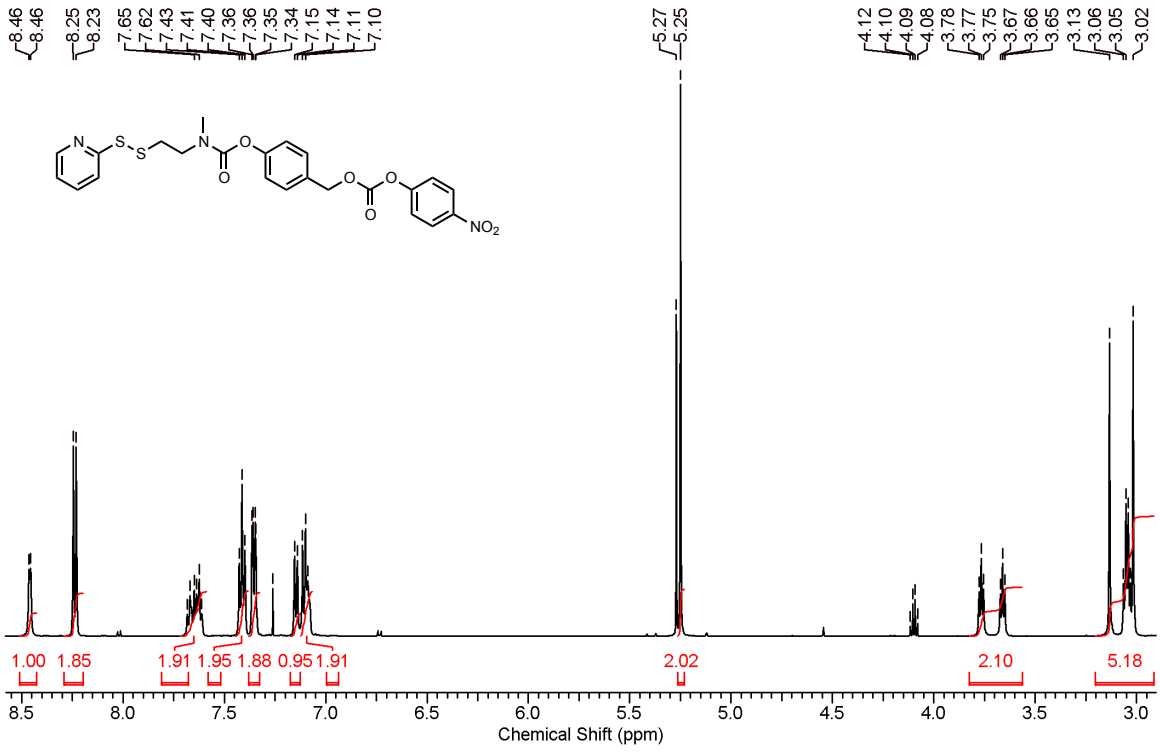

Figure A27: ^{1}H NMR spectrum of compound **3.13** (600 MHz, $CDCl_3$)

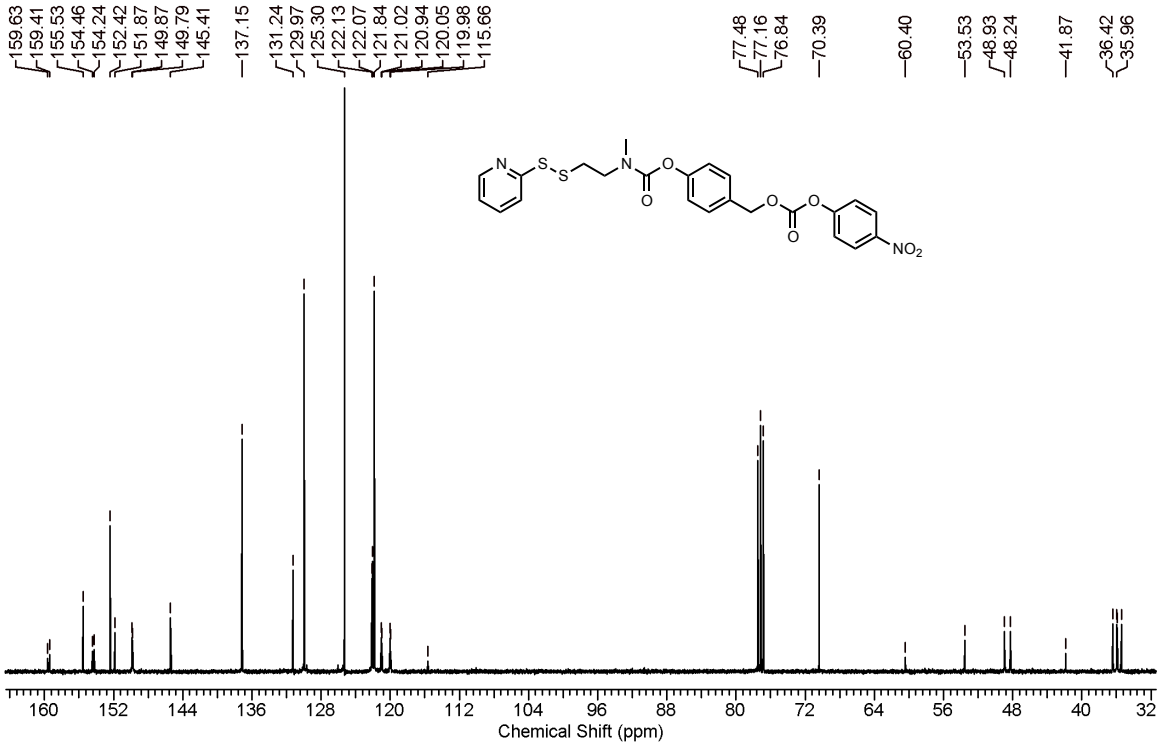

Figure A28: ^{13}C NMR spectrum of compound **3.13** (100 MHz, $CDCl_3$)

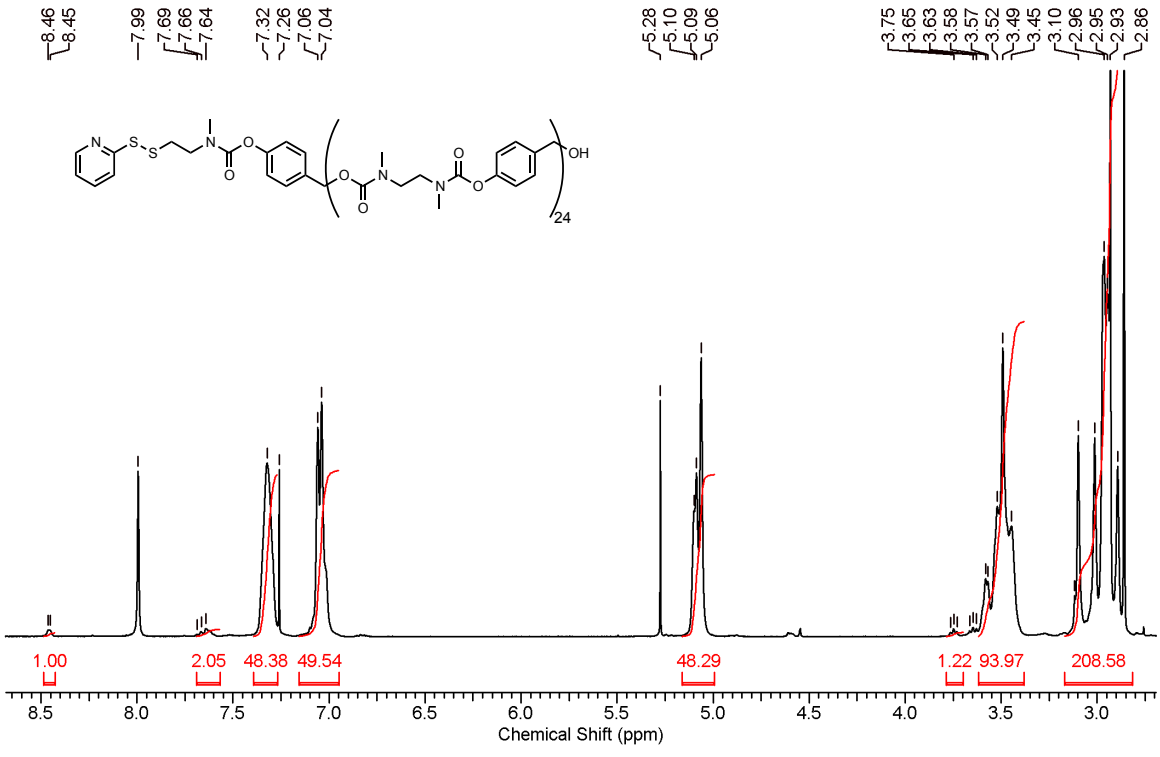

Figure A29: ^{1}H NMR spectrum of polymer **3.14** (400 MHz, $CDCl_3$)

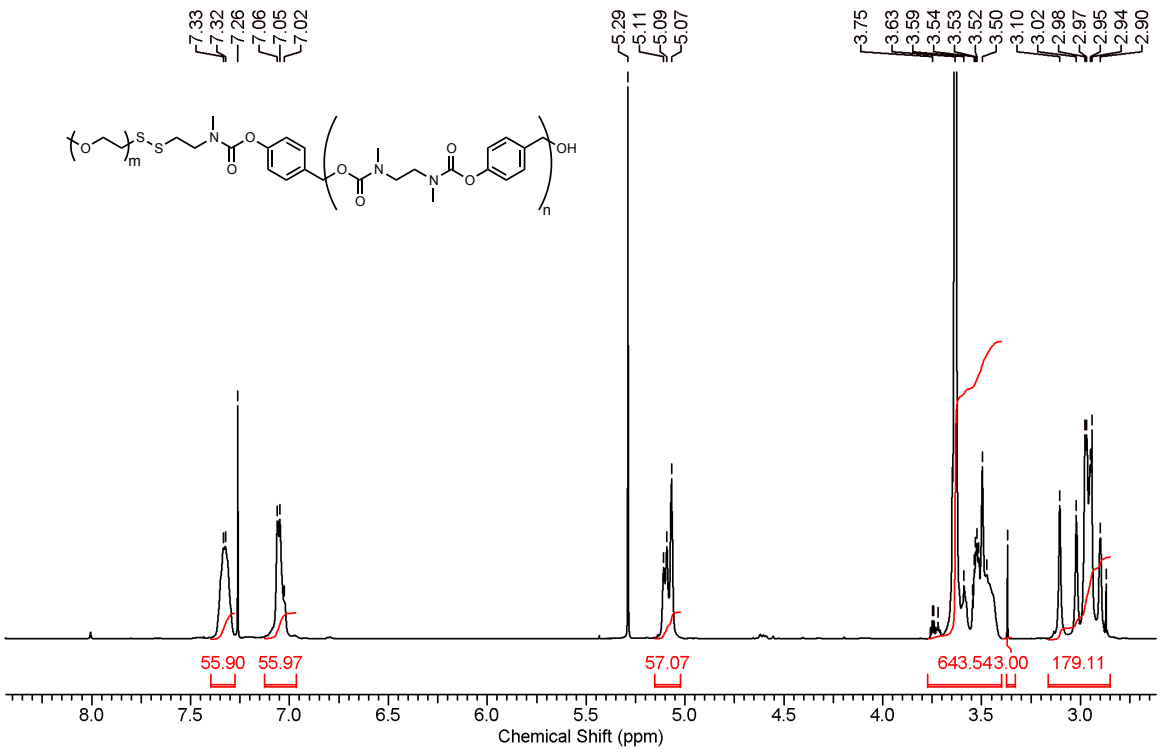

Figure A30: ^{1}H NMR spectrum of polymer **3.16** (600 MHz, $CDCl_3$)

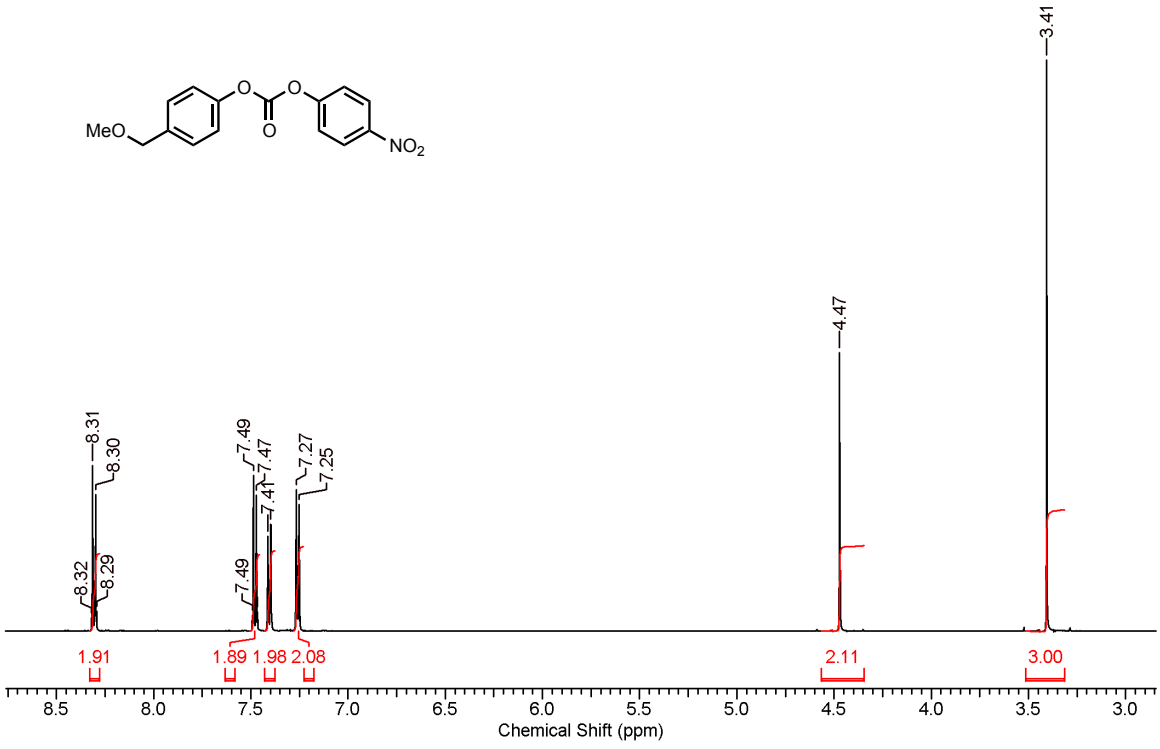

Figure A31: ^{1}H NMR spectrum of compound **3.18** (600 MHz, $CDCl_3$)

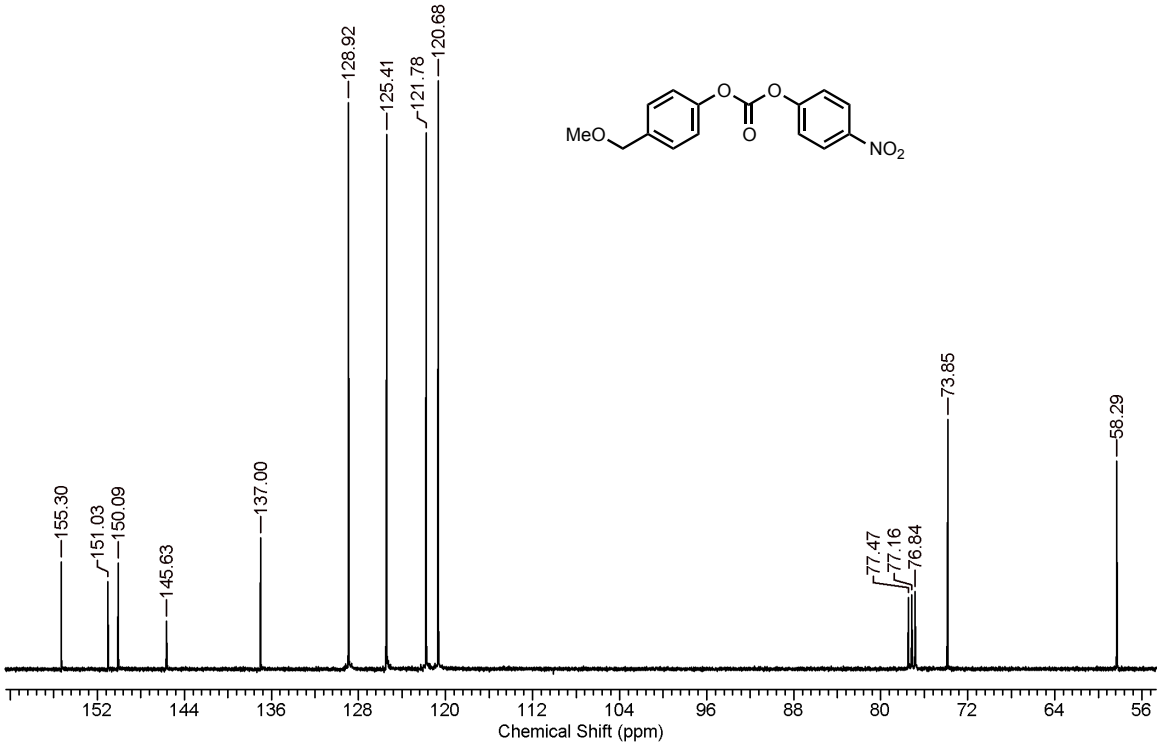

Figure A32: ^{13}C NMR spectrum of compound **3.18** (600 MHz, $CDCl_3$)

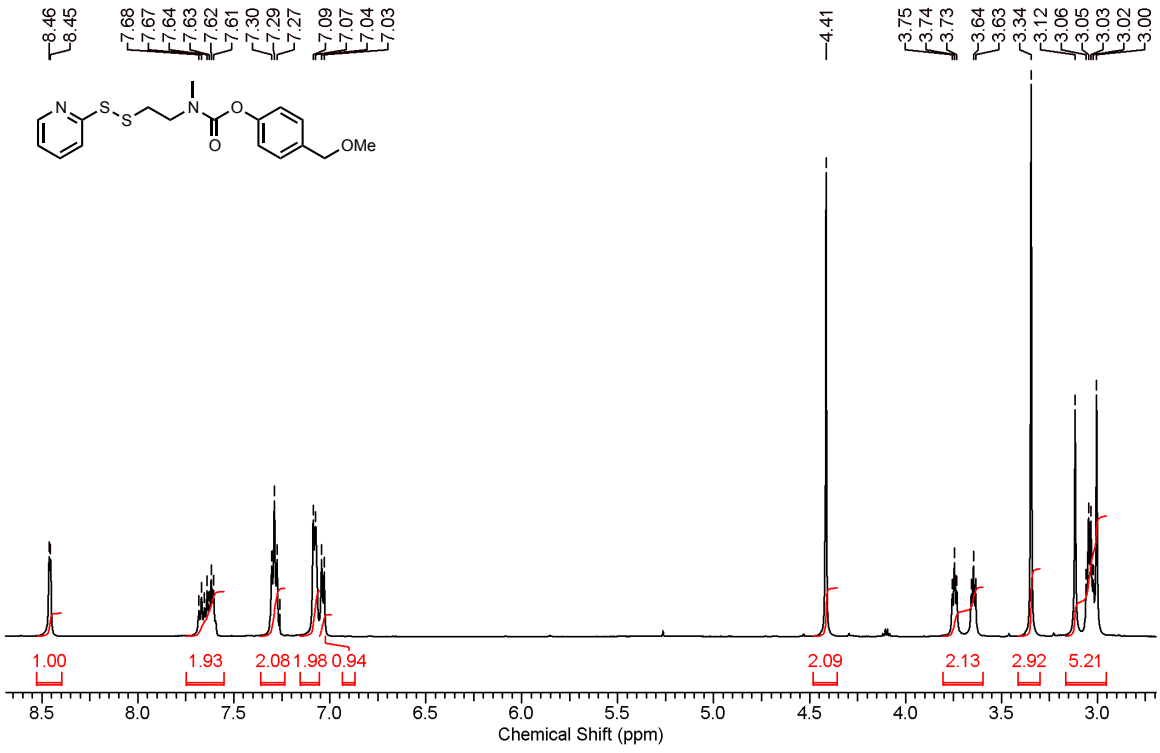

Figure A33: ^{1}H NMR spectrum of compound **3.19** (600 MHz, $CDCl_3$)

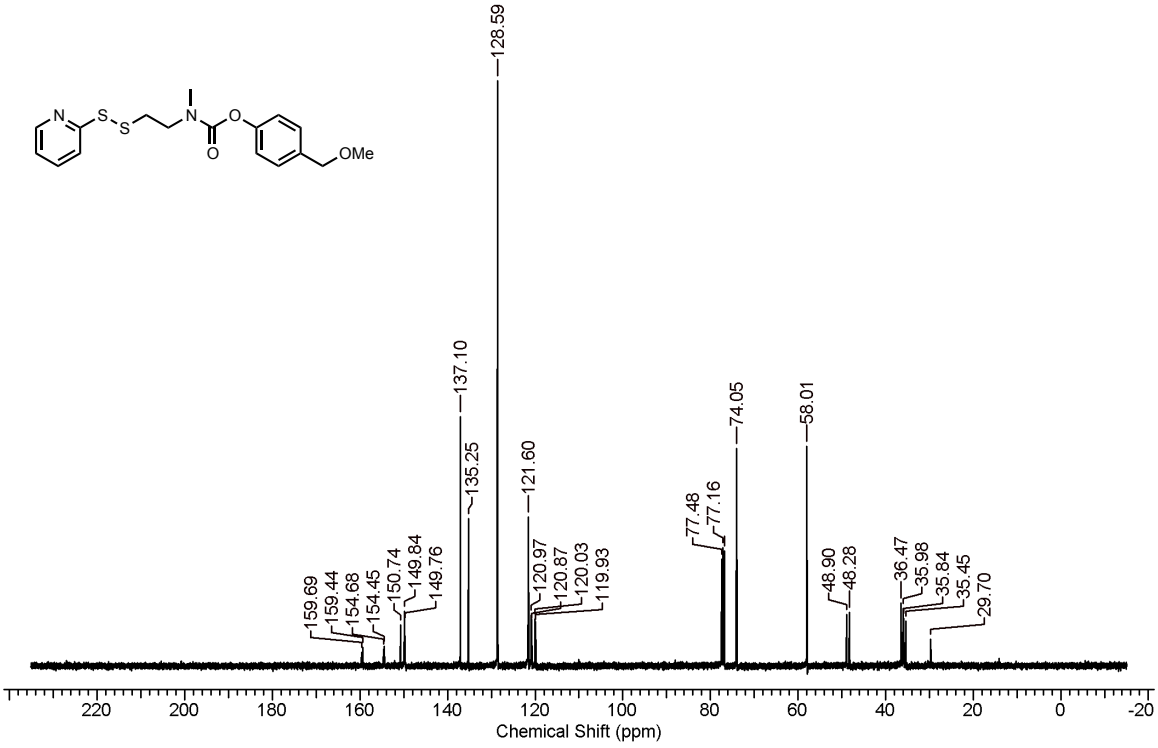

Figure A34: ^{13}C NMR spectrum of compound **3.19** (100 MHz, $CDCl_3$)

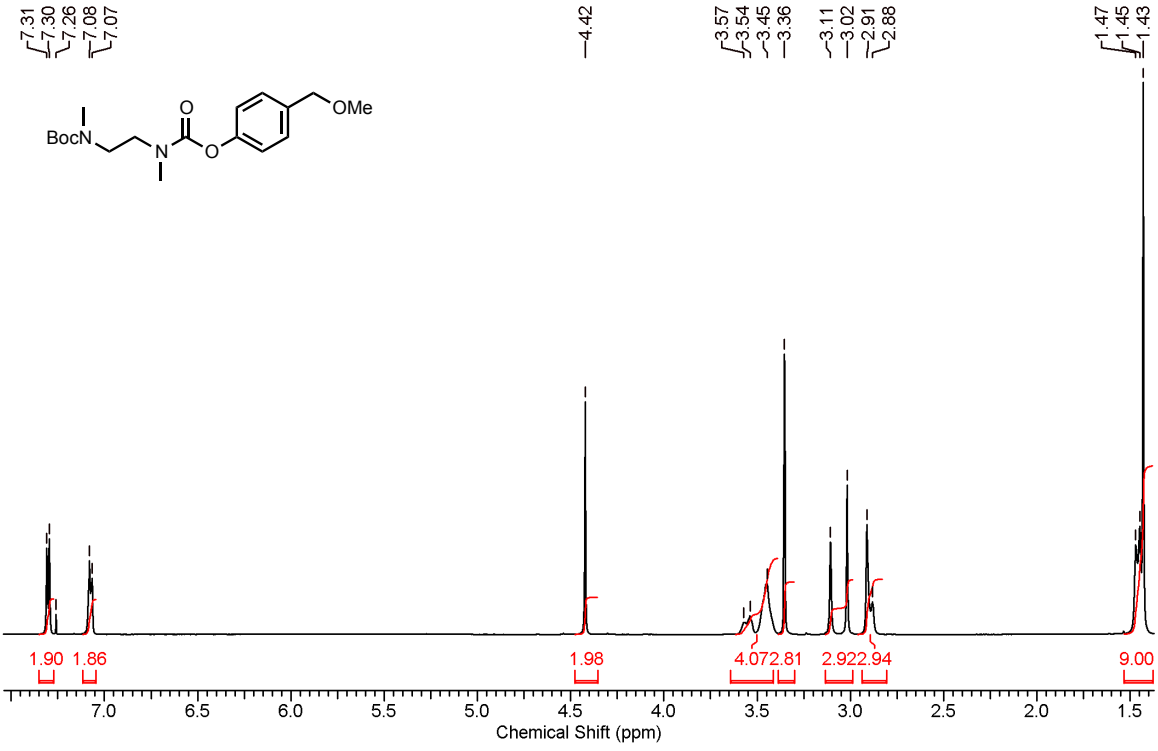

Figure A35: ^{1}H NMR spectrum of compound **3.21** (600 MHz, $CDCl_3$)

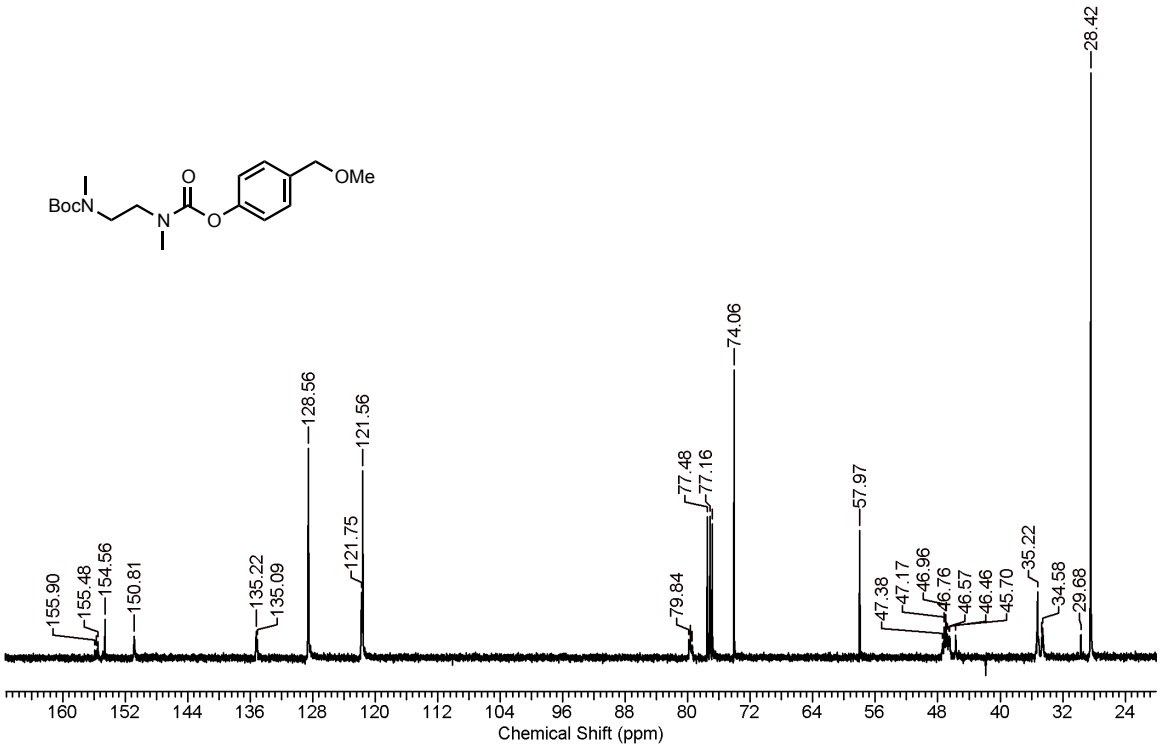

Figure A36: ^{13}C NMR spectrum of compound **3.21** (100 MHz, $CDCl_3$)

Appendix B: HPLC Chromatograms

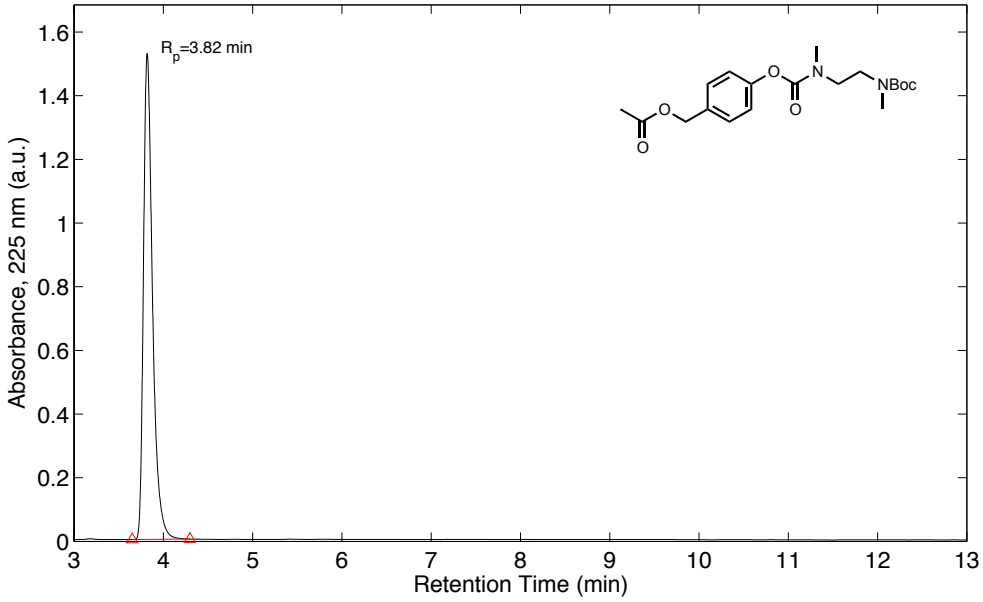

Figure B1. HPLC chromatogram of compound **2.1a**

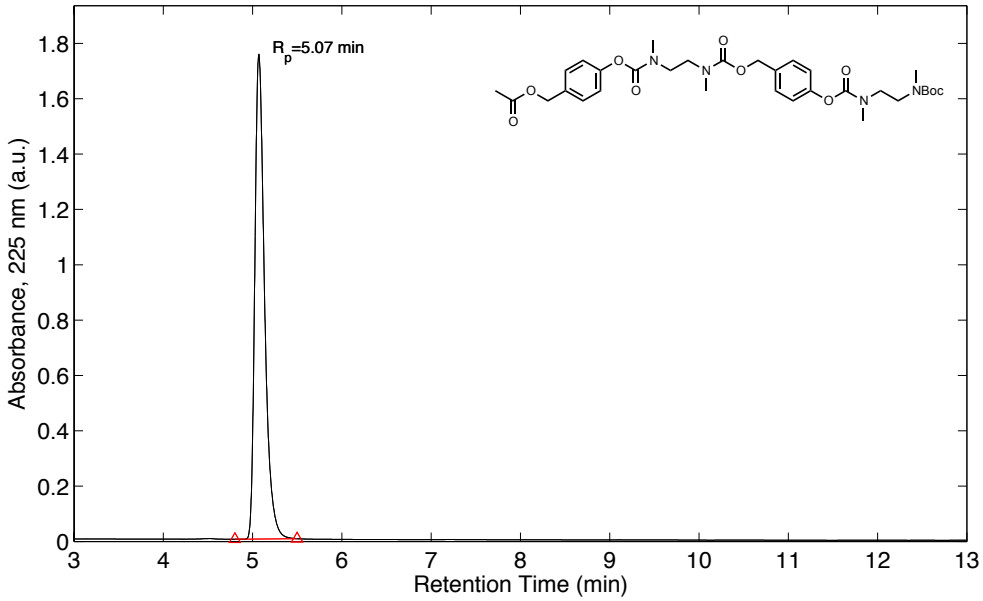

Figure B2. HPLC chromatogram of compound **2.2a**

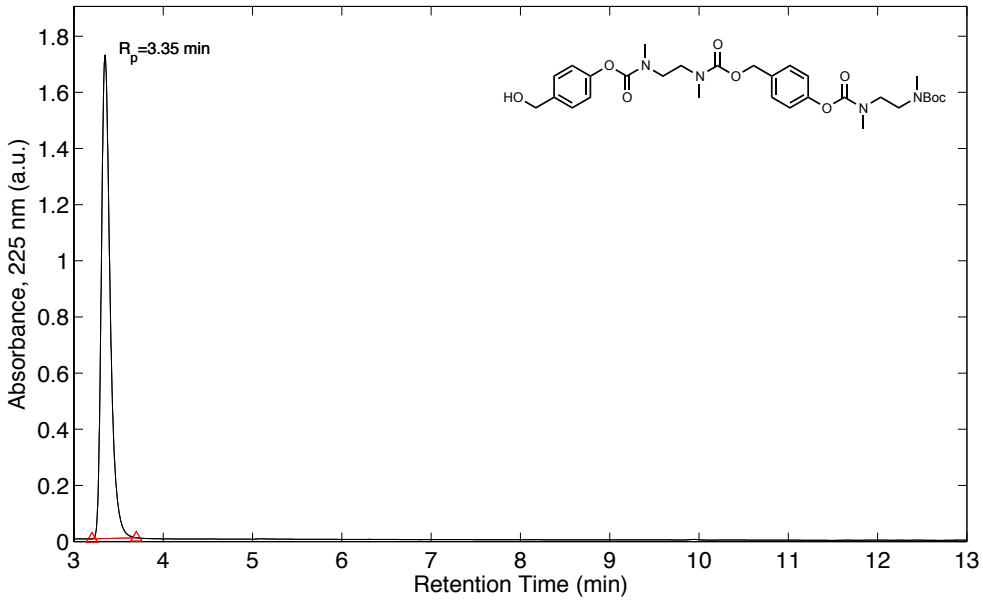

Figure B3. HPLC chromatogram of compound **2.2b**

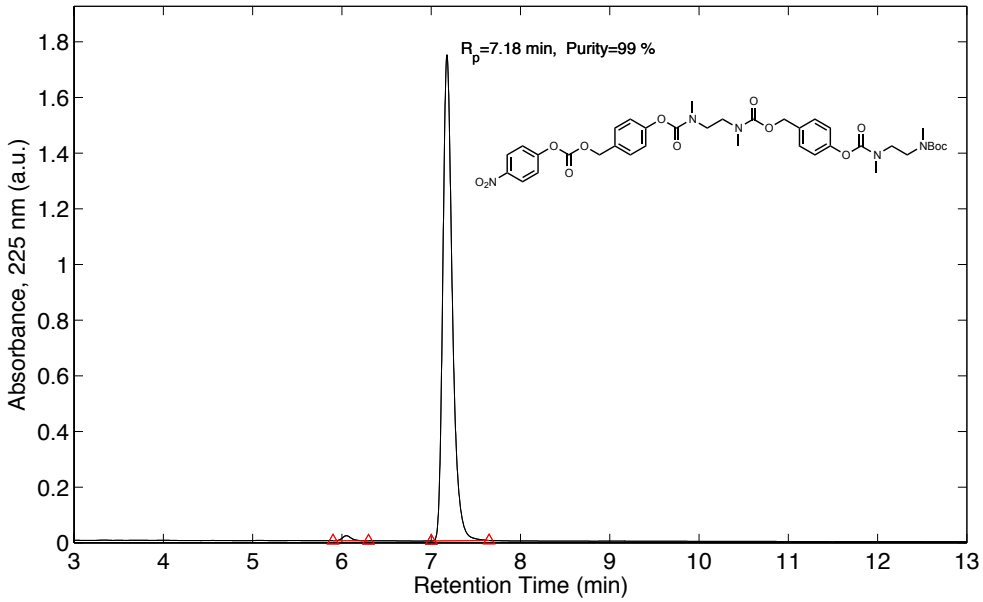

Figure B4. HPLC chromatogram of compound **2.2c**

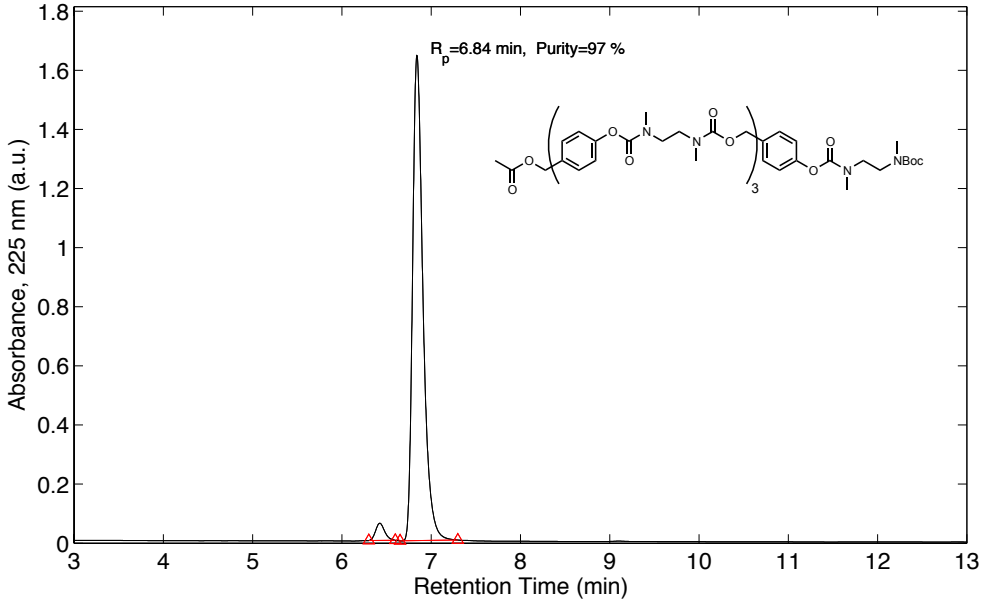

Figure B5. HPLC chromatogram of compound **2.3a**

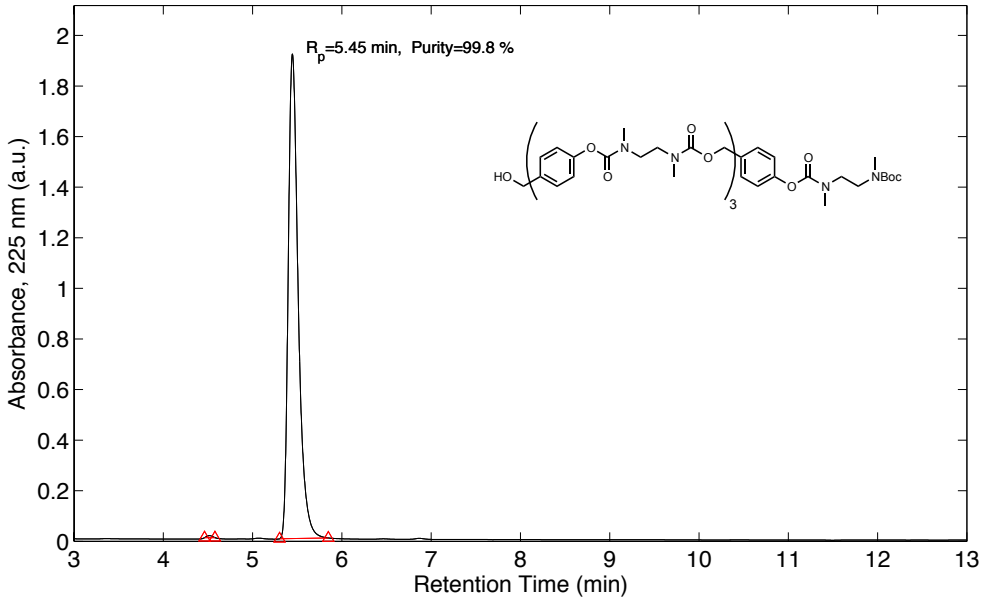

Figure B6. HPLC chromatogram of compound **2.3b**

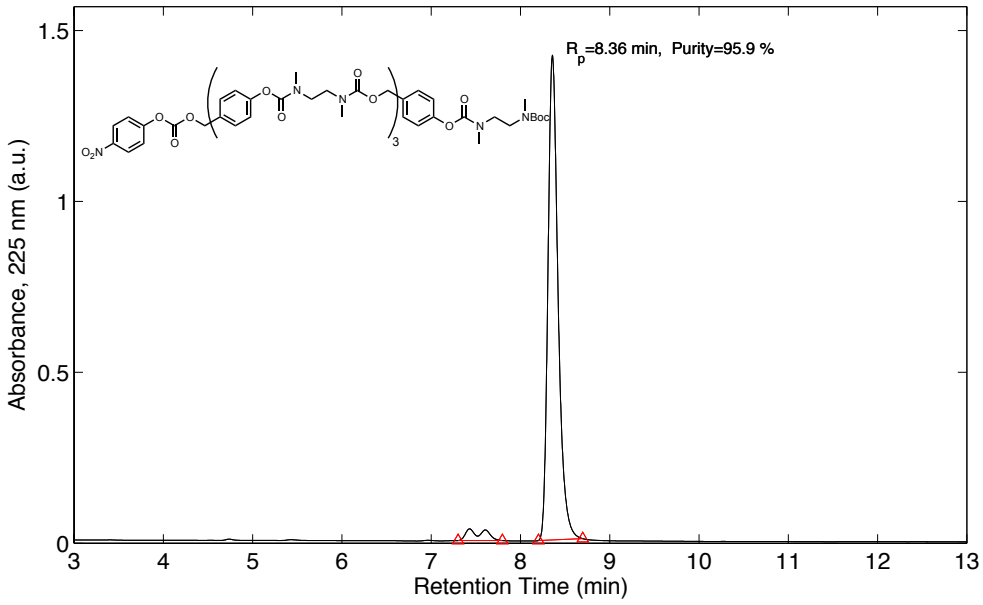

Figure B7. HPLC chromatogram of compound **2.3c**

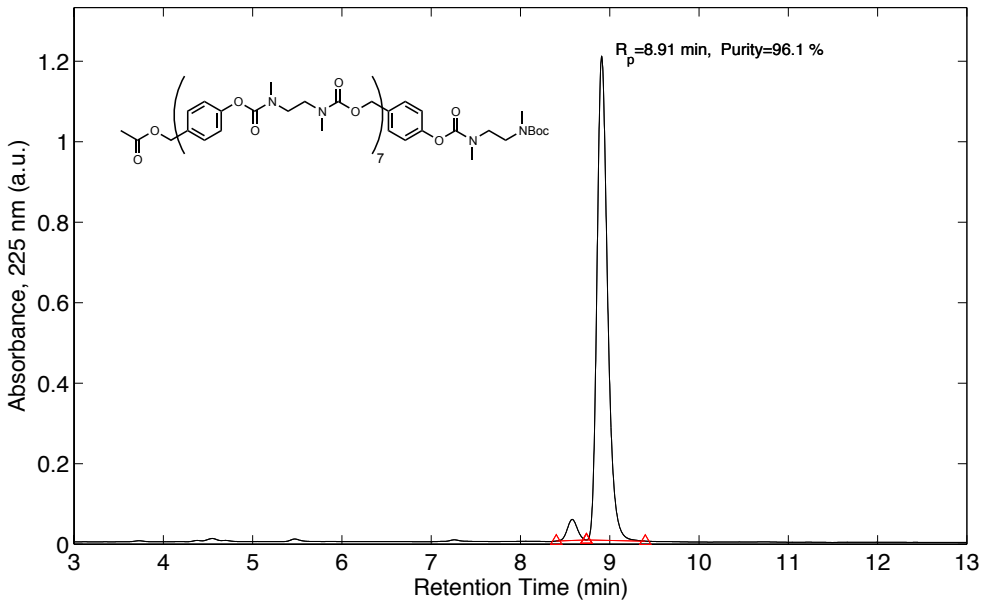

Figure B8. HPLC chromatogram of compound **2.4a**

Appendix C: Supplemental Degradation Study Spectra

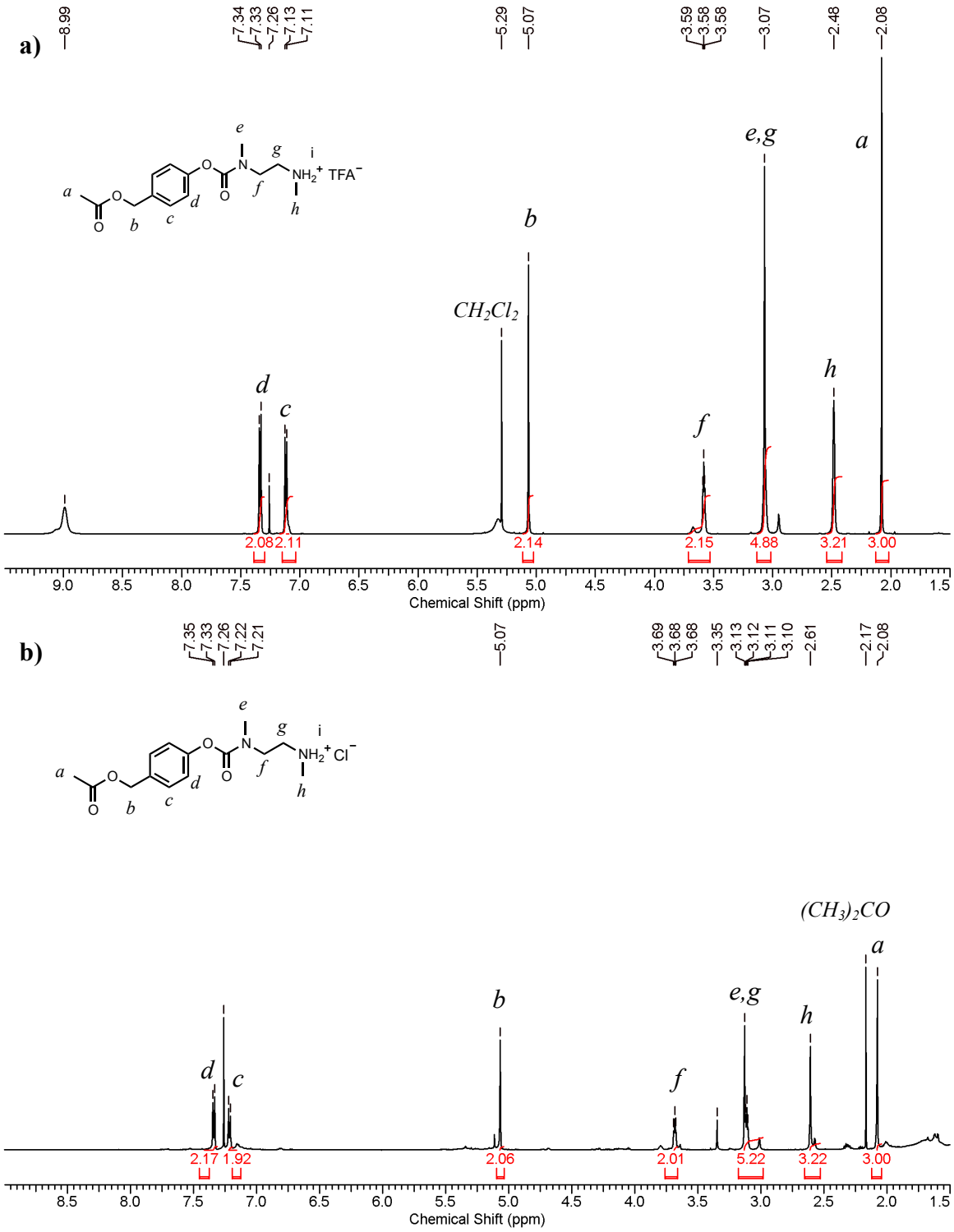

Figure C1: ^{1}H NMR spectrum of compound 2.1d: a) prior to and b) timmediately following a 1:1 1 M citric acid:brine wash (600 MHz, CDCl3)

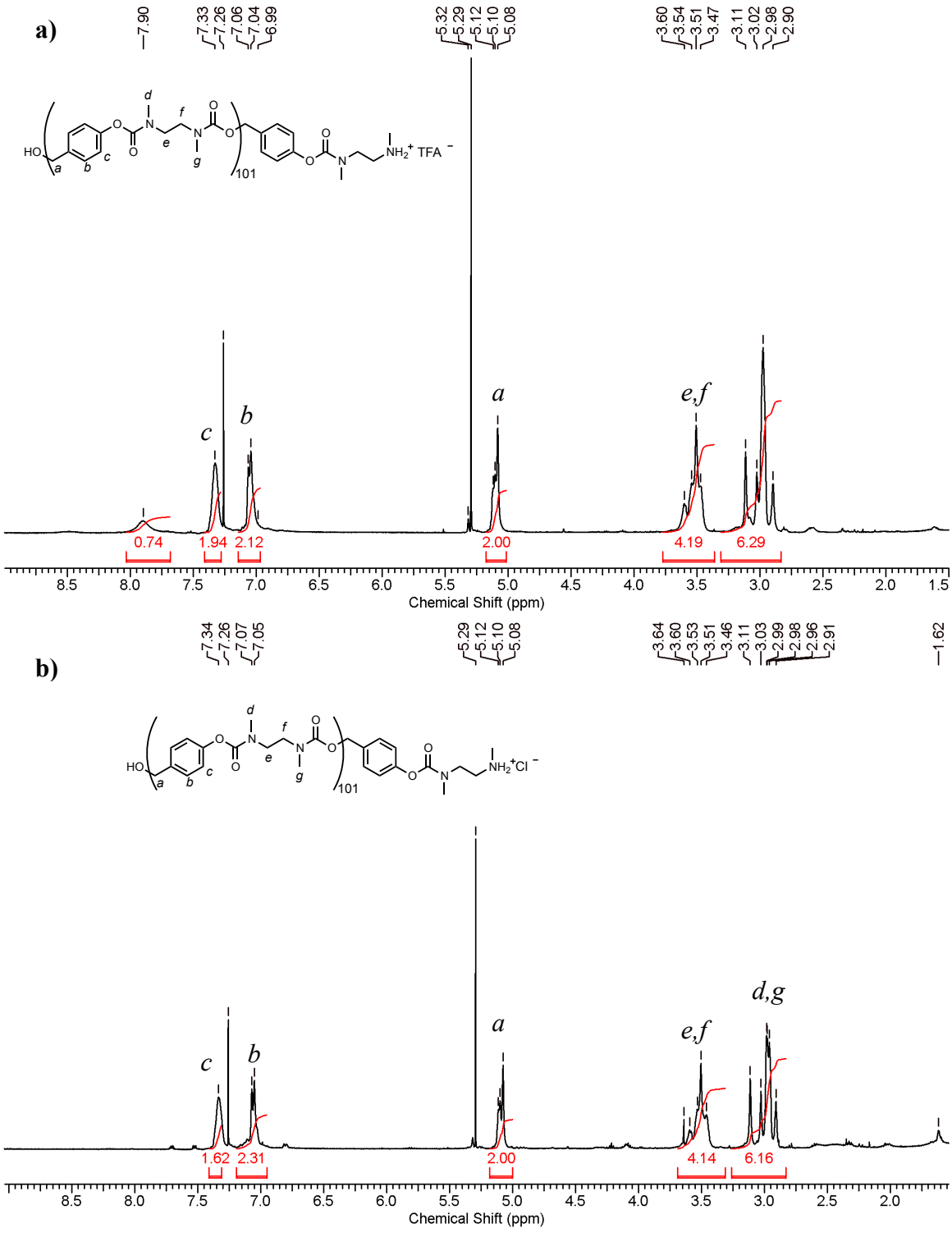

Figure C2: ^{1}H NMR spectrum of Boc-deprotected polymer 2.7: a) prior to and b) immediately following a 1:1 1 M citric acid:brine wash (400 MHz, CDCl3)

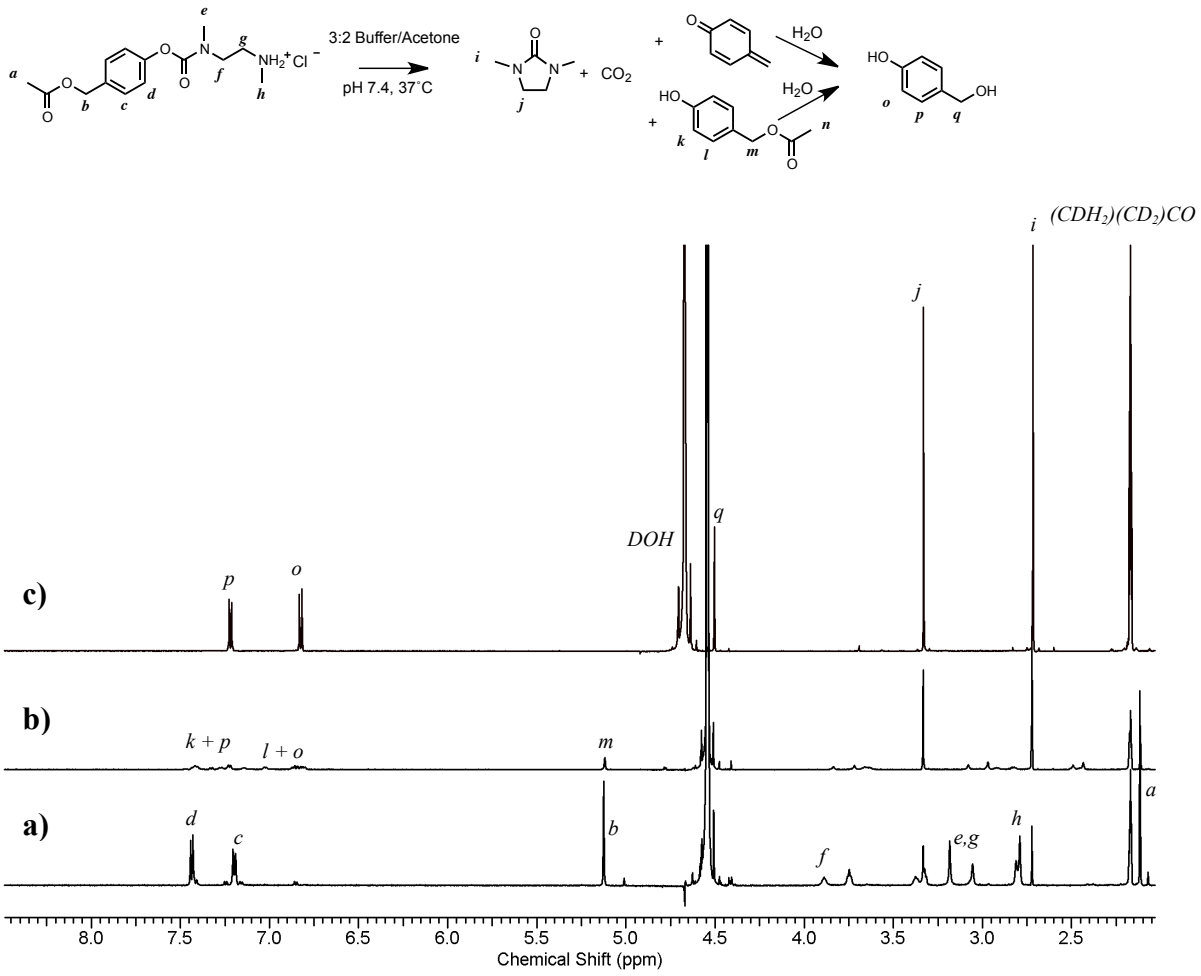

Figure C3: ^{1}H NMR spectra of compound 2.1d (a) following end-cap removal in 0.1 M pH 7.4 phosphate buffer (D_2O):acetone-d_6 (3:2) at the first time point reading in the degradation process; (b) following complete cyclization after 2 h at 37˚C; and (c) following hydrolysis of all acetate end-groups

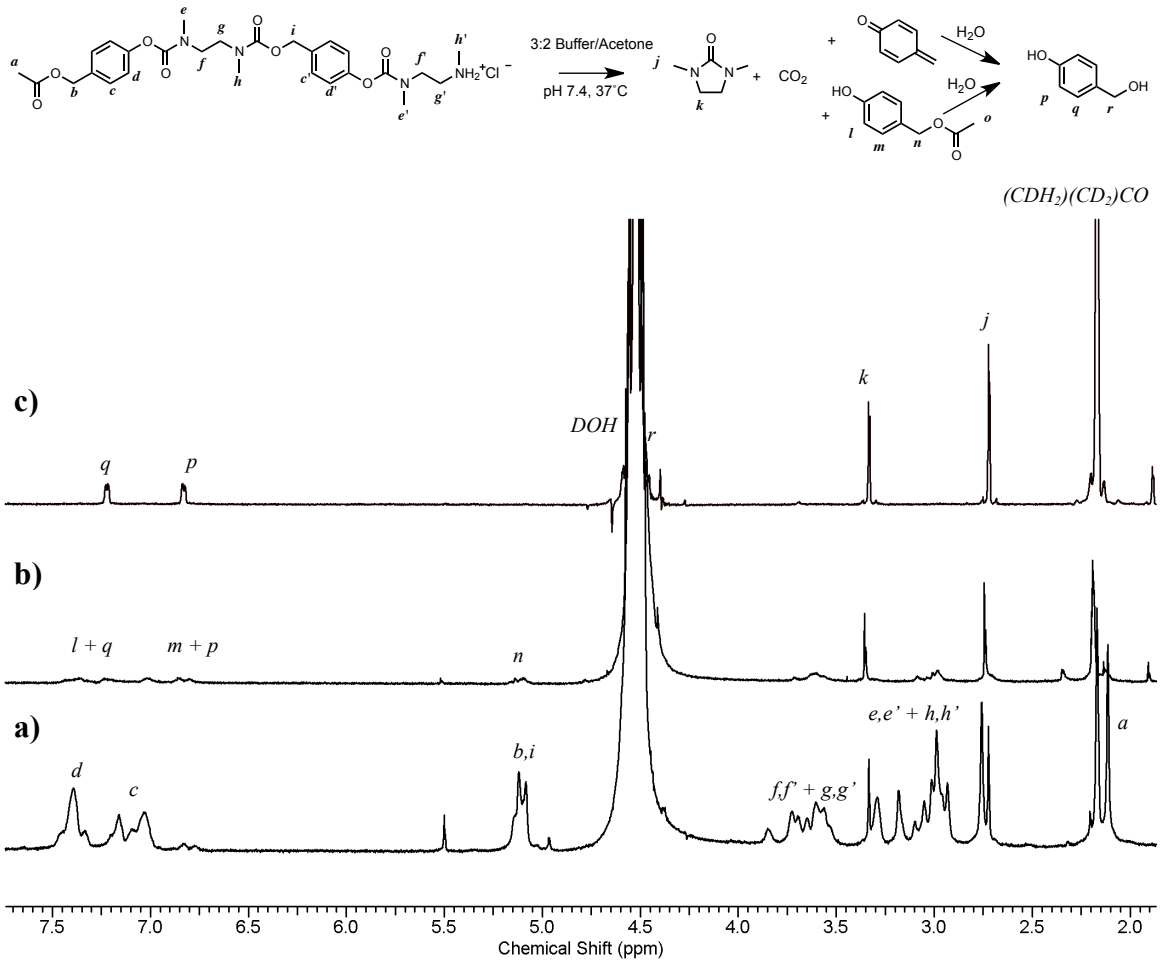

Figure C4: ^{1}H NMR spectra of compound 2.2d (a) following end-cap removal in 0.1 M pH 7.4 phosphate buffer (D_2O):acetone-d_6 (3:2) at the first time point reading in the degradation process; (b) following complete cyclization after 2 h at 37˚C; and (c) following hydrolysis of all acetate end-groups

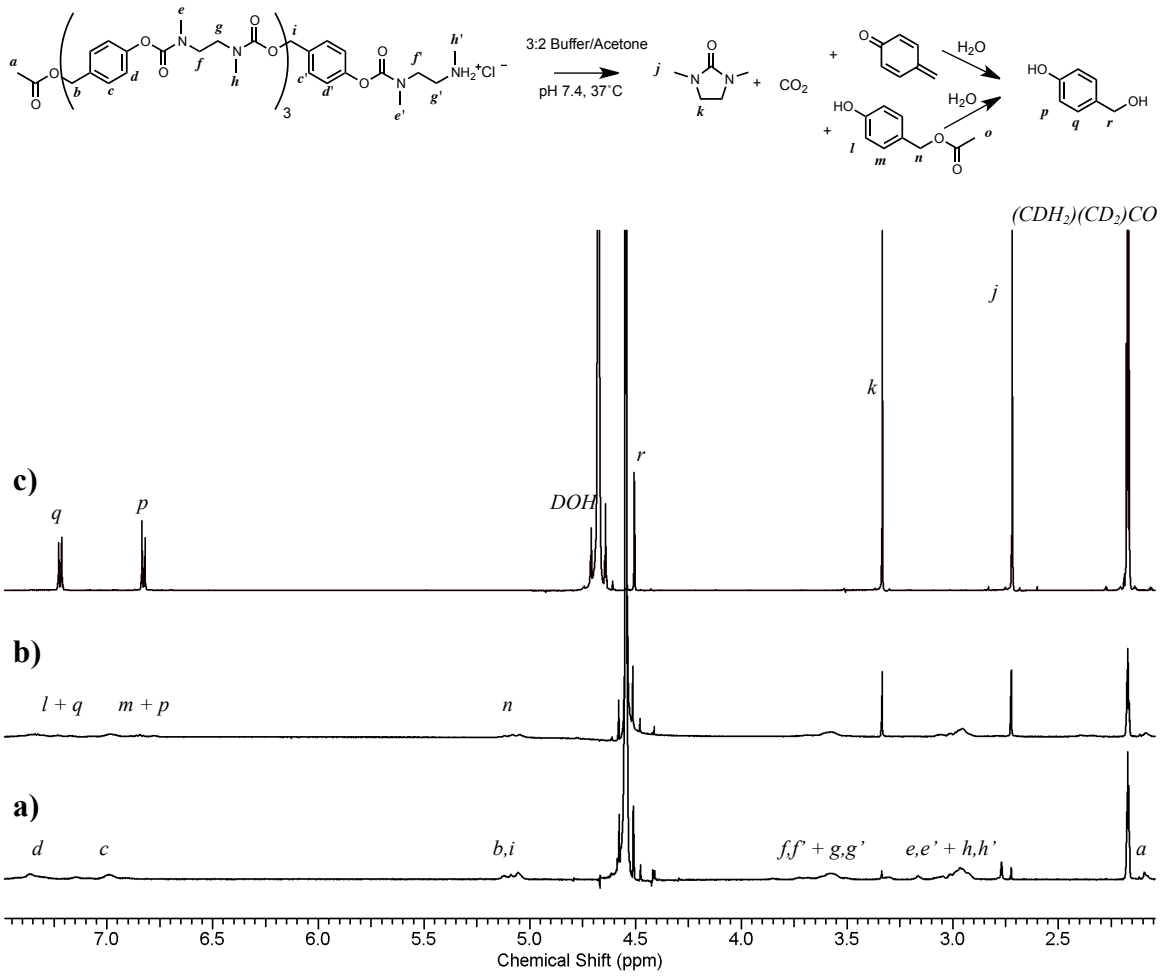

Figure C5: ^{1}H NMR spectra of compound 2.3d (a) following end-cap removal in 0.1 M pH 7.4 phosphate buffer (D_2O):acetone-d_6 (3:2) at the first time point reading (t=5 min) in the degradation process; (b) following complete cyclization after 2 h at 37˚C; and (c) following hydrolysis of all acetate end-groups

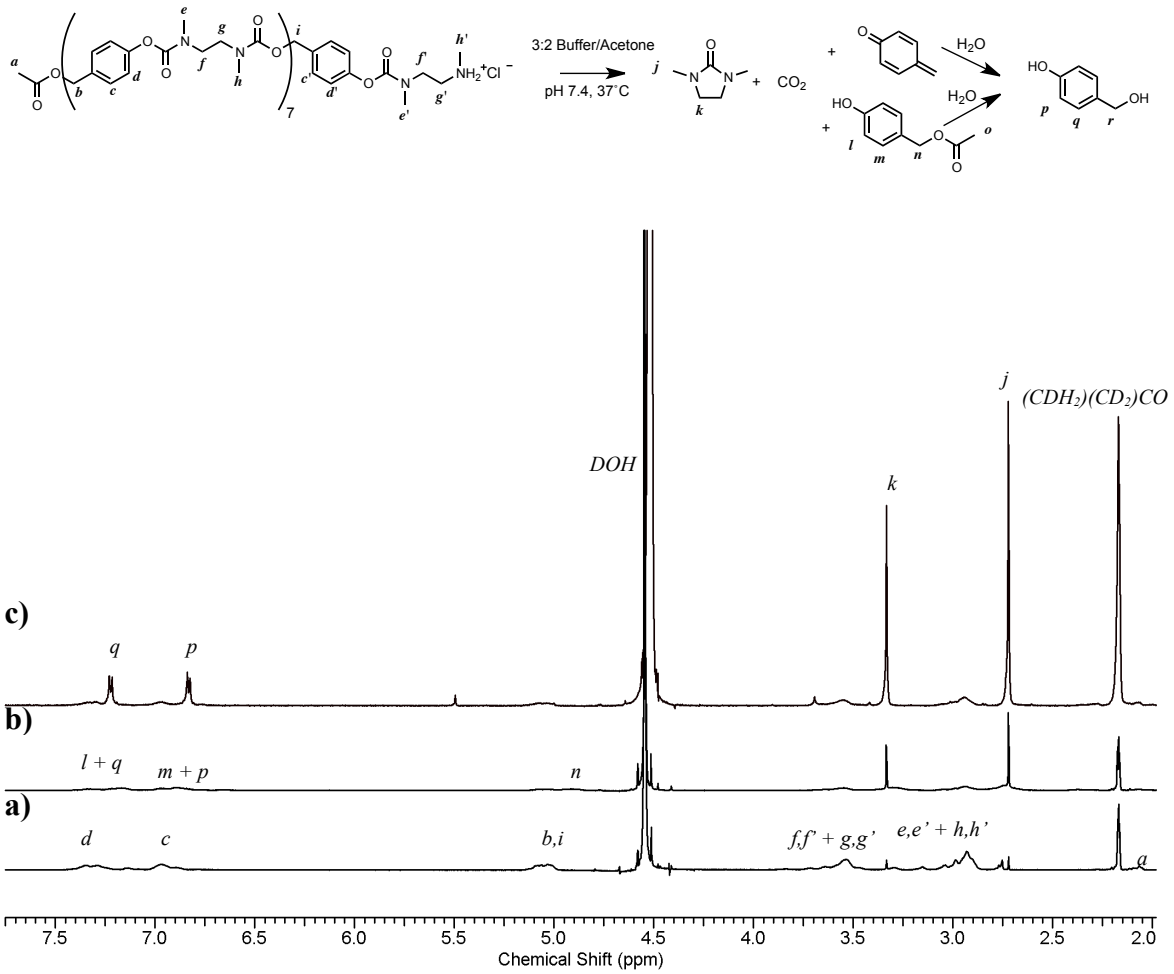

Figure C6: ^{1}H NMR spectra of compound 2.4d (a) following end-cap removal in 0.1 M pH 7.4 phosphate buffer (D_2O):acetone-d_6 (3:2) at the first time point reading (t=5 min) in the degradation process; (b) following complete cyclization after 2 h at 37˚C; and (c) following hydrolysis of all acetate end-groups

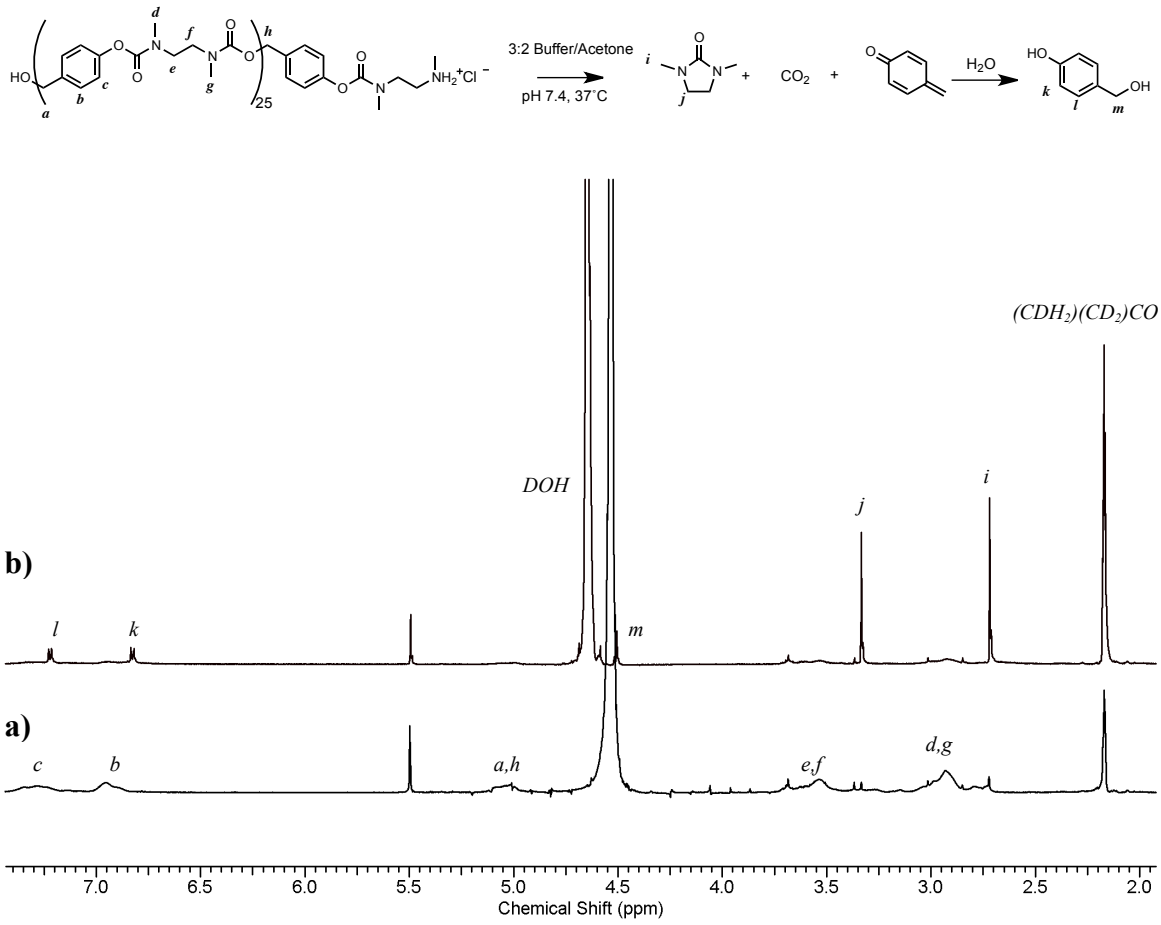

Figure C7: ^{1}H NMR spectra of polymer 2.6 (a) following end-cap removal in 0.1 M pH 7.4 phosphate buffer (D_2O):acetone-d_6 (3:2) at the first time point reading (t=5 min) in the degradation process; and (b) following complete cyclization after 4 h at 37˚C

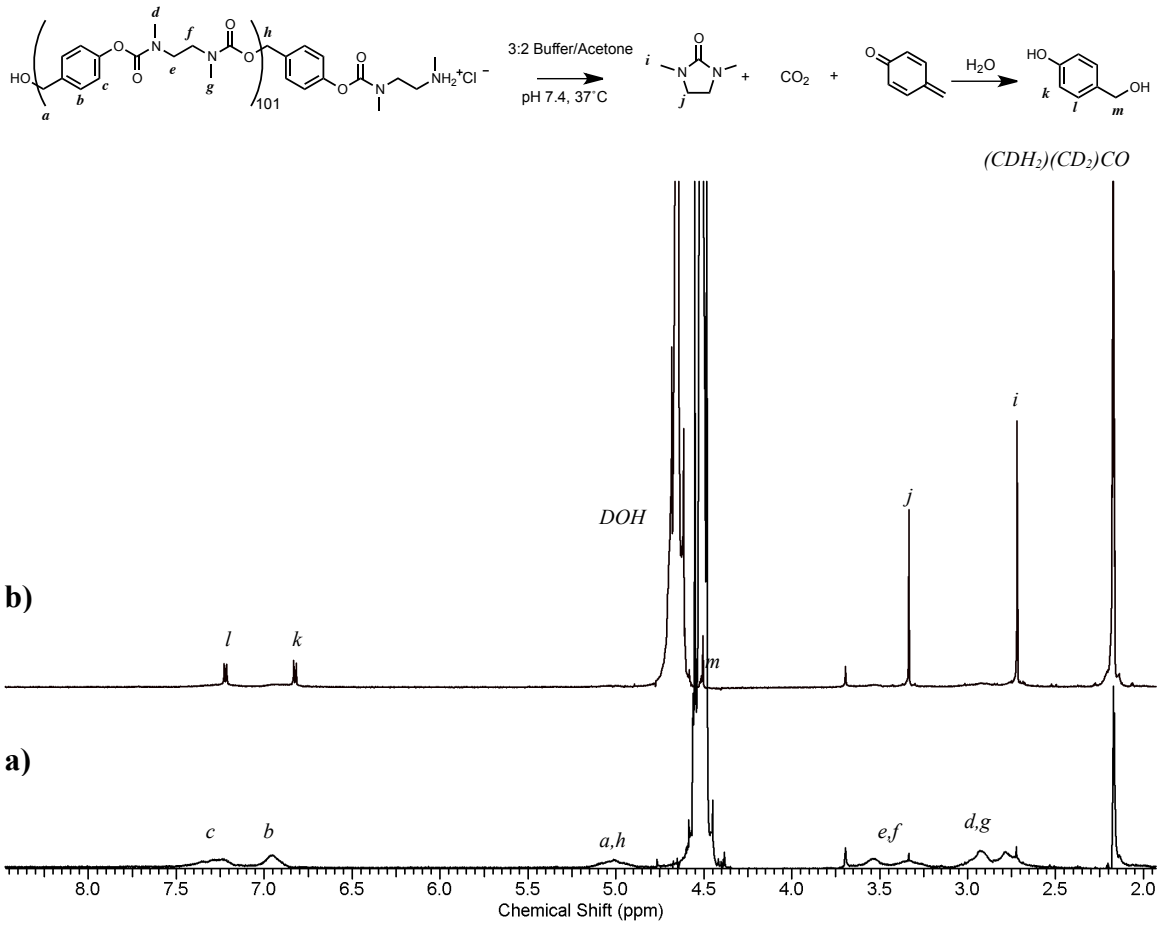

Figure C8: ^{1}H NMR spectra of polymer 2.7 (a) following end-cap removal in 0.1 M pH 7.4 phosphate buffer (D_2O):acetone-d_6 (3:2) at the first time point reading (t=5 min) in the degradation process; and (b) following complete cyclization after 4 h at 37˚C.

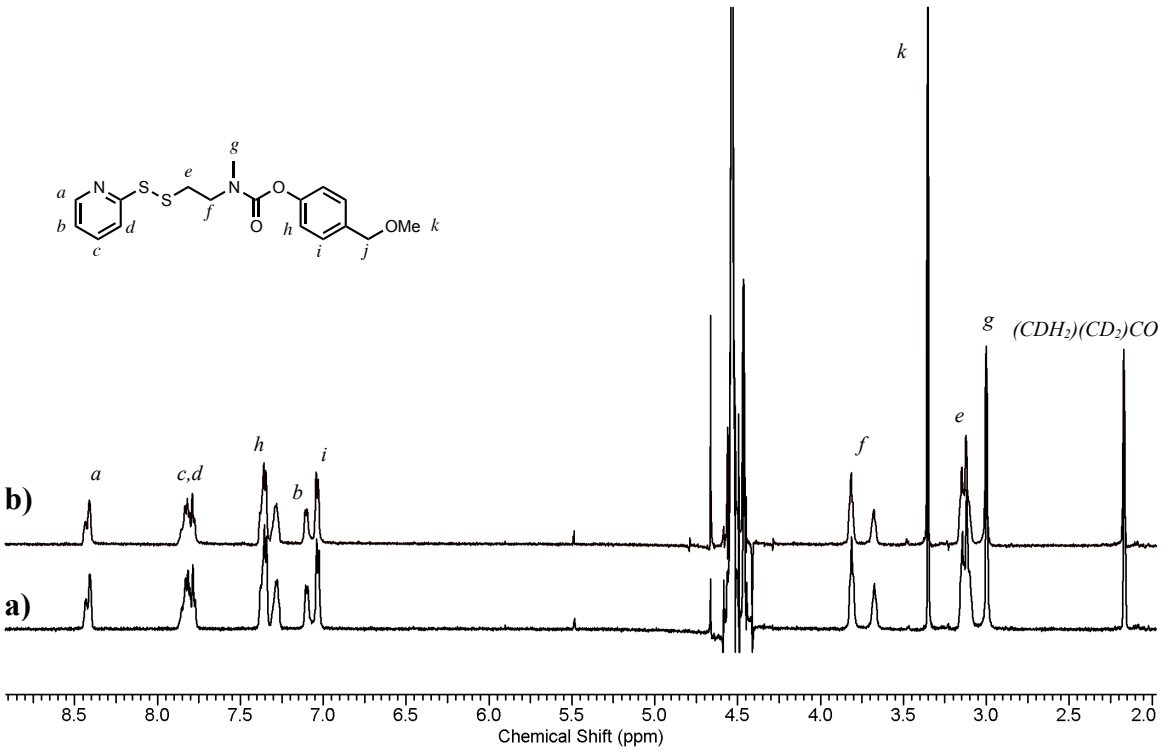

Figure C9: Control ^{1}H NMR study of compound 3.19 in 0.1 M pH 7.4 phosphate buffer (D_2O) :acetone-d_6 (3:2) in the absence of DTT at (a) the first time point reading (t=5 min) and (b) following incubation for 2 h.

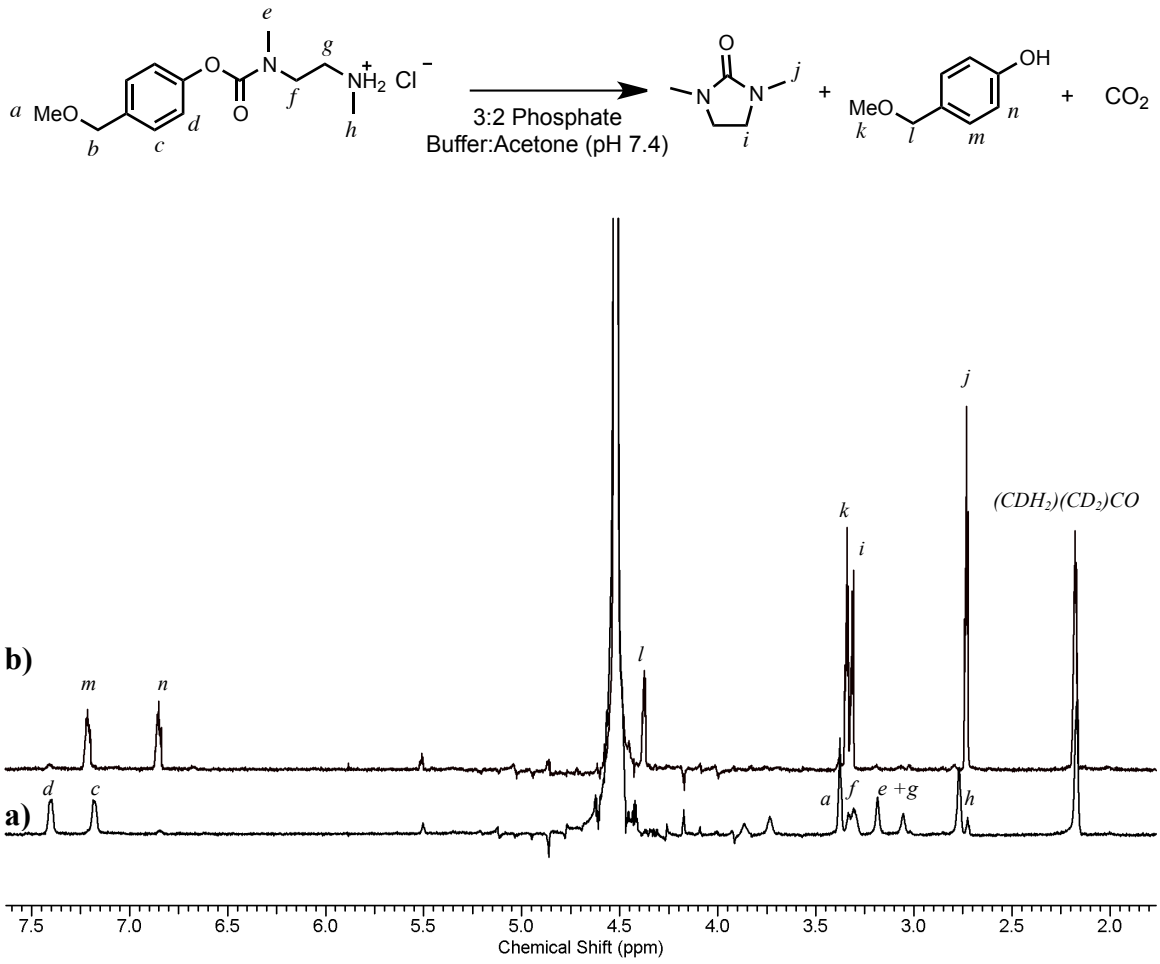

Figure C10: ^{1}H NMR spectra of compound 3.21 (a) following Boc-group removal in 0.1 M pH 7.4 phosphate buffer (D_2O):acetone-d_6 (3:2) at the first time point reading (t=5 min) in the degradation process; and (b) following complete cyclization after 1 h at 37˚C.

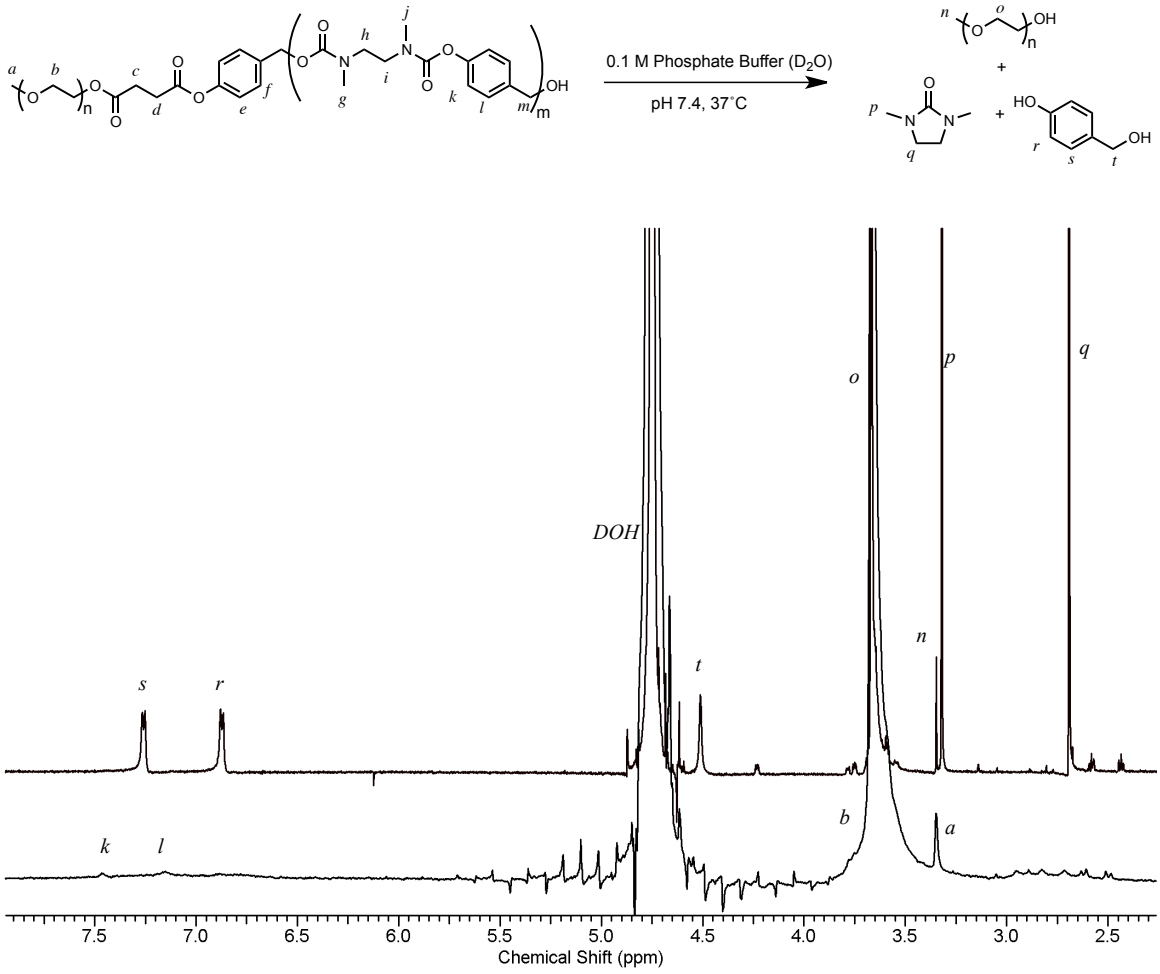

Figure C11: ^{1}H NMR spectra of polymer 3.7a (a) following dissolution and sonication in 0.1 M pH 7.4 phosphate buffer (D_2O) at the first time point reading (t=15 min) in the degradation process; and (b) following complete cyclization after 32 d at 37˚C.

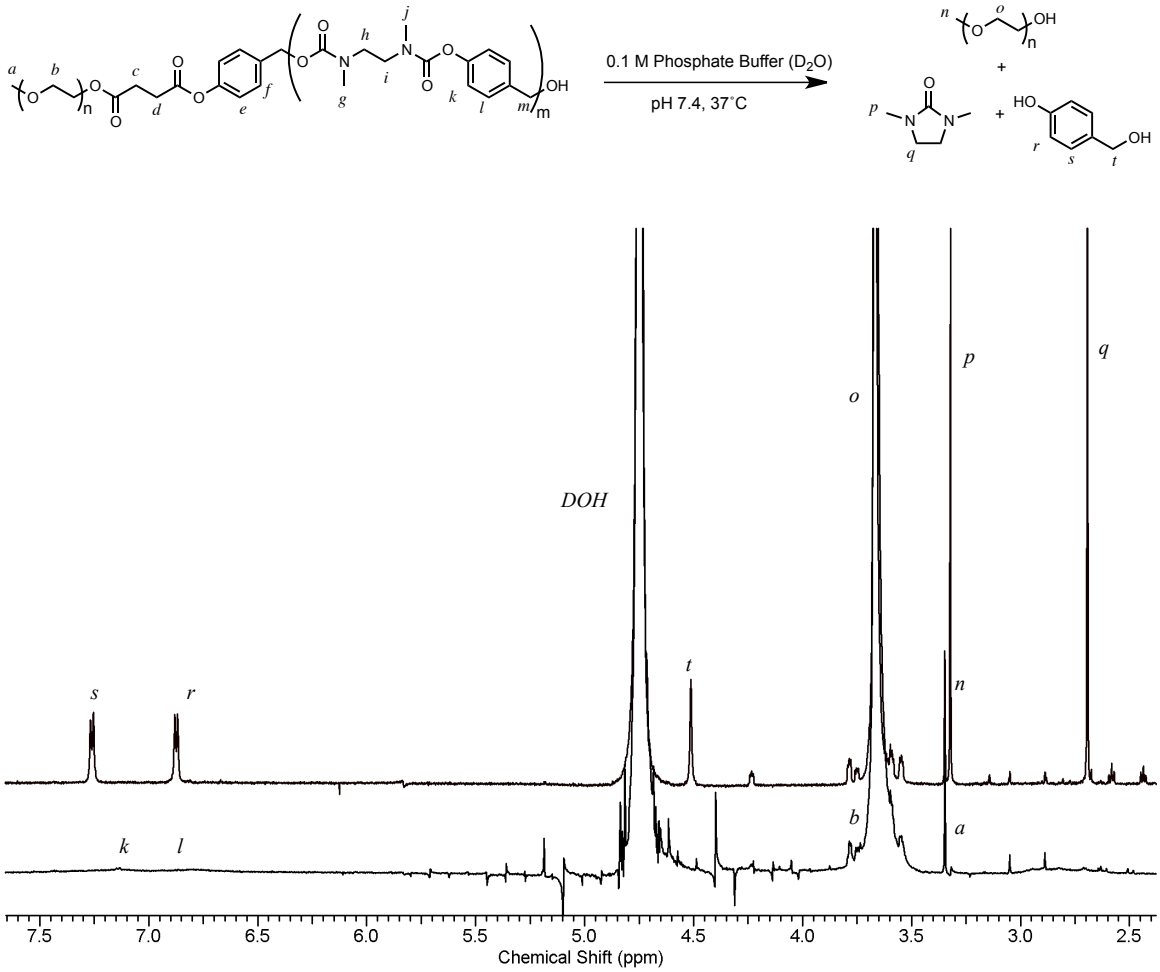

Figure C12: ^{1}H NMR spectra of polymer 3.7b (a) following dissolution and sonication in 0.1 M pH 7.4 phosphate buffer (D_2O) at the first time point reading (t=15 min) in the degradation process; and (b) following complete cyclization after 32 d at 37˚C.

Appendix D: Factorial DOE Experiments

D1. Factorial Design: Varying the Molecular Weight Obtained from the Polymerization of Compound 2.5

3 Factor, 2 Level Design with Blocking:

Factor	Low Level (-)	High Level (+)
1. Reaction Duration	6 h	24 h
2. Temperature	0˚C	Room Temperature
3. Equivalents of End-Cap	0.025	0.05
4. Amine Base (Blocked Variable)	NEt_3	DIPEA

DOE Structure:

Experiment	Duration (x_D)	Temperature (x_T)	End Cap (x_{EC})	Blocking Pattern (x_B)	M_P (g/mol)
1	-	-	-	-	30,558
2	+	-	-	+	25,453
3	-	+	-	+	29,096
4	+	+	-	-	28,743
5	-	-	+	+	17,770
6	+	-	+	-	23,962
7	-	+	+	-	21,507
8	+	+	+	+	18,416

M_P – Peak molecular weight (g/mol) relative to polystyrene standards

Experimental Details: Activated monomer **2.1c** (1 equiv) was dissolved in 6 mL of 1:1 TFA:CH_2Cl_2 and stirred at room temperature for 2 h. The solvent was then blown off prior to subjecting the reaction mixture three times to a repeat cycle of dilution with CH_2Cl_2 followed by concentration under reduced pressure to remove residual TFA and provide the deprotected monomer **2.5**. End-cap **2.1c** (0.025 or 0.05 equiv) was added and the resulting mixture was dissolved in 12 mL of anhydrous toluene and cooled to 0˚C or maintained at room temperature. The amine base (NEt_3 or DIPEA) and DMAP (0.066 g, 0.54 mmol, 0.22 equiv) were sequentially added and the solution was stirred at 0˚C or room temperature for 6 or 24 h. The solvent was then evaporated under reduced pressure and the crude polymer was dissolved in 2 mL of DMF and dialyzed against DMF for 24 h (200, mL, 1 solvent change) using a regenerated cellulose membrane (6000-8000 g/mol MWCO). The contents of the dialysis membrane were then concentrated *in vacuo* and lyophilized to afford the purified polymers.

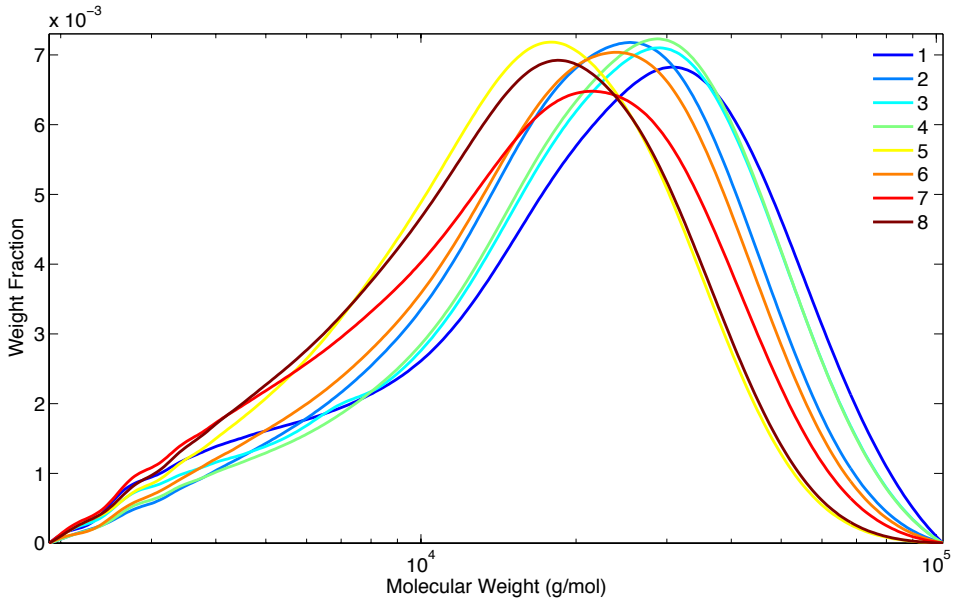

Figure D1. SEC chromatograms of DOE polymers 1-8 (DMF, PS standards)

Appendix E: Regression Fits

a)

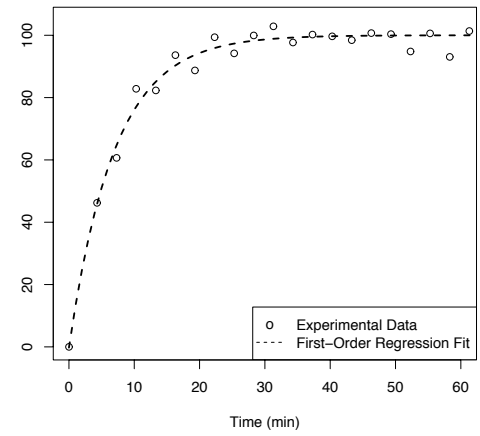

b)

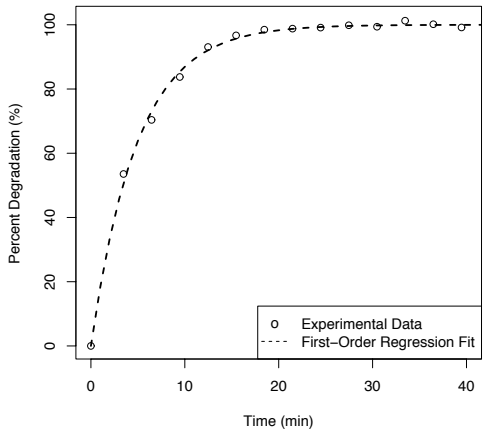

c)

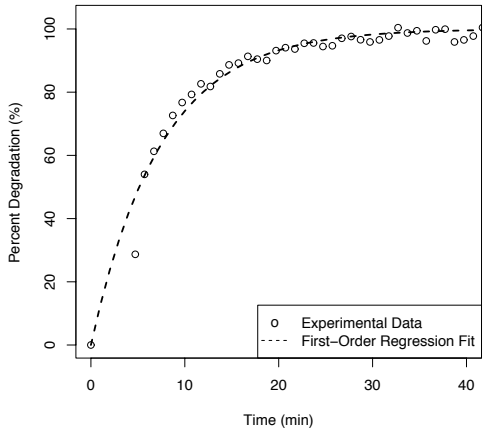

Figure E1. Degradation plots for monomer compound 2.1d. a) Run 1: $k=1.52\times10^{-1}$ min^{-1}, $h_{1/2}$=4.56 min , SE= 5.7%; b) Run 2: $k=2.03\times10^{-1}$ min^{-1}, $h_{1/2}$=3.41 min , SE= 1.2%; and c) Run 3: $k=1.35\times10^{-1}$ min^{-1}, $h_{1/2}$=5.14 min , SE= 2.9%.

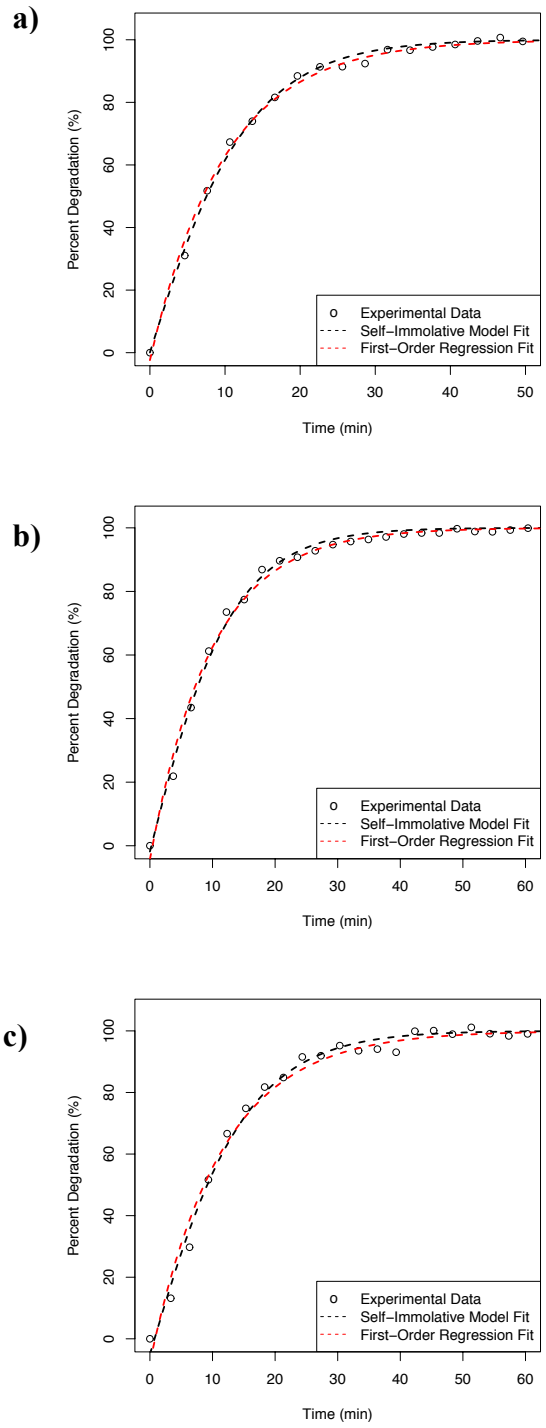

Figure E2. Degradation plots for dimer compound 2.2d. a) Run 1: $k=1.52\times10^{-1}$ min^{-1}, $h_{1/2}$=4.56 min , SE= 2.4%; b) Run 2: $k=1.55\times10^{-1}$ min^{-1}, $h_{1/2}$=4.46 min , SE= 1.8%; and c) Run 3: $k=1.36\times10^{-1}$ min^{-1}, $h_{1/2}$=5.10 min , SE= 3.0%.

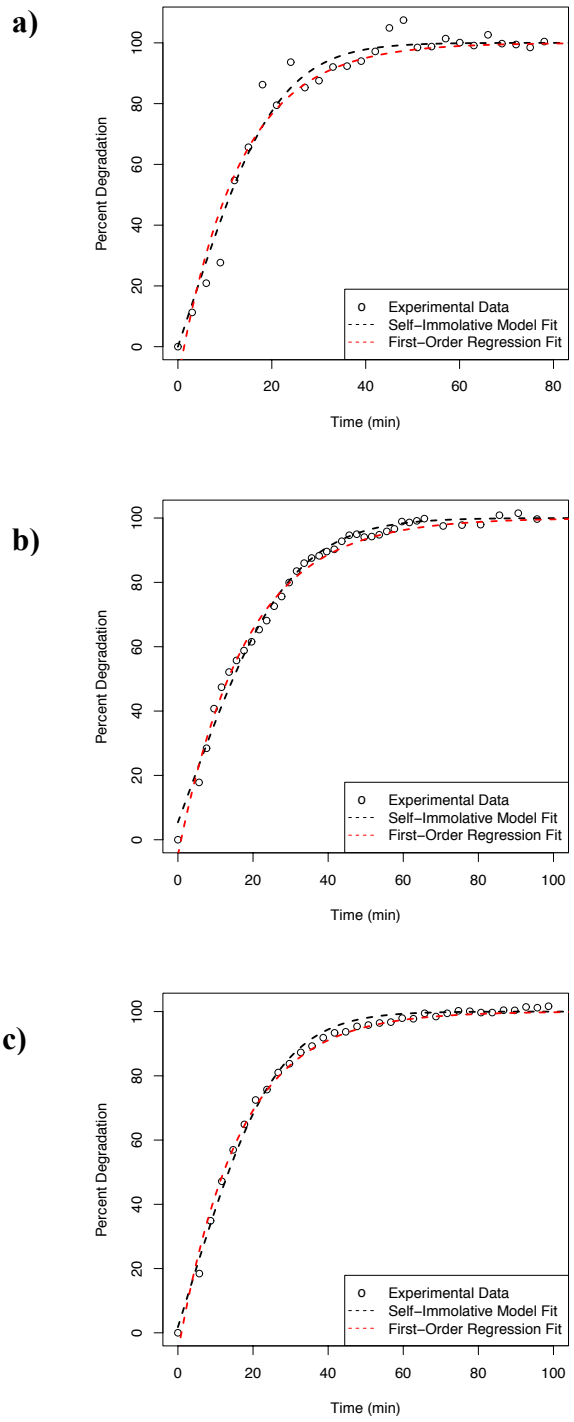

Figure E3. Degradation plots for tetramer compound 2.3d. a) Run 1: $k=1.28\times10^{-1}$ min^{-1}, $h_{1/2}=5.43$ min , SE= 5.4%; b) Run 2: $k=1.50\times10^{-1}$ min^{-1}, $h_{1/2}=4.62$ min , SE= 1.9%; and c) Run 3: $k=2.01\times10^{-1}$ min^{-1}, $h_{1/2}=3.44$ min , SE= 5.1%.

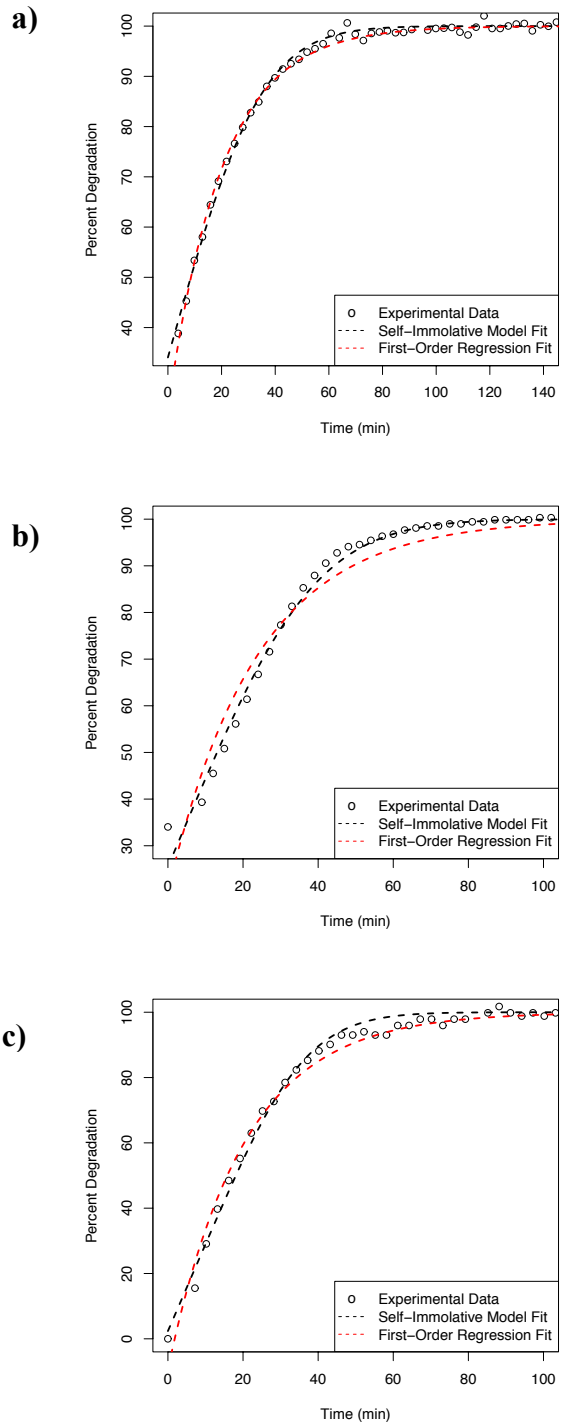

Figure E4. Degradation plots for octamer compound 2.4d. a) Run 1: $k=1.53\times10^{-1}$ min^{-1}, $h_{1/2}=4.52$ min , SE= 1.1%; b) Run 2: $k=1.52\times10^{-1}$ min^{-1}, $h_{1/2}=4.54$ min , SE= 2.0%; and c) Run 3: $k=2.12\times10^{-1}$ min^{-1}, $h_{1/2}=3.26$ min , SE= 2.5%.

Table E1. Regression statistics for compounds 2.1d-2.4d

Compound	Run	First-Order Model			Self-Immolative Model		
		SE	AIC	BIC	SE	AIC	BIC
2.1d	1	5.65	/	/			
	2	1.20	/	/			
	3	2.91	/	/			
2.2d	1	2.5	129.9	133.8	2.4	126.8	130.7
	2	2.2	127.8	131.8	1.8	117.6	121.6
	3	3.5	186.5	191.1	3.0	175.1	179.7
2.3d	1	2.3	174.3	179.2	2.4	179.6	184.5
	2	2.0	144.5	149.0	1.9	141.1	145.6
	3	6.4	180.7	184.6	5.1	168.2	172.1
2.4d	1	1.1	178.3	184.5	1.1	181.1	184.5
	2	4.1	220.0	224.9	2.0	162.8	167.7
	3	2.9	183.1	187.9	2.5	173.2	178.0

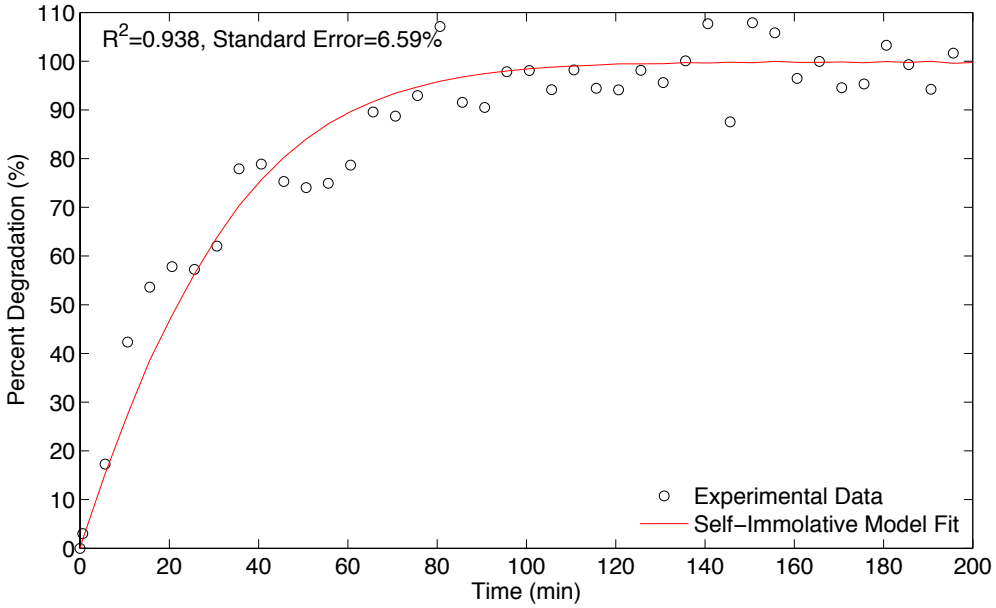

Figure E5: Numerical regression of the self-immolative degradation model applied to polymer 2.6

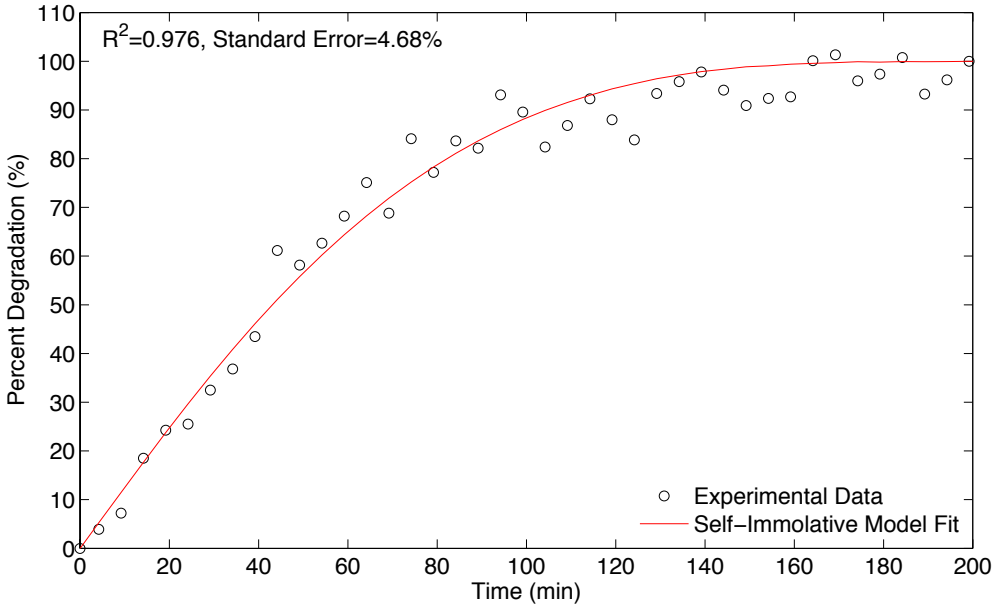

Figure E6: Numerical regression of the self-immolative degradation model applied to polymer 2.7.

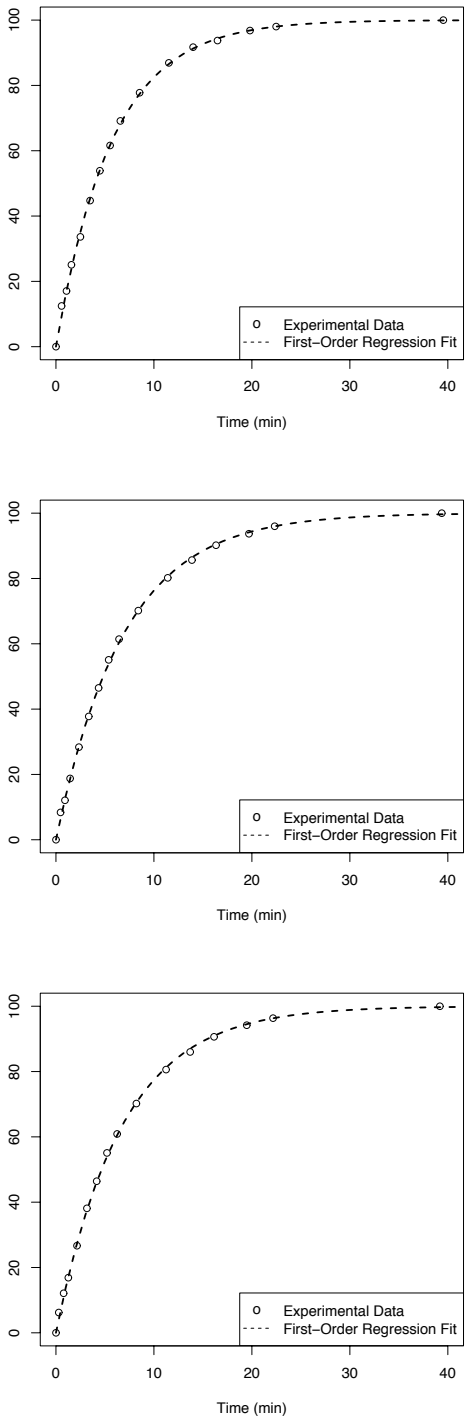

Figure E7. Degradation plots for model compound 3.19. a) Run 1: $k=1.74\times10^{-1}$ h^{-1}, $h_{1/2}$=3.97 h, SE= 1.0%; b) Run 2: $k=1.44\times10^{-1}$ h^{-1}, $h_{1/2}$=4.81 h , SE= 0.7%; and c) Run 3: $k=1.49\times10^{-1}$ h^{-1}, $h_{1/2}$=4.65 h , SE= 0.8%.

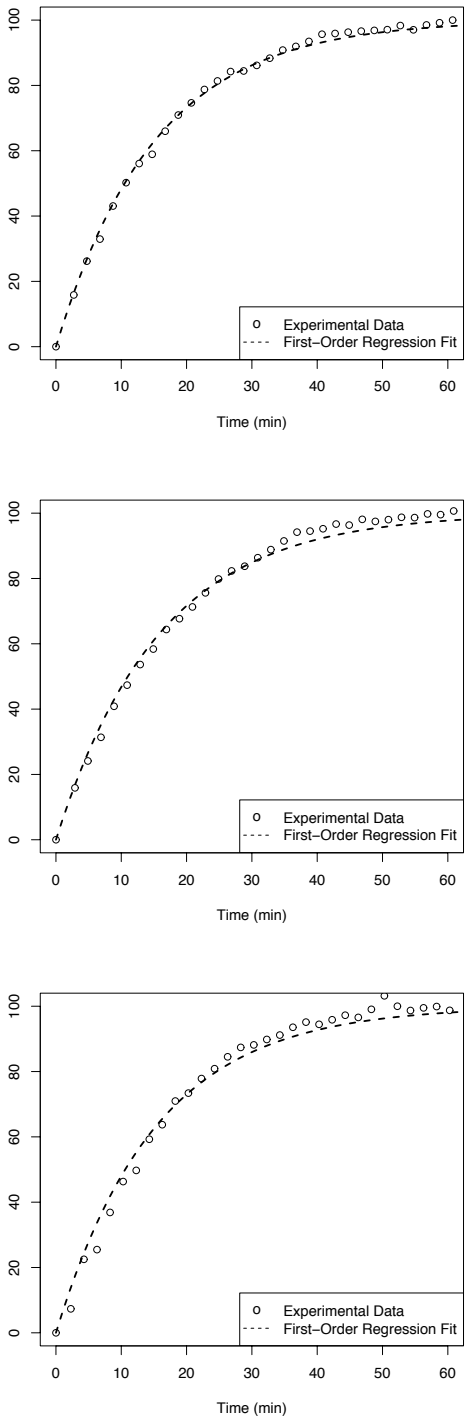

Figure E8. Degradation plots for model compound 3.21. a) Run 1: $k=6.59\times10^{-2}$ min^{-1}, $h_{1/2}$=10.5 min , SE= 1.3%; b) Run 2: $k=6.30\times10^{-2}$ min^{-1}, $h_{1/2}$=11.0 min , SE= 2.3%; and c) Run 3: $k=6.54\times10^{-1}$ min^{-1}, $h_{1/2}$=10.6 min , SE= 3.3%.

Appendix F: Permission to Reuse Copyrighted Material

American Chemical Society's Policy on Theses and Dissertations

If your university requires you to obtain permission, you must use the RightsLink permission system.
See RightsLink instructions at http://pubs.acs.org/page/copyright/permissions.html.

This is regarding request for permission to include **your** paper(s) or portions of text from **your** paper(s) in your thesis. Permission is now automatically granted; please pay special attention to the **implications** paragraph below. The Copyright Subcommittee of the Joint Board/Council Committees on Publications approved the following:

> Copyright permission for published and submitted material from theses and dissertations
> ACS extends blanket permission to students to include in their theses and dissertations their own articles, or portions thereof, that have been published in ACS journals or submitted to ACS journals for publication, provided that the ACS copyright credit line is noted on the appropriate page(s).
> Publishing **implications** of electronic publication of theses and dissertation material
> Students and their mentors should be aware that posting of theses and dissertation material on the Web prior to submission of material from that thesis or dissertation to an ACS journal may affect publication in that journal. Whether Web posting is considered prior publication may be evaluated on a case-by-case basis by the journal's editor. If an ACS journal editor considers Web posting to be "prior publication", the paper will not be accepted for publication in that journal. If you intend to submit your unpublished paper to ACS for publication, check with the appropriate editor prior to posting your manuscript electronically.

Reuse/Republication of the Entire Work in Theses or Collections: Authors may reuse all or part of the Submitted, Accepted or Published Work in a thesis or dissertation that the author writes and is required to submit to satisfy the criteria of degree-granting institutions. Such reuse is permitted subject to the ACS' "Ethical Guidelines to Publication of Chemical Research" (http://pubs.acs.org/page/policy/ethics/index.html); the author should secure written confirmation (via letter or email) from the respective ACS journal editor(s) to avoid potential conflicts with journal prior publication*/embargo policies. Appropriate citation of the Published Work must be made. If the thesis or dissertation to be published is in electronic format, a direct link to the Published Work must also be included using the ACS Articles on Request author-directed link − see http://pubs.acs.org/page/policy/articlesonrequest/index.html

* Prior publication policies of ACS journals are posted on the ACS website at http://pubs.acs.org/page/policy/prior/index.html

If your paper has **not** yet been published by ACS, please print the following credit line on the first page of your article: "Reproduced (or 'Reproduced in part') with permission from [JOURNAL NAME], in press (or 'submitted for publication'). Unpublished work copyright [CURRENT YEAR] American Chemical Society." Include appropriate information.

If your paper has already been published by ACS and you want to include the text or portions of

the text in your thesis/dissertation, please print the ACS copyright credit line on the first page of your article: “Reproduced (or 'Reproduced in part') with permission from [FULL REFERENCE CITATION.] Copyright [YEAR] American Chemical Society." Include appropriate information.

Submission to a Dissertation Distributor: If you plan to submit your thesis to UMI or to another dissertation distributor, you should not include the unpublished ACS paper in your thesis if the thesis will be disseminated electronically, until ACS has published your paper. After publication of the paper by ACS, you may release the entire thesis (**not the individual ACS article by itself**) for electronic dissemination through the distributor; ACS’s copyright credit line should be printed on the first page of the ACS paper.

Curriculum Vitae for Ryan A. McBride

EDUCATION

The University of Western Ontario, London, ON 2011-2013
Master of Engineering Science, Chemical & Biochemical
- Supervisor: Dr. Elizabeth Gillies
- Thesis Project: Degradation Kinetics and Functional Design of Linear Self-Immolative Polymers

McMaster University, Hamilton, ON 2006-2011
Bachelor of Engineering and Biosciences, Chemical
- Graduated *summa cum laude* (11.5/12 GPA) with co-op specialization

HONOURS AND AWARDS

Ontario Graduate Scholarship, $15000, Ontario Government, 2012
Alexander Graham Bell Scholarship (CGS-M), $17500, NSERC, 2011
Dr. Harry Lyman Hooker Scholarship, $800, McMaster University, 2010
Undergraduate Student Research Award, $4500, NSERC, 2010
University Senate Scholarship, $800, McMaster University, 2008 & 2009
Yates Scholarship, $800, McMaster University, 2007
President's Award, $12000, McMaster University, 2006-2010
Nortel Networks Entrance Scholarship, $6000, McMaster University, 2006-2008

PUBLICATIONS

Articles submitted to refereed journals:

McBride, R. A., Gillies, E. R. Kinetics of Self-Immolative Degradation in a Linear Polymeric System: Demonstrating the Effect of Chain Length, *Macromolecules* **2013**. doi: 10.1021/ma4009753

Chen, E. K. Y., McBride, R. A., Gillies, E. R. Self-Immolative Polymers Containing Rapidly Cyclizing Spacers: Toward Rapid Depolymerization Rates, *Macromolecules* **2012**, 45 (18): 7364-7374.

Wallace, M., McBride, R., Aumi, S., Mhaskar, P., Salsbury, T., and House, J. Energy efficient model predictive building temperature control, *Chemical Engineering Science* **2012**, 69: 45-58.

CONFERENCE PRESENTATIONS

McBride, R. A., Gillies, E. R. "Stimuli-Responsive Linear Self-Immolative Polymers: Tuning the Rate of Degradation." 96th Canadian Chemistry Conference and Exhibition, May 26-30, 2013. **Oral Presentation.**

McBride, R. A., Chen, E. K. Y., DeWit, M. A., Gillies, E. R. "Design and synthesis of linear self-immolative polymers with tunable rates of degradation." 35th Canadian High Polymer Forum, August 15-18, 2012. **Oral Presentation**.

McBride, R. A., Gillies, E. R. "Kinetic Evaluation and Mechanistic Modelling of the Effect of Chain Length on Self-Immolative Degradation in a Linear Polymeric System." 24th Canadian Materials Science Conference, June 5-8, 2012. **Poster Presentation**- Received 3rd Place

PROFESSIONAL EXPERIENCE

The University of Western Ontario, London, Ontario
Research Assistant, Department of Chemistry — May – Aug. 2011

McMaster Advanced Control Consortium, Hamilton, ON
USRA Summer Student — May – Aug. 2010

Agviro, Inc., Guelph, ON
Engineering Co-op Student — May – Aug. 2008 & 2009

Centre for Nutritional Modelling, Guelph, ON
Research Assistant — May – Aug. 2007

TEACHING EXPERIENCE

The University of Western Ontario, London, Ontario
Teaching Assistant

CBE 2291 Computational Methods	Jan. – Apr. 2013
CBE 4485 Energy and Society	Sept. – Dec. 2012
CBE 2291 Computational Methods	Jan. – Apr. 2012